

N65-29717

TOPICAL REPORT **VOLUME 1** SELECTION CRITERIA

**BRUSHLESS ROTATING ELECTRICAL GENERATORS
FOR SPACE AUXILIARY POWER SYSTEMS**

by

J. N. Ellis and F. A. Collins

prepared for

NATIONAL AERONAUTICS AND SPACE ADMINISTRATION

CONTRACT NO. NAS 3-2783

LEAR SIEGLER, INC.



*POWER EQUIPMENT DIVISION
CLEVELAND 1, OHIO*

NOTICE

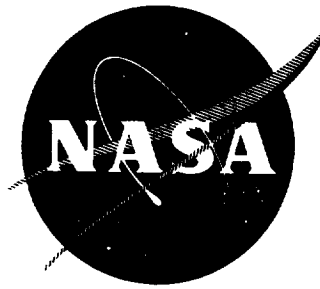
This report was prepared as an account of Government sponsored work. Neither the United States, nor the National Aeronautics and Space Administration (NASA), nor any person acting on behalf of NASA:

- A.) Makes any warranty or representation, expressed or implied, with respect to the accuracy, completeness, or usefulness of the information contained in this report, or that the use of any information, apparatus, method, or process disclosed in this report may not infringe privately owned rights; or
- B.) Assumes any liabilities with respect to the use of, or for damages resulting from the use of any information, apparatus, method or process disclosed in this report.

As used above, "person acting on behalf of NASA" includes any employee or contractor of NASA, or employee of such contractor, to the extent that such employee or contractor of NASA, or employee of such contractor prepares, disseminates, or provides access to, any information pursuant to his employment or contract with NASA, or his employment with such contractor.

Requests for copies of this report
should be referred to:

National Aeronautics and Space Administration
Office of Scientific and Technical Information
Washington, D. C. 20546
Attention: AFSS-A



TOPICAL REPORT

BRUSHLESS ROTATING ELECTRICAL GENERATORS
FOR SPACE AUXILIARY POWER SYSTEMS

by

J. N. Ellis and F. A. Collins

prepared for

NATIONAL AERONAUTICS AND SPACE ADMINISTRATION

April 26, 1965

Contract No. NAS 3-2783

Technical Management
Howard A. Shumaker
NASA Lewis Research Center
Space Power System Division
Solar and Chemical Power Branch

LEAR SIEGLER, INC.
Power Equipment Division
Cleveland, Ohio

ABSTRACTING SUMMARY

This report contains ten (10) design manuals and nine (9) computer programs for use in calculating the performance and characteristics of brushless a. c. generators. It contains a computer program for use in calculating generator operating temperatures. It contains selection aids for use in choosing the proper generator for a specific application and has derivations and other supplemental aids to support the design manuals.

TABLE OF CONTENTS

SELECTION CRITERIA & MECHANICAL STUDIES FOR AC GENERATORS

VOL. I

BRIEF DESCRIPTIONS AND SCHEMATICS

SECTION A, VOL. I

Wound Pole, Salient Pole Generator	Page A-1
Wound-Rotor, Non-Salient-Pole Generator	Page A-8
Rotating Coil Lundell	Page A-15
Single, Inside, Stationary Coil Lundell Generator	Page A-25
Two, Inside, Stationary Coil Lundell Generator (Becky Robinson)	Page A-33
Two, Outside-Coil Lundell	Page A-41
Single, Outside-Coil Lundell	Page A-46
Axial Air Gap Lundell	Page A-52
Homopolar Inductor	Page A-59
Permanent-Magnet Generator	Page A-73
How to Start a Design	Page A-116

GENERATOR SELECTION CRITERIA

SECTION B, VOL. I

Discussion	Page B-1
Family Tree Diagram of Generators	Page B-4
Comparison Chart for Brushless AC Generator Applications (Good- Better-Best Type Comparison)	Page B-5

Approximate Dimensions for Homopolar Inductor and Two, Outside Coil Lundell AC Generators	Page B-6
Weight vs. Output, Wound-Pole, Salient- Pole, Synchronous Generator	Page B-7
Volume vs. Output for Wound-Pole, Salient-Pole Synchronous Generator	Page B-8
Weight vs. Output, Two, Inside, Stationary Coil Lundell (Becky Robinson) with 4 Poles	Page B-9
Weight vs. Output, Two, Inside, Stationary Coil Lundell (Becky Robinson) with 6 Poles	Page B-10
Weight vs. Output, Two, Inside, Stationary Coil Lundell (Becky Robinson) with 8 Poles	Page B-11
Weight vs. Output, Two, Outside Coil or Single, Outside Coil Lundell (4 Poles)	Page B-12
Weight vs. Output, Two, Outside Coil or Single, Outside Coil Lundell (6 Poles)	Page B-13
Weight vs. Output, Two, Outside Coil or Single, Outside Coil Lundell (8 Poles)	Page B-13a
Weight vs. Output, Homopolar Inductor (4 Poles)	Page B-14
Weight vs. Output, Homopolar Inductor (6 Poles)	Page B-15
Weight vs. Output, Homopolar Inductor (8 Poles)	Page B-15a

Weight vs. Output for Wound, Laminated Stators of AC Electro- magnetic Generators	Page B-16
Weight vs. Output, Axial Air-Gap Lundell	Page B-17
Stator Diameter vs. Output for Disk-Type Lundell	Page B-18
Pole Face Losses at No- Load and Full- Load for Rotors of Various Diameters	Page B-19
Rotor Diameter vs. Rotor Speed for Solid Pole Face Alternators Limited to 20 Watts/in² Pole Face Losses Based on Stator Bore Area	Page B-20
Comparison of No- Load and Full- Load Losses When the Slot Pitch is Changed	Page B-21
Pole- Face Losses in a Solid Pole Face Rotor at No- Load as a Function of Speed	Page B-22
Surface Heat Dissipation from a Generator Rotor	Page B-23
Discussion of the Performance of Synchronous Generators When Used as Motors	Page B-24
MECHANICAL AND THERMAL STUDIES	VOL. I
GENERATOR THERMAL ANALYSIS	SECTION C, VOL. I
Table of Contents	Page C-0
Rotor Friction Analysis	Page C-A-1

GENERATOR ROTOR DYNAMICS

Table of Contents

SECTION D, VOL. I

Page D-0

DISCUSSION OF GAS BEARINGS

Table of Contents

SECTION E, VOL. I

Page E-0

Rolling Contact Bearings

Page E-81

DESIGN FORMULAE FOR BRUSHLESS A-C GENERATORS

VOL. II

DESIGN CURVES & TABLES

SECTION F, VOL. II

Chord Factors, Table 1

Page F-1

Distribution Factors, Table 2

Page F-2

Wire Table, Round Copper
Table 3

Page F-3

Wire Table, Round Half Size
Table 4

Page F-4

End-Winding Constant, Curve 1

Page F-5

Pole Face Loss Constants,
Curve 2

Page F-6

Pole Face Load Loss Factor,
Curve 3

Page F-7

C_1 and C_p , Salient Pole,
Curve 4

Page F-8

C_1 , C_m and C_p Non-Salient Pole,
Curve 4a, 4b

Page F-7a, b

C_x , Curve 5

Page F-9

Damper Loss Constants, Curve 7

Page F-10

Damper Loss Constants, Curve 8

Page F-11

C_m and C_q , Curve 9	Page F-12
Magnetization Curve, Pure Iron, Curve 10	Page F-13
Magnetization Curve, M-43 Silicon Irons, Curve 11A	Page F-14
Magnetization Curve, M36, Curve 11B	Page F-14
Magnetization Curve M-22, Curve 11C and 11E	Page F-14
Magnetization Curve M-15, Curve 11D	Page F-14
Magnetization Curve, 1% Max. Carbon, Curve 12	Page F-18
Magnetization Curve, Cobalt- Iron, Curve 13	Page F-19
Magnetization Curve For Cast and Forged Cobalt-Iron Alloy, Curve 13b	Page F-21
Magnetization Curve, 4620, 4130, 4140, 6302, Curve 14	Page F-22
Magnetization Curve, 6427, Hy-TUF 410 SS, VASCOJET, Curve 15	Page F-23
Magnetization Curve, 1095, P-6, Curve 16	Page F-24
Magnet Stabilization Point (A_T) Versus Out-of-Stator Leakage Permeance for Alnico V and Alnico VI, Curve 17	Page F-25
Magnet Stabilization Point (A_T) Versus Out-of-Stator Leakage Permeance for Alnico VIII, Curve 18	Page F-26

Magnet Stabilization Point (A_T) Versus Out-of-Stator Leakage Permeance for Alnico V7, Curve 19	Page F-27
Demagnetization Curves for High Energy Product Cast Alnicos, Curve 20	Page F-28
Demagnetization Curve for Cast Alnico VIII, Curve 21	Page F-29
Demagnetization Curve for Cast Alnico VIII, Curve 22	Page F-30
Demagnetization Curve for Cast Alnico V7, Curve 23	Page F-31
Demagnetization Curve for Cast Alnico VI, Curve 24	Page F-32
Demagnetization Curve for Cast Alnico V, Curve 25	Page F-33
Iron Losses for Cobalt-Iron Alloy, Curve 13a	Page F-20
Iron Losses for Si-Fe Alloys at Various Frequencies, Curve 11H	Page F-17
Iron Losses for Silicone-Iron Alloys, at 400 cps, Curve 11F	Page F-15
Iron Losses for Si-Fe Alloys at 60 cps, Curve 11G	Page F-16
Curve Points of Magnetic Metals	Page F-34
Magnetic Properties of Cr-Ni Steels	Page F-36
MASTER DESIGN MANUAL (SALIENT-POLE, WOUND-POLE, SYNCHRONOUS AC GENERATOR	SECTION G, VOL. II
Input Sheet	Page G-01

Output Sheet	Page G-03
Design Procedure	Page G-1
DESIGN MANUAL FOR NON-SALIENT, WOUND-ROTOR, SYNCHRONOUS AC GENERATOR	SECTION H, VOL. II
Input Sheet	Page H-01
Output Sheet	Page H-02
Design Procedure	Page H-1
DESIGN MANUAL FOR ROTATING-COIL AC LUNDELL TYPE GENERATORS	SECTION J, VOL. II
Input Sheet	Page J-01
Output Sheet	Page J-03
Design Procedure	Page J-1
DESIGN MANUAL FOR SINGLE, INSIDE, STATIONARY-COIL AC LUNDELL- TYPE GENERATOR	SECTION K, VOL. II
Input Sheet	Page K-01
Output Sheet	Page K-03
Design Manual	Page K-1
DESIGN MANUAL FOR TWO, INSIDE- COIL, STATIONARY-COIL AC LUNDELL- TYPE GENERATOR (BECKY ROBINSON PATENT)	SECTION L, VOL. II
Input Sheet	Page L-01
Output Sheet	Page L-04
Design Manual	Page L-1

DESIGN MANUAL FOR TWO COIL AND
SINGLE-COIL, OUTSIDE COIL AC
LUNDELL-TYPE GENERATORS

SECTION M, VOL. II

Input Sheet

Page M-01

Output Sheet

Page M-03

Design Manual For Two-Coil Lundell

Page M-1

Design Manual For One-Coil Lundell

Page M-41

DESIGN MANUAL FOR AXIAL AIR-GAP,
STATIONARY-COIL, SALIENT-POLE,
SYNCHRONOUS AC GENERATOR

SECTION N, VOL. III

Discussion

Page N-1

Design Sheet

Page N-4

Design Manual

Page N-5

DESIGN MANUAL FOR HOMOPOLAR
INDUCTOR, AC GENERATOR

SECTION P, VOL. III

Input Sheet

Page P-01

Output Sheet

Page P-03

Design Manual

Page P-1

DESIGN MANUAL FOR PERMANENT
MAGNET, SALIENT-POLE AC
GENERATORS

SECTION R, VOL. III

Discussion

Page R-1

Input Sheet

Page R-01

Output Sheet

Page R-03

Design Manual

Page R-22

EQUIVALENT CIRCUITS

SECTION S, VOL. III

SYMBOL TABLES

SECTION T, VOL. III

GENERATOR THERMAL ANALYSIS
COMPUTER PROGRAM (FORTRAN)

SECTION CA, VOL. IV

SALIENT-POLE WOUND-POLE
SYNCHRONOUS GENERATOR COMPUTER
PROGRAM AND TEST DATA

SECTION GA, VOL. IV

Computer Input 30 KVA Generator

Page GA-1

Computer Output 30 KVA Generator

Page GA-2

Test Data 30 KVA Generator

Page GA-5

Computer Program (Fortran)

Page GA-14

NON-SALIENT-POLE, WOUND-ROTOR
SYNCHRONOUS GENERATOR COMPUTER
PROGRAM AND TEST DATA

SECTION HA, VOL. IV

Computer Input 120 KVA Generator

Page HA-1

Computer Output 120 KVA Generator

Page HA-2

Test Data 120 KVA Generator

Page HA-4

Computer Program (Fortran)

Page HA-29

ROTATING-COIL LUNDELL, A-C
GENERATOR COMPUTER PROGRAM
AND TEST DATA

SECTION JA, VOL. IV

Computer Input 840 Watt Generator

Page JA-1

Computer Output 840 Watt Generator

Page JA-5

Test Data 840 Watt Generator

Page JA-7

Computer Program 840 Watt Generator	Page JA-25
INSIDE, SINGLE-COIL, STATIONARY- COIL LUNDELL, A-C GENERATOR COMPUTER PROGRAM AND TEST DATA	Page KA, VOL. IV
Computer Input	Page KA-1
Computer Output	Page KA-3
Computer Program	Page KA-22
INSIDE, TWO-COIL STATIONARY COIL LUNDELL A-C GENERATOR COMPUTER PROGRAM AND TEST DATA	SECTION LA, VOL. IV
Computer Input 30 KVA Generator	Page LA-3
Computer Output 30 KVA Generator	Page LA-1
Test Data 30 KVA Generator	Page LA-6
Computer Program	Page LA-37
TWO-COIL AND SINGLE-COIL OUTSIDE- COIL, LUNDELL, A-C GENERATOR COMPUTER PROGRAM AND TEST DATA	SECTION MA, VOL. V
Computer Input 840 Watt Generator	Page MA-1
Computer Output 840 Watt Generator	Page MA-3
Test Data 840 Watt Generator	Page MA-7
Computer Program	Page MA-20
HOMOPOLAR INDUCTOR A-C GENERATOR COMPUTER PROGRAM AND TEST DATA	SECTION PA, VOL. V
Computer Input	Page PA-01

Computer Output	Page PA-03
Test Data	Page PA-05
Computer Program	Page PA-19
PERMANENT MAGNET A-C GENERATOR COMPUTER PROGRAM AND TEST DATA	SECTION RA, VOL. V
Computer Input	Page RA-1
Computer Output	Page RA-3
Test Data	Page RA-5
Computer Program	Page RA-22
DERIVATIONS	SECTION SA, VOL. V
Pole Face Losses in Solid-Pole Generators	Page SA-1
Graphical Flux Analysis	Page SA-29
The Maximum $\frac{l}{d}$ Ratio for Rotating Coil Lundell A-C Generators	Page SA-38
The Maximum $\frac{l}{d}$ Ratio for Two, Inside, Stationary- Coil Lundell A-C Generators	Page SA-40
The Development of Equations Describing the Weights of Electromagnetic Parts for Three Generator Types	Page SA-43
Generator Stator Ampere Load- ing - A Discussion	Page SA-50
Grouping of Fractional Slot Windings	Page SA-53
Distribution Factor	Page SA-58

Fractional Slot Distribution Factor	Page SA-60
Skew Factor	Page SA-61
Pitch Factor	Page SA-64
Reactances, Per-Unit System	Page SA-67
Synchronous Reactance	Page SA-69
Reactance of Armature Reaction	Page SA-72
Transient Reactance	Page SA-74
Subtransient Reactance	Page SA-78
Negative Sequence Reactance	Page SA-79
Zero Sequence Reactance	Page SA-79
Leakage Reactance	Page SA-80
Potier Reactance	Page SA-86
Time Constants	Page SA-89
Resistance	Page SA-95
Generator Voltage and Output Equations	Page SA-96
C_m	Page SA-100
C_q	Page SA-103
Permeance Calculations	Page SA-110
EFFECT OF INCREASING THE AIR GAP	SECTION TA, VOL. V

FIGURES

	<u>Figure No.</u>	<u>Page No.</u>
Wound-Pole, Salient-Pole AC Generator	A-1	A-1
Wound-Pole, Salient-Pole AC Generator	A-2	A-4
Wound-Pole, Rotating-Rectifier AC Generator	A-3	A-5
Wound-Pole Synchronous AC Generator	A-4	A-6
Photograph of Wound-Pole Synchronous Generator	A-5	A-7
Field Form for Non-Salient Pole Wound-Pole AC Generator	A-6	A-9
Rotor Views - NSP AC Generator	A-7	A-10
Photograph of Rotor & Stator (NSP Generator)	A-8	A-11
Photograph of Rotor & Stator (NSP Generator)	A-9	A-12
Exploded View of Complete NSP AC Generator	A-10	A-13
Rotating-Coil Lundell AC Generator	A-11	A-14
Step 1 of Conversion to Outside-Coil Lundell	A-12	A-15
Step 2 of Conversion	A-13	A-16

	<u>Figure No.</u>	<u>Page No.</u>
Conversion of Rotating-Coil to Stationary-Coil Lundell	A-14	A-17
How to Make a Becky-Robinson Lundell	A-15	A-18
How to Make a Homopolar Inductor	A-16	A-19
Patent Drawing, Rotating Coil Lundell	A-17	A-20
Photo Rotating-Coil Lundell	A-18	A-21
Rotor, Rotating-Coil Lundell	A-19	A-22
Photo, Rotating Coil Lundell	A-20	A-23
Single-Inside, Stationary-Coil Lundell	A-21	A-24
Single-Inside, Stationary-Coil Lundell	A-22	A-26
Single-Inside, Stationary-Coil Lundell	A-23	A-27
Single-Inside, Stationary-Coil Lundell Patent Drawing	A-24	A-29
Photo of Single, Inside, Stationary- Coil Lundell	A-24a	A-30
Photo of Single, Inside, Stationary- Coil Lundell	A-24	A-31
MG Set	A-26	A-32
Two-Inside Stationary Coil Lundell	A-27	A-33
Two-Inside Stationary Coil Lundell Photo	A-28	A-36

	<u>Figure No.</u>	<u>Page No.</u>
Two-Inside Stationary Coil Lundell Photo	A-29	A-37
Two-Inside Stationary Coil Lundell Photo	A-30	A-38
Two-Inside Stationary Coil Lundell Flux Circuit	A-31	A-39
Two-Inside Stationary Coil Lundell Flux Circuit	A-32	A-40
Two-Outside Coil Lundell Flux Circuit Schematics	A-33	A-42
Two-Outside Coil Lundell Drawing	A-34	A-43
Two-Outside Coil Lundell Patent Drawing	A-35	A-44
Photo Two-Outside Coil Lundell	A-36	A-45
Single-Coil Outside Coil Lundell	A-37	A-48
Pole Configuration	A-38	A-49
Single Coil Outside-Coil Lundell	A-39	A-50
Pole Configuration	A-40	A-51
Axial Air-Gap Lundell	A-41	A-52
Axial Air-Gap Lundell Patent Drawing	A-42a	A-55
Axial Air-Gap Lundell Rotor Photo	A-42c	A-56
Axial Air-Gap Lundell Stator Photo	A-42b	A-57
Double Axial-Gap Generator	A-42c	A-58

	<u>Figure No.</u>	<u>Page No.</u>
Homopolar Inductor	A-43	A-59
Homopolar Inductor	A-44	A-60
Homopolar Inductor Rotor	A-45	A-64
Homopolar Inductor Rotor	A-46	A-66
Patent Drawing for Homopolar Inductor	A-47a	A-68
Patent Drawing for Homopolar Inductor	A-47b	A-69
Permanent-Magnet AC Generator	A-48	A-73
PM Rotor Types	A-49	A-77
Earliest PM Generator	A-50	A-78
Patent Drawing for Axial Gap PM Generator	A-51	A-79
PM Hysteresis Loop	A-52	A-81
PM Hysteresis Loop	A-53	A-84
Volt Ampere Characteristic	A-54	A-86
Saturation Curve	A-55	A-88
Saturation Curve & B_r	A-56	A-89
Air Gap Shear Line	A-57	A-90
F_{dm}	A-58	A-91
Short Circuit Stabilization	A-59	A-92
Out of Stator Permeance Shear Line	A-60	A-93
In-Stator Permeance Shear Line	A-61	A-96

	<u>Figure No.</u>	<u>Page No.</u>
Useful Flux	A-62	A-98
Construction of Load Points On The PM Generator Hysteresis Loop	A-63	A-99
Air Gap Energy Storage	A-64	A-100
Air Gap Energy Storage	A-65	A-101
Vector Diagram	A-66	A-105
Vector Diagrams for AC Generators Having High Stator Winding Resistance	A-67	A-106
Vector Diagrams for AC Generators Having Low Stator Winding Resistance	A-68	A-107
Locus of Terminal Voltage	A-69	A-108
Locus of Terminal Voltage	A-70	A-109
Volt-Ampere Characteristic	A-71	A-110
Weight vs. Rating for Salient-Pole Wound-Pole, Rotating-Rectifier AC Generators	B-1 B-1	B-7 B-7
Volume vs. Rating for Salient-Pole Wound-Pole, Rotating-Rectifier AC Generators	B-2	B-8
Weight Breakdown for Two, Inside- Coil Lundell Generators (Becky- Robinson)	B-3 B-4 B-5	B-9 B-10 B-11
Weight Breakdown for a Two-Coil Outside-Coil, Lundell Generator	B-6 B-7 B-8	B-12 B-13 B-14

	<u>Figure No.</u>	<u>Page No.</u>
Weight Breakdown for a Homopolar Inductor AC Generator	B-9 B-10 B-11	B-15 B-16 B-17
Weight vs. Rating for Wound Stators	B-12	B-18
Weight vs. Stator O.D. for Disk- Type Lundell Generators	B-13	B-19
KVA Output vs. Stator O.D. for Disk-Type Lundell Generators	B-14	B-20
Pole-Face Loss Curves	B-15 B-16 B-17 B-18	B-22 B-23 B-24 B-25
Heat Dissipation From a Generator Rotor	B-19	B-26
Induction Motor Speed Torque Curves	B-20	B-28
Lundell Motor Speed Torque Curves	B-21	B-30
Wound Pole Motor Speed-Torque Curves	B-22	B-31
Induced Field Voltage During Start of Salient, Wound Pole Motor	B-23	B-34
Alternator Configuration for Thermal Analysis	CA-1	C-60
Friction Design Charts	CA-2	C-61
Homopolar Inductor Rotor	D-1	D-8a

written in Fortran, for Lear Siegler, a thermal analysis program for small generators. The same company (MTI) has written for this study a discussion on gas bearings and a discussion of rotor dynamic characteristics.

The design manuals used in this report are based in part on work done by L. A. Kilgore, E. I. Pollard, and E. C. Barnes.⁽¹⁾

Source references are given on the design curves used in Section F and the Appendix to this report contains derivations for most of the formulas used in the design programs. We are indebted to J. N. Hibbard for the hand-calculation design manuals from which the manuals in this report evolved.⁽²⁾

The investigators believe that the design manuals presented here can be used to provide better communication between purchasing agencies and manufacturers.

(1) See Bibliography on Page A-124 at end of Section A.

(2) J. N. Hibbard also provided many of the derivations published in the appendix.

	<u>Figure No.</u>	<u>Page No.</u>
Weight Breakdown for a Homopolar Inductor AC Generator	B-9 B-10 B-11	B-15 B-16 B-17
Weight vs. Rating for Wound Stators	B-12	B-18
Weight vs. Stator O.D. for Disk- Type Lundell Generators	B-13	B-19
KVA Output vs. Stator O.D. for Disk-Type Lundell Generators	B-14	B-20
Pole-Face Loss Curves	B-15 B-16 B-17 B-18	B-22 B-23 B-24 B-25
Heat Dissipation From a Generator Rotor	B-19	B-26
Induction Motor Speed Torque Curves	B-20	B-28
Lundell Motor Speed Torque Curves	B-21	B-30
Wound Pole Motor Speed-Torque Curves	B-22	B-31
Induced Field Voltage During Start of Salient, Wound Pole Motor	B-23	B-34
Alternator Configuration for Thermal Analysis	CA-1	C-60
Friction Design Charts	CA-2	C-61
Homopolar Inductor Rotor	D-1	D-8a

	<u>Figure No.</u>	<u>Page No.</u>
Outside Coil Lundell Rotor	D-2	D-8b
Becky Robinson Rotor	D-3	D-8c
Rotor Model	D-4	D-8d
Bearing Stiffness Curves	D-5	D-8e
Critical Speeds for Outside-Coil Lundell	D-6	D-8f
Critical Speeds for Inside-Coil Lundell	D-7	D-8g
Dynamic Response for Homopolar Inductor	D-8	D-8h
Dynamic Response for Homopolar Inductor	D-9	D-8i
Dynamic Response for Homopolar Inductor	D-10	D-8j
Absolute Viscosity of Various Gases	E-1	E-11a
Self Acting Gas Bearings	E-7	E-22a
Tilting-Pad Bearing Schematic	E-8	E-22b
Load Calculating Charts for Cylindrical Journal Bearings	E-9	E-22c
Curves for Tilting-Pad Bearings	E-10	E-22d
Self Acting Thrust Bearings	E-11	E-43a
Pressure Rise in Bearing Caps	E-12	E-43b
Friction Vectors in Bearings	E-13	E-43c
Spiral-Groove Thrust Bearings	E-14	E-43d

	<u>Figure No.</u>	<u>Page No.</u>
Curvature Effects-on Load and Bearing Stiffness	E-15	E-43e
End-Leakage in Spiral-Grooved Bearings	E-16	E-43f
Effects of Grooves on Pressure Profile	E-17	E-43g
Hydrostatic Bearing Stiffness vs. Restrictor Coefficient	E-21	E-54a
Hydrostatic Bearing Stiffness vs. Restrictor Coefficient	E-22	E-54b
Hydrostatic Bearing Flow vs. Restrictor Coefficient	E-23	E-54c
Hydrostatic Bearing Flow vs. Restrictor Coefficient	E-24	E-54d
Hybrid Journal Bearing Load vs. Compressibility Number	E-25	E-54e
P ₁ , Pole Head Leakage Permeance	J-4	J-9
P ₂ , Pole Head Side Leakage Permeance	J-5	J-11
P ₃ Pole Body End Leakage Permeance	J-6	J-12
P ₄ Pole Body Side Leakage Permeance	J-8	J-15
P ₅ Coil Leakage Permeance	J-9	J-16
P ₇ Stator Leakage Permeance	J-10	J-18
MMF Drops	J-11	J-19
Diagram of Leakages	J-12	J-20

	<u>Figure No.</u>	<u>Page No.</u>
Pole Dimensions	K-2	K-7
Rotor & Stator Dimensions	K-3	K-9
Permeance Path P_2	K-4	K-11
Permeance Path P_3 , P_5	K-5	K-12
Permeance Path P_1 , P_2 , P_4	K-6	K-13
MMF Drops and Leakage Fluxes	K-7	K-14
Becky Robinson Lundell Pole Types and Dimensions	L-2	L-8
Rotor Dimensions	L-3	L-10
Types of Auxiliary Gap and Gap Dimensions	L-4	L-11
Rotor Dimensions	L-5	L-13
Leakage Permeance P_3	L-6	L-17
Leakage Permeance P_4 and MMF Drops	L-7	L-18
Leakage Permeance P_4	L-8	L-19
Leakage Permeance P_4	L-9	L-20
Coil Leakage Permeance P_5	L-10	L-22
Coil Leakage Permeance P_6	L-11	L-23
Coil Leakage Permeances P_5 and P_6	L-12	L-24
Leakage Permeance P_7 from Stator to Rotor	L-13	L-25

	<u>Figure No.</u>	<u>Page No.</u>
Outside-Coil Lundell Stator and Rotor Dimensions	M-3	M-9
Leakage Permeance P_1	M-4	M-13
Leakage Permeance P_2	M-5	M-14
Leakage Permeance P_3	M-6	M-15
Leakage Permeance P_4	M-7	M-16
MMF Drops and Leakage Paths in Outside-Coil Lundell	M-8	M-17
Three Possible Locations and Permeances P_5, P_7	M-9	M-18
Leakage Flux ϕ_7 From Stator to Rotor	M-10	M-21
Leakage Permeances for 1-coil Outside-Coil Lundell	M-14	M-52
Stator Leakage Flux ϕ_7	M-15	M-53
MMF Drops in Outside-Coil Lundell and Leakage Flux ϕ_7	M-16	M-54
Disk-Type Lundell Generator	N-1	N-2
Flux Circuit for Disk-Type Lundell	N-2	N-3
Design Sheet for Disk-Type Lundell	N-3	N-4
Pole Dimensions	N-4a	N-26
Pole Dimensions	N-4b	N-26
Rotor Leakage Permeances	N-5	N-27
Rotor Leakage Permeance P_4	N-6	N-29

	<u>Figure No.</u>	<u>Page No.</u>
Homopolar Inductor Housing Type 1 Item (78)		P-8
Types 2 and 3		P-9
Homopolar Inductor Shaft Dimensions Item (78a)		P-10
PM Generator	R-1	R-2
Rotor Leakage Permeances	R-2	R-4
Rotor Leakage Permeance P_1	R-3	R-5
Curve for P_1	R-5	R-7
Rotor Leakage Permeance P_s	R-6	R-8
Rotor Leakage Permeance P_f	R-7	R-9
Curve for Leakage Permeance P_2	R-8	R-10
Rotor Leakage Permeance P_{s1}	R-9	R-11
Rotor Pole Tip Leakage	R-10	R-13
Rotor Leakage Permeance P_{s2}	R-11	R-14
Rotor Leakage Permeance P_3	R-12	R-15
Curve for P_3	R-13	R-16
Magnet Comparisons	R-14	R-20
Magnet Comparisons	R-15	R-21
Equivalent-Circuit Representation for Synchronous AC Generator Carrying a Balanced Load		S-33

	<u>Figure No.</u>	<u>Page No.</u>
Equivalent-Circuit Representation for Synchronous AC Generator Carrying a Balanced Load		S-35
Equivalent Circuit for Synchronous AC Generator Carrying an Unbalanced Load		S-73
Equivalent Circuit for Synchronous AC Generator Carrying an Unbalanced Load		S-74

TABLES

List of Cobalt Steels	Page A-111
Table of PM Steel Characteristics	Page A-113
Table of PM Steel Characteristics	Page A-114
Table of PM Steel Composition	Page A-115
Family Tree of Brushless AC Generators	Page B-4
Comparison Chart for Brushless AC Generators	Page B-4
Approx. Dimensions for Homopolar Inductors and for Outside-Coil Lundell AC Generators	Page B-6
Gas Bearings	Page E-7
Operating Requirements of Gas Bearing Types	Page E-8
Gas Lubricated Journal Bearing Family Tree	Page E-9
Gas Lubricated Thrust Bearing Family Tree	Page E-10
Required Design Information	Page E-11
Bearing Parameter for Maximum Load Capacity	Page E-41
Bearing Tolerance Ranges	Page E-42
Effects of Grooves in Gas Bearings	Page E-43

Alloy Classes Useful as Base Materials for Shaft and/or Bearings	Page E-76
Material Combinations that Have Been Used for Large Bearings	Page E-77
Bearing (Rolling Element) Life Dispersion Curve	Page E-82
Speed and Size of Light and Extra Light Superprecision Ball Bearings	Page E-84
Inner-Race RPM for Oil Jet or Oil-Mist Lubrication Extra Light Series Ball Bearings	Page E-85
Limiting Speeds for Grease Lubricated Ball Bearings	Page E-86
Temperature Limitation of Ball Bearings	Page E-87

INTRODUCTION

Most of the brushless, solid-pole a-c generators that are now considered new were used before 1900. The wound-pole a-c generators are circa 1900 though the accessory rectifiers that allow the wound-pole generators to be brushless were developed in the 1950's.

Though the brushless a-c generators are old as electrical devices are compared, the procedures for designing them are not widely understood and the design limits (or performance limits) of the machines are not well known. Because design procedures for these generators are considered proprietary when existent at all and because the performance limits of the generators are not well understood, impossible generator designs have sometimes been proposed.

With no way to evaluate proposed generator designs except by comparing them with other offerings proposed for the same application, purchasing agencies have been placed at a disadvantage, especially when the generators are for use in space applications.

The purpose of this investigation is to provide a means of selecting and evaluating generators for specific applications. Further aims of this investigation are to provide means of calculating generator performance, means of determining generator limitations, and a means of determining the effect of improved materials on the generator performance.

The investigators decided that the only satisfactory method of calculating generator performance would be to use a design manual programmed in Fortran computer language. Further, they decided that, in order to select the best generators for use in space and other environments, it would be necessary to write design manuals and computer programs for all of the generators that might logically be considered for space or severe environment applications. The design manuals and computer programs would then allow the users of the results of the study to evaluate designs for themselves and to verify or disprove the findings of the investigators.

Toward fulfilling the purposes and objectives of the investigation, the investigators have written ten (10) design manuals and nine (9) Fortran computer programs. To calculate operating temperatures of the generators, Mechanical Technology, Inc. of Latham, New York has

written in Fortran, for Lear Siegler, a thermal analysis program for small generators. The same company (MTI) has written for this study a discussion on gas bearings and a discussion of rotor dynamic characteristics.

The design manuals used in this report are based in part on work done by L. A. Kilgore, E. I. Pollard, and E. C. Barnes.⁽¹⁾

Source references are given on the design curves used in Section F and the Appendix to this report contains derivations for most of the formulas used in the design programs. We are indebted to J. N. Hibbard for the hand-calculation design manuals from which the manuals in this report evolved.⁽²⁾

The investigators believe that the design manuals presented here can be used to provide better communication between purchasing agencies and manufacturers.

(1) See Bibliography on Page A-124 at end of Section A.

(2) J. N. Hibbard also provided many of the derivations published in the appendix.

Section A



Section B



Section CA or Section C



Section D



Section E



Section F



Section GA or Section G



Section HA or Section H



Section JA or Section J



Section KA or Section K



Section LA or Section L



Section MA or Section M



Section N



Section PA or Section P



Section RA or Section R



Section SA or Section S

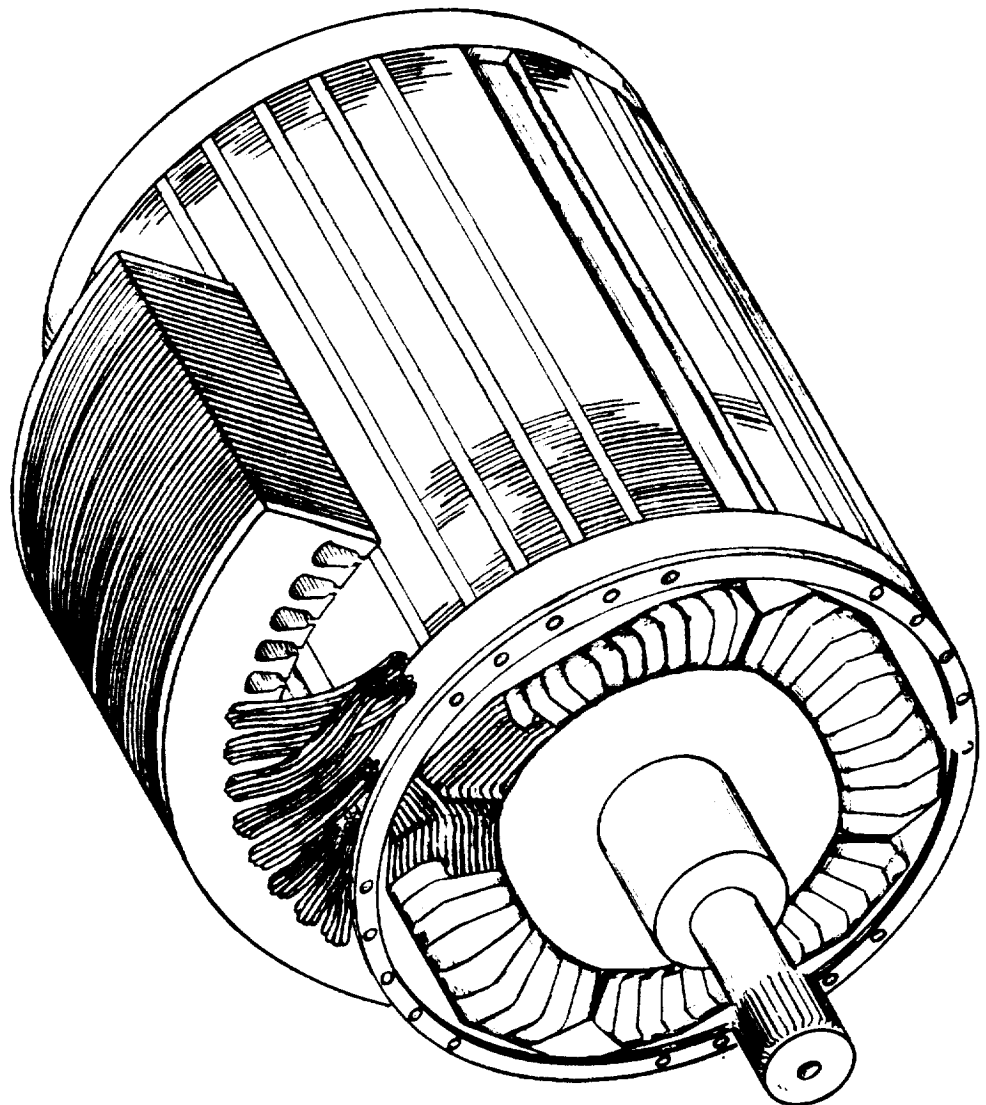


Section TA or Section T



DESCRIPTIONS AND SCHEMATICS
FOR THE GENERATORS TREATED
IN THE STUDY

THE WOUND-POLE, SALIENT-POLE, A-C
GENERATOR



THE WOUND-POLE, SALIENT-POLE, A.C. GENERATOR

The salient-pole, synchronous generator with wound poles is the standard generator of the electrical industry. It is the standard generator because it has the highest electrical output per pound per rpm of any practical generator yet known. Its reactances are the lowest of any of the generators which means that its regulation and performance under transient load conditions are the best of all the a.c. generators.

The wound-pole, salient-pole synchronous generator is used on both aircraft and utility systems almost to the exclusion of any other types except non-salient pole, wound rotor, generators (or turbine generators) which are used with 1800 rpm and 3600 rpm steam turbines in central station generating plants.

In addition to its use as an electrical generator, the salient-pole, wound-pole, machine makes the best synchronous motor known. The pole heads can be designed with cage windings so that the machine can start a substantial load as an induction motor. The cage windings can be made double to give good starting characteristics and good pull-in characteristics.

Within its usable range, the wound-pole synchronous generator has no equal, but its range of usefulness is limited. Its maximum rotor peripheral

speed is low because the field windings are supported by the poles and high stresses result from the centrifugal loading of the field coils. The maximum output frequency of the generator is low because the possible number of poles is restricted by electrical and mechanical limits imposed by the field windings, pole construction and the need for having at least one slot/phase/pole in the stator. Its maximum operating temperature is about 600° F for the copper and insulation on the rotor and 350° F for the rotating (silicon) rectifiers.

For extreme temperature, high radiation environments and for high peripheral speeds, the rotating-rectifier wound-pole, salient-pole generator is not usable and other more rugged generators are used. The more rugged generators are all heavier, on a KVA per revolution basis, than the wound-pole, salient-pole machines.

Although generators other than the wound-pole, salient-pole synchronous generator are now often used in both aerospace and ground power applications, it is well to remember that within its application range, no other type of a-c generator can compare with the wound-pole, salient-pole machine and it should be used whenever feasible.

**DISCUSSION OF THE
WOUND-POLE, SALIENT POLE A. C. GENERATOR**

THE WOUND-POLE, SALIENT-POLE, A-C
GENERATOR

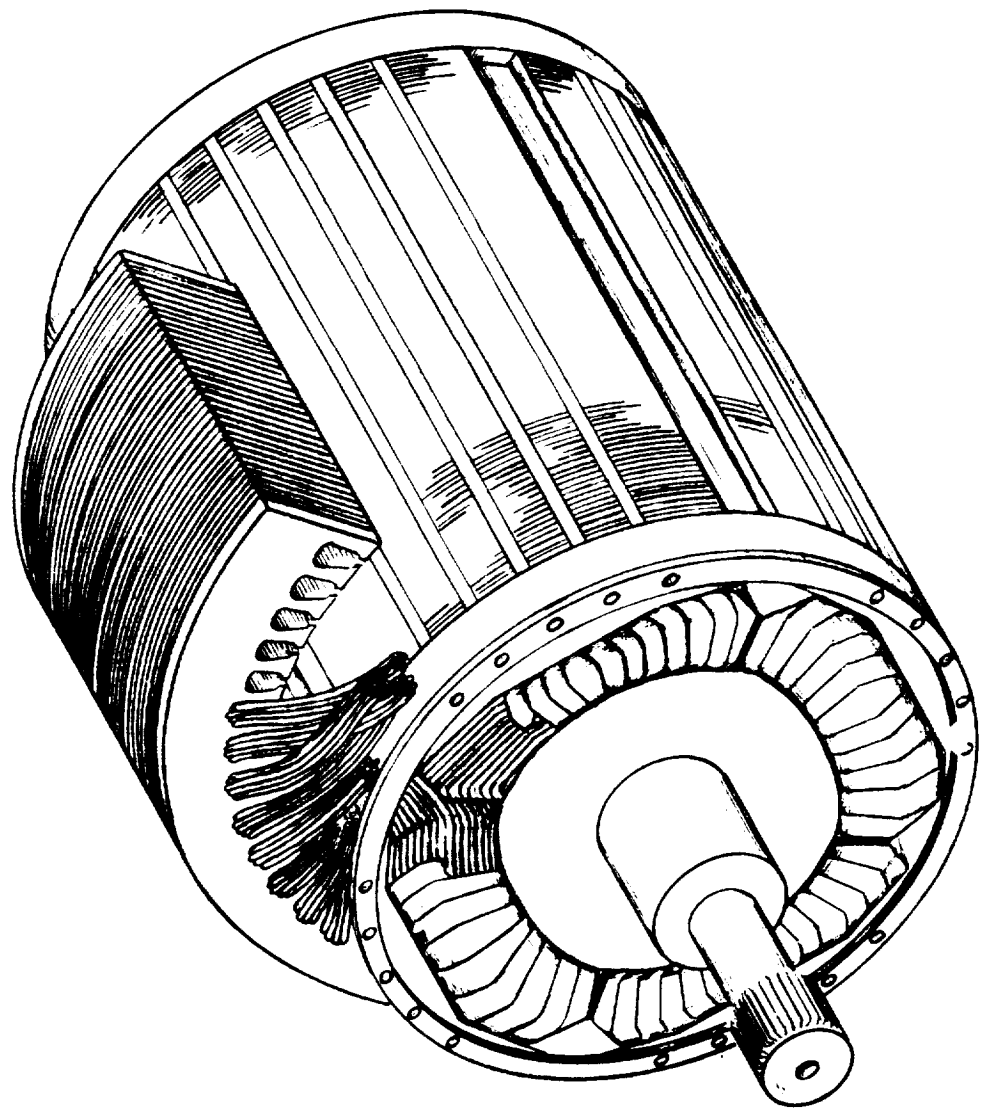
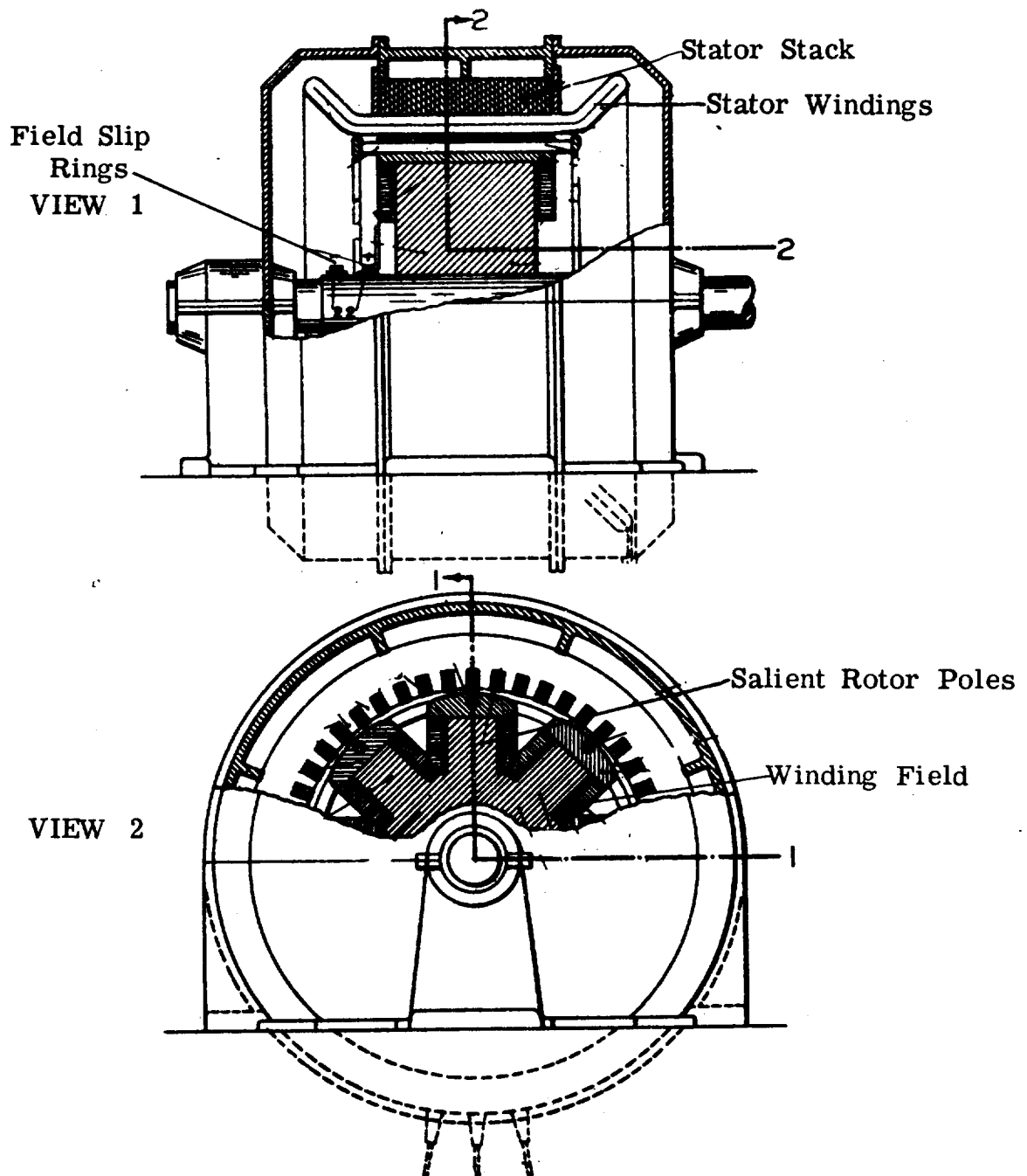


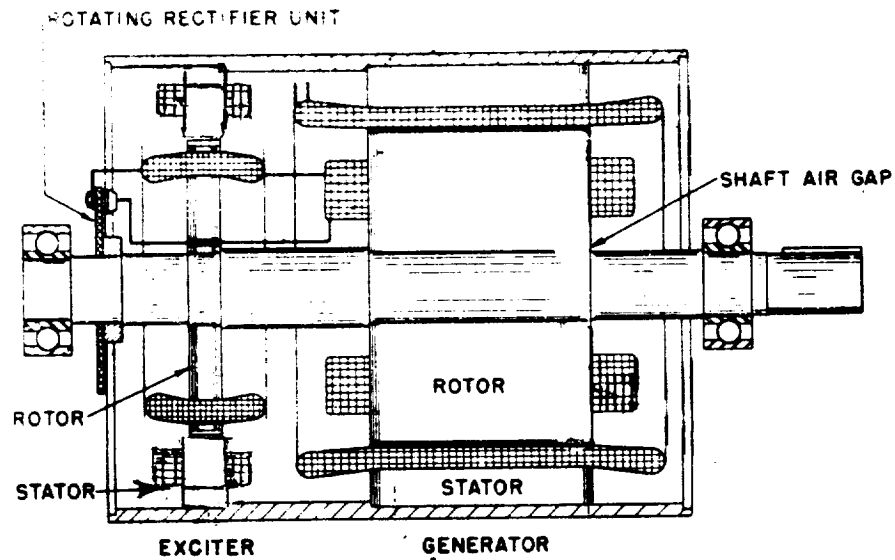
FIGURE A 1

A-1a



**TWO VIEWS OF A WOUND-POLE, SYNCHRONOUS
GENERATOR THAT USES SLIP-RINGS TO CONVEY
THE EXCITATION CURRENT TO THE FIELD WINDINGS**

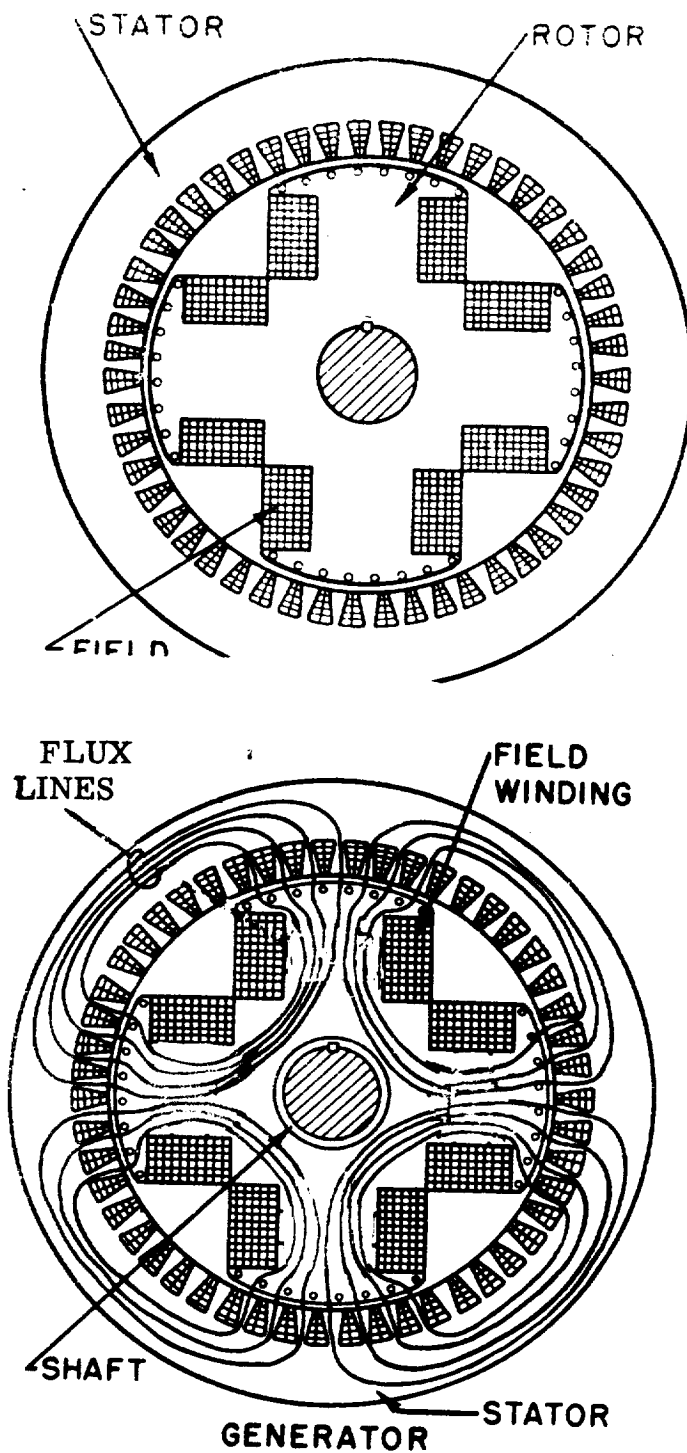
FIGURE A2



A-C Generator

SCHEMATIC SHOWING THE ARRANGEMENT USED TO MAKE THE WOUND-POLE GENERATORS BRUSHLESS. THE A-C CURRENT IN THE EXCITER ROTOR IS RECTIFIED BY THE ROTATING RECTIFIERS AND THE D-C OUTPUT OF THE RECTIFIERS IS FED INTO THE MAIN GENERATOR FIELD WINDINGS

FIGURE A 3



SECTION VIEWS OF A WOUND-POLE, SYNCHRONOUS GENERATOR SHOWING THE ARRANGEMENT OF THE WINDINGS AND THE PATH OF THE MAGNETIC FLUX

FIGURE A 4

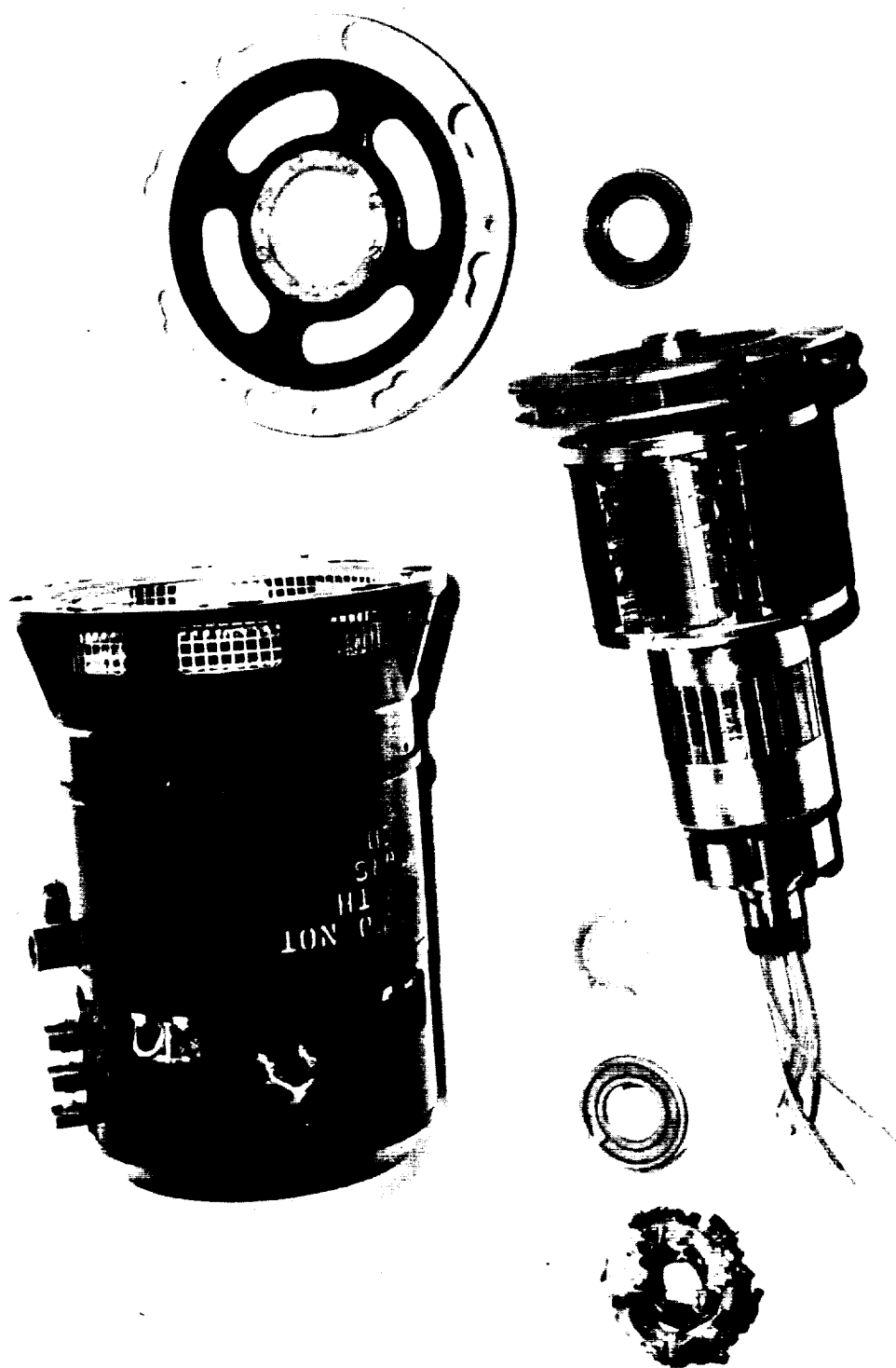


FIGURE A5

ROTATING RECTIFIER GEN.

DISCUSSION OF THE
WOUND-POLE, NON-SALIENT POLE A. C. GENERATOR

WOUND-POLE, NON-SALIENT-POLE A. C. GENERATOR

The non-salient pole or round-rotor a. c. generator is widely used in central station power plants where the generator is coupled to a steam turbine and operated at 1800 rpm or 3600 rpm. Because its pole windings are contained in slots in the rotor, this generator is capable of higher peripheral speeds than are possible with the salient pole wound-pole generator.

A round-rotor, inner-cooled generator producing 460,000 KVA at 19 KV was delivered on 1963 to the Texas Electric Service Company for use at Fort Worth, Texas. This is a 3600 rpm generator that will produce 506,000 KVA continuously at 60 PSI cooling hydrogen pressure. This Texas machine probably is close to the practical physical limit for its speed and type, using today's materials and technology.

Several 8000 rpm and 12000 rpm generators have been built as non-salient, wound-rotor machines for aircraft and auxiliary power where wound-pole salient-pole generators could not be used for the ratings and speeds desired.

When two-pole, wound-pole generators are built, they are usually non-salient pole machines because the rotor construction of the non-salient

generator is stronger and more practical than that of a two-pole, salient-pole generator.

The wound-rotor, non-salient pole is the best electrical generator to use in mild environments when the peripheral speeds are too high for the salient-pole wound-pole generator, but not so high that the rotor winding creeps and allows the rotor to change balance.

A section of a two-pole, non-salient-pole rotor without its field winding and a field form of a similar rotor.

The field form was made with an oscillograph and a search coil. The rotor represented by the record had the same number of rotor slots as the section shown.

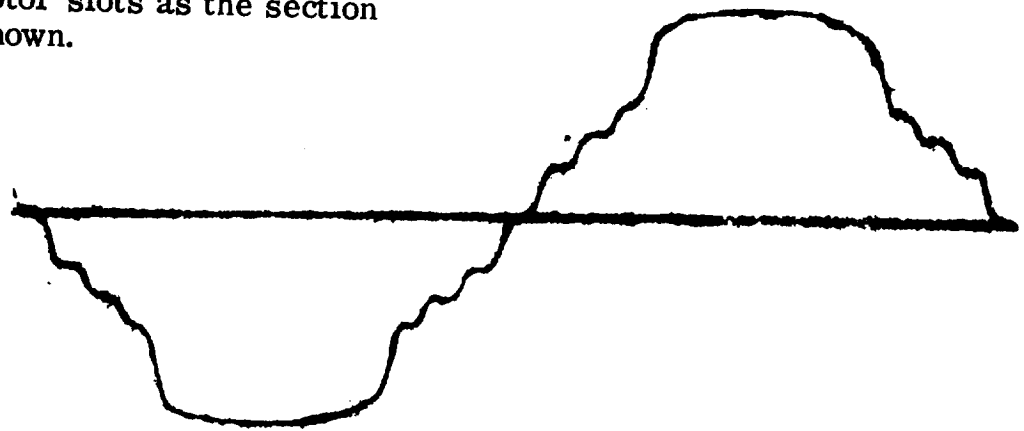
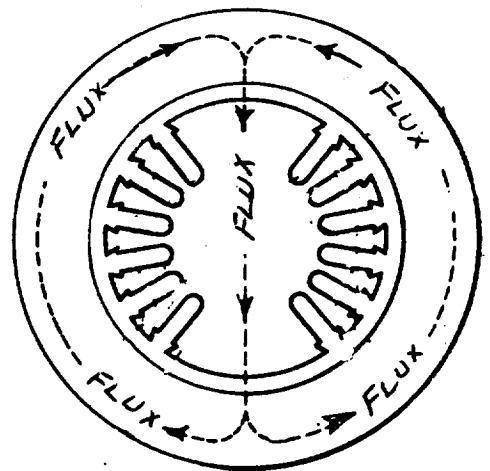
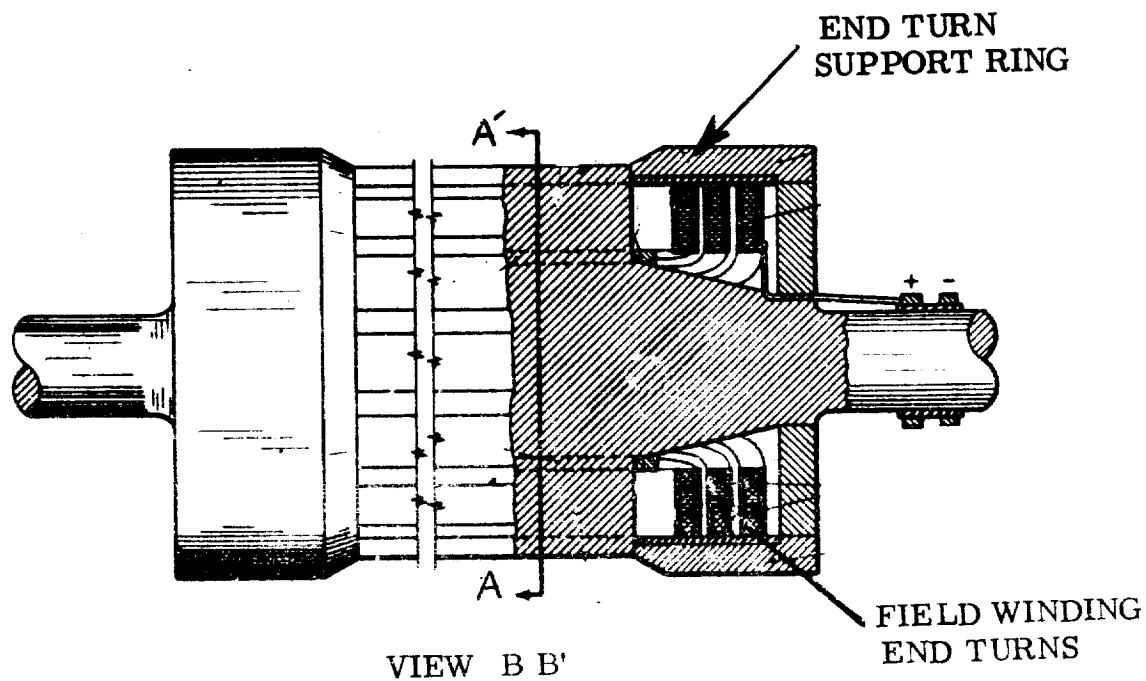
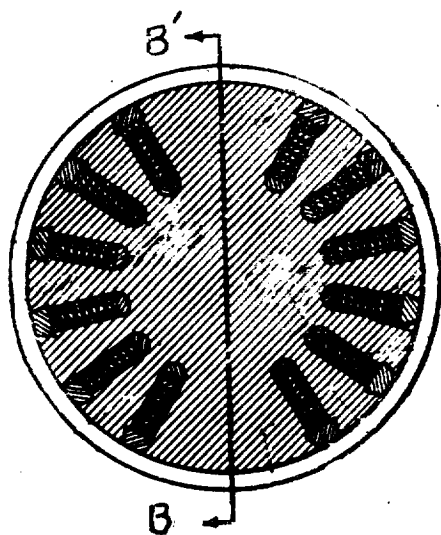


FIGURE A6

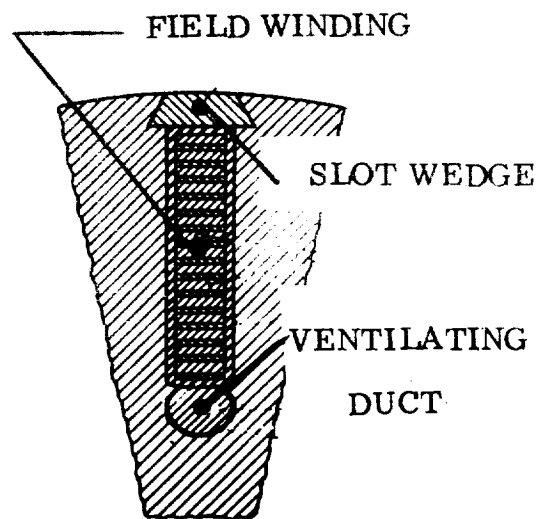


ROTOR OF NON-SALIENT-POLE
SYNCHRONOUS A-C GENERATOR



SECTION A A'

CROSS-SECTION OF ROTOR



SECTION VIEW OF SLOT
AND FIELD WINDING

FIGURE A7

PARTIALLY COMPLETED ROTOR AND STATOR OF A 125 KVA
NON-SALIENT POLE, OR ROUND-ROTOR A-C GENERATOR
4 POLES, 12000 RPM

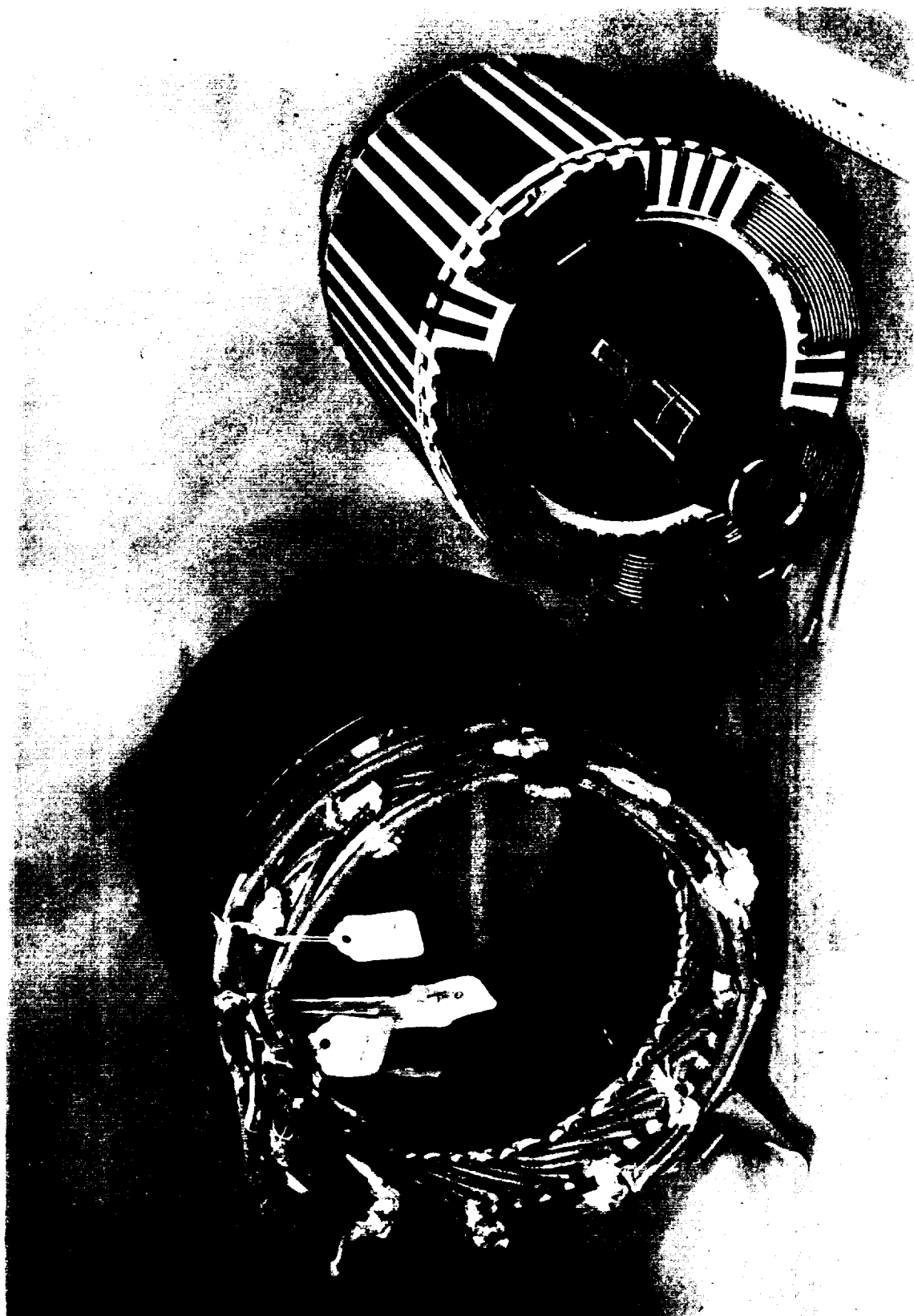
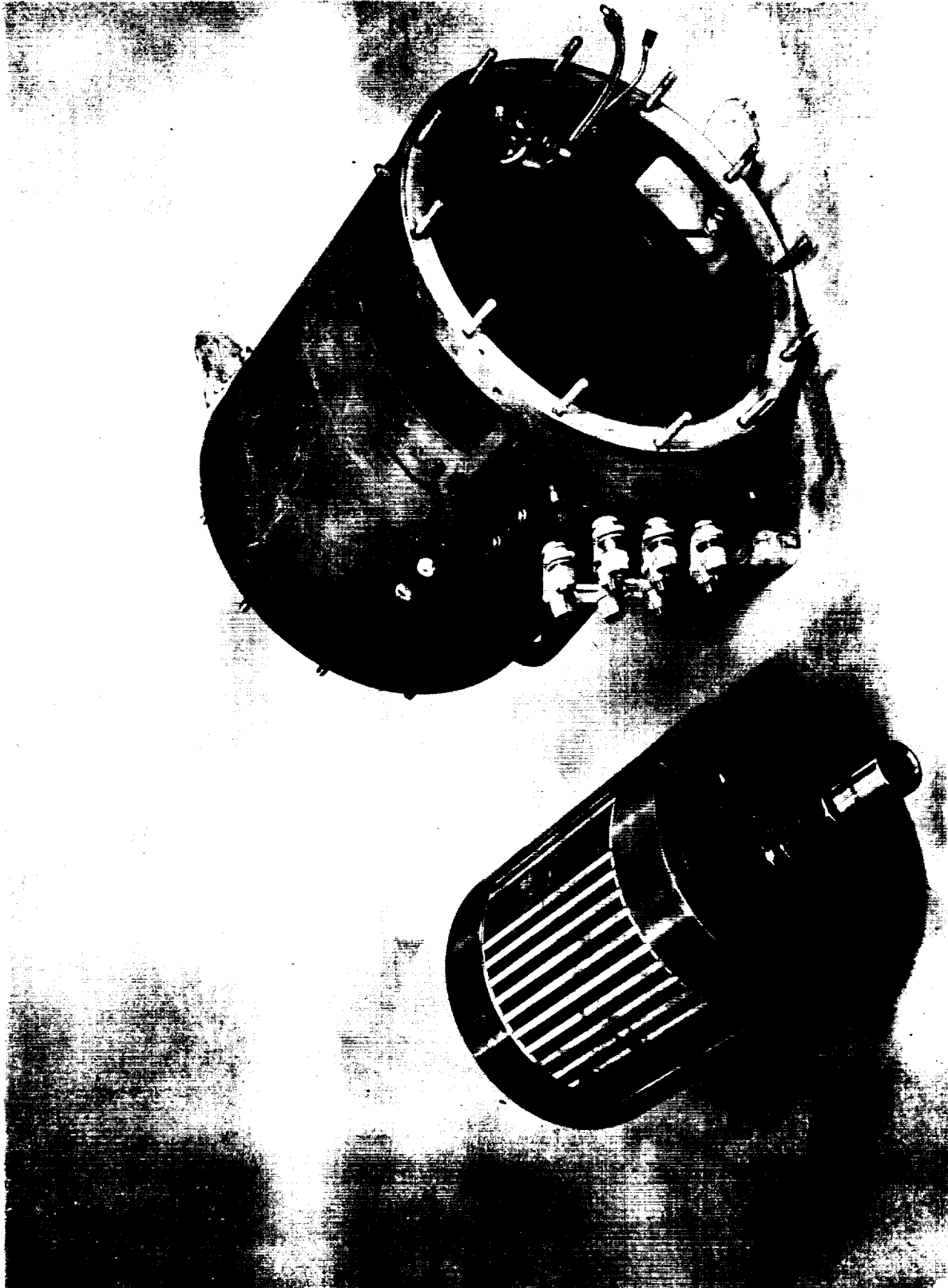


FIGURE A8

**COMPLETED ROTOR AND STATOR FOR A 125 KVA,
NON-SALIENT POLE, OR ROUND-ROTOR A-C GENERATOR
4 POLES, 12000 RPM**



EXPLODED VIEW OF A 125 KVA, ROUND-ROTOR OR NON-SALIENT POLE, A-C GENERATOR. SPEED 12000 RPM, FREQUENCY 400 CPS, POLES 4, WEIGHT 175 LBS.

MEETS REQUIREMENTS
OF MIL-C-6099 A

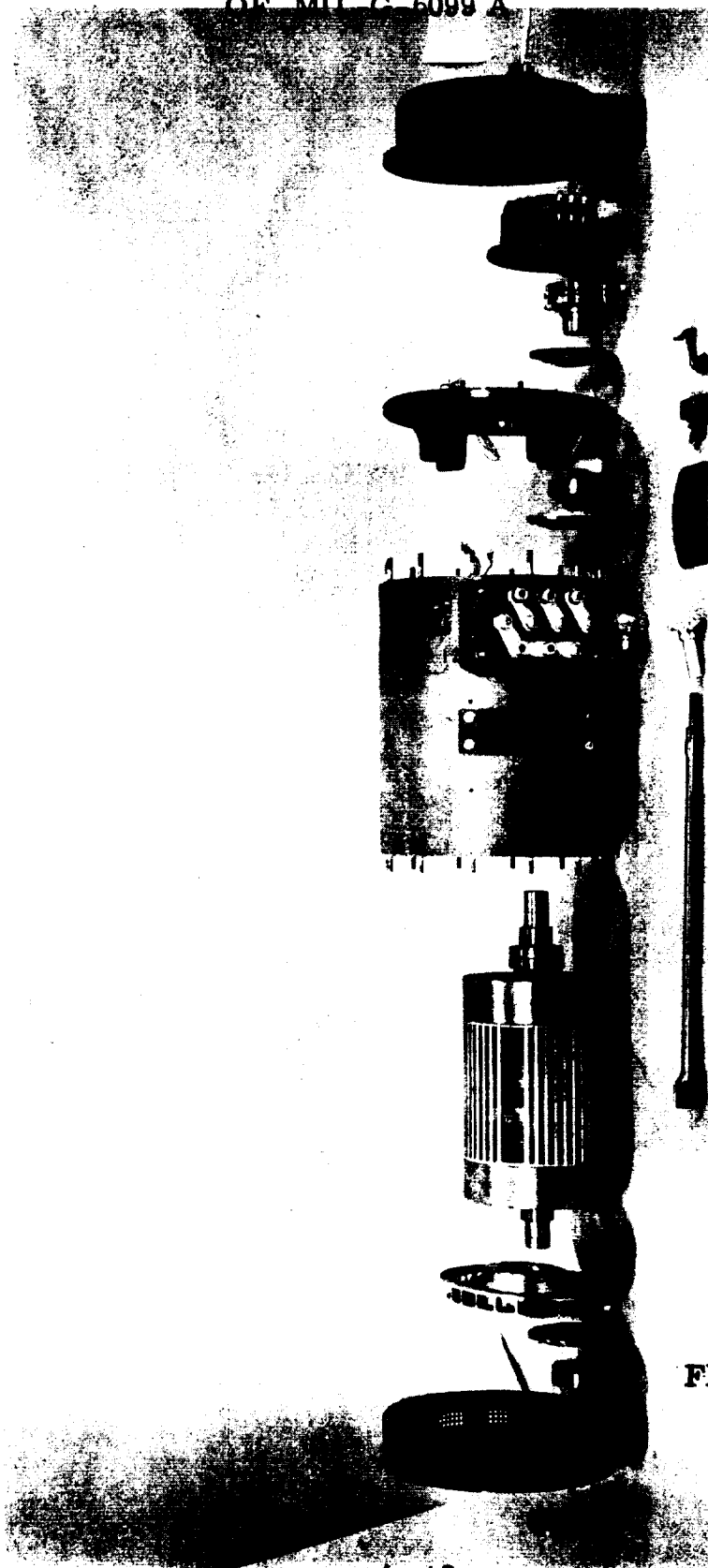
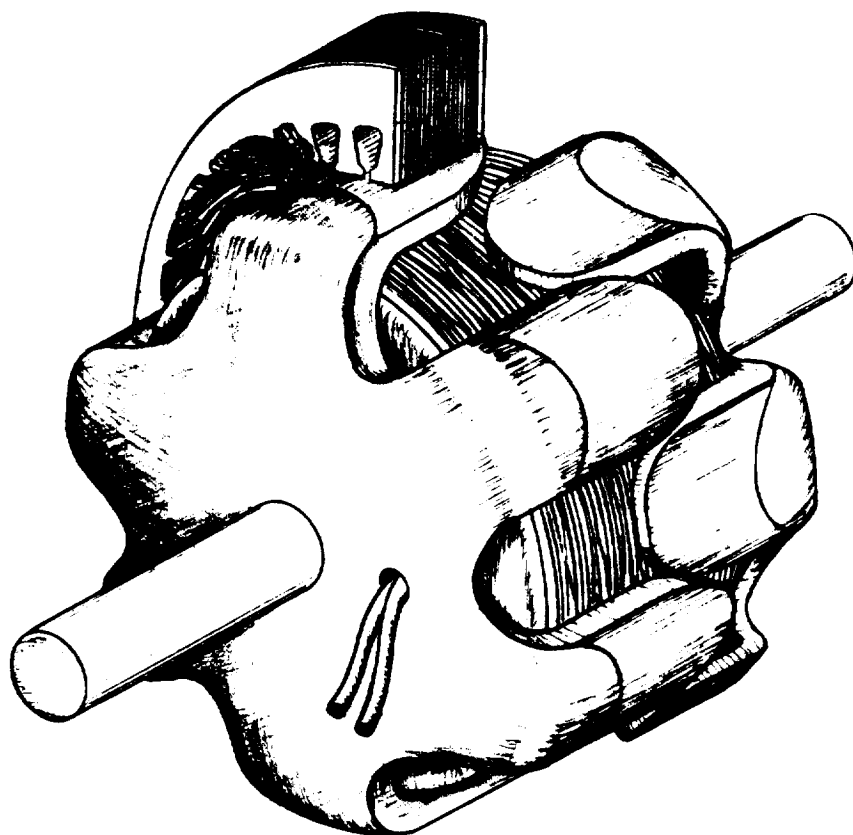


FIGURE A 10

**DISCUSSION OF THE
ROTATING COIL
LUNDELL TYPE A. C. GENERATOR**



ROTATING COIL
LUNDELL A-C GENERATOR

FIGURE A 11

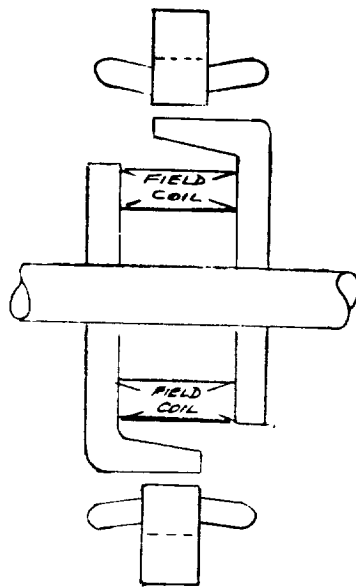
INSIDE-COIL, ROTATING-COIL LUNDELL A.C. GENERATOR

The Lundell generator with a rotating excitation coil is the a. c. generator that has been used for years on automobiles, trucks and busses. To make this generator brushless, an exciter and rotating rectifiers must be used.

The rotating-coil Lundell a. c. generator is limited to the same temperatures and radiation environments that the wound-pole generators are capable of withstanding. It is of interest in this study because it is a basic generator type and can be considered a transition step or link between the so-called solid-rotor brushless generators and the wound-pole, rotating-rectifier, brushless generators.

The following discussion will help the reader to understand the basic similarities and differences of various machine types in this report. By showing how one type of machine can be transformed to another type, the reader can see the electromagnetic relationships existing among these machine types. An understanding of these relationships may make it easier for the reader to follow the analytical steps described in the design manuals.

To show how the rotating-coil Lundell a. c. generator can be made into an outside-coil brushless a. c. generator, take the basic generator below:



STEP 1

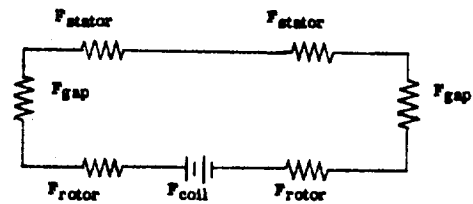
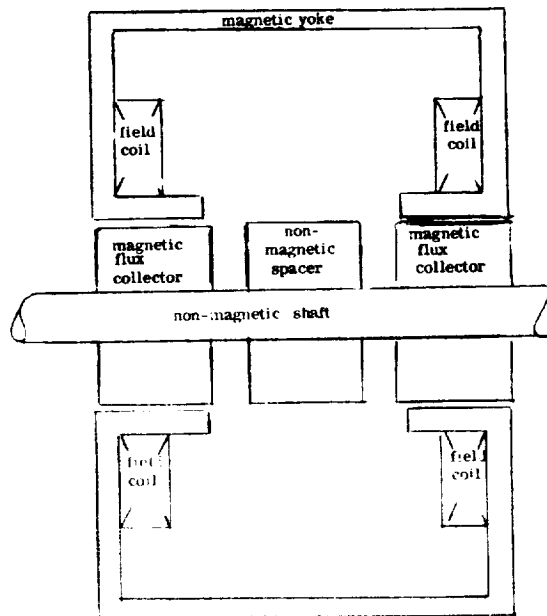


FIGURE A 12

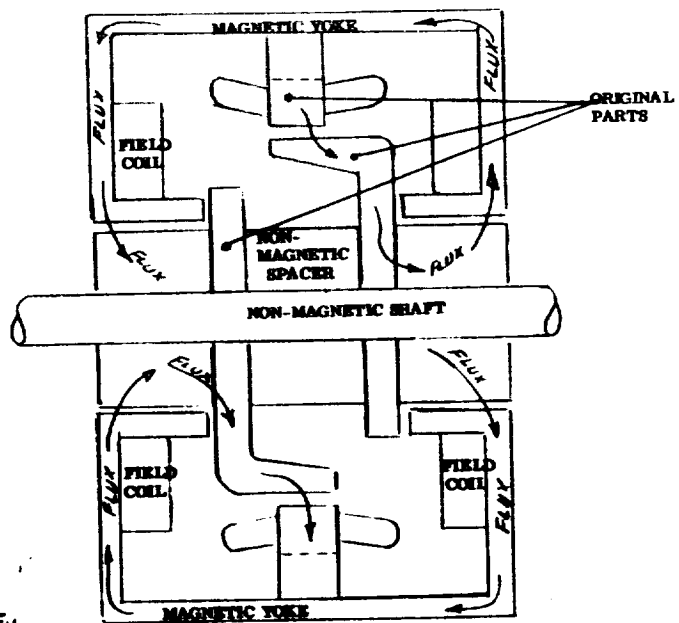
REMOVE THE
FIELD COIL
AND ADD
THESE PARTS

TO MAKE THE
GENERATOR
SHOWN BELOW
AS STEP 3



STEP 2

THE RESULT IS
A TWO-COIL,
OUTSIDE-COIL
BRUSHLESS,
LUNDELL, A-C
GENERATOR
SIMILAR TO THAT
PATENTED BY
L. C. RICE IN
1897.



STEP 3

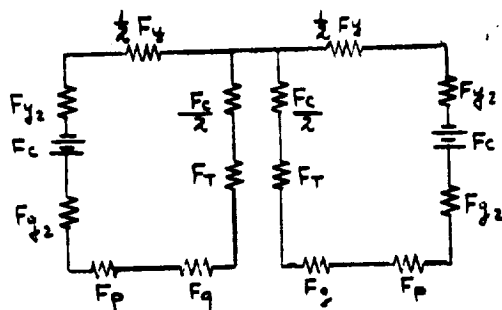
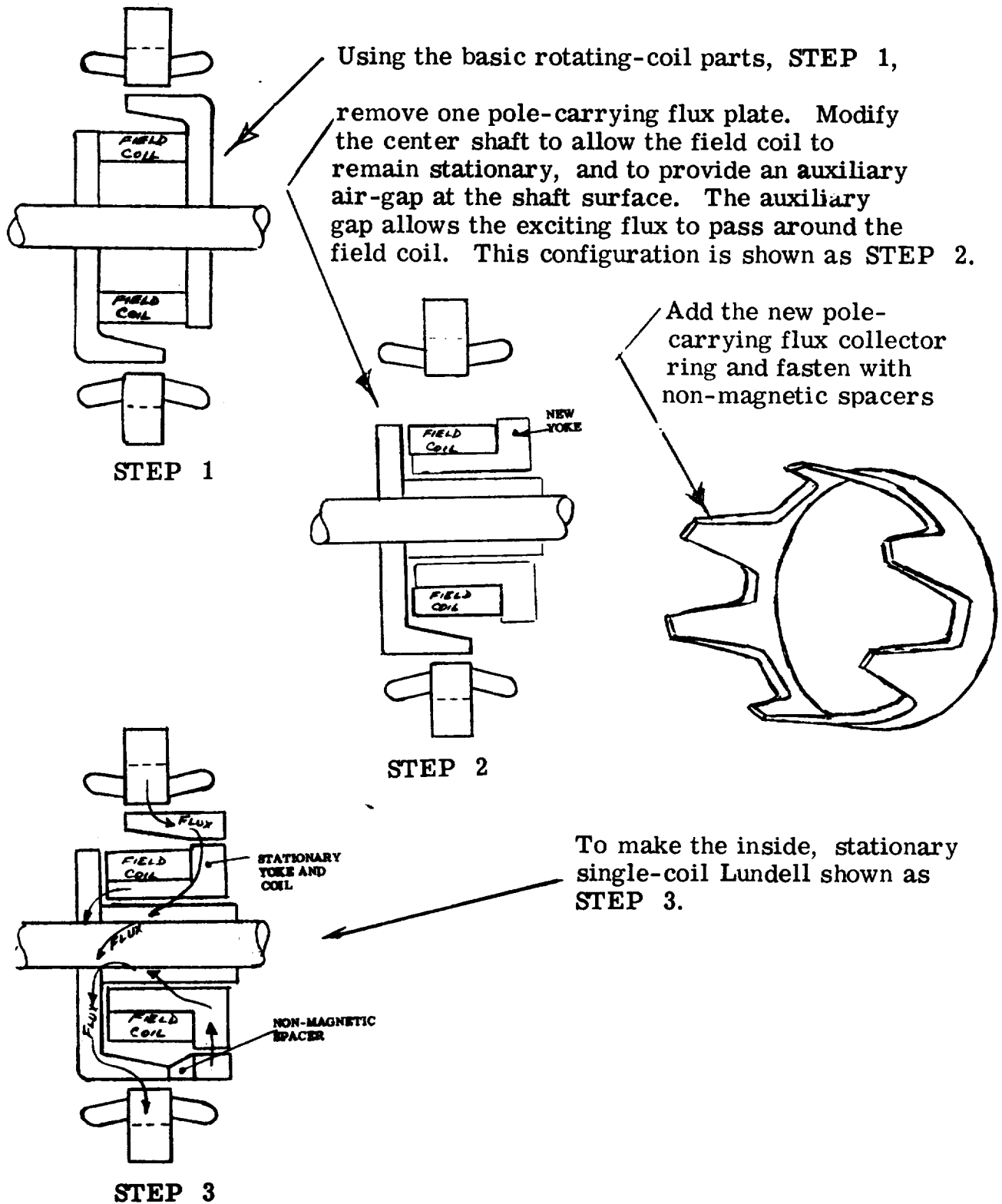


FIGURE A 13

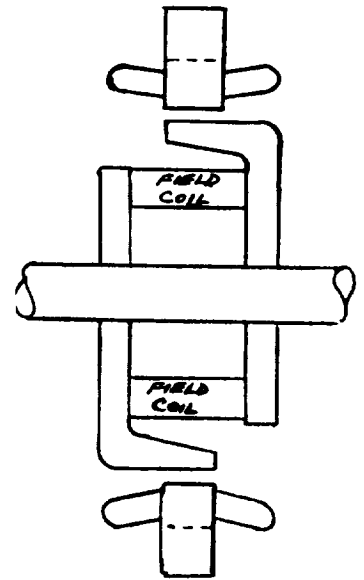


Use two of the inside, single, stationary-coil generators back-to-back to make a two, inside, stationary-coil Lundell a-c generator (Becky-Robinson).

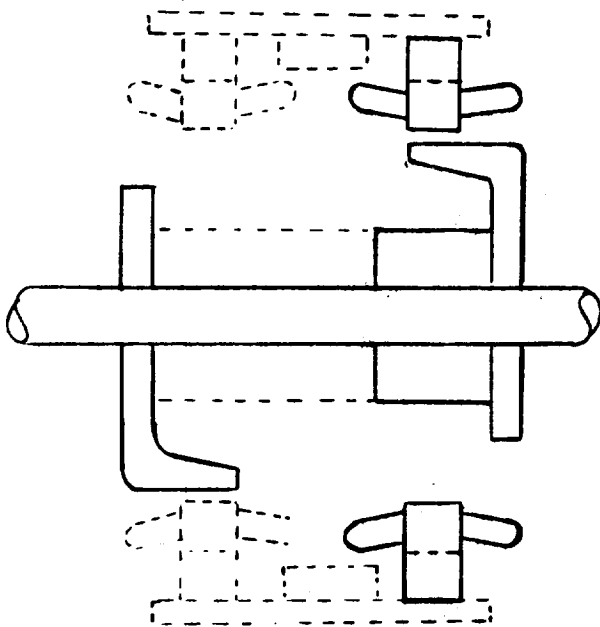


TO MAKE A HOMOPOLAR GENERATOR

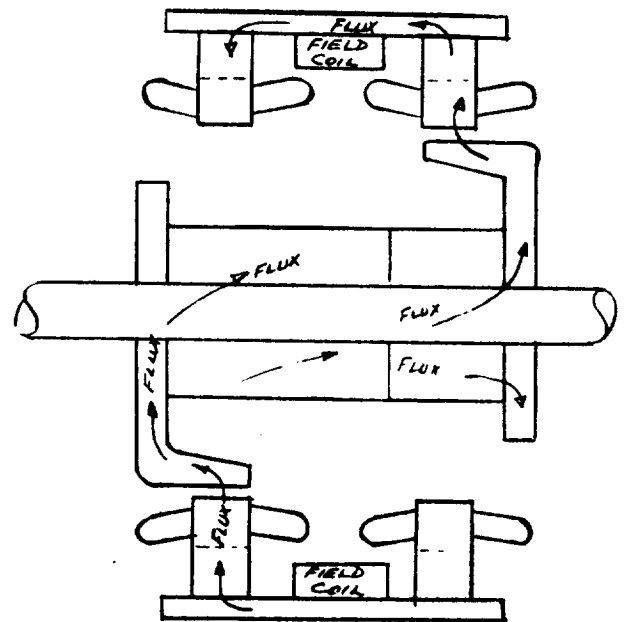
Use the basic rotating coil parts, step 1.
Remove the field coil. Separate the rotor parts as shown in step 2, and add the parts shown in phantom to make the complete homopolar inductor shown in step 3.



STEP 1



STEP 2



STEP 3

FIGURE A 16

PATENT DRAWING FOR A
ROTATING COIL
LUNDELL A. C. GENERATOR

March 4, 1952

S. F. STEWART ET AL
INDUCTOR ALTERNATOR

2,588,175

Filed Sept. 23, 1950

2 SHEETS—SHEET 1

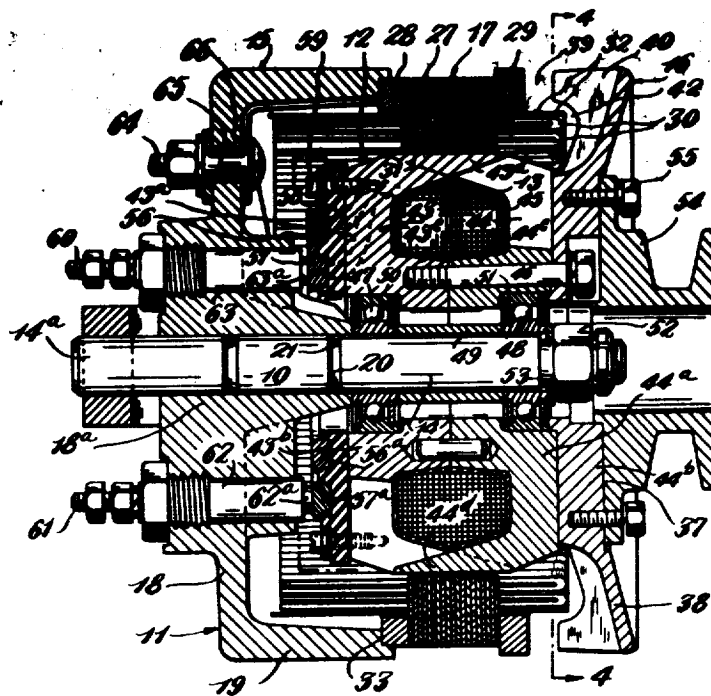


FIG. 2

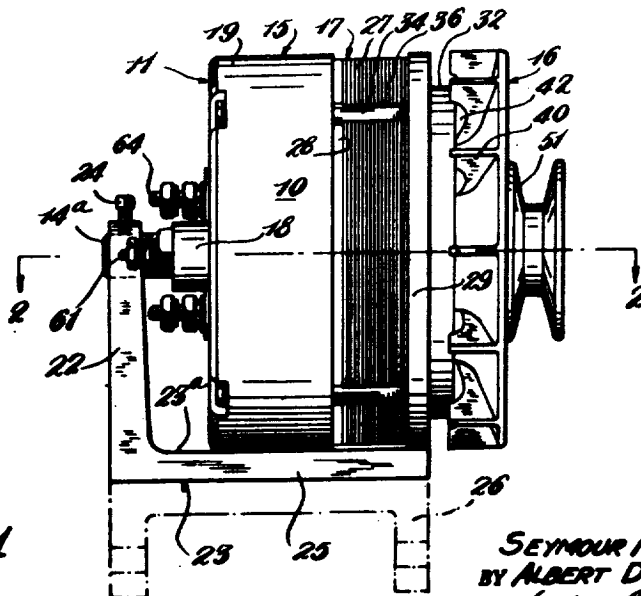


FIG. 1

INVENTORS
SEYMOUR FLOYD STEWART
BY ALBERT D. GILCHRIST
Hyden, Baughman,
Williams, David & Hoffmann,
ATTORNEYS

FIGURE A 17

ROTATING COIL A. C. LUNDELL
A. C. GENERATOR

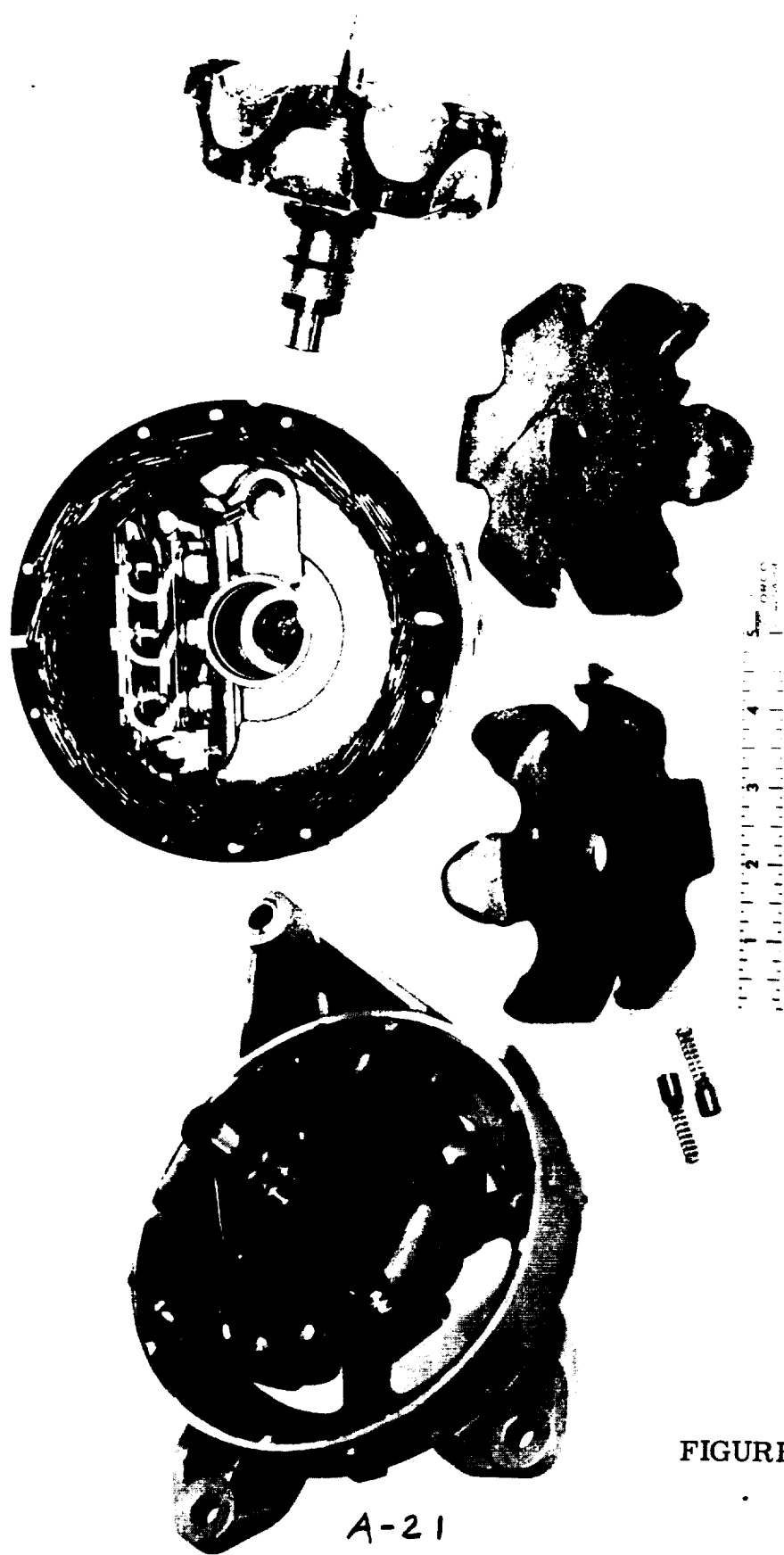


FIGURE A 18

ROTOR FROM ROTATING COIL
(AUTOMOTIVE TYPE) LUNDELL
A. C. GENERATOR

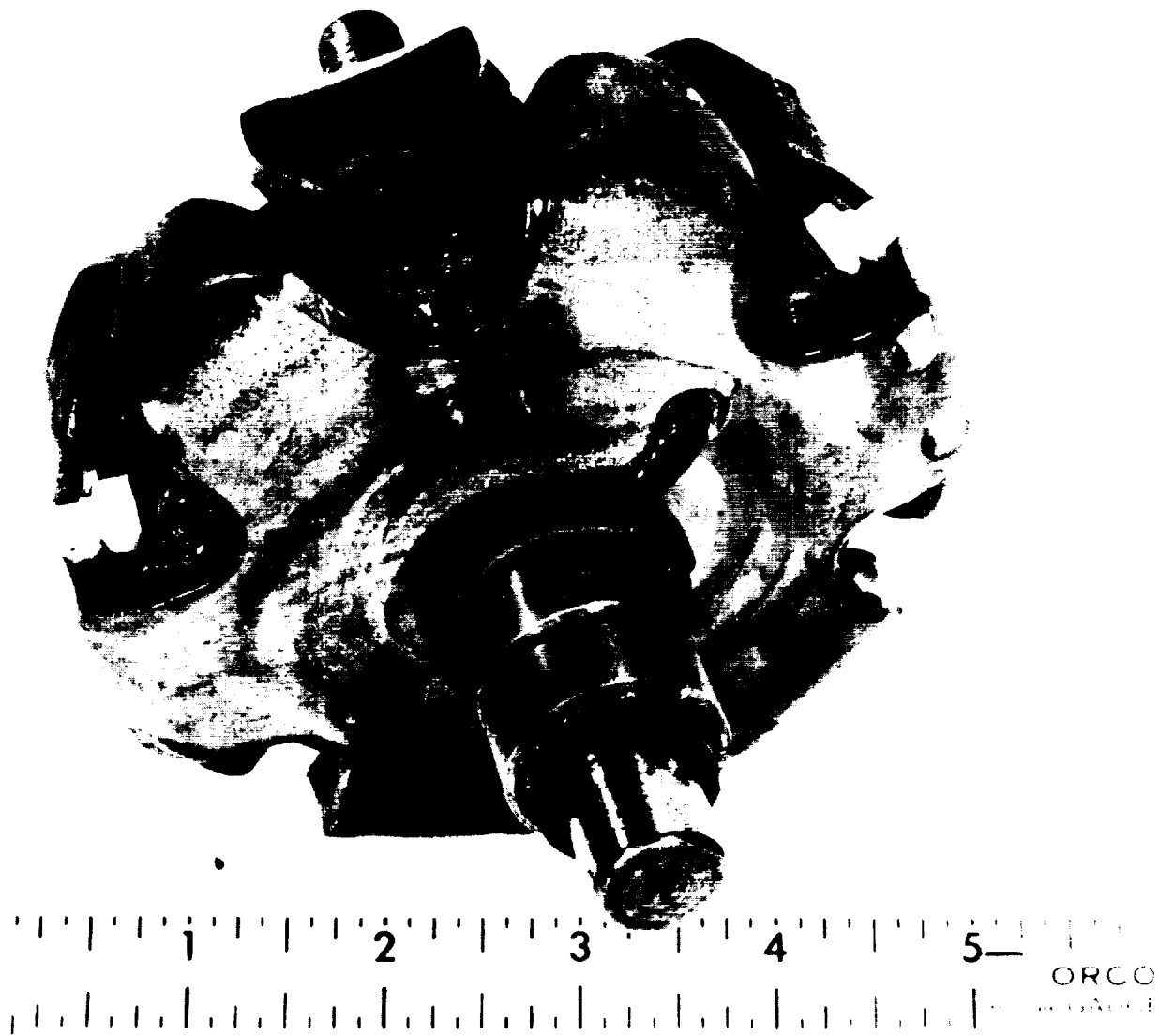


FIGURE A 19

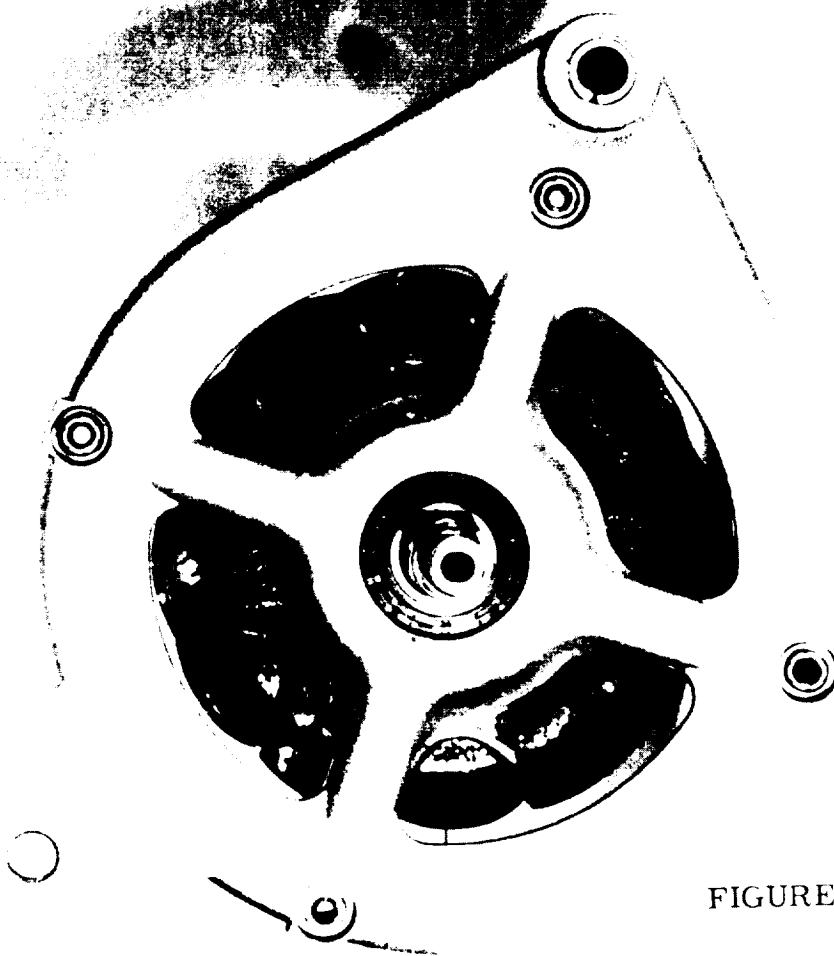


FIGURE A 20

STATOR OF ROTATING COIL
LUNDELL A. C. GENERATOR

**DISCUSSION OF THE
SINGLE INSIDE COIL
STATIONARY COIL
LUNDELL A. C. GENERATOR**

A SINGLE, INSIDE, STATIONARY-COIL, LUNDELL, A-C GENERATOR

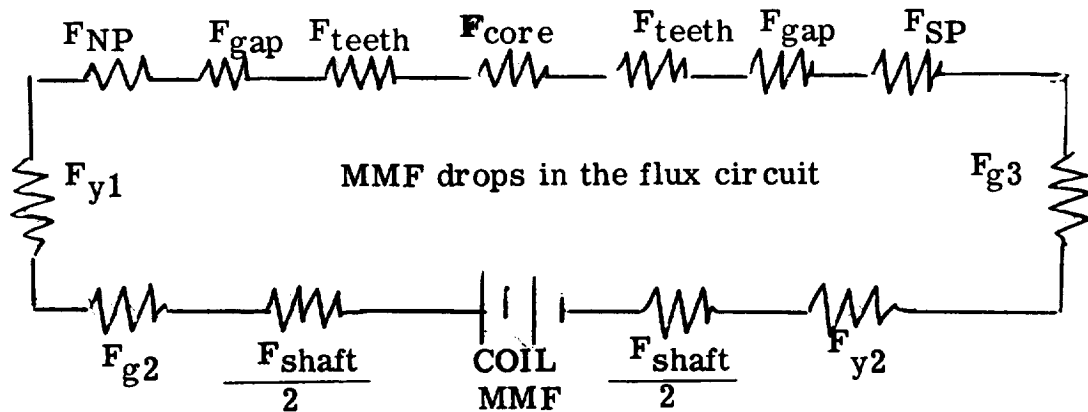
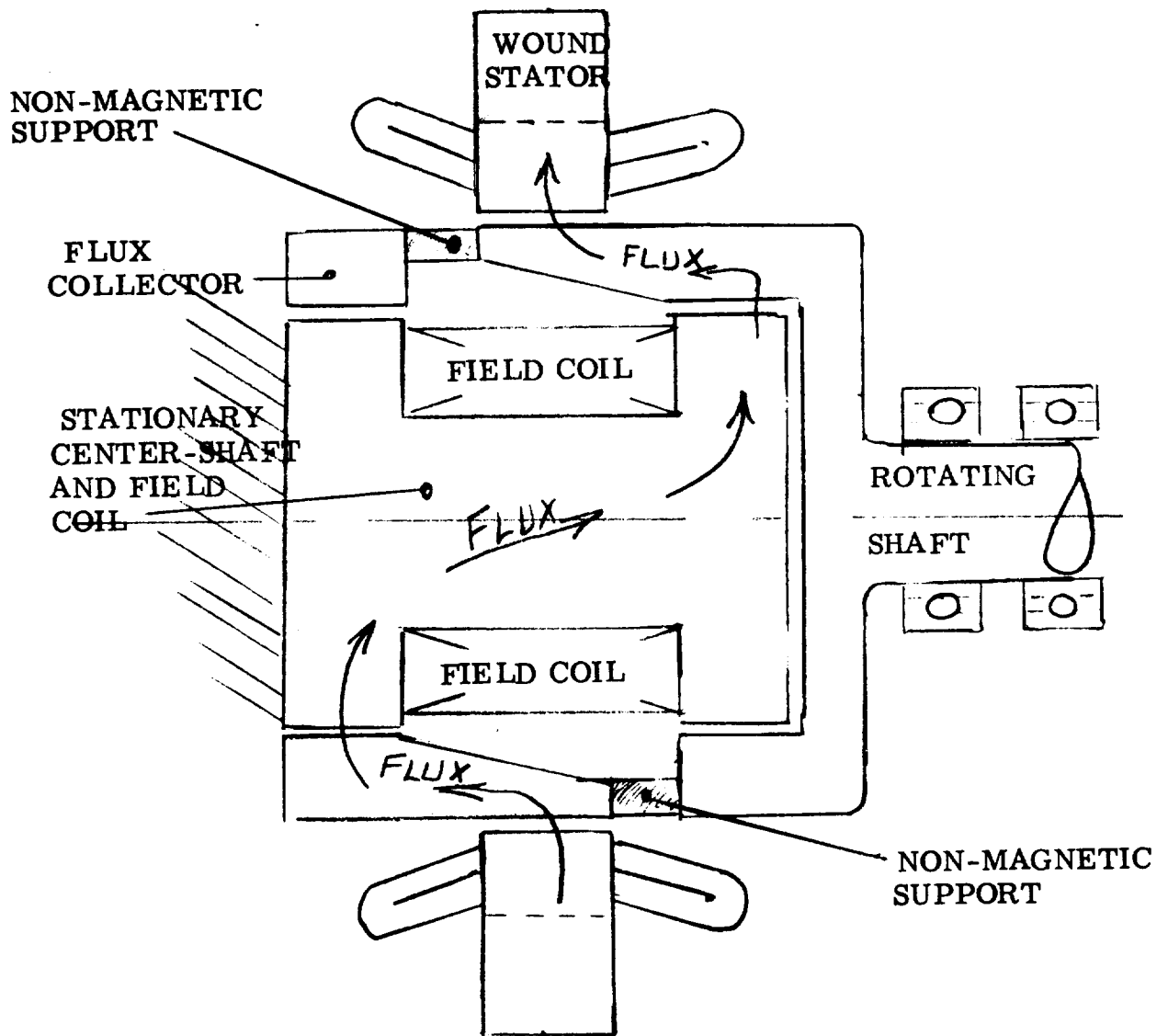


FIGURE A 21

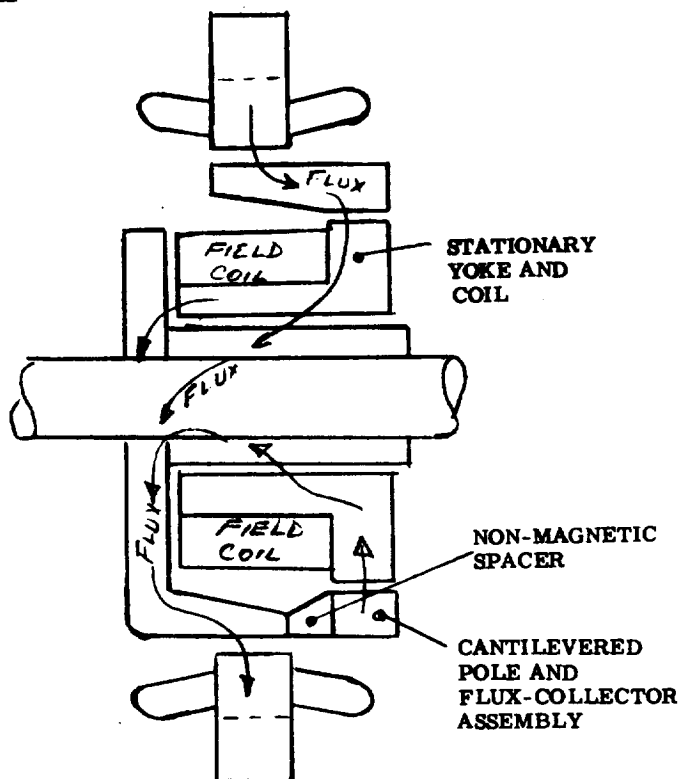
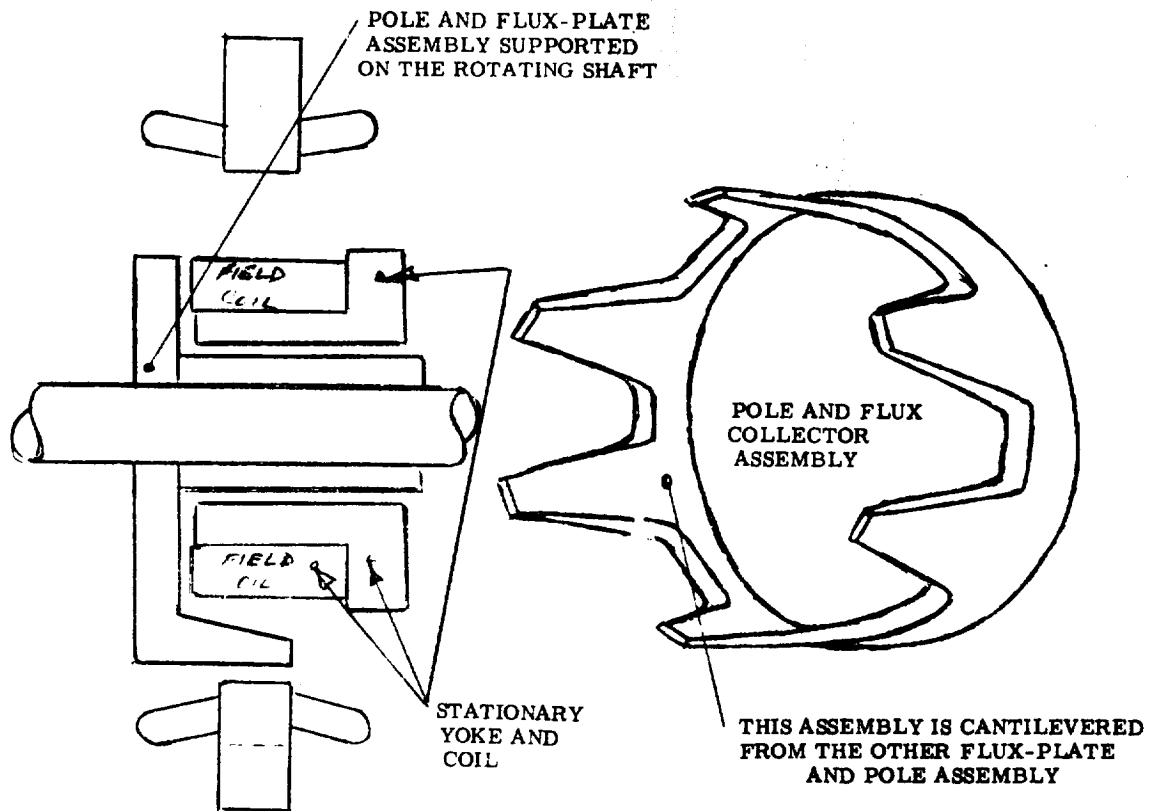
SINGLE, STATIONARY, INSIDE-COIL LUNDELL GENERATOR

This brushless generator is similar to the rotating-coil Lundell except that it has two auxiliary air-gaps and the excitation coil remains stationary. A flux carrying member rotates above the auxiliary air gap.

The single, stationary, inside-coil Lundell has been made in this country for several years. Its application has been on trucks, busses and other heavy vehicles requiring a husky, low maintenance electrical power supply.

In the description of the rotating coil Lundell generator, you are shown the steps required to make a rotating coil generator into the stationary-coil type of AC generator. By using two of these single, stationary-coil generators back-to-back, we can make a two, inside, stationary-coil Lundell or Becky-Robinson generator. These demonstrations show the close relationship of all of the Lundell-type generators.

The sketches immediately following show the generator without the overhung pole and flux collector assembly attached. Another accompanying sketch shows the completely assembled electromagnetic parts for a

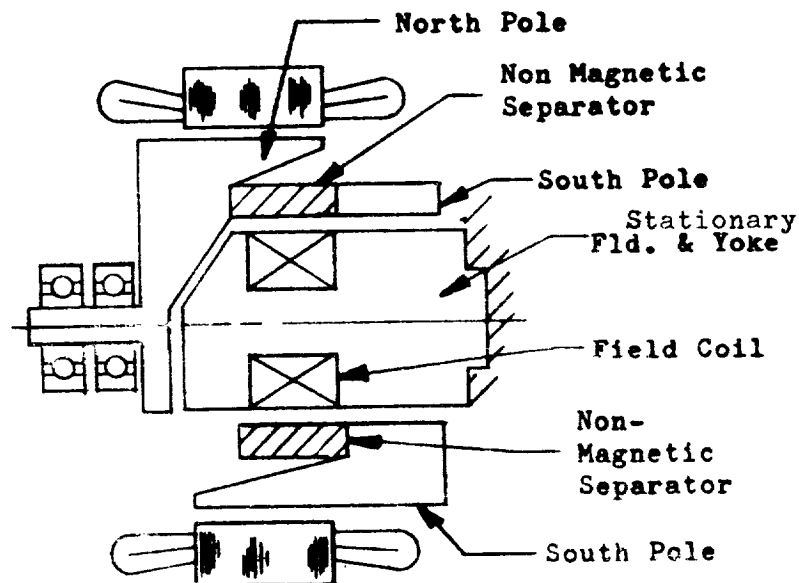


THE GENERATOR SHOWN HERE ABOVE HAS BEARINGS AT EACH END OF THE ROTOR AND THE YOKE AND COIL MUST BE SUPPORTED FROM THE HOUSING OR END-BELL

FIGURE A 22

stationary, single, inside-coil generator with bearings at each end of the rotor.

FIGURE A 23



The generator configuration shown above has a coil support cantilevered from the housing and the rotating structure is overhung. The configuration with bearings at each end of the rotor and the one with the overhung rotor are electrically and magnetically equal. The requirements of a specific application might dictate which type is to be used.

This brushless generator can operate successfully at temperatures above the capability of the wound-pole generators. There are no rotating semi-conductors and the stationary excitation coil is not subjected to stress.

The rotational speed is limited by the stresses in the cantilevered pole structure and vibration limits for this generator are lower than those for some of the other generators.

See the comparison table in the selection criteria for environmental and mechanical limits.

Feb. 19, 1963

R. H. BERTSCHE, JR., ETAL

3,078,409

ELECTRICAL POWER CONVERTER

Filed Feb. 26, 1959

6 Sheets-Sheet 4

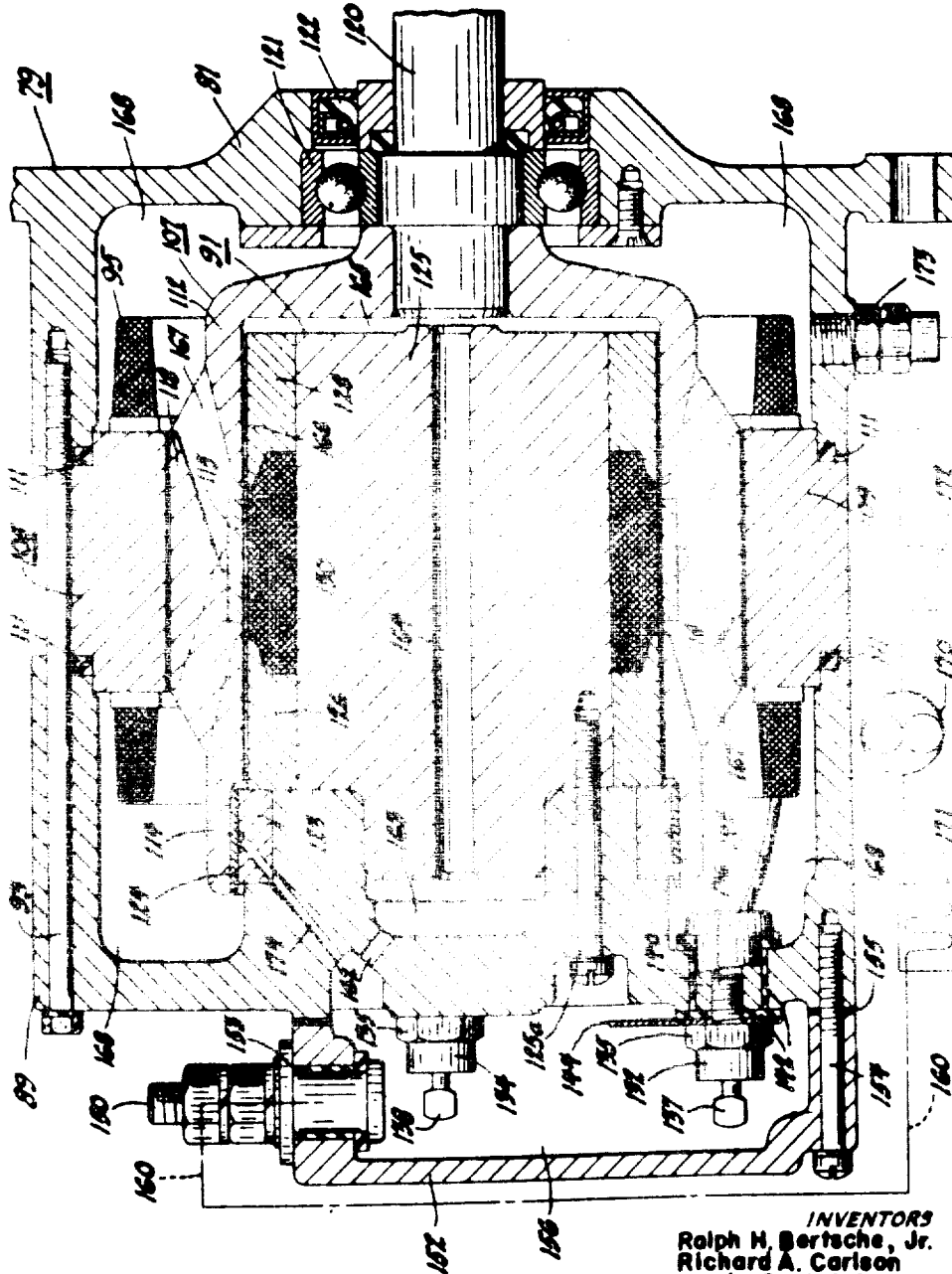
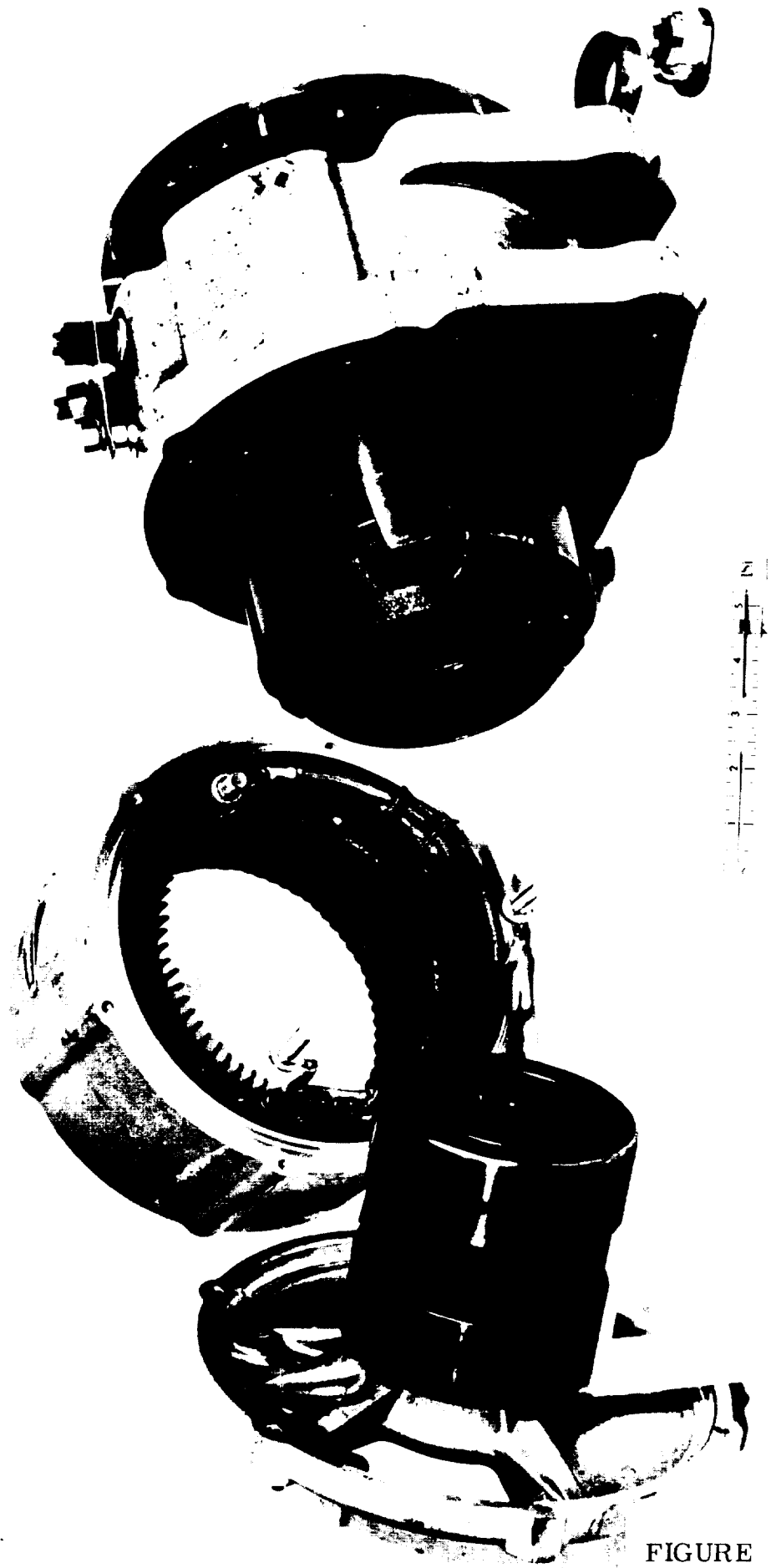


Fig. 6

INVENTORS
Rolph H. Bertsche, Jr.
Richard A. Carlson
Lewis R. Metzler
Louis J. Raver
BY *John T. Mann*
THEIR ATTORNEY

FIGURE A 24

PATENT DRAWING FOR
INSIDE STATIONARY COIL, LUNDELL
A. C. GENERATOR



AN INSIDE STATIONARY COIL
LUNDELL, A. C. GENERATOR

FIGURE A 24 a

ROTOR PARTS FOR AN INSIDE, STATIONARY, SINGLE-
COIL LUNDELL GENERATOR--SHOWN WITH AN INDUCTION
MOTOR ROTOR AND COMMON SHAFT

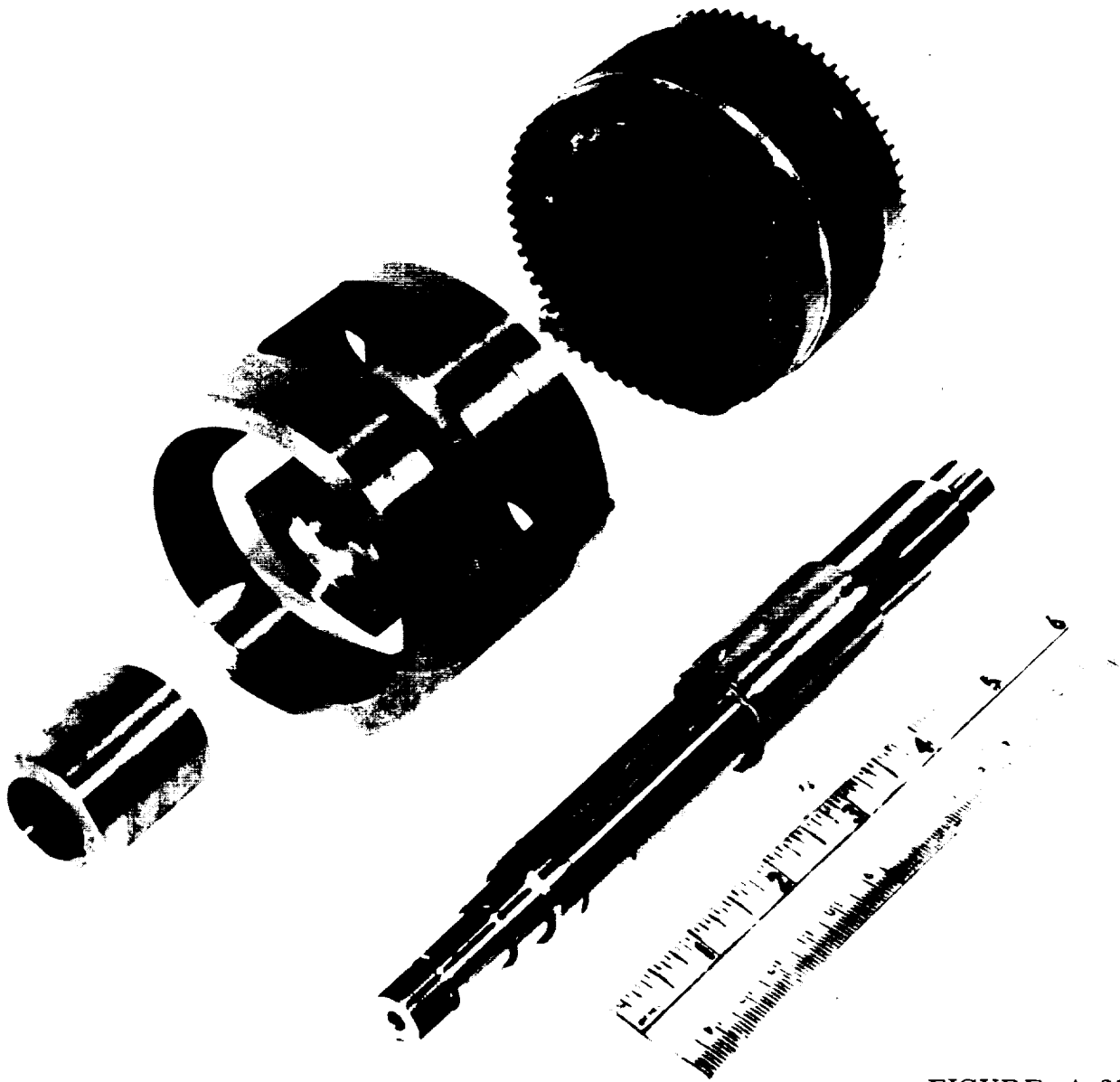


FIGURE A 25

EXPLODED VIEW OF AN INSIDE, STATIONARY, SINGLE-
COIL LUNDELL GENERATOR---INDUCTION MOTOR, M-G
SET.



FIGURE A 26

DISCUSSION OF THE
INSIDE STATIONARY TWO-COIL
LUNDELL A. C. GENERATOR
(BECKY-ROBINSON)

INSIDE-COIL, STATIONARY, TWO-COIL
LUNDELL A. C. GENERATOR (BECKY-ROBINSON)

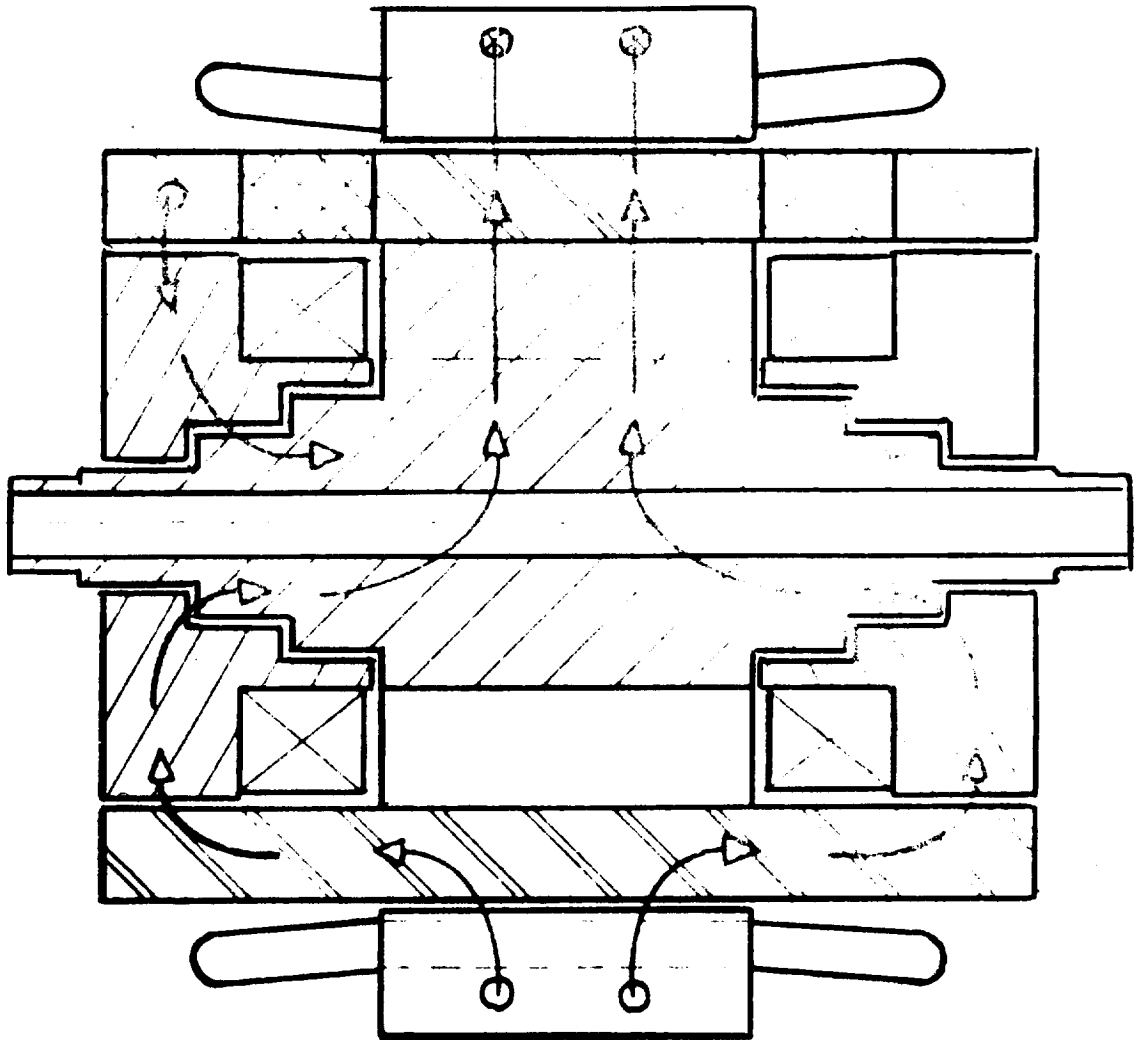


FIGURE A 27

A brushless, stationary-coil Lundell-type generator that uses two exciting coils is described in U. S. Patent 2,796,542 issued to A. Becky and

H. M. Robinson. This machine can be thought of, for calculating purposes, as essentially two single, inside, stationary-coil Lundell a. c. generators back-to-back. The description and discussion of rotating-coil Lundell generators explains how the Becky Robinson generator can be evolved from the rotating coil generator by making single stationary coil machines first, then putting two of them together back-to-back.

The Becky-Robinson generator can be made in ratings twice as large for the same stator inside diameter as is possible for the single, inside-coil Lundell, or the rotating coil Lundell. This advantage allows the Becky-Robinson machine to be used in larger ratings and/or at higher rotational speeds than the ratings and speeds of the single coil configuration.

The peripheral speed limits for the two-coil, inside-coil generator are about the same as for the single coil, inside-coil generator. The tolerable speeds are probably a little higher because the Becky-Robinson machine has less overhang on the tube, or pole and flux collector assembly. The environmental limits for the Becky-Robinson generator are tabulated and compared with the other generators in Section B, "Generator Selection Criteria".

This Becky-Robinson generator is the lightest weight of all of the stationary-coil brushless generators when compared at the same KVA and RPM. It can be used in environments too severe for the wound-rotor generators and its best application area appears now to be auxiliary electrical power generators or system electrical power generators for use in supersonic aircraft when the temperature of the cooling medium is too high for wound-pole generators and semiconductor rectifiers. The same generator is suitable for ordnance vehicles under the same circumstances - when the wound rotor or rotating coil generators cannot be used because the temperature of the coolant is too high.

ROTORS FOR THREE, TWO-COIL, INSIDE-COIL
LUNDELL A-C GENERATORS. THE SMALLEST
ROTOR IS FOR A 1.2 KVA, 12000 RPM GENERATOR.
THE MIDDLE ROTOR IS FOR A 2.5 KVA, 8000 RPM
GENERATOR. THE LARGE ROTOR IS FOR A 6000
RPM, 60 KVA GENERATOR.

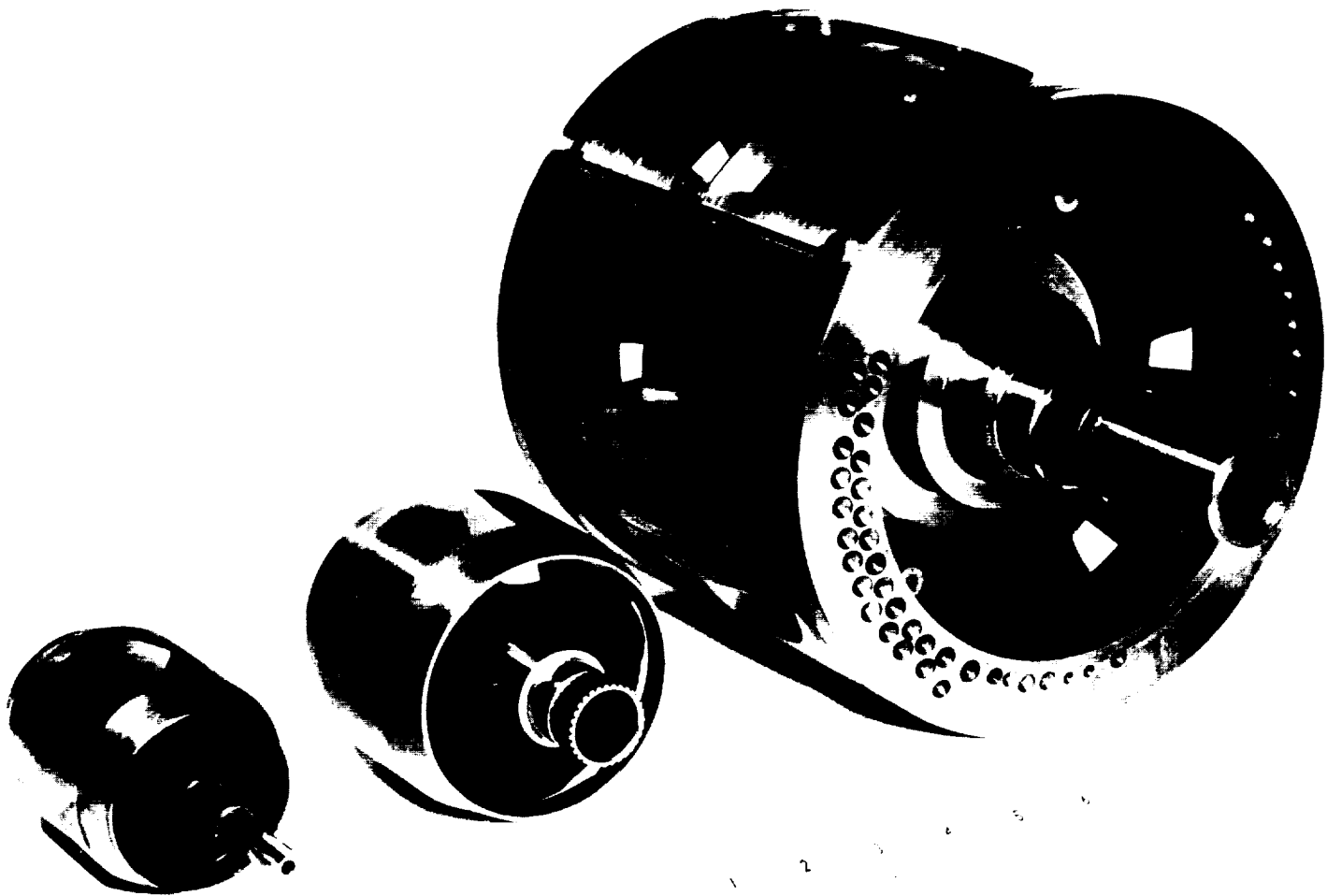


FIGURE A 28

A ROTOR FOR A 60 KVA, 6000 RPM, TWO, INSIDE--
COIL LUNDELL, A-C GENERATOR

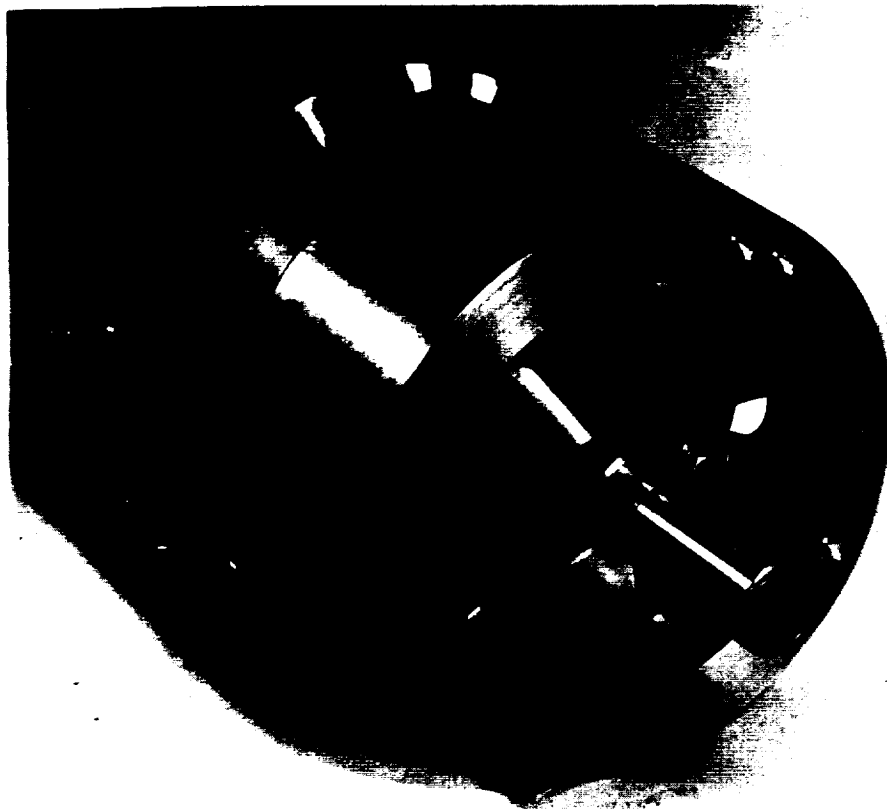
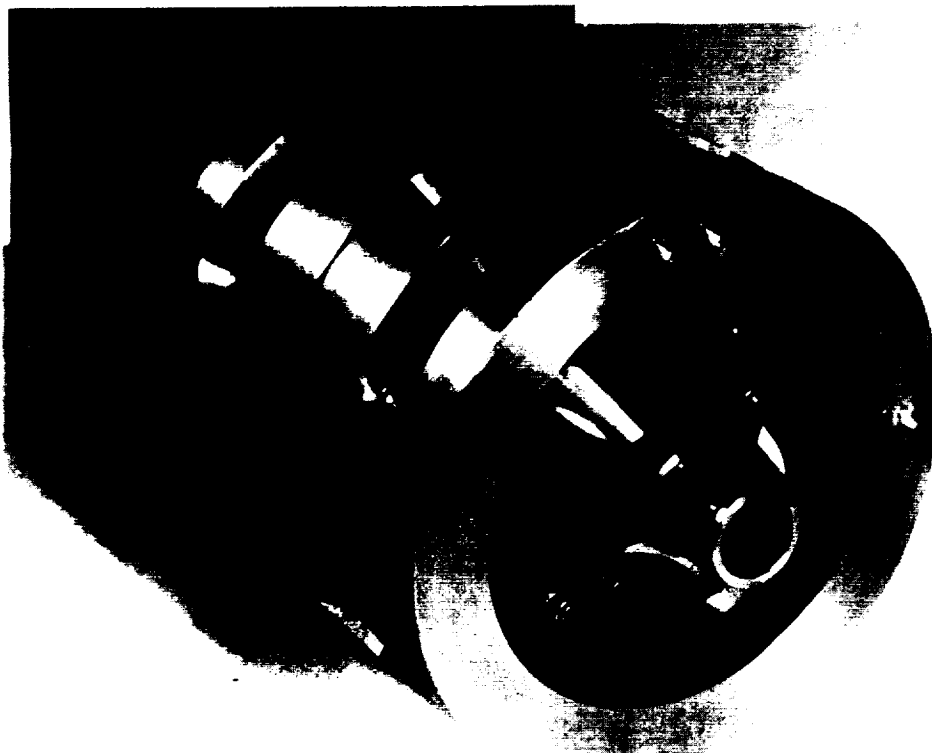


FIGURE A 29



TWO COIL LUNDELL
(BECKY-ROBINSON TYPE)



FIGURE A 30

The schematic below shows the MMF drops in the flux circuit of a two, inside, stationary-coil Lundell, a-c generator (Becky-Robinson generator).

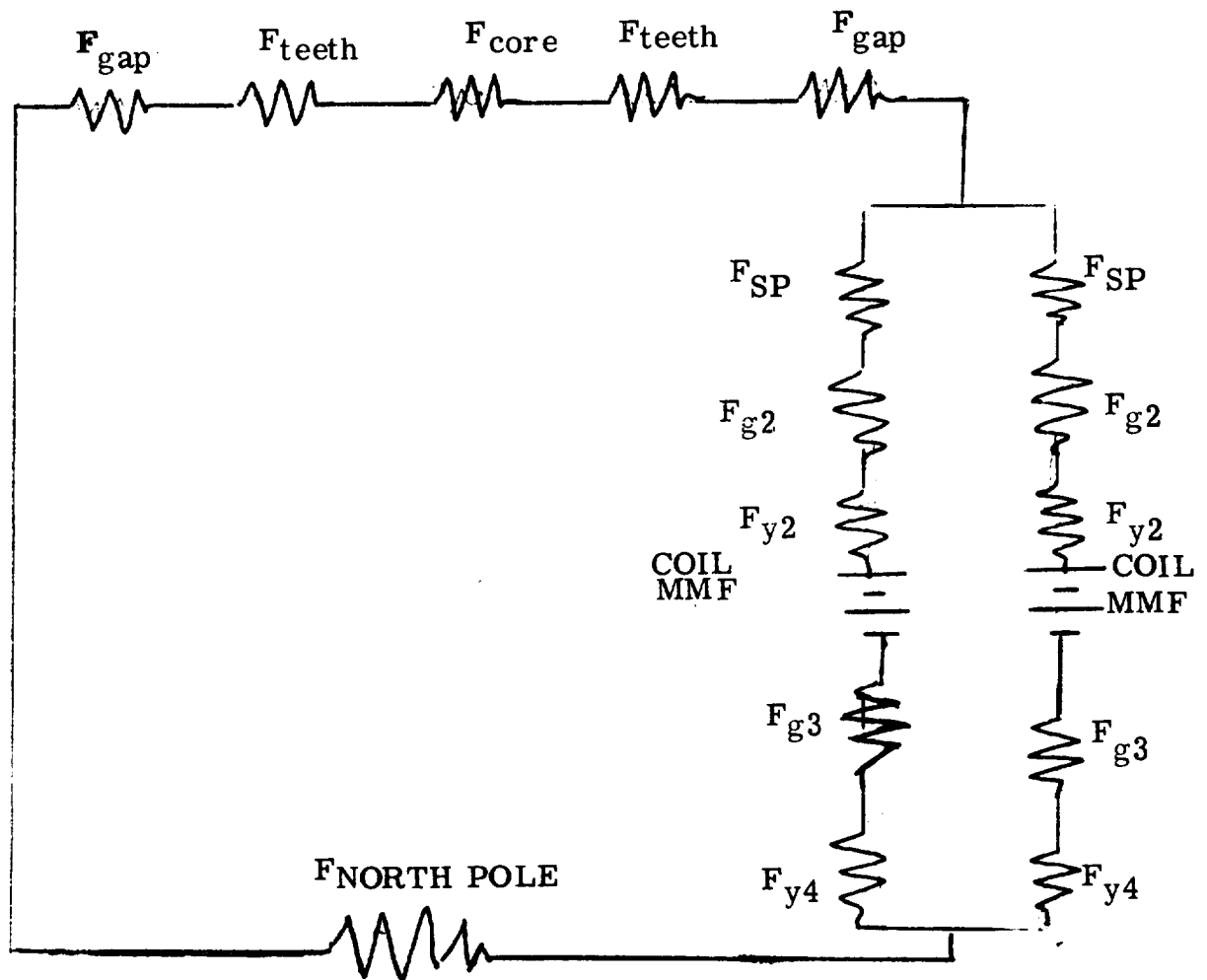


FIGURE A 31

Instead of using both of the parallel flux paths shown in Figure A 31, the calculation procedure uses only one of those parallel branches and the calculations are adjusted to the single circuit. The final circuit is shown below with the leakage paths. For a definition of the leakage fluxes and their paths, see the calculation procedure in section L.

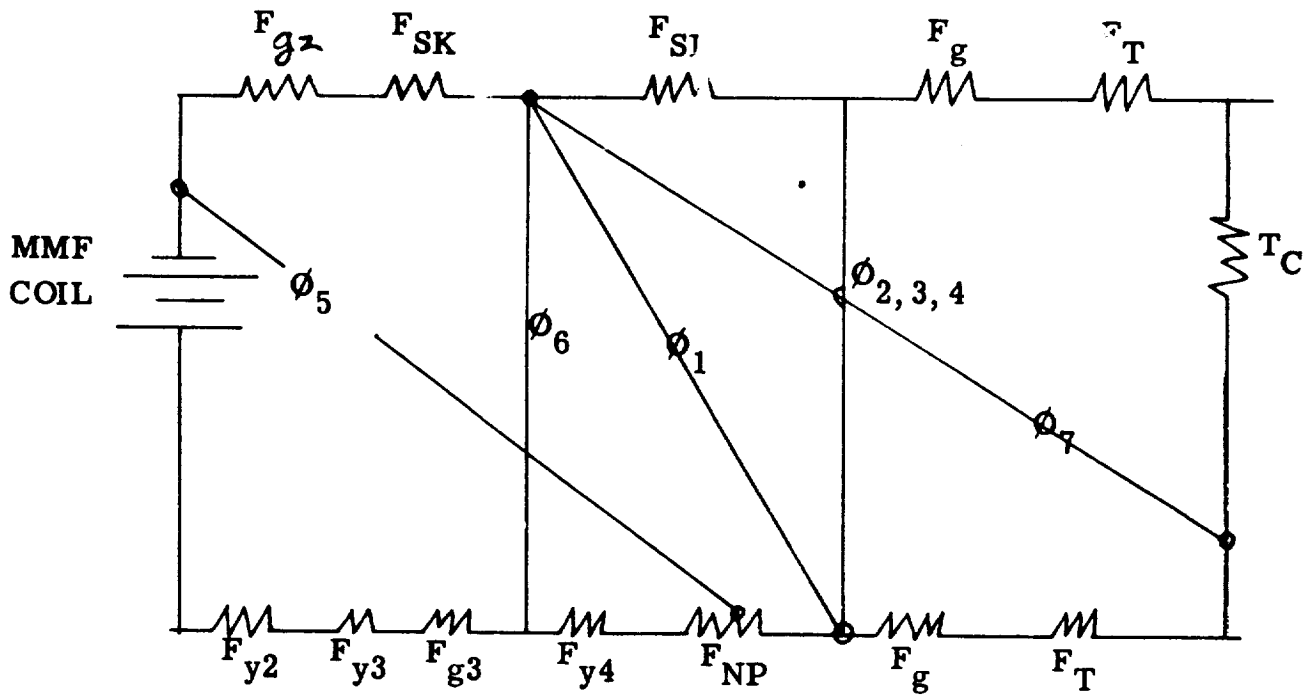


FIGURE A 32

**OUTSIDE-COIL, STATIONARY-COIL, LUNDELL,
A-C GENERATORS**

OUTSIDE-COIL, STATIONARY-COIL LUNDELL A. C. GENERATORS

Two-Coil, Outside-Coil Lundell

The two-coil, outside-coil Lundell a. c. generator and the single-coil outside-coil Lundell a. c. generator are two variations of the same machine. The two coil configuration was patented by Mr. L. C. Rice in 1897 and probably by many others in recent years.

The two-coil configuration is built by Allgemeine Elektricitate Gesellschaft in Western Germany, by Siemens-Schuckertwerke, Erlangen, Germany, and is used in Russian railway service. It is offered by several U.S.A. companies for aerospace use and is potentially one of the best generators for use in severe environments.

The flux paths through the two-coil version can be represented by the mmf drops shown in Figure A 33. The flux circuit shown in Figure A-33 A is for a machine having its stator iron touching the housing or yoke.

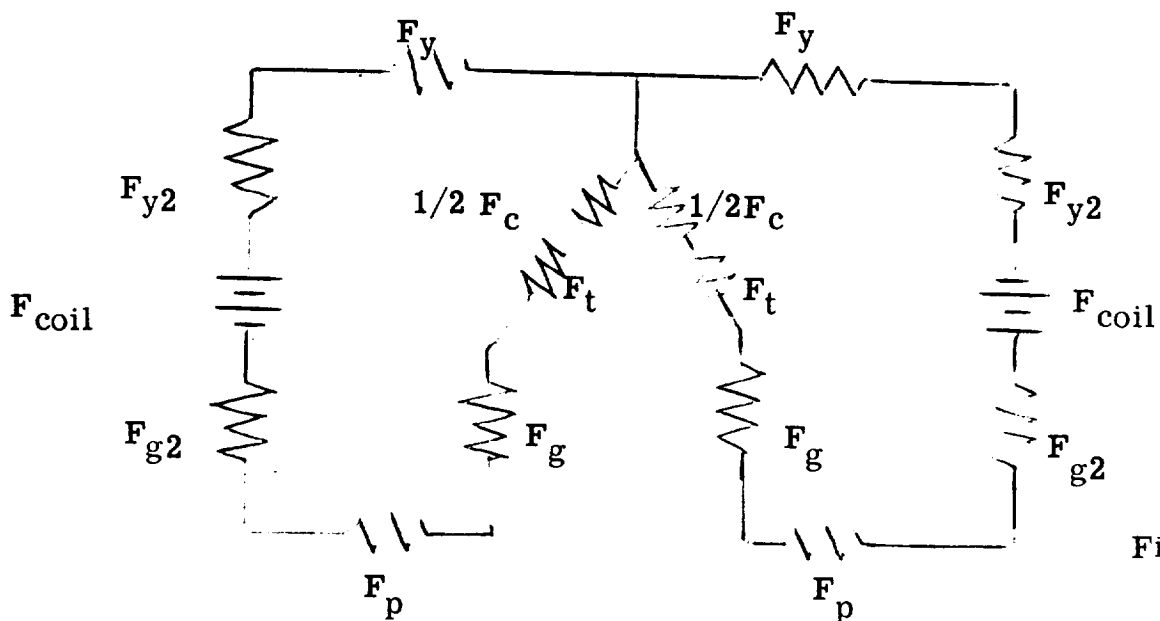


Figure A 33-A

If the stator iron is separated from the housing or yoke by a non-magnetic spacer, the mmf drops can be represented by the following schematic which is for calculating purposes, exactly the same as the circuit for the machine having its back-iron touching the yoke.

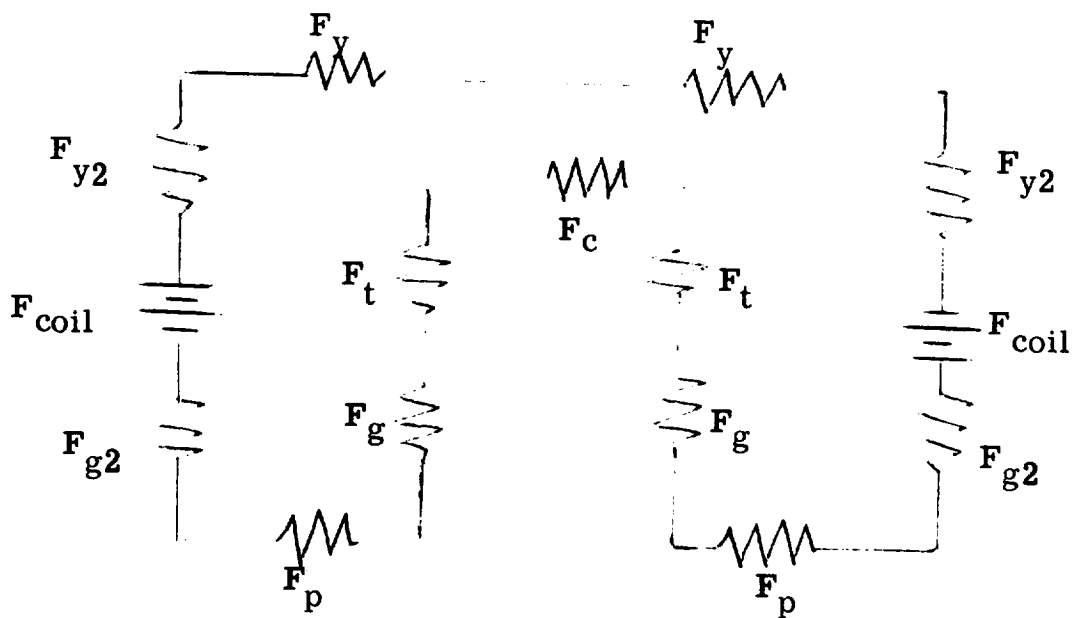
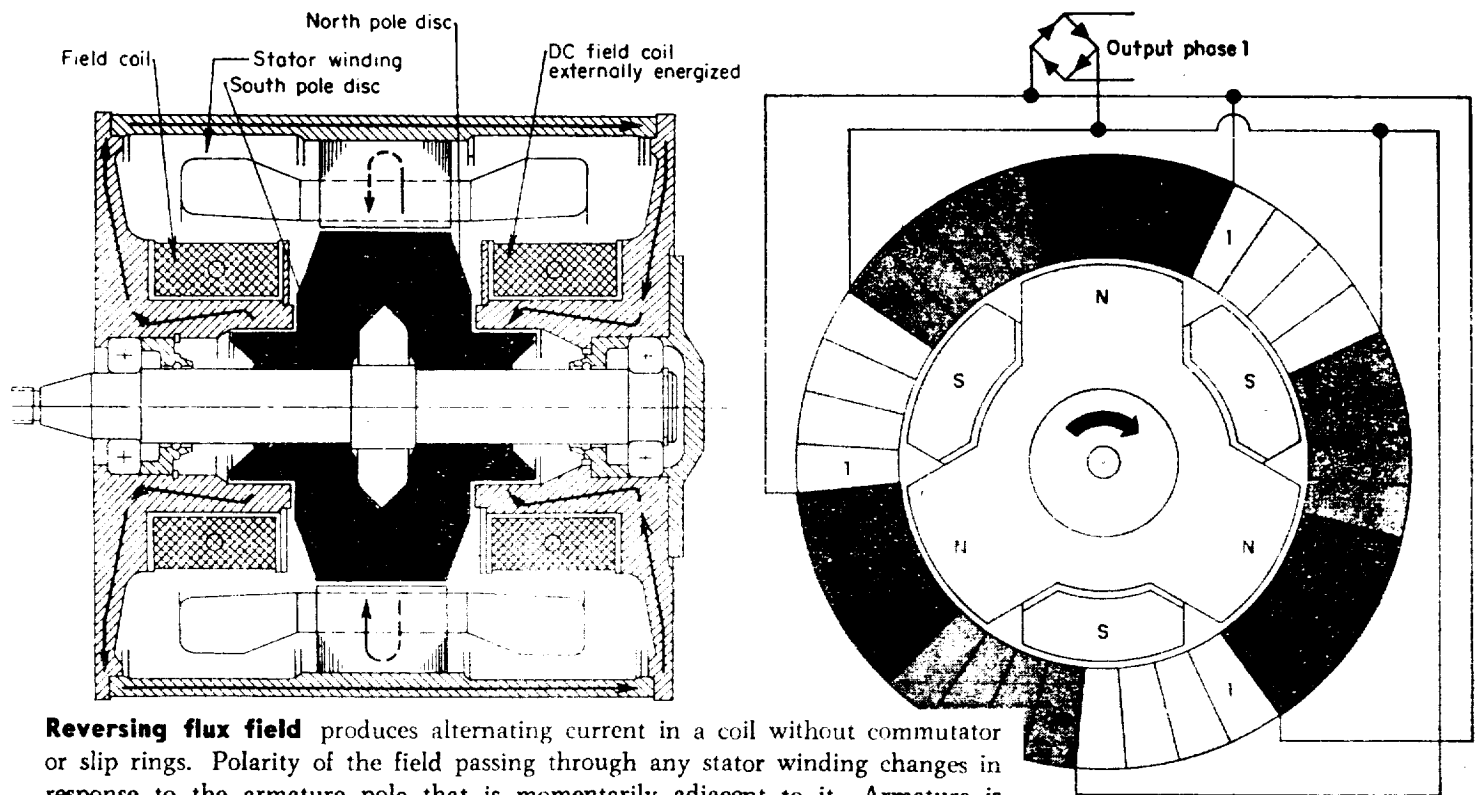


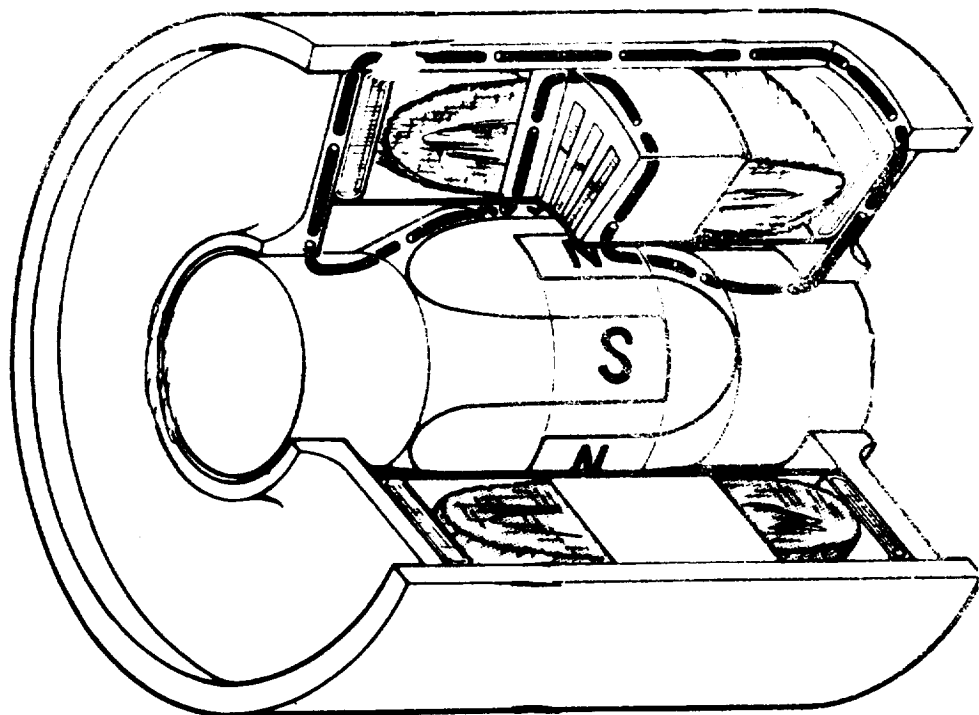
FIGURE A 33 B

TWO VERSIONS OF THE OUTSIDE-COIL LUNDELL



Reversing flux field produces alternating current in a coil without commutator or slip rings. Polarity of the field passing through any stator winding changes in response to the armature pole that is momentarily adjacent to it. Armature is composed of two discs with interlocking poles—all north on one disc and all south on the other. Stationary field windings are inside the ends of the stator windings. There is no moving armature winding. Principle used in a railroad coach alternator by Siemens-Schuckertwerke, Erlangen, Germany.

FIGURE A 34



A PATENT DRAWING FOR AN OUTSIDE COIL LUNDELL A. C. GENERATOR

(No Model.)

2 Sheets—Sheet 2.

L. C. RICE.
DYNAMO ELECTRIC MACHINE.

No. 588,602.

Patented Aug. 24, 1897.

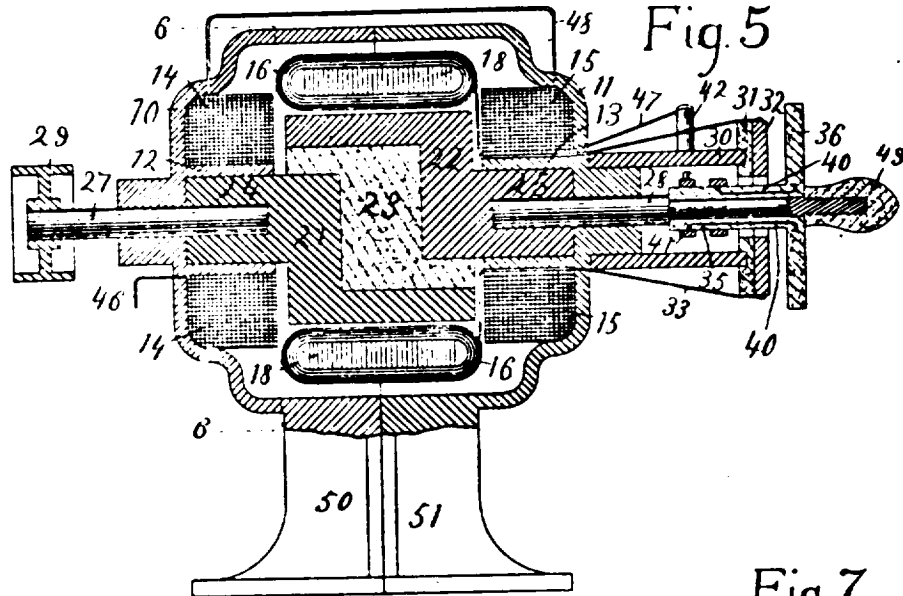


Fig. 6.

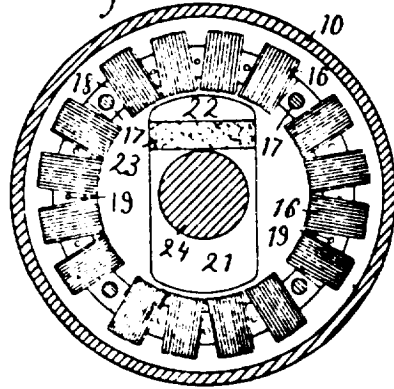


Fig. 7.

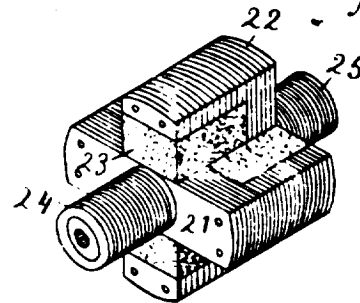
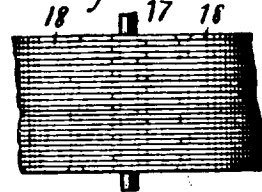


Fig. 8.



Witnesses
W. C. Alexander.
E. L. Kimball

Inventor
Lewis C. Rice
By Attorney
Fowler & Fowler

FIGURE A 35

AN OUTSIDE COIL, LUNDELL
A. C. GENERATOR MADE FROM A ROTATING
COIL LUNDELL GENERATOR



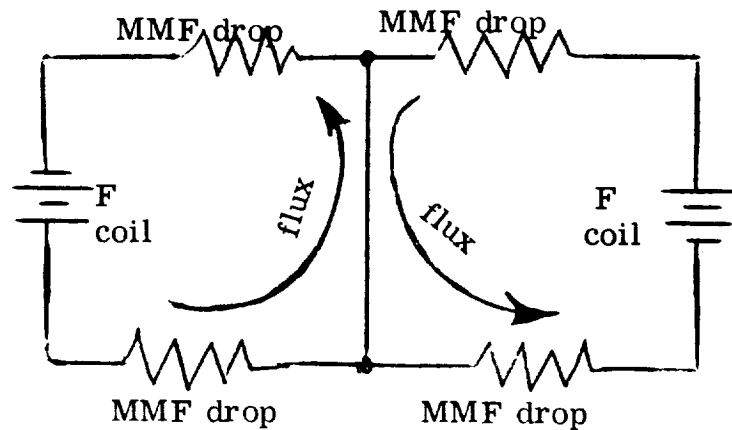
FIGURE A 36

SINGLE-COIL, OUTSIDE-COIL LUNDELL

The rotor and stator of the single-coil machine are identical to those of the two-coil configuration. Leakage permeances around the stator and coil are different and the flux circuit is different. There can be only one long single loop or circuit for the flux of the single coil machine and there are two series loops for the two-coil machine.

The single outside coil Lundell probably should be used if the generator has only two poles. In the single coil configuration, there is no direct flux circuit from the stator into the yoke and the flux in the air-gap over each pole is more nearly equal. This reduces but does not eliminate the possibility of a rotating couple due to unbalanced pole fluxes.

There are two ways the two-pole Lundell can have an unbalance or a rotating magnetic couple on its rotor. In the two, outside coil Lundell, if the stator is mounted in the magnetic steel housing, there are two possible magnetic paths through the stator. Shown schematically, the two paths look like this -

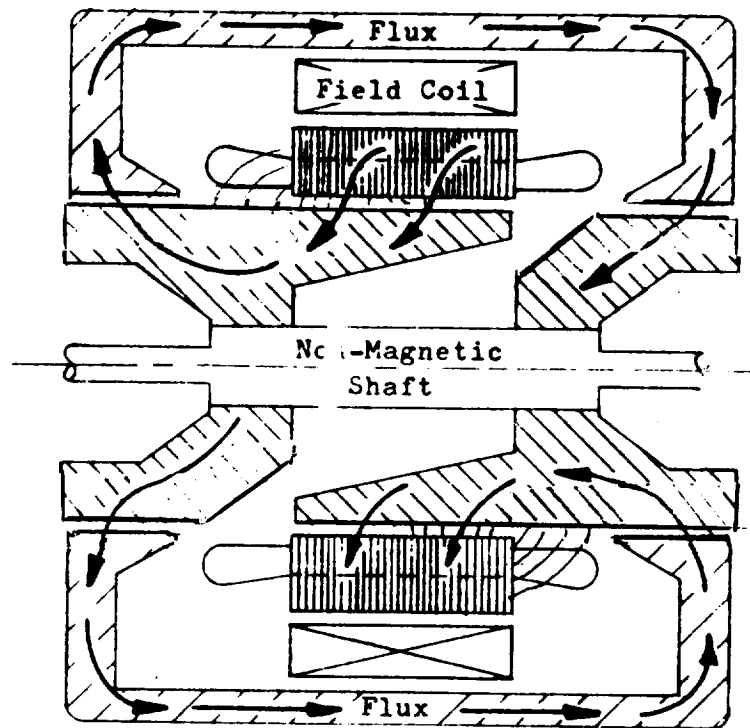


If the two fluxes are equal, the magnetic attraction between each rotor pole and the stator are equal. If the fluxes are different values because of different numbers of coil turns, varying magnetic permeability of yoke and end bells, difference in lengths of the auxiliary air-gaps, etc., one pole will have greater attractive force between it and the stator than the other pole has between it and the stator. This causes a rotating unbalance that increases with an increase in excitation.

If either the two-coil or single-coil, outside-coil Lundell is mounted in the housing with a large air-gap or non-magnetic spacer between the stator back-iron and the housing or yoke, the flux cannot easily cross the non-magnetic space and the flux in the two poles is more certain to be equal. In this case, the possible difficulty with rotor dynamics

may be a rotating couple caused by the effective magnetic centers of the two poles being in different planes of rotation.

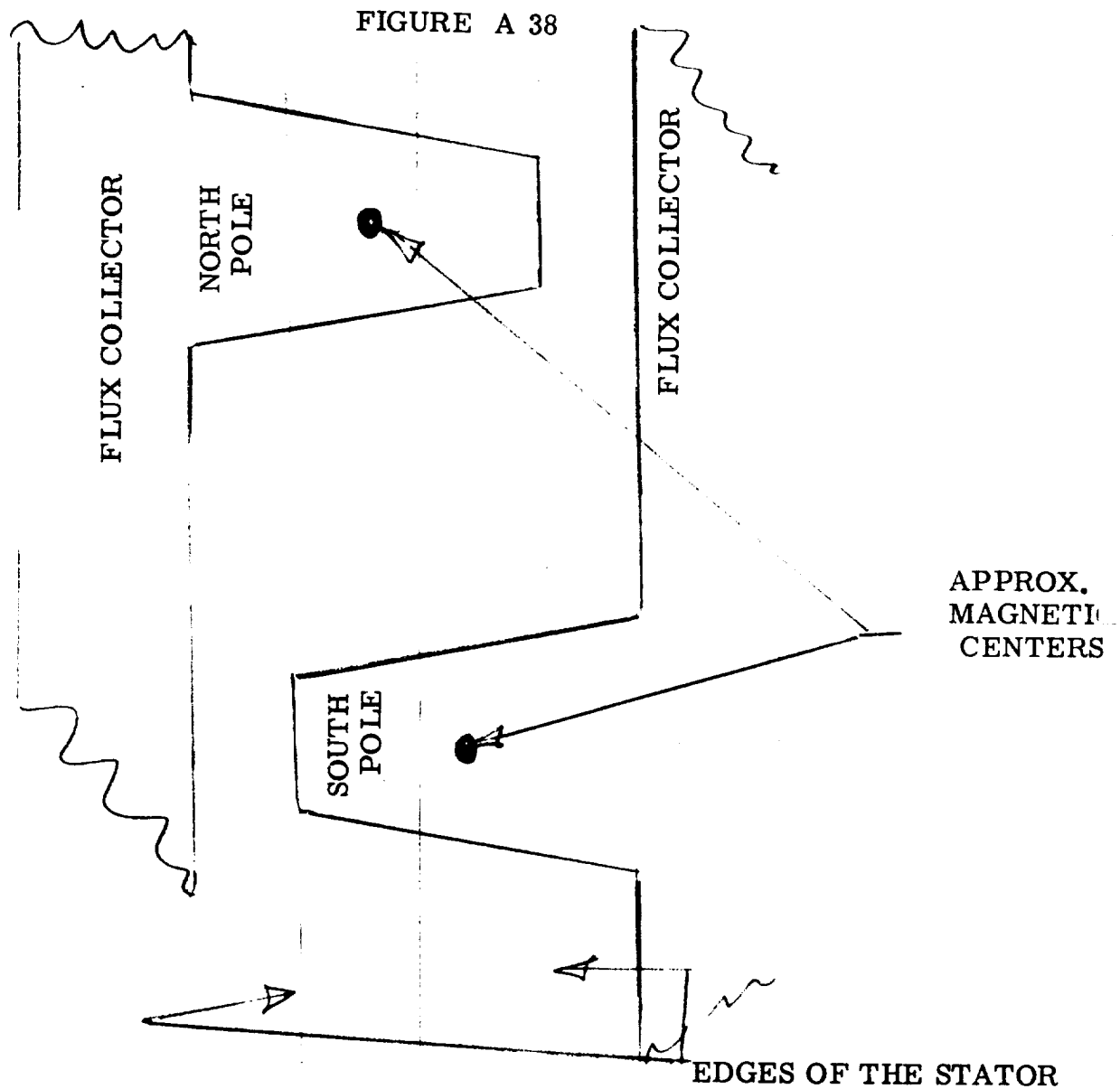
FIGURE A 37



A two-pole Lundell generator with the excitation-coil external to the rotor can be built with the flux collector section of the shaft on the same diameter as the rotor diameter at the pole surface. This configuration causes a maximum amount of fringing flux to enter or leave the stator at the bases of the cantilevered poles and from that cause alone the magnetic center of the pole must shift away from a plane through the center of the stator.

If in addition, the poles are made trapezoidal as is commonly done in Lundell generators, the magnetic center of the pole is shifted away from

the center-plane of the stator because of the markedly different amounts of flux passing from the pole to the stator on each side of the centerline of the stator. The combination of these two causes of displaced magnetic centers can cause a large rotating couple that varies with variation in excitation.



If the flux-collector section of the shaft is made appreciably smaller in diameter than the surface of the rotor poles and in addition if the poles are made rectangular in shape, the dynamic unbalance can be made to be small and conceivably can be made as small as desired. Rotating couples in such a case would be eliminated at the expense of increased weight.

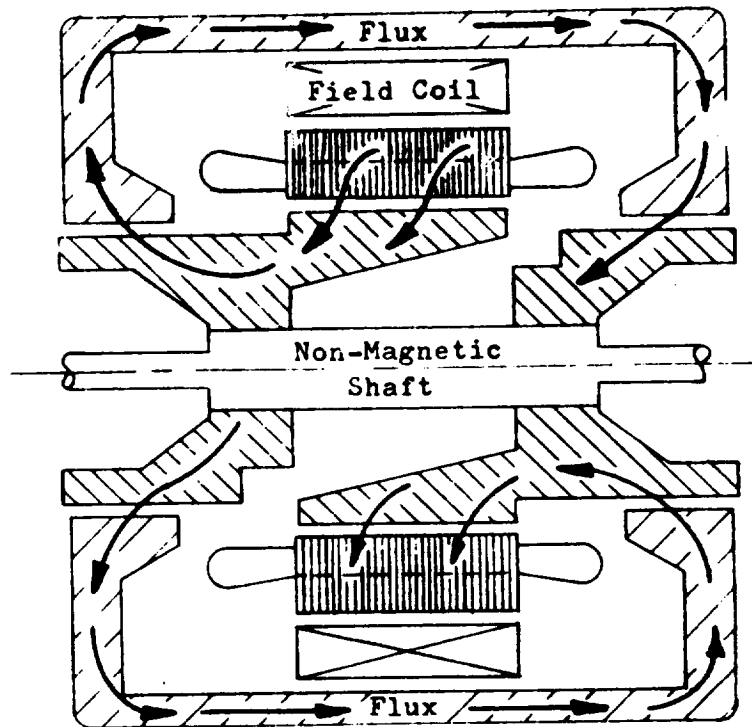
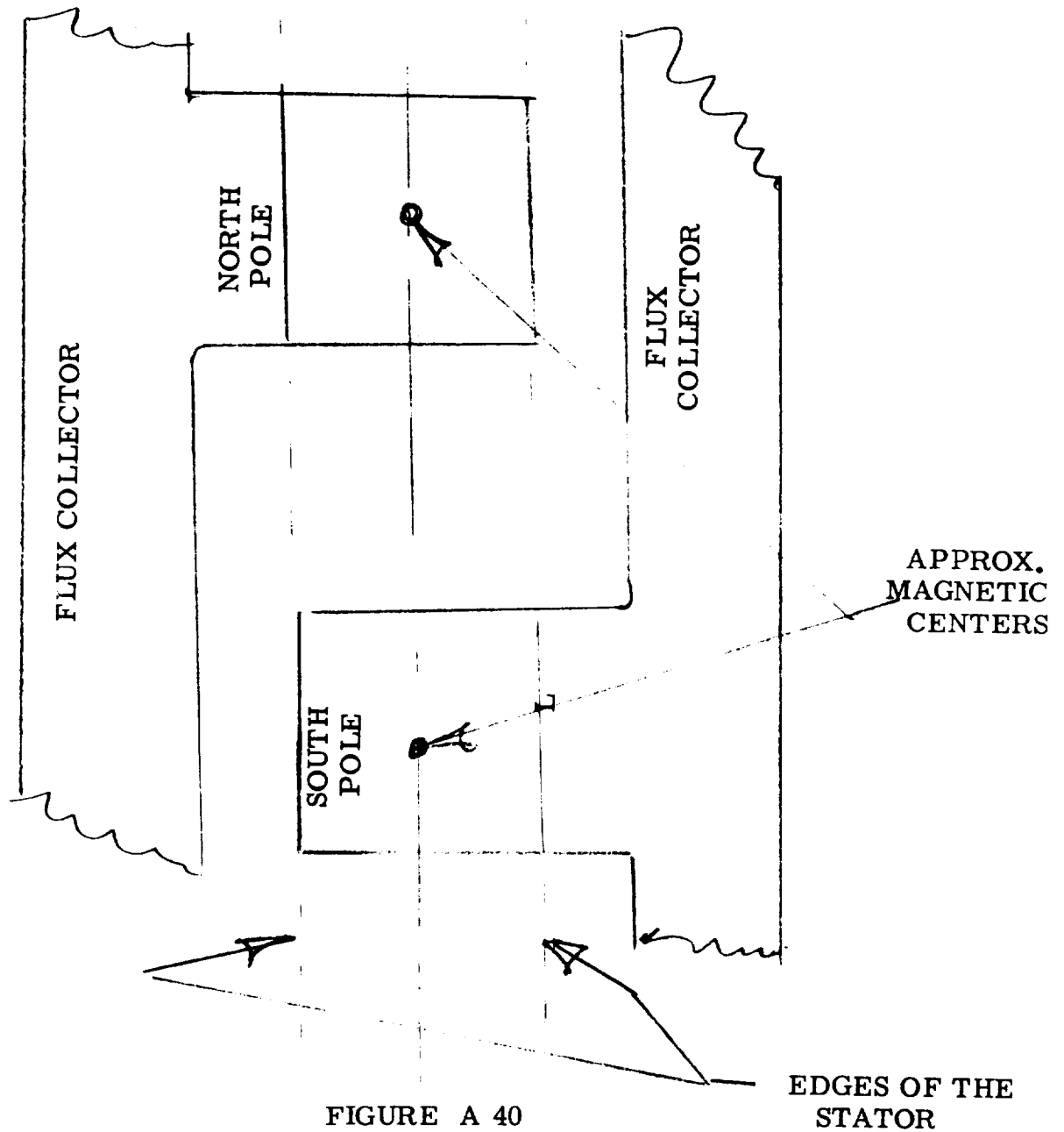


FIGURE A 39

The sketch above shows the step-down shaft in the flux collector region. This reduces fringing flux at the base of the cantilevered pole and reduces the shift of the magnetic center of the pole away from a plane through the stator centerline.



The sketch above shows the two poles made rectangular. The poles can be shaped so that no appreciable shift of the poles magnetic centers will occur.

AXIAL AIR-GAP, LUNDELL, A-C GENERATOR

A-51a

AXIAL AIR-GAP, LUNDELL TYPE, A. C. GENERATOR

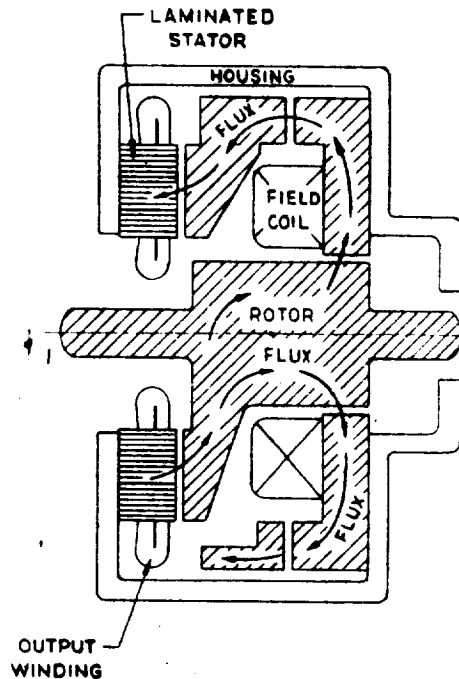


FIGURE A 41

The axial air-gap Lundell a. c. generator with a stationary excitation coil is of recent origin and this type of generator has been tried for several applications. At least one design is being used in production quantities for electrical power in an undersea weapons system.

The original Lundell generator patented by Robert Lundell in 1893 was an axial air-gap generator with the output windings rotating.

The newer brushless, axial air-gap generator has the field structure rotating and the output winding is stationary. The brushes are eliminated through the use of auxiliary air-gaps.

The weight of this machine is approximately the same in small ratings as that of a radial gap Lundell generator of the same rating, speed and frequency. It can be built with two stators and one field coil for maximum output at a given diameter.

The output of any Lundell-type a. c. generator with a rotating pole structure is some function of the stator inside diameter. The equivalent stator diameter for the axial air-gap generator is the square root of the average of the $(OD)^2$ and $(ID)^2$ or $\sqrt{\frac{D^2 + d^2}{2}}$.

If a single-stator axial-gap generator and a radial-gap generator are built with the same KVA, frequency, RPM, air-gap flux density, and stator ampere loading (or the same reactances) the rotor of the disk-type generator will be a minimum of two (2) times the diameter of the radial-gap generator. See derivations in the Appendix.

At the same rating and conditions of load, the single-stator axial air-gap machine operates at four (4) times the stress level of the radial-gap machine.

The axial-gap generator is difficult to build and has high rotor flux leakage. In large ratings, the single-stator generator produces high attractive forces between the rotor and stator. These forces are hard to eliminate though they can be reduced by designing the auxiliary gaps to give an opposite attractive force. Because of the attractive force between rotor and stator, the single-stator configuration cannot be used with fluid bearings. The more balanced two-stator design must be used if fluid bearings are necessary. The axial air-gap Lundell a.c. generator may, in small ratings, be useful because of its shape and the design procedure for hand calculation is included to make the study more complete. No computer program is provided.

PATENT DRAWING FOR AN EARLY
LUNDELL AXIAL AIR-GAP A. C. GENERATOR

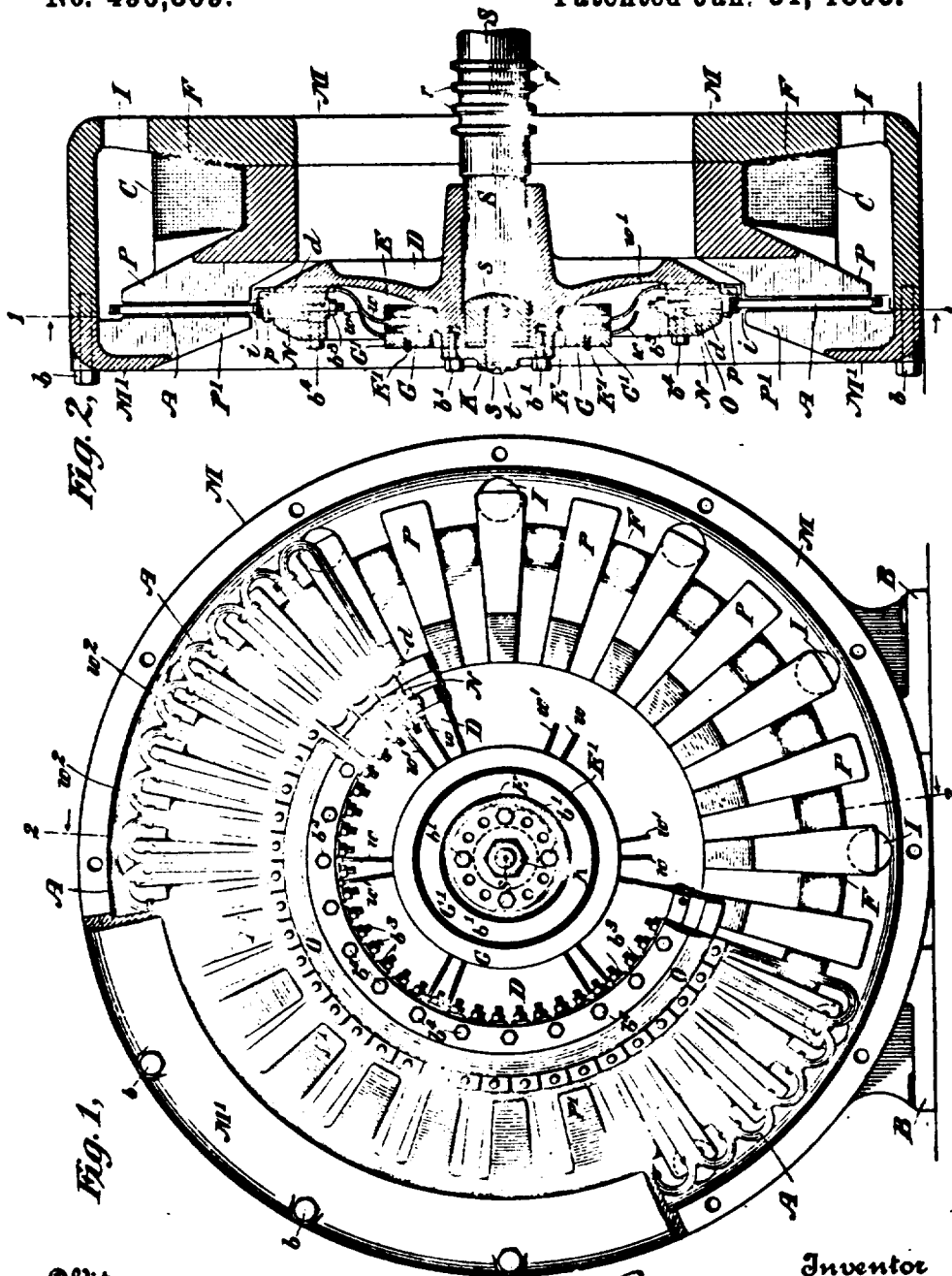
(No Model.)

2 Sheets—Sheet 1.

R. LUNDELL.
DYNAMO ELECTRIC MACHINE.

No. 490,809.

Patented Jan. 31, 1893.



Witnesses
C. E. Ashley
L. W. Chamberlain

Inventor
Robert Lundell
By his Attorney
Charles I. Kintner

FIGURE A 42 a

ROTOR FOR A SMALL, AXIAL AIR GAP
LUNDELL A. C. GENERATOR

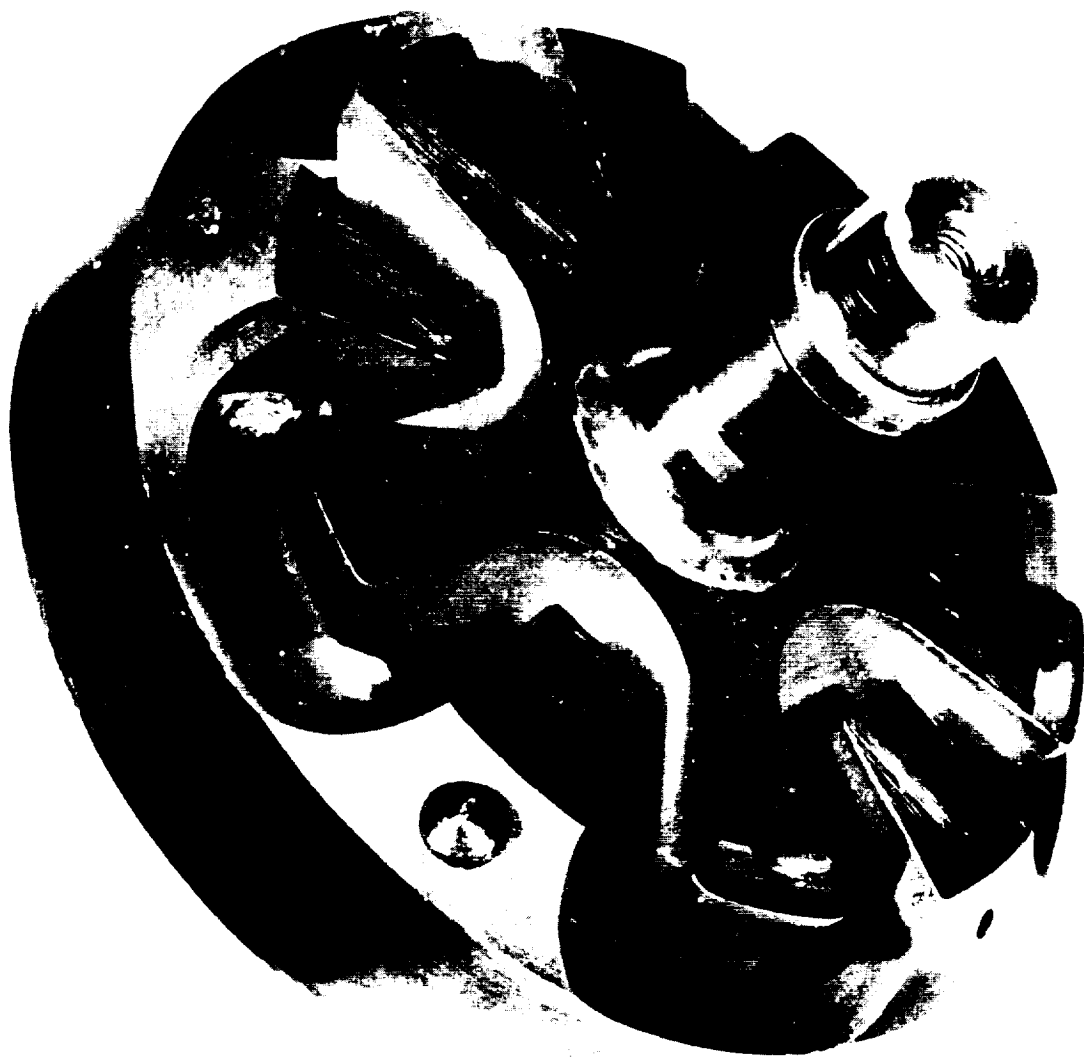


FIGURE A 42 c

STATOR FOR A SMALL AIR-GAP
LUNDELL A. C. GENERATOR

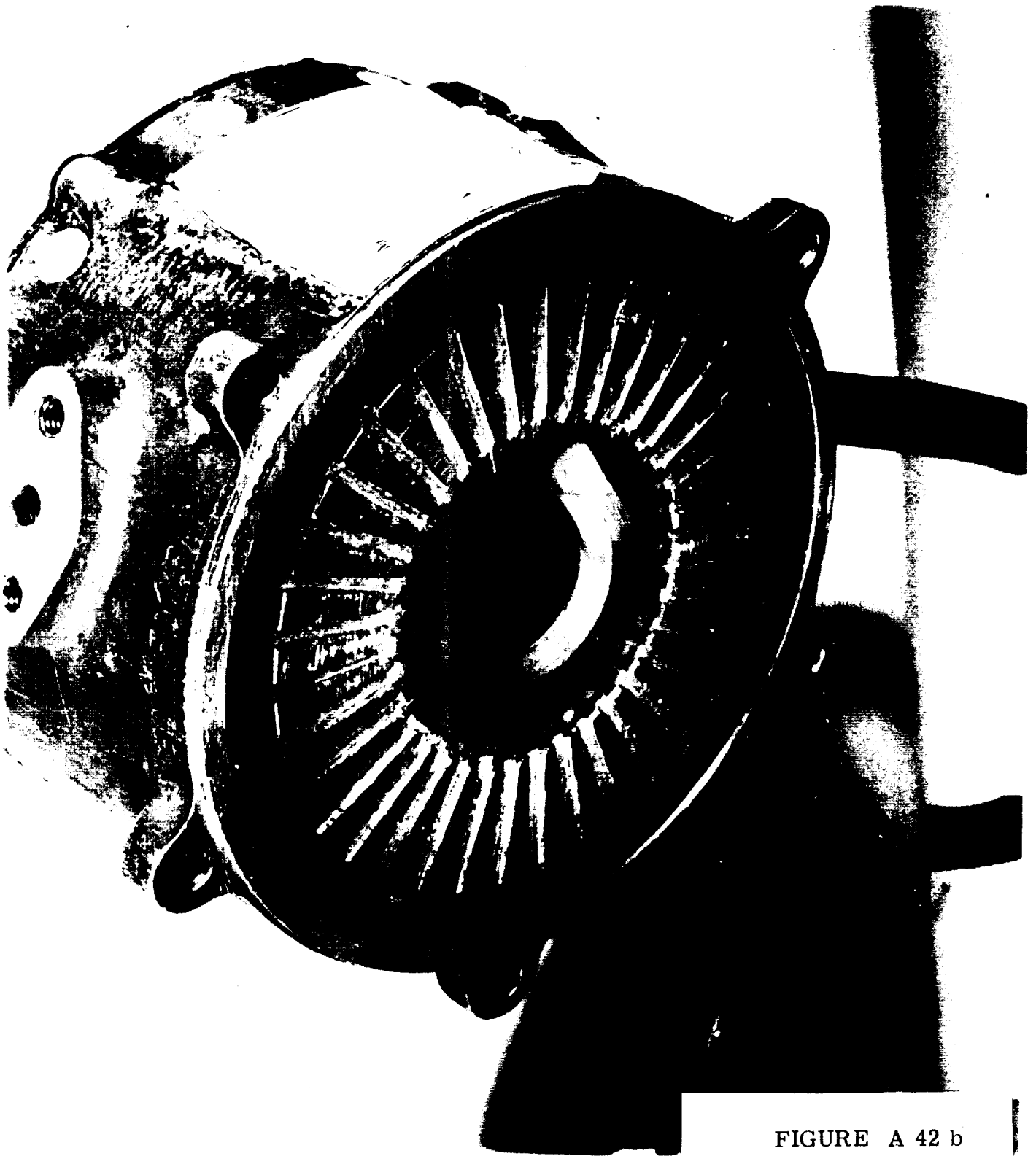
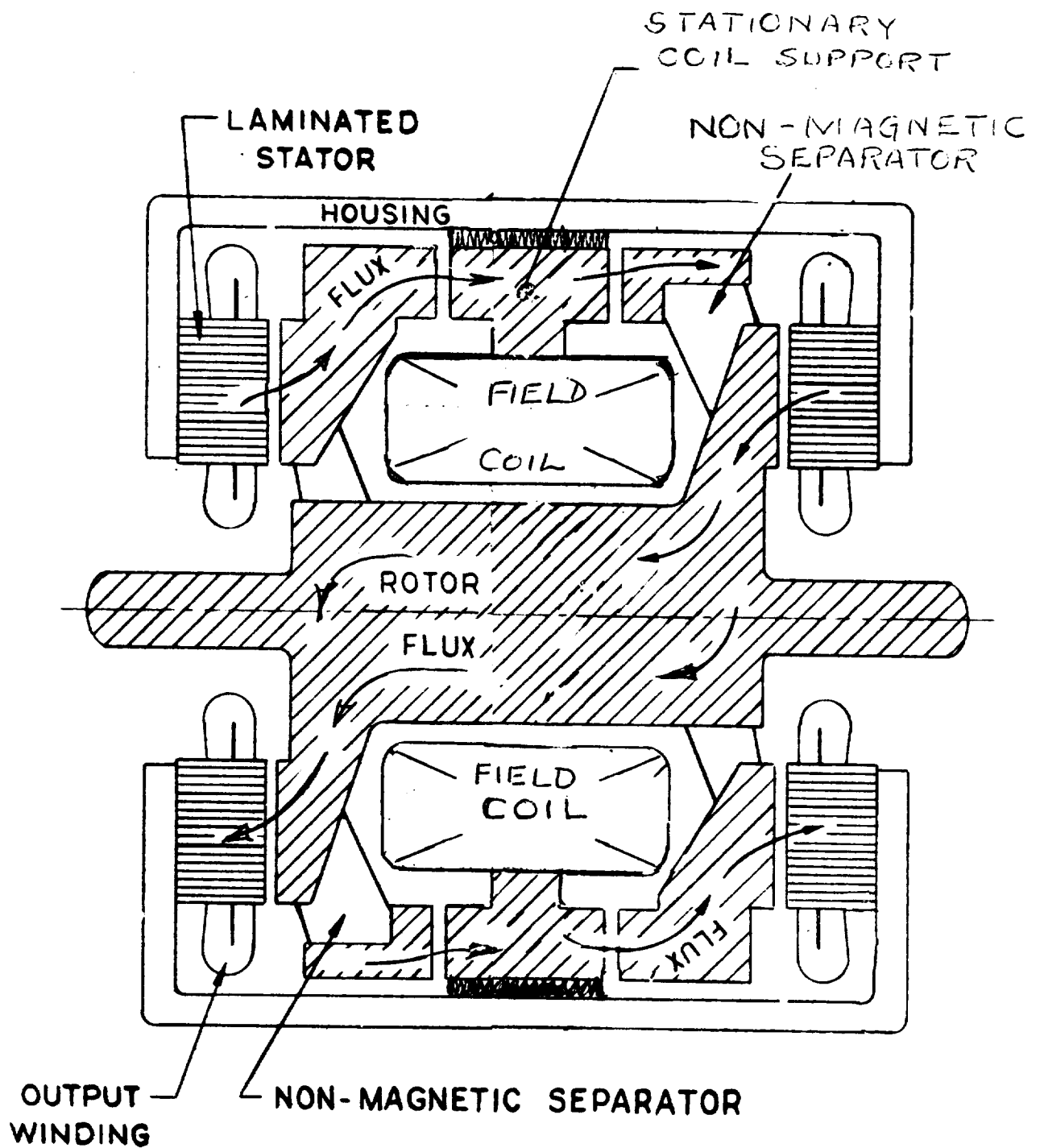


FIGURE A 42 b



DOUBLE, DISK-TYPE, LUNDELL, A-C
GENERATOR

FIGURE A 42 c

DISCUSSION OF THE
HOMOPOLAR INDUCTOR A. C. GENERATOR

THE HOMOPOLAR INDUCTOR, A-C GENERATOR

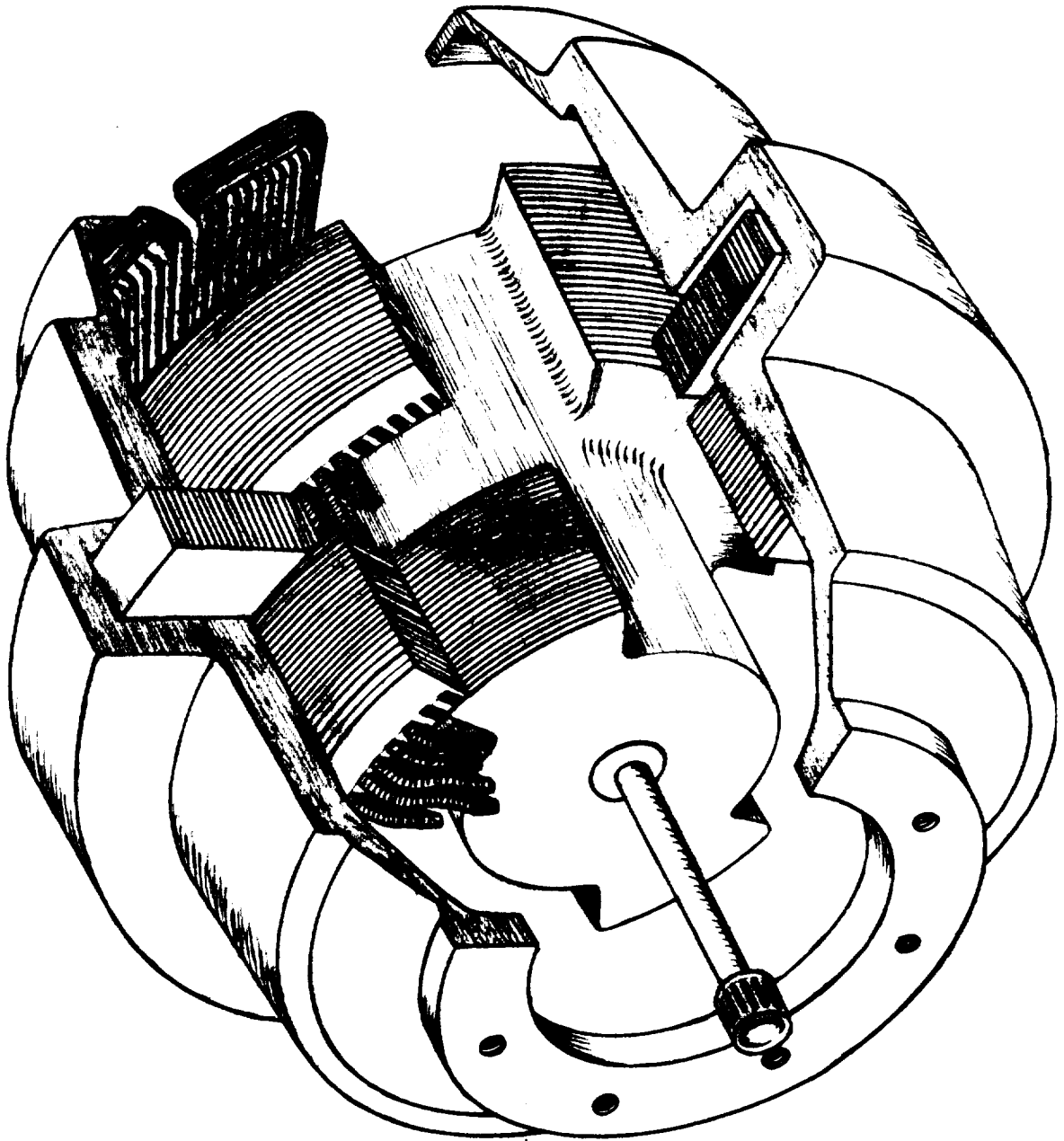


FIGURE A 43

HOMOPOLAR INDUCTOR, AC GENERATOR

Before 1900, in the young age of electrical power engineering, many different generator designs were proposed and patented. One of those old designs, widely used since its conception, is described in U. S. Patent No. 499446 issued to William Stanley, Jr. and John F. Kelly in 1893.

The same configuration is now made by every company building homopolar inductor AC generators.

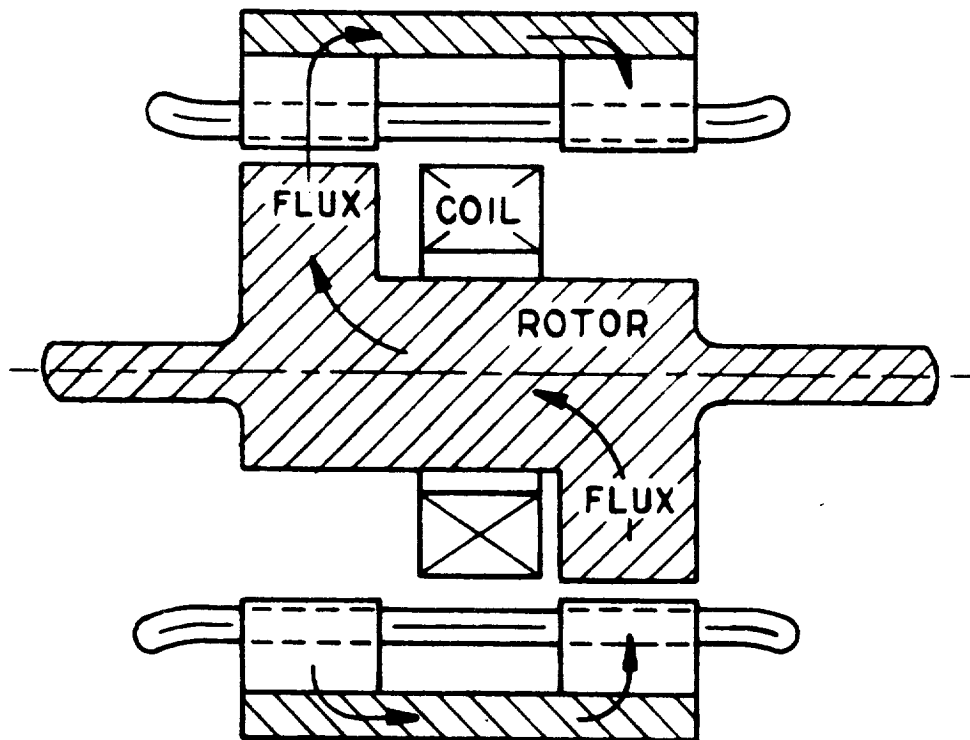


FIGURE A 44

SMALL HOMOPOLAR INDUCTOR GENERATOR

The usual homopolar inductor consists of two identical stators wound with a common winding, a double rotor having all north poles on one end and all south poles on the other end, and a field coil enclosed in the magnetic path formed by the outer shell or yoke, the stators, and the rotor.

When the field coil is excited and the rotor is rotating, unidirectional fields of flux cut the windings of each stator in such a manner that approximately the same voltage is generated in the two stators combined as would be generated in one stator by a single rotor having both the north and south poles of the two ends of the homopolar inductor rotor. In other words, two stators and two rotor ends are electrically and magnetically accomplishing what one stator and its corresponding rotor would do in a conventional salient-pole, synchronous, wound-field generator.

The magnetic flux from the rotor poles passing through each stator section and linking the output windings, is unidirectional and pulsating. Since the magnetic flux never changes direction in a stator and the poles of a rotor section are of one polarity, the generator has been called a homopolar generator (or alike-pole generator).

The AC generator known as the homopolar inductor is confused in the literature with a DC generator that is also called a homopolar inductor. The DC generator is called both a unipolar generator and an acyclic generator to distinguish it from the AC machine. A paper given by B. G. Lamme, AIEE Transactions 1912, PP 1811-1835, describes the development problems of a 2000 KW acyclic DC generator. The acyclic generators are of interest for generating the high direct currents needed for pumping liquid metals but are not discussed in this study.

During the seventy odd years of its existence, the homopolar inductor alternator has been used mainly in industrial applications where size and weight were of little consequence. One of its uses has been to supply high frequency electrical power for induction heating of steel products.

Homopolar inductor designs used in industrial applications have poles, or rotor teeth as they are often called, protruding far out of the shaft so that only a very small amount of unwanted flux passes from the shaft to the stator between the poles of a single polarity (on one end of the stator.)

Recently, the homopolar inductor is being used in airborne and space applications where size and weight are of primary importance. In these appli-

cations, the area of the shaft between the two groups of poles of opposite polarities directly limits the maximum output of the machine. In these minimum weight designs, the shaft is the largest diameter practicable and the poles or rotor teeth do not protrude far from the shaft. The unwanted flux passing from the shaft to the stator in the region between poles of like polarity is significant. It is of the order of several percent in a practical, useable design. This unwanted flux generates a voltage opposite to the output voltage in the output windings and reduces the output of the machine.

To get the maximum output from a given rotor diameter, when a small number of poles is used, it is necessary to remove all excess magnetic material from the rotor - to reduce the rotor diameter between adjacent poles or rotor teeth. This treatment is shown by the two following before and after pictures.

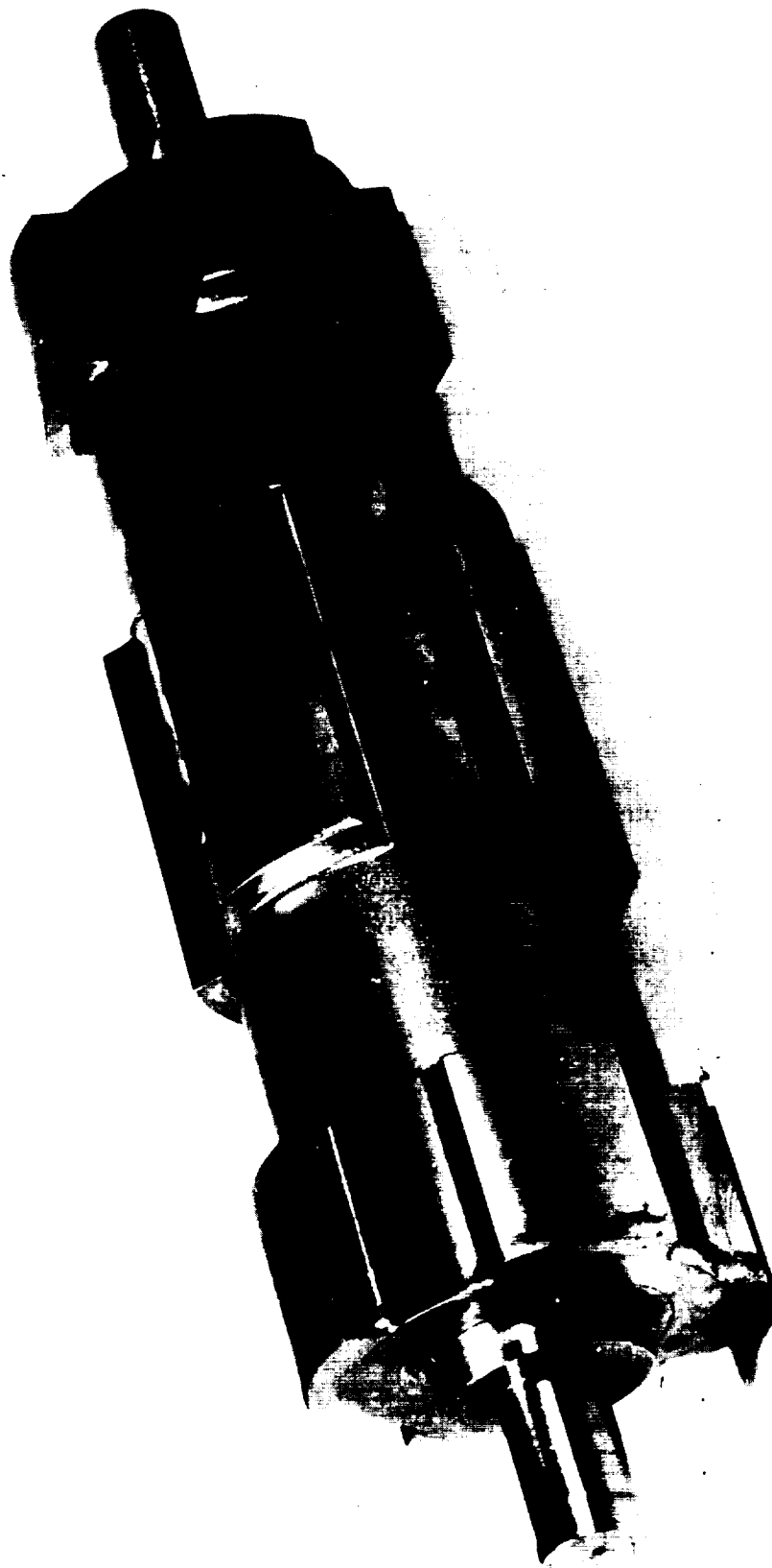


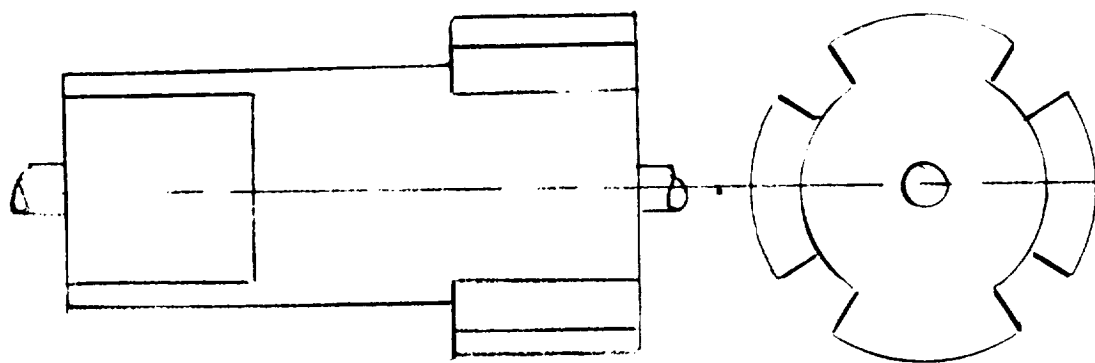
FIGURE A 46

DOUBLE HOMOPOLAR GEN.

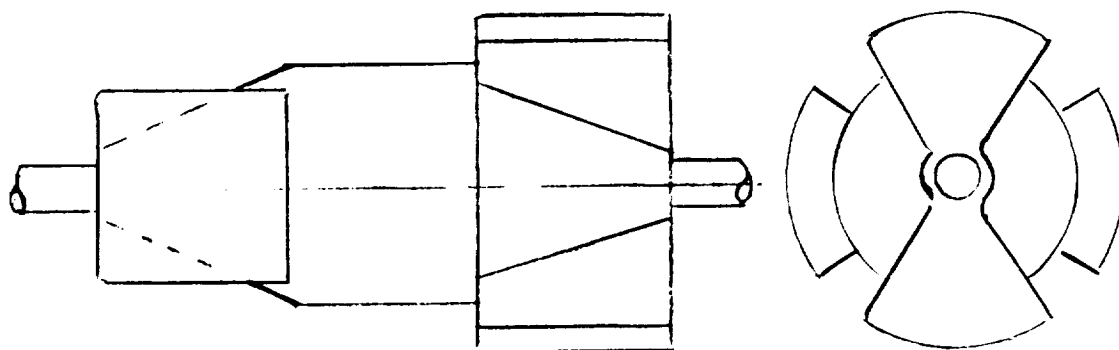
cations, the area of the shaft between the two groups of poles of opposite polarities directly limits the maximum output of the machine. In these minimum weight designs, the shaft is the largest diameter practicable and the poles or rotor teeth do not protrude far from the shaft. The unwanted flux passing from the shaft to the stator in the region between poles of like polarity is significant. It is of the order of several percent in a practical, useable design. This unwanted flux generates a voltage opposite to the output voltage in the output windings and reduces the output of the machine.

To get the maximum output from a given rotor diameter, when a small number of poles is used, it is necessary to remove all excess magnetic material from the rotor - to reduce the rotor diameter between adjacent poles or rotor teeth. This treatment is shown by the two following before and after pictures.

FIGURE A 45



View of a conventional four-pole, homopolar inductor rotor with no excess metal removed to reduce the interpolar leakage ϕ_m



The same generator rotor after the excess metal has been removed from between the poles of like polarity.

Reducing the rotor diameter between poles in the manner shown above reduces the unwanted flux between poles and has the effect of increasing the effective pole height.

The output of a homopolar inductor is limited by the diameter of the rotor section between pole-carrying ends (we call the section the Center Shaft Section). Reducing the important interpolar flux leakage (called ϕ_m in the design manual) reduces the flux carried in the center-shaft at full load and allows the designer to use longer stator stacks. The designer obtains a larger rating from the same rotor diameter and the total generator weight is reduced to a minimum.

When the diameter of the rotor cannot be increased to increase the generator rating, two homopolar inductors can be put together to make a duplex or double homopolar inductor. The photo following shows such a rotor from a generator originally designed for 70 KVA at 60,000 rpm.

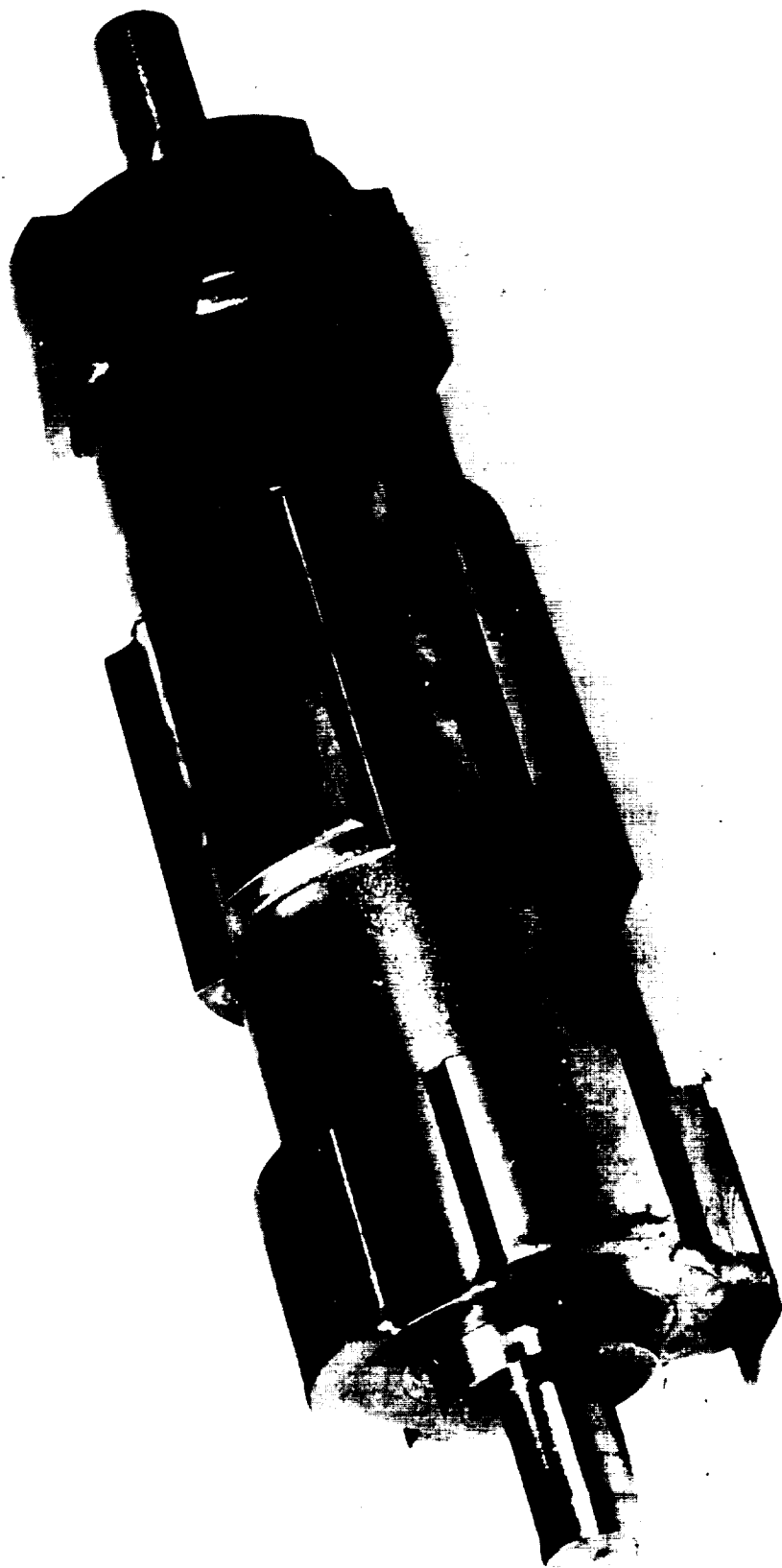


FIGURE A 46

DOUBLE HOMOPOLAR GEN.

Advantages of the homopolar inductor generator for use in space power systems are:

1. It is simple in design and inherently reliable.
2. The homopolar rotor has high strength and can be used for high rotational speeds if bearing problems permit.
3. At lower speeds the rotors can be laminated to remove the output limits imposed by pole-face losses.

Disadvantages of the machine for the same applications are:

1. It is a heavy machine -- the heaviest of all of the AC generators if compared at the same rpm.
2. Stator protection problems are compounded by the two stators when used in a hostile environment.
3. The solid pole faces limit the output unless the poles are treated to reduce the pole-face losses.
4. The long, double rotor is sometimes not as stiff as desirable for high-speed applications where fluid or gas bearings are used.

A PATENT DRAWING FOR A HOMOPOLAR INDUCTOR A. C. GENERATOR

(No Model.)

W. STANLY, Jr. & J. F. KELLY.
ALTERNATING CURRENT GENERATOR.

No. 499,446.

Patented June 13, 1893.

Fig. 2

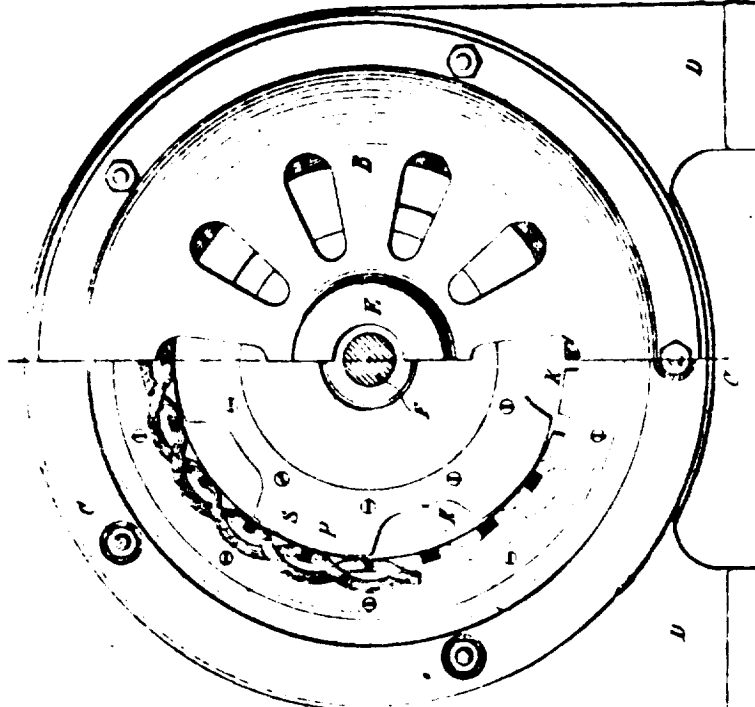
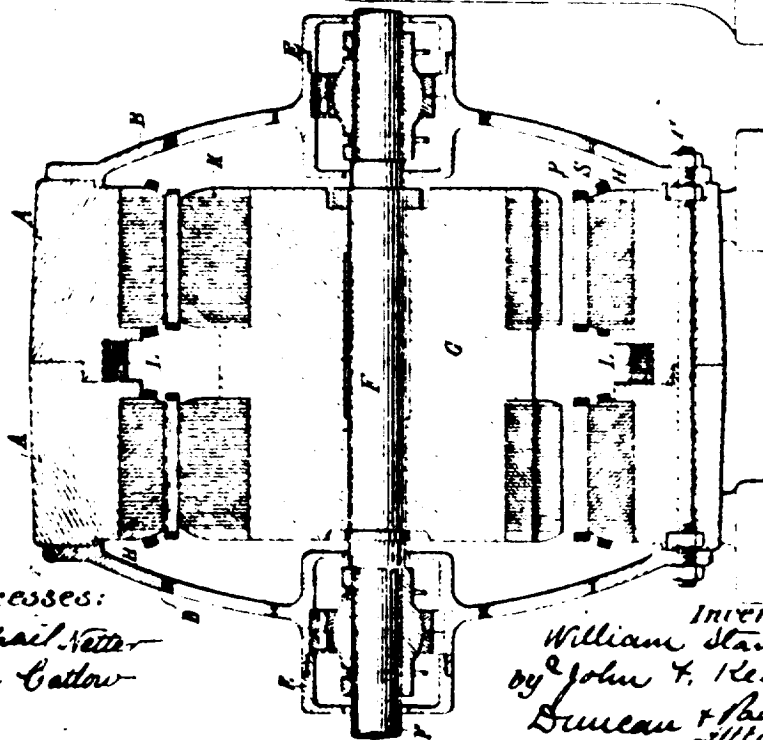


Fig. 1



Witnesses:
Raphael Vetter
James Callow

Inventors
William Stanley, Jr.
by John F. Kelly
Duncan & Page
Attorneys

FIGURE A 47 a

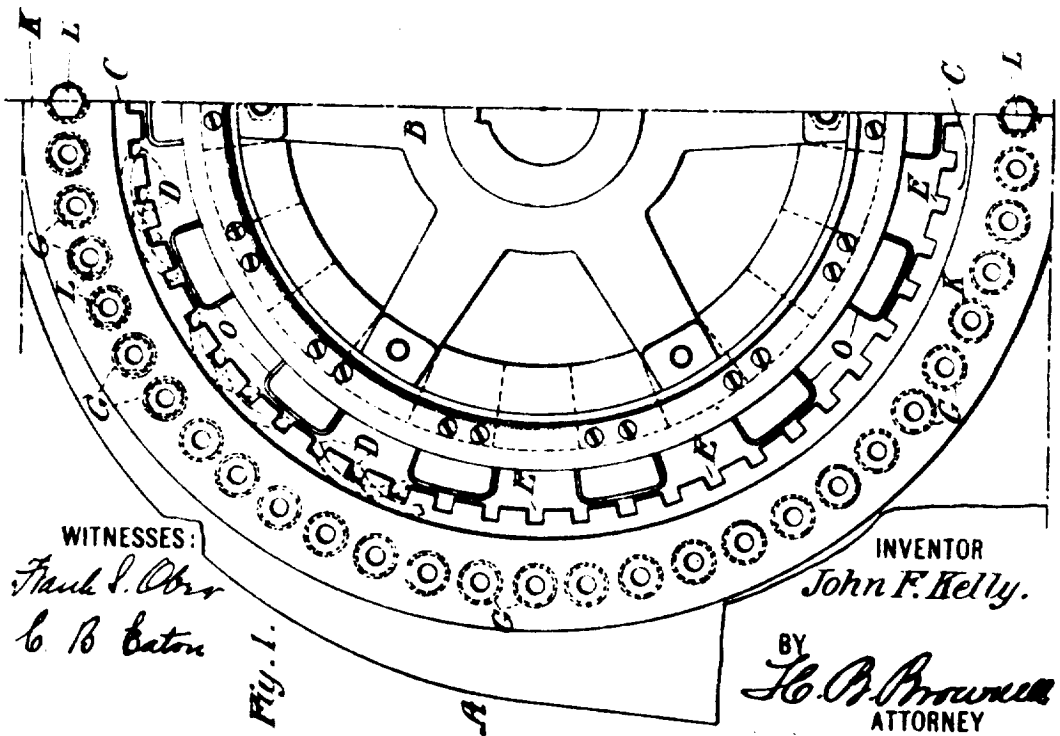
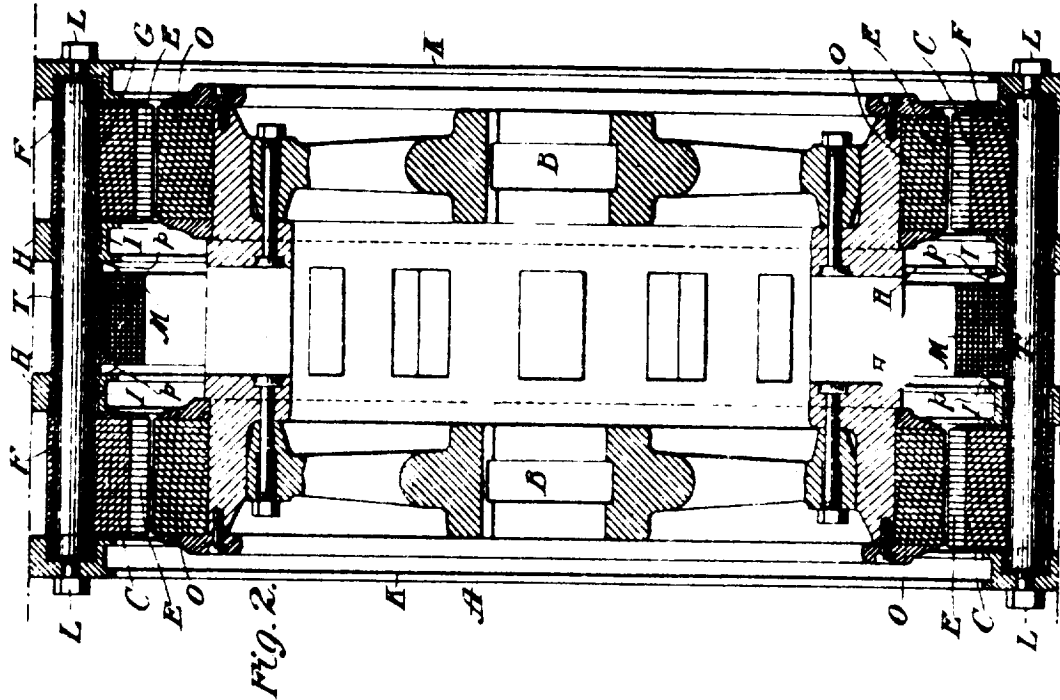
A PATENT DRAWING FOR A HOMOPOLAR INDUCTOR A. C. GENERATOR

(No Model.)

J. F. KELLY.
DYNAMO ELECTRIC MACHINE.

No. 559,531.

Patented May 5, 1896.



WITNESSES:
Frank S. Ober
C. B. Eaton

INVENTOR
John F. Kelly.

BY
H. B. Brown
ATTORNEY

FIGURE A 47 b

BIBLIOGRAPHY OF PAPERS ON HOMOPOLAR
INDUCTOR AC GENERATORS

N. Oboukhoff, "A Method of Designing Medium and High-Frequency Alternators", Oklahoma Agricultural and Mechanical College Publication Vol. 1 No. 7, December, 1930.

J. H. Walker, "The Theory of the Inductor Alternator", Journal of IEE Vol. 89, Pt. 2, 1942, pp 227-41.

J. H. Walker, "High-Frequency Alternators", J of IEE, Vol. 93, Pt. 2, 1947, pp 67-80.

A. Mandl, "Short-Circuit Characteristics and Load Performance of Inductor Alternators", J of IEE, Vol. 94, 1947, pp 102-117.

J. T. Duane, "A Brushless D-C Generator for Aircraft Use", AIEE Trans. Paper No. 58-916.

J. T. Bateman, "A Solid-Rotor A. C. Generator for High-Temperature Electrical Systems", AIEE Trans. Paper No. 59-848.

H. Weier, A. Finzi, "Medium Frequency Converters", Brown Boveri Review, Vol. 45, No. 1, Jan, 1958.

N. W. Bucci, C. L. Doughman, F. C. Stump, "Space Electrical Power Systems Study", Progress Report, 4th Quarter Contract NAS5-1234.

E. J. Davies, N. P. Pedersen, "An Experimental and Theoretical Study of the Lorentz-Type Inductor Alternator Under Load", IEEE Conf. Paper No. 63-341.

E. A. Erdelyi, F. C. Trutt and R. E. Hopkins, "Flux Distribution in Saturated High-Speed Homopolar Inductor Alternators with Purely Reactive Loads", IEEE Trans. on Aerospace, Vol. AS-1 No. 2, pp 407-411.

E. A. Erdelyi, F. C. Trutt, "No Load Flux Distribution in Saturated High-Speed Homopolar Inductor Alternators", IEEE Trans. on Aerospace, Vol. AS-1 No. 2, pp 417-429.

G. A. Osborn, T. W. Salmon, "Application of the Electromagnetic Generator to Space Power System", IEEE Trans. on Aerospace, Vol. AS-2, pp 857-866.

E. A. Erdelyi, F. C. Trutt, and R. E. Hopkins, "Saturated High-Speed Homopolar Alternators at Balanced Loads", IEEE Trans. on Aerospace, Vol. AS-2, April, 1964, No. 2, pp 929-935.

K. K. Syrti, E. A. Erdelyi, "The Effects of Slotting on the Flux Distribution in Saturated High-Speed Homopolar Inductor Alternators", IEEE Trans. on Aerospace, Vol., AS-2, April, 1964, No. 2, pp 937-947.

R. W. Landgraff, E. A. Erdelyi, "Influence of Air-Gap Curvature on Flux Distribution in Saturated Homopolar Alternators", IEEE Trans. on Aerospace, Vol. AS-2, April, 1964, No. 2, pp 904-912.

Robert Pohl, "Theory of Pulsating-Field Machines", Journal of the Institution of Electrical Engineers, Vol. 93, Part II, February, 1946, pp 37-47.

A. Mandl, "Short-Circuit Characteristics and Load Performance of Inductor-Type Alternators", Journal of the Institution of Electrical Engineers, Vol. 94, Part I, April, 1947, pp 102-17.

PERMANENT MAGNET, A. C. GENERATORS

PERMANENT-MAGNET, A-C GENERATOR

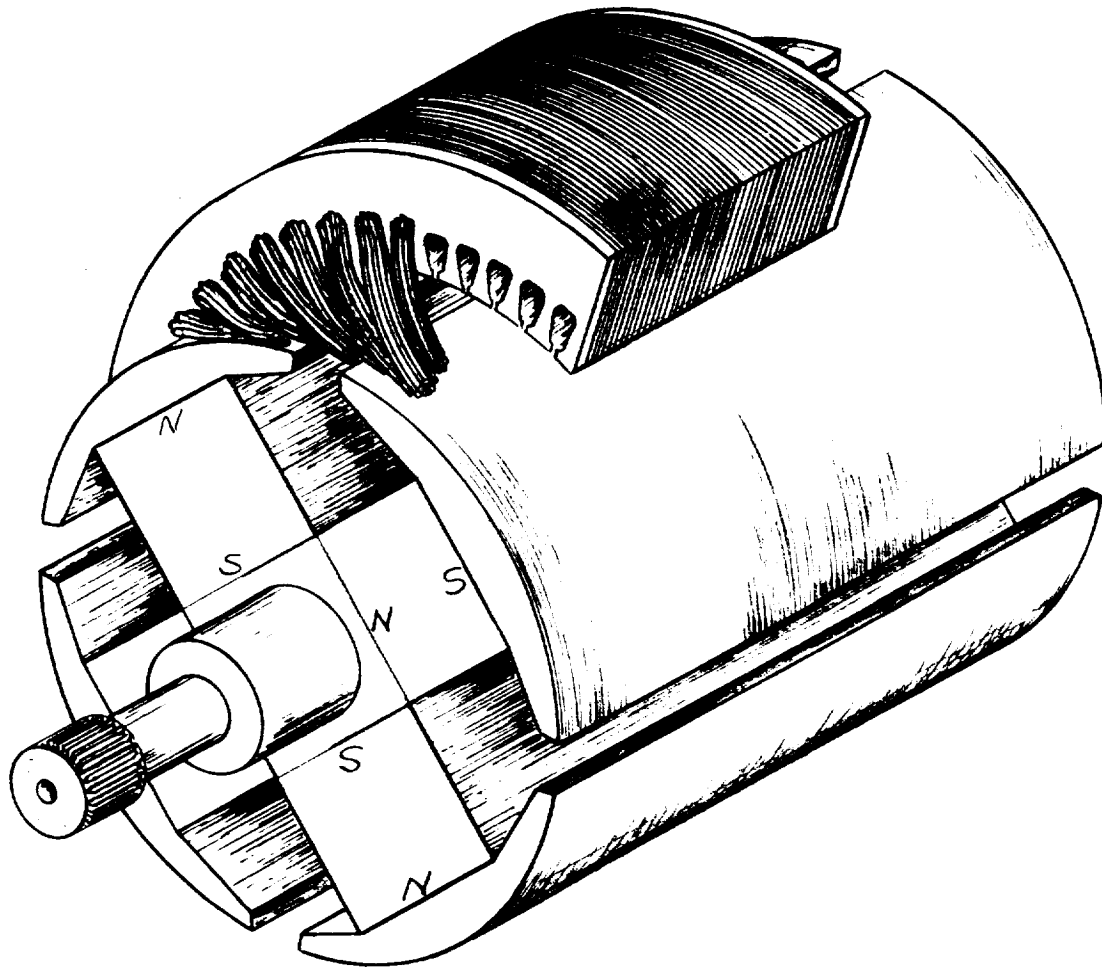


FIGURE A 48

PERMANENT MAGNET GENERATORS

GENERAL DISCUSSION

One of the first, if not the first, low voltage A.C. generator ever built was a permanent magnet generator built by M. Hyppolyte Pixii and demonstrated before the Paris Academie des Sciences in 1832. *

FIG. A 50 is the photograph of a replica of the Pixii machine, which had an axial air gap. FIG. A 51 is a patent drawing of a recently developed permanent magnet generator, which also has an axial air gap.

Permanent magnet generators were at first built for demonstration and for amusement, later for telegraph use, for lighting, for telephone ringing and engine ignition.

P.M. Generators built by a man named Frederick H. Holmes were installed in 1857 and 1858 to power arc-lights in lighthouses at Blackwell, South Foreland, and Dungeness, England. These generators operated at 90 rpm and produced about 1.7 kw each. (See History of Electrical Engineering, Part 3, Journal of IEEE, May, 1955, pp. 280-286.)

* The first electric generators were the influence machines (or electrostatic generators.)

The permanent-magnet generators operate on the same principle as the wound-pole electromagnetic generators. The permanent-magnet replaces the iron pole and exciting coil and furnishes the flux that the iron pole and exciting coil would have furnished.

A permanent-magnet generator can be made in nearly every type of generator known. Some, if not most, of the configurations would be impractical and the most often encountered PM generators are DC generators with commutators salient pole AC generators with rotating magnets, flux-switch generators with stationary magnets, round rotor or non-salient-pole generators with rotating magnets. The last named generator is usually encountered as a tachometer.

Alnico 5 and Alnico 6 magnets are the most widely used permanent magnets because they are the strongest magnetically of all the well-known production materials. These materials yield at their ultimate strength and are hard and brittle. Cast Alnico 5 has an advertised tensile strength of 5450 PSI and cast Alnico 6 has an advertised tensile strength of 23,000 PSI. Both of these materials can easily have casting flaws and are seldom trusted to their tensile limits.

GENERAL DISCUSSION (Contd)

Until 1910, the magnets of the PM generators were almost always made of high carbon steel. Then after 1910, alloy steels began to be used more commonly and magnet performance was improved. Finally, in 1931, a Japanese Metallurgist named Mishima discovered an alloy system of aluminum, nickel, iron, and Cobalt. The Alnicos developed from this alloy system have made high performance permanent magnet generators possible.

SOME OF THE ROTOR TYPES USED IN A-C
PERMANENT - MAGNET GENERATORS WITH
RADIAL AIR - GAPS

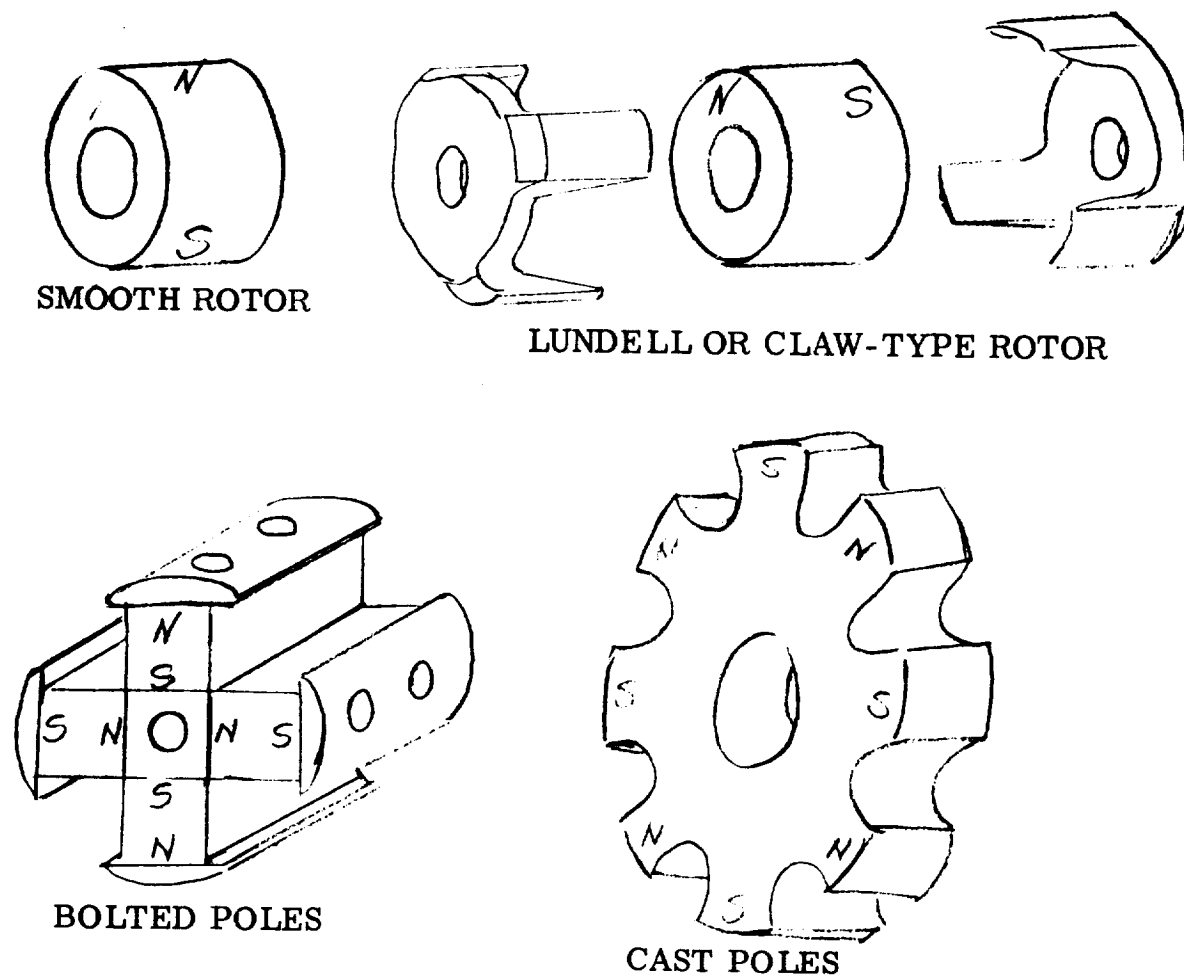
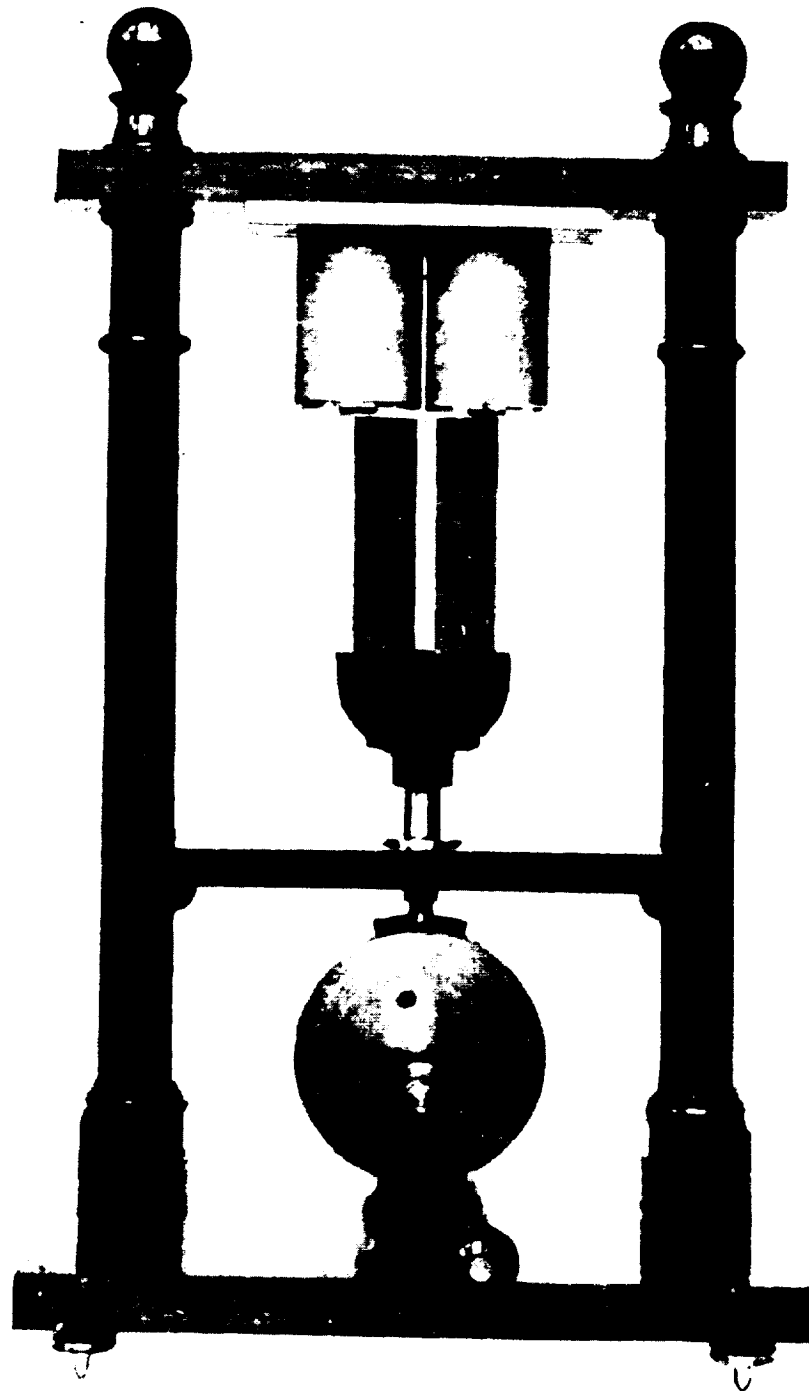


FIGURE A 49

THE FIRST (?) AXIAL AIR-GAP
PERMANENT MAGNET GENERATOR



1 *Replica of Pixii hand-driven magneto-electric generator
(about 1832)*

Crown copyright. From an exhibit in the Science Museum,
South Kensington.

FIGURE A 50

A PATENT DRAWING FOR A
PERMANENT MAGNET, AXIAL AIR-GAP GENERATOR

Aug. 21, 1962

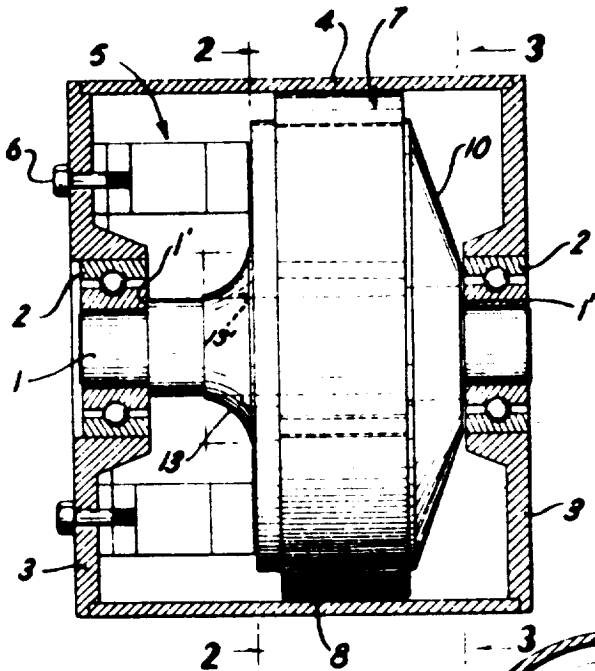
W. KOBER

3,050,648

ROTOR AND METHOD OF ASSEMBLY THEREOF

Filed Jan. 14, 1959

FIG. 1



Having fully disclosed and completely described my invention, and its mode of operation, what I claim as new is
1. A dynamoelectric rotor comprising, a shaft journaled for rotation about substantially its lengthwise axis, an end plate fixed to said shaft for rotation therewith, a rotor body carrying magnets positioned on said shaft against said end plate, a pole piece structure positioned against the opposite end of said rotor body, and a collar gripping said shaft circumferentially thereof and clamping said pole piece structure and said rotor body against said end plate for rotation therewith.

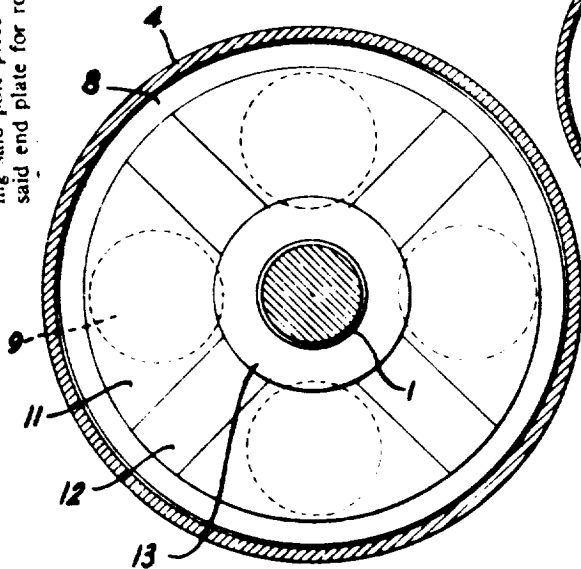


FIG. 2

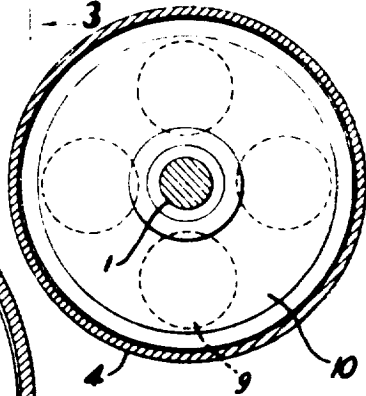


FIG. 3

INVENTOR
WILLIAM KOBER

BY

Beau, Brook, Buckley & Beau
ATTORNEYS

PERMANENT MAGNET GENERATORS

DESCRIPTION OF PM GENERATOR OPERATION

Permanent Magnets

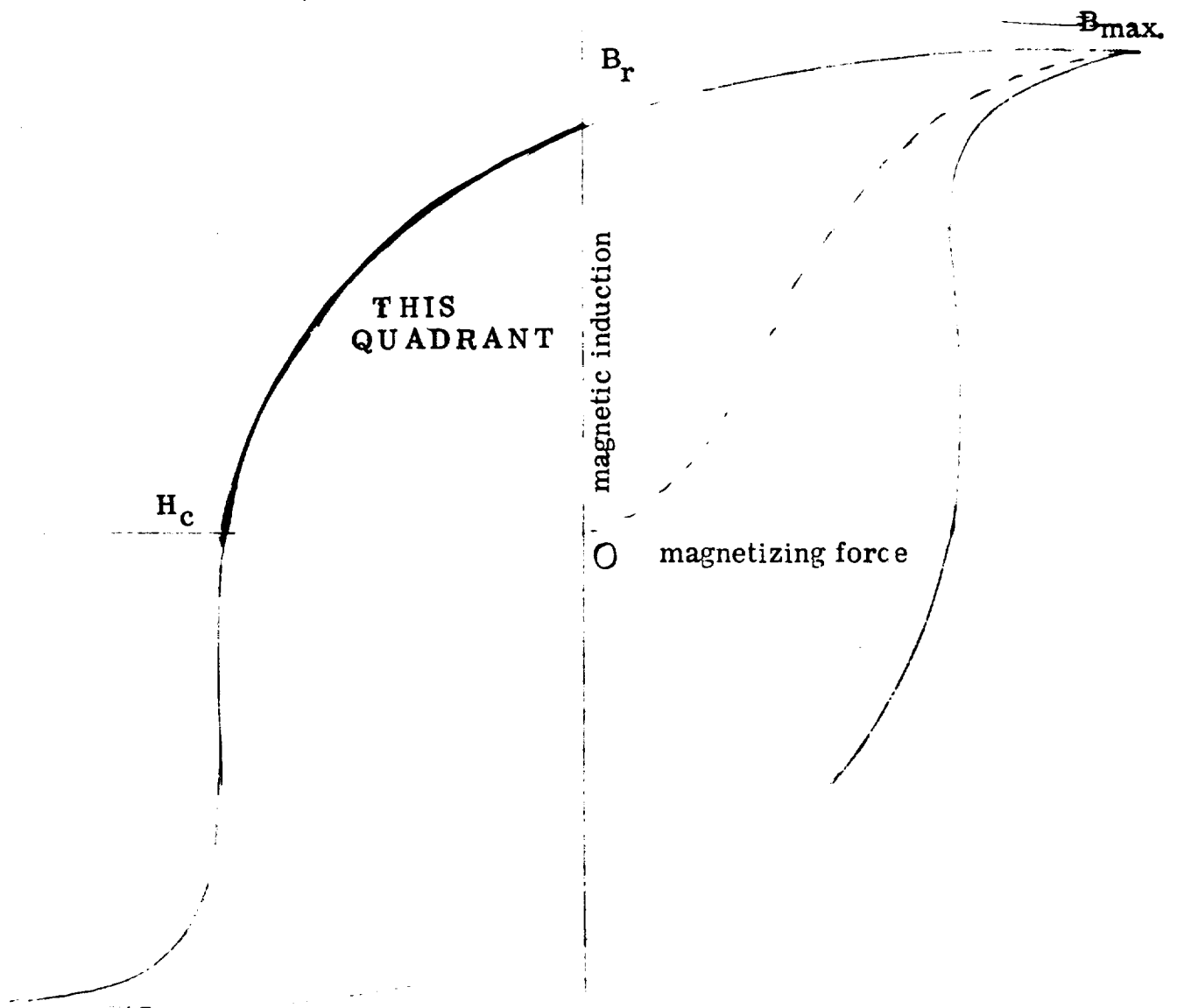
All permanent magnets resist changes in their magnetic state. It is this property that makes the permanent magnet useful.

Most early-day permanent magnets were made of high carbon steel in hard condition. This high carbon steel was used in magnets for magnetos in engine ignition systems, in telephone ringers, toys, etc. It is still used in some applications.

Newer permanent magnets are alloys of nickel, aluminum, Cobalt, copper and iron. The alloy system is called Alnico and magnets made from these alloys are so much stronger than other commercial magnet alloys, that high performance PM generators almost always use them.

A ceramic permanent magnet material is sometimes used for generators when low-cost or high coercive force is of primary importance. The ceramic magnets are used mostly on small d. c. generators and are not of interest for this study.

All good permanent magnet materials have large hysteresis loops and in designing permanent magnet generators one quadrant of the hysteresis loop is used to predict performance.



HYSTERESIS LOOP OF A
PERMANENT MAGNET

FIGURE A 52

If a toroid or closed annular ring of permanent magnet steel is excited to its saturation value and then the exciting mmf is removed, the flux density will decrease from the maximum saturation induction value B_{max} to the residual induction B_r . For the flux density in the ring to stabilize at the value B_r , there must be no air gap in the toroid or closed magnetic circuit. If the magnet material is Alnico 5, the flux density in the ring under these conditions will be 78,000 lines per square inch.

If an air gap is introduced in the toroid, the ampere turns required to send flux across the air gap must be supplied by the magnet and this causes the magnet flux density to decrease, still along the hysteresis loop, to some lower value. The actual value depends upon the length of the air gap and upon the length of the magnet.

Think of the magnet as furnishing a certain number of ampere-turns of mmf per inch of magnet. Then when an air gap is introduced into the magnetic circuit, each inch of magnet will contribute its portion of the mmf required to force flux across the air gap.

If an air gap of .010 inches length is introduced in a magnet toroid having a magnet length of ten (10) inches, each inch of magnet will contribute 24 ampere turns toward forcing 77 Kilolines/in² across the gap. Ignore fringing!

$$\text{mmf} = B_g \frac{l_g}{u} = 77000 \frac{(.010)}{3.19} = 241 \text{ AT}$$

The magnet AT/inch = $\frac{241}{10} = 24$ and the demagnetizing effect on the magnet is negligible.

If the air gap length is .100" and the magnet length is 10 inches, the mmf required is only 241 ampere-turns per inch of magnet and the demagnetizing effect is still negligible. If, however, the air gap is .100 inches and the magnet length is only 1.0", the ampere-turns required for the one inch of magnet to force 77 KL across the gap is 2410 which is two times the ampere-turns needed to demagnetize the Alnico 5 magnet completely.

What actually happens in the case of a 1.0" magnet and a 0.100" air gap is that the magnet demagnetizes to a point on the hysteresis curve where the mmf available will force the now lower flux density across the gap. For Alnico 5, the magnet density will be 37 KL/in² and the mmf/inch = 1200 AT.

In the case of a 1.0" magnet and .100" gap, if the gap is later closed, the magnet density will increase along a minor hysteresis loop having the same slope as the main loop and in this example the magnet density will be 45 KL/in² when the gap is completely closed.

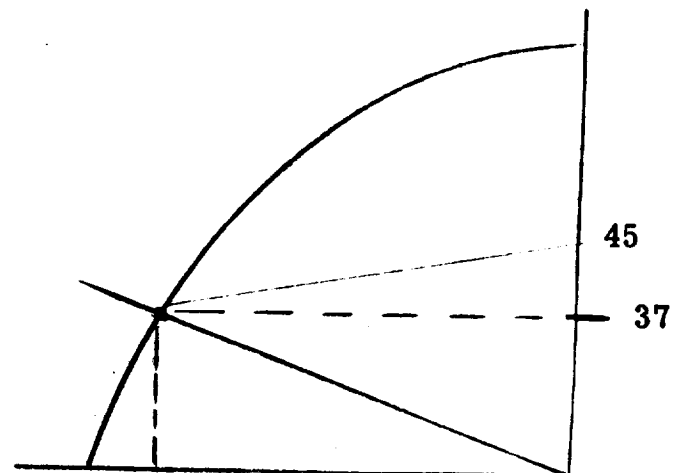
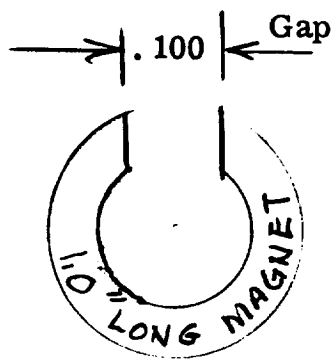
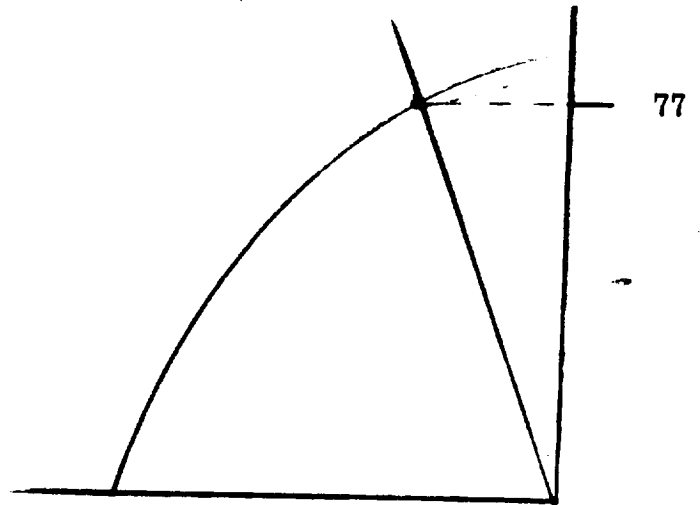
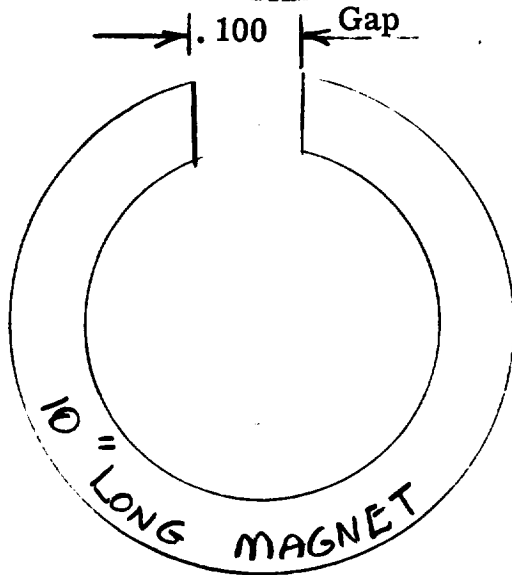
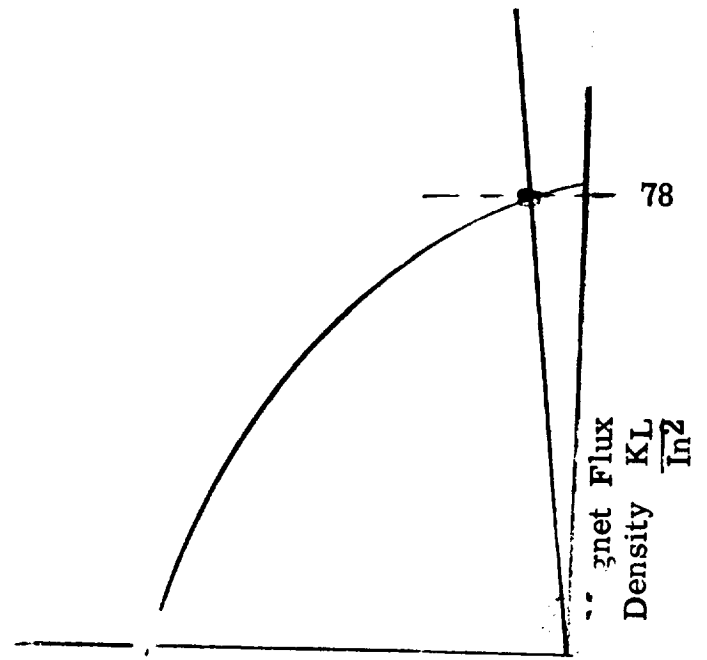
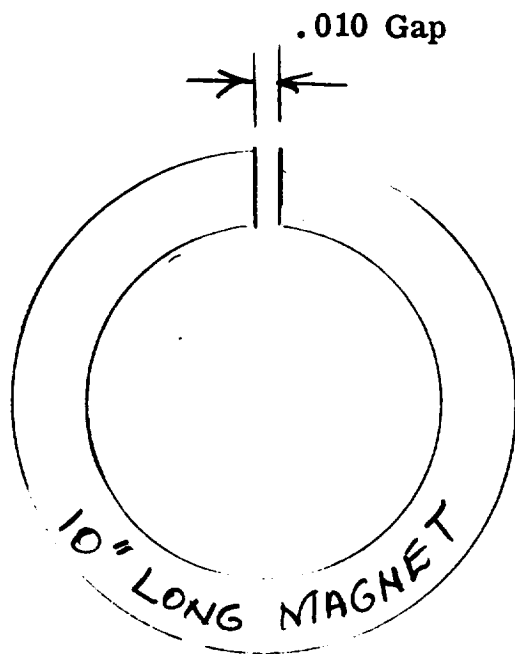


FIGURE A 53

When a permanent magnet rotor is constructed and magnetized, then taken out of the magnetizing fixture without a keeper or metal piece to close the magnetic circuit, the magnet density drops to some low value similar to the 1.0" long magnet with .100" air gap. The magnet rotor is said to be air stabilized and the flux circuit is through leakage paths in the air. If the leakage is high enough, the magnet density will remain fairly high. If there were no leakage, the magnet would demagnetize almost completely.

When the air stabilized magnet is placed in a stator, the air gap is partially closed and the magnet density increases along the minor hysteresis loop to a new value that depends on the length of the new air gap. From this time on, the permanent magnet operates along the same minor hysteresis loop unless the demagnetizing ampere-turns of the stator produced by the load on the stator become too great and further demagnetize the magnet. If the armature reaction due to the load does demagnetize the magnet further, the machine is said to be load stabilized and if short circuits are repeatedly applied to the output leads, the magnets are said to be short circuit stabilized.

All permanent magnet materials have large hysteresis loops and, in general, those permanent magnet materials having the largest hysteresis loops are the most useful.

When a magnet is properly applied and stabilized, the level of maximum flux is fixed and the magnet mmf is fixed. To reduce the voltage generated at fixed speed in a permanent magnet generator for a given load condition, it is customary to reduce the permeance of the flux path so that less flux flows through the output windings and less voltage is generated. To increase voltage, the converse conditions apply.

When no controls are applied to a PM generator, the voltage current characteristics curve looks like this:

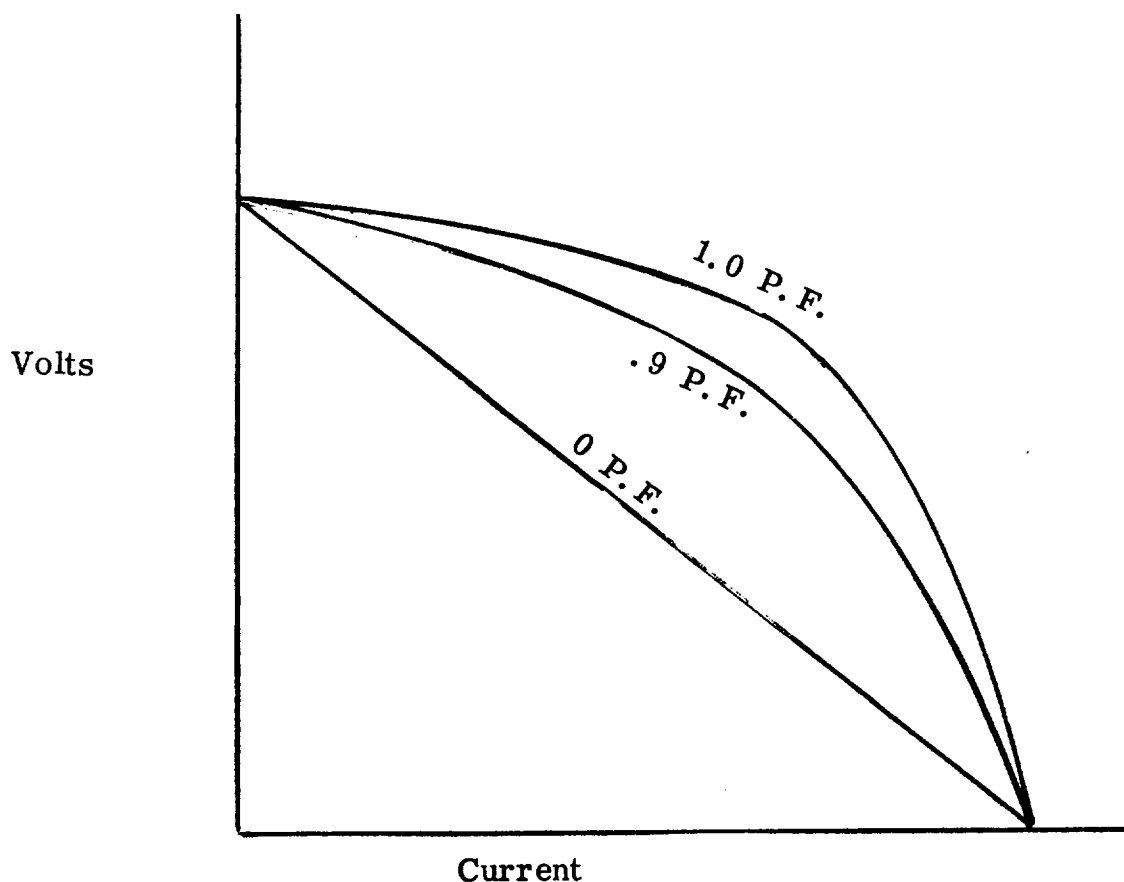


FIGURE A 54

\

If a permanent magnet generator is required to produce a constant voltage from no load to full load, at a fixed speed, the no load voltage is usually depressed by saturating part of the iron circuit so that less flux links the output winding at no load.

One widely used method of saturating part of the iron circuit is called back-iron control or back-iron saturation and U.S. Patent No. 2564320 issued to N. W. Brainard describes this scheme. Voltage control by this method is usually limited to 10 or 15% of maximum.

Another control method varies the air gap length. In radial gap machines, the rotor is sometimes tapered and designed so that it can be moved axially to increase or decrease the air gap length and the flux linkages in the winding.

U.S. Patent No. 2861238 issued to W. Kober describes a mechanism for adjusting the air gap of an axial gap permanent magnet generator. By adjusting the length of the air gap, the no load voltage can be varied from its maximum to nearly any desired lower level. The air gap control method is effective though relatively slow in response.

When magnets are attached to a rotor and magnetized in a fixture, the magnetic material is subjected to a high magnetomotive force

(mmf) or a high number of ampere turns per inch of magnet. About 4000 ampere-turns per inch are applied to Alnico 5 magnets and the Alnico saturates from zero flux along a saturation curve that looks like this:

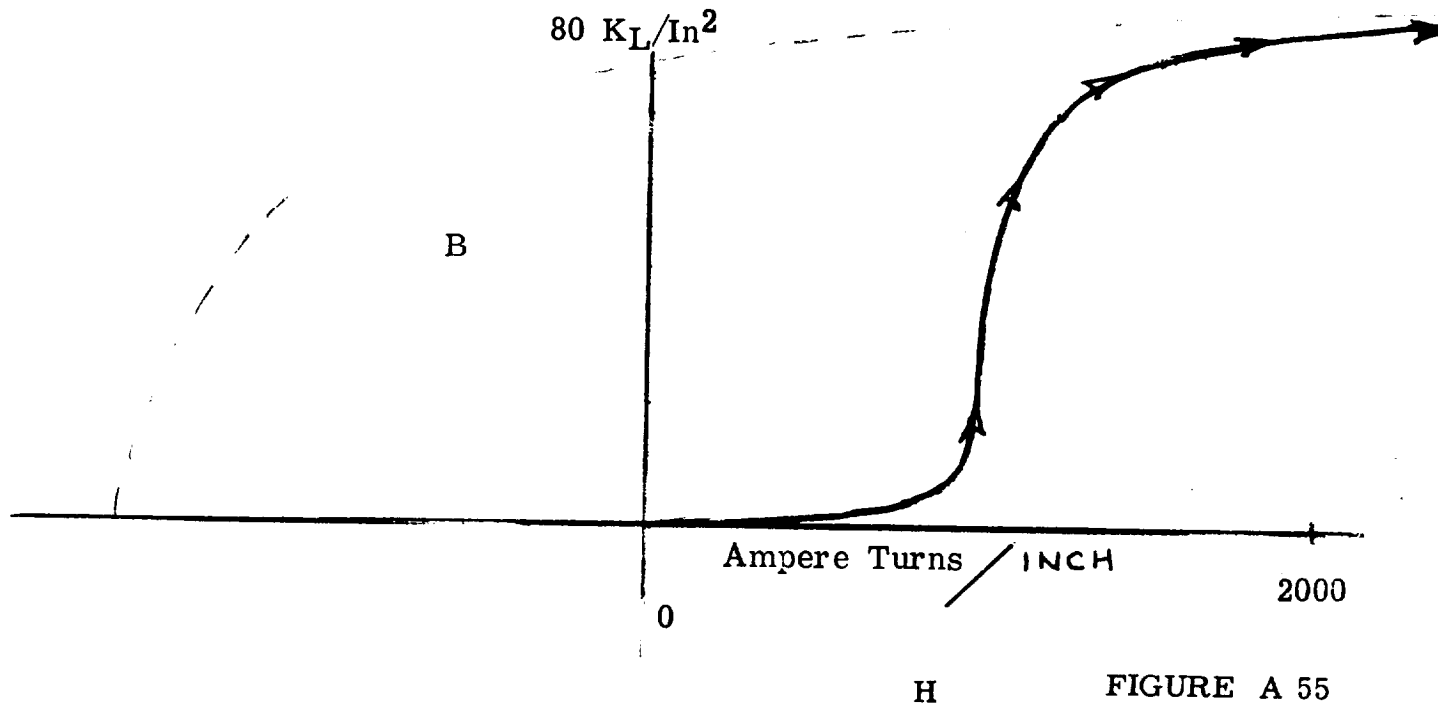


FIGURE A 55

As the current in the magnetizer coil is reduced to zero, the flux in the magnet reduces along a hysteresis loop to a residual value B_r .

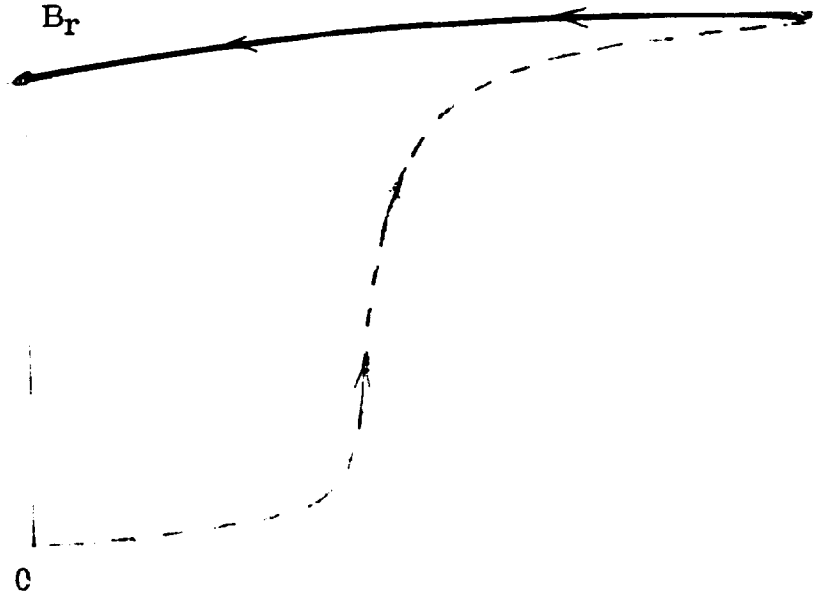


FIGURE A 56

As long as the magnet or magnets are in a closed, iron circuit such as the magnetizer or a Keeper, the flux density in the magnet will remain at the value B_r . The magnet is not useable under a closed-circuit condition and an air-gap must be introduced in order to use the magnet.

If the rotor is inserted in a wound stator, and a keeper is kept on the magnets until the magnets are in the stator, the air gap and additional permeance that is introduced will be minimal.

The flux density in the magnet may have dropped to a value about like this:

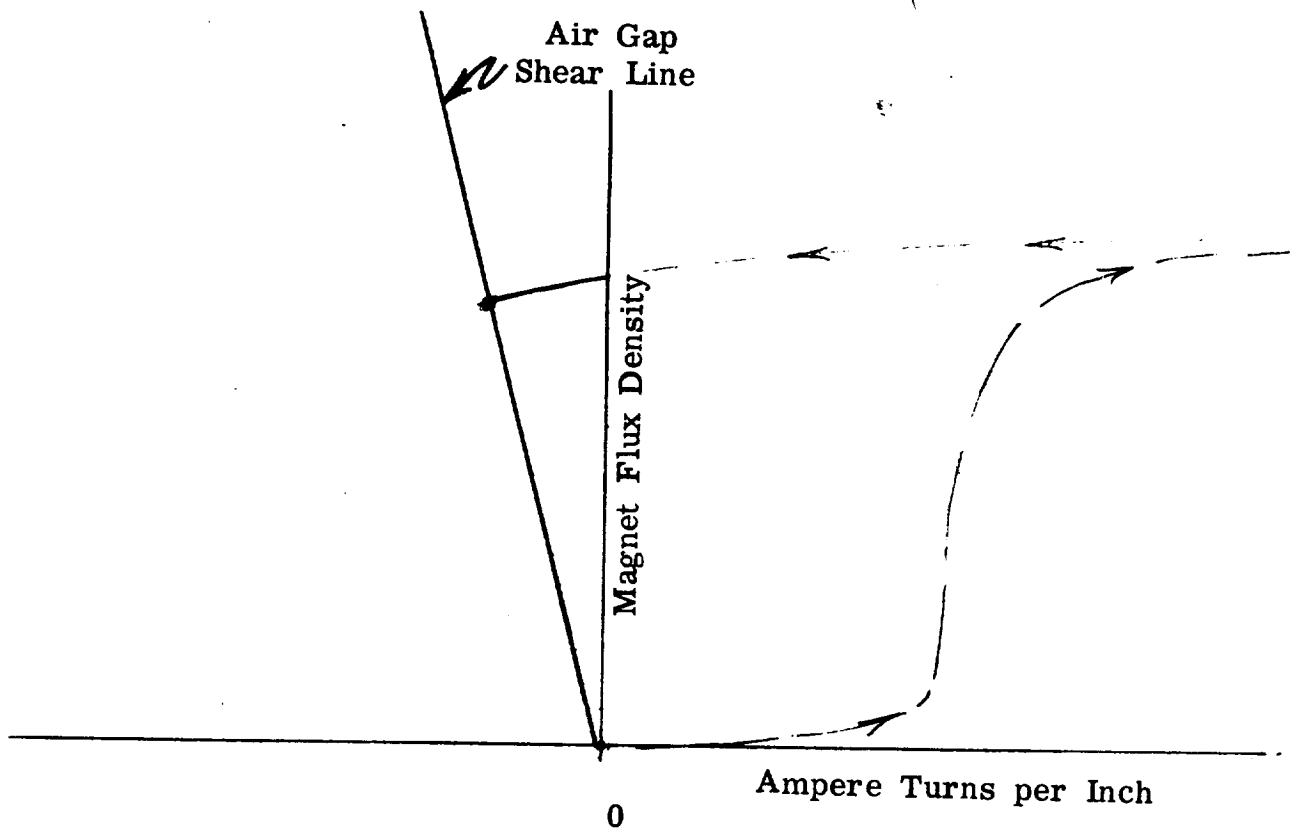


FIGURE A 57

The flux in the circuit is now at its maximum useable level.

When load is applied, the demagnetizing ampere-turns from the stator oppose the mmf of the magnet and the effect is the same as if the air gap line were shifted over an amount equal to the stator demagnetizing mmf (as related to the magnets per inch.)

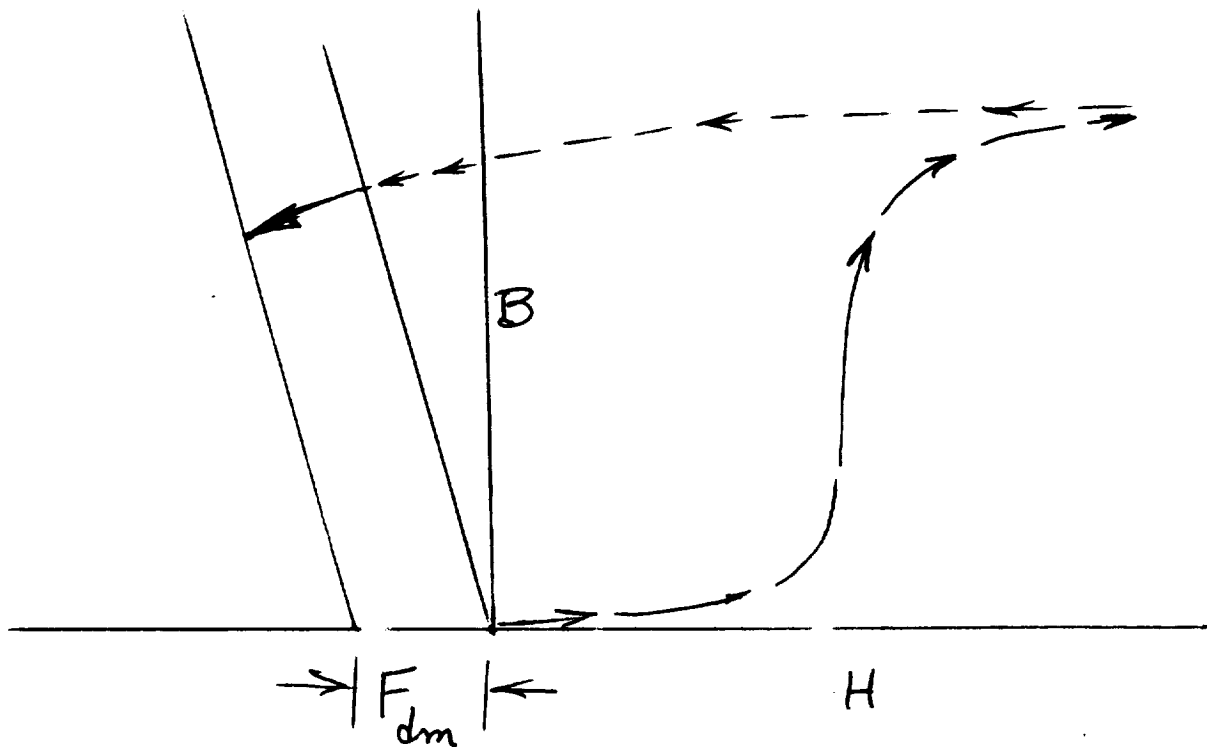


FIGURE A 58

Under the stated conditions, the flux density in the magnet never returns to the value it had before load was applied. The flux density returns to a slightly lower value, along a minor hysteresis loop and the generator can be said to be load stabilized. Some tachometers are treated this way and sometimes a larger PM generator for a special application is so treated.

If a short-circuit is applied to the generator, it experiences the maximum demagnetizing force that is possible except for transient demagnetizing forces or external demagnetizing forces. If repeated short circuits are applied by switching them on and off, the

magnets are subjected to many transient demagnetizing mmf's and the magnets are probably stable for most of the possible conditions of loading. The generator is said to be short circuit stabilized. The flux density in the magnets does this:

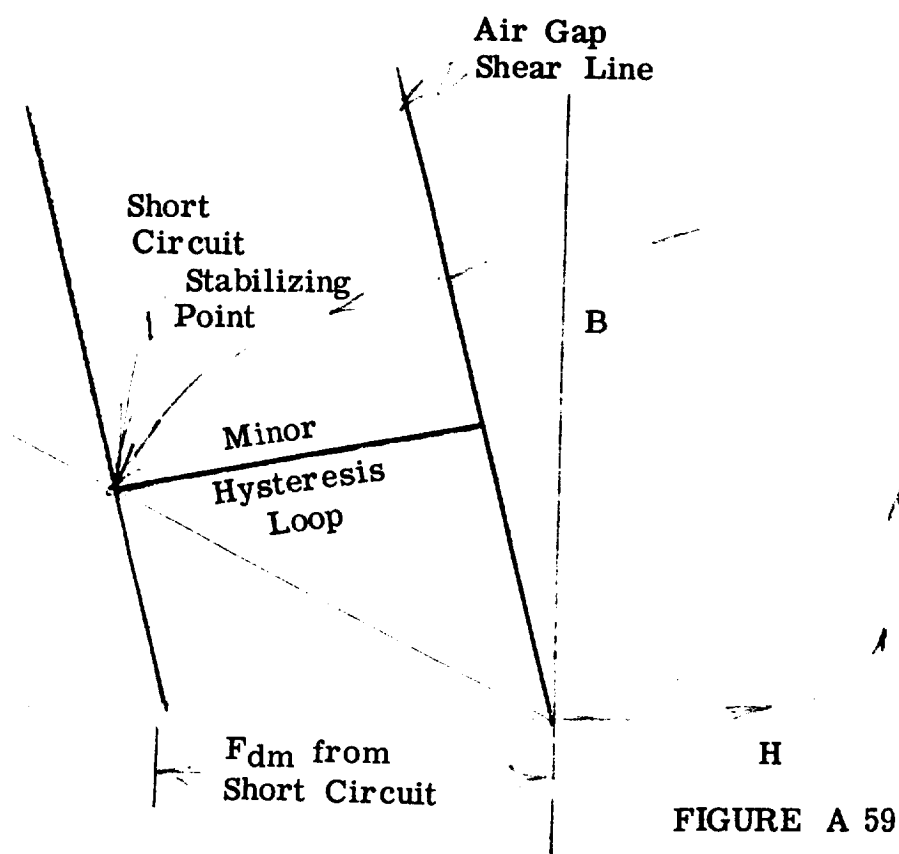


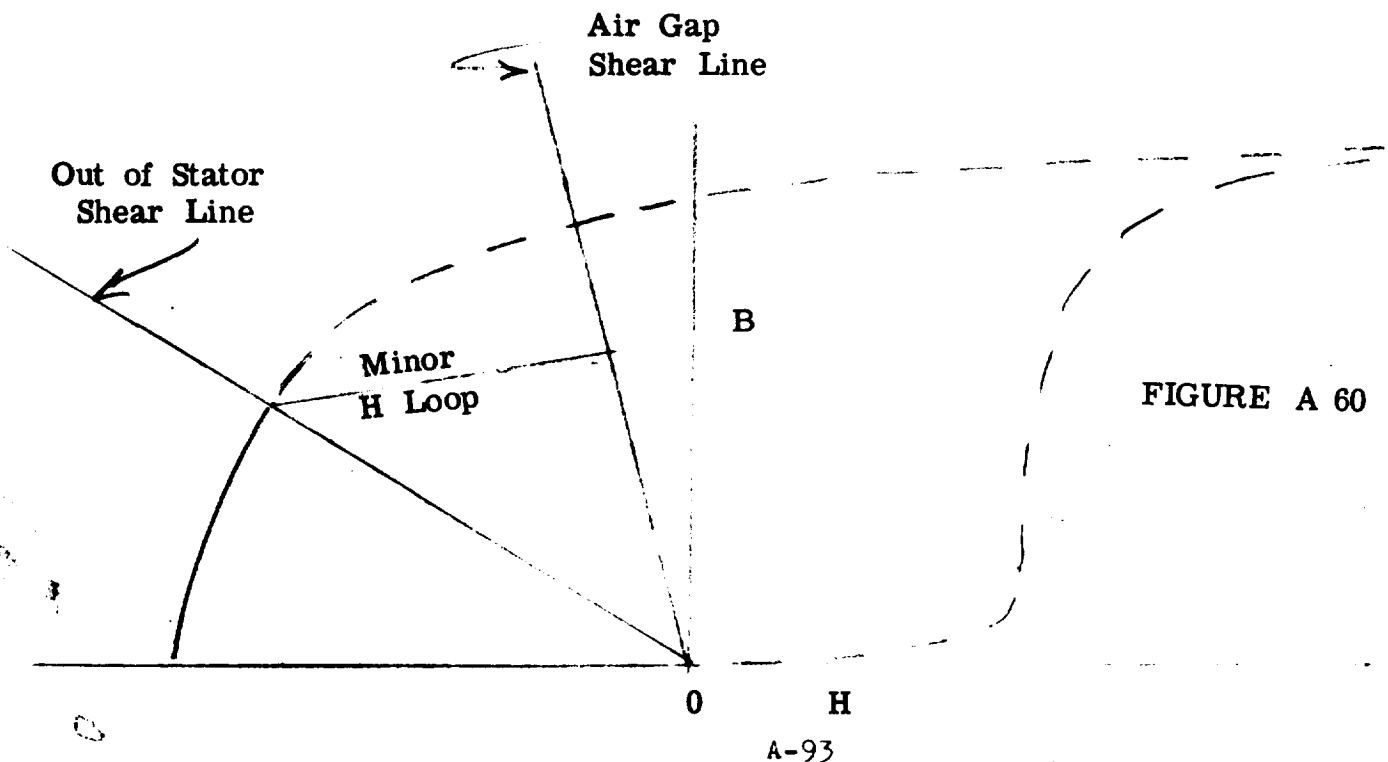
FIGURE A 59

If no other severe disturbance affects the magnet adversely, the flux in the magnet will always be a value on the minor hysteresis loop between the air-gap line (at no load) and the short circuit line.

A generator can be designed so that short circuit will demagnetize the magnets almost completely. Then the transients normally associated with testing may cause the magnets to demagnetize beyond their useable strength. When that happens, the rotor must be remagnetized.

If the rotor is taken from the magnetizing fixture without a keeper on it, the circuit for the magnet flux is through the air and, in effect, a huge air gap has been introduced into the circuit. The air gap is the leakage path of the magnets when the rotor is out of the generator stator. This is called air stabilization of the rotor and the permeance of the leakage path air gap is called out-of-stator permeance.

The magnet flux density is represented like this:



Right here, we define the permeance terms that are used from here on, even though they are defined later.

Out-stator or Out-of-stator Permeance - This is the permeance of the pole-to-pole flux when the rotor is in air. All of the flux paths are in air and all of the flux is leakage flux since no stator or output winding is present to utilize the magnet flux. The symbol is P_o .

In-Stator Permeance - When the rotor is placed in the stator, some of the flux enters the stator to link the output winding and this is the flux that becomes useful flux.

Some flux still leaks from pole-to-pole and can never be utilized. The permeance path for the never-to-be-utilized leakage flux that is leaking from pole to pole when the rotor is inserted in the stator is called In-stator permeance. It is a leakage permeance and when you see the words in-stator permeance in this document they mean the permeance of the in-stator leakage paths of the rotor.

The symbol is P_i .

Air-gap Permeance - The permeance of the air-gap. The symbol is P_g .

Working Air-gap Permeance - The total apparent permeance of the working air-gap. It is the sum of the permeances of the air-gap and the in-stator leakage flux paths. The symbol is P_w .

Magnet Spatial Permeance - This is the adjustment factor to convert the permeance values to the proper scale for use in the conventional hysteresis loop representation. The symbol is P_m .

NOTE --- In the illustrative drawings showing the permeance shear lines, the air-gap shear line is the air-gap permeance plus the in-stator leakage permeance or P_w .

If no further adverse operating conditions are imposed on the magnet, the flux density in the magnet will always be a value on the minor hysteresis loop shown, between the out-stator leakage line and the air gap line.

When the rotor is inserted in the stator, the path for the magnet flux includes the leakage paths between the rotor magnets and around the ends of the magnets. This permeance path is called the in-stator permeance.

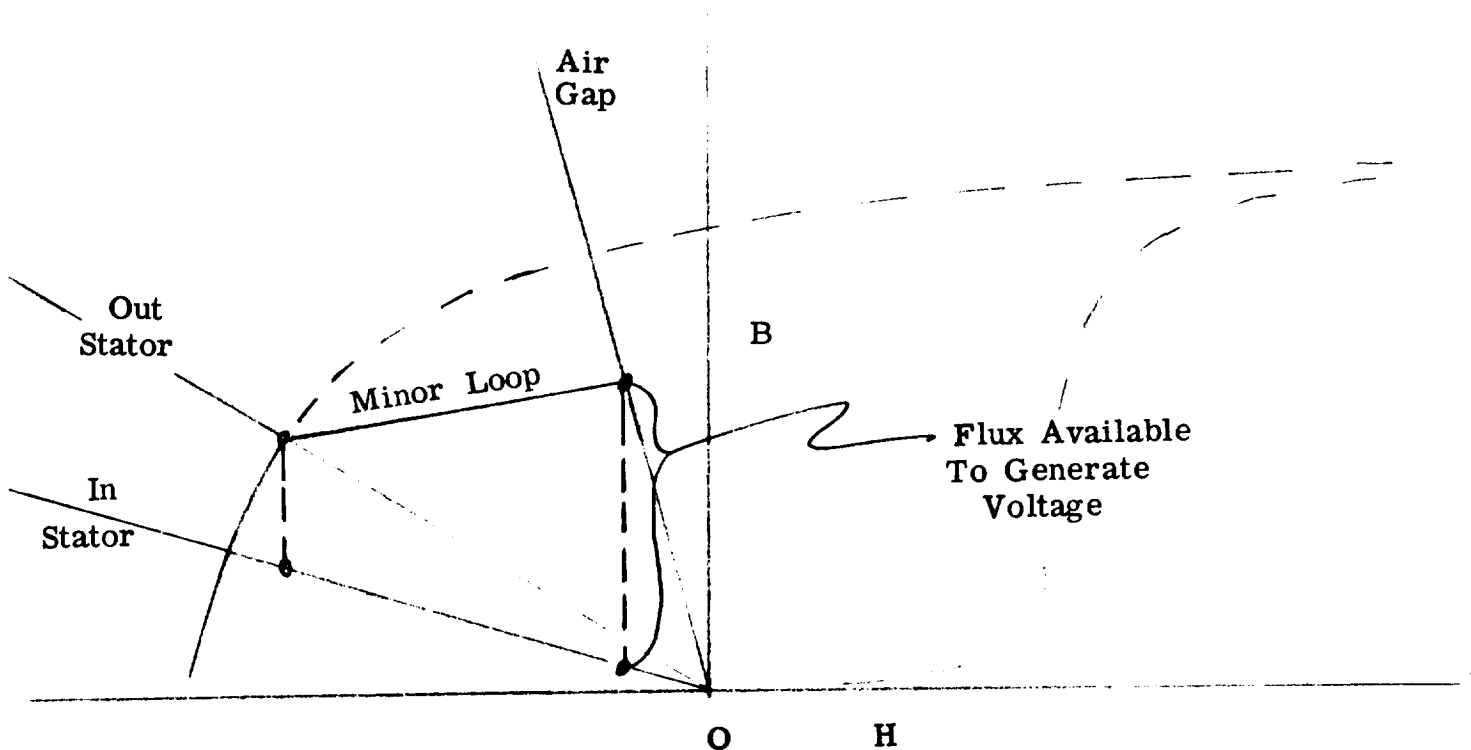


FIGURE A 61

The in-stator permeance is the out-stator permeance minus a few leakage paths. Some out-stator leakage paths no longer exist when the rotor is in the stator because the stator iron completes the flux circuit.

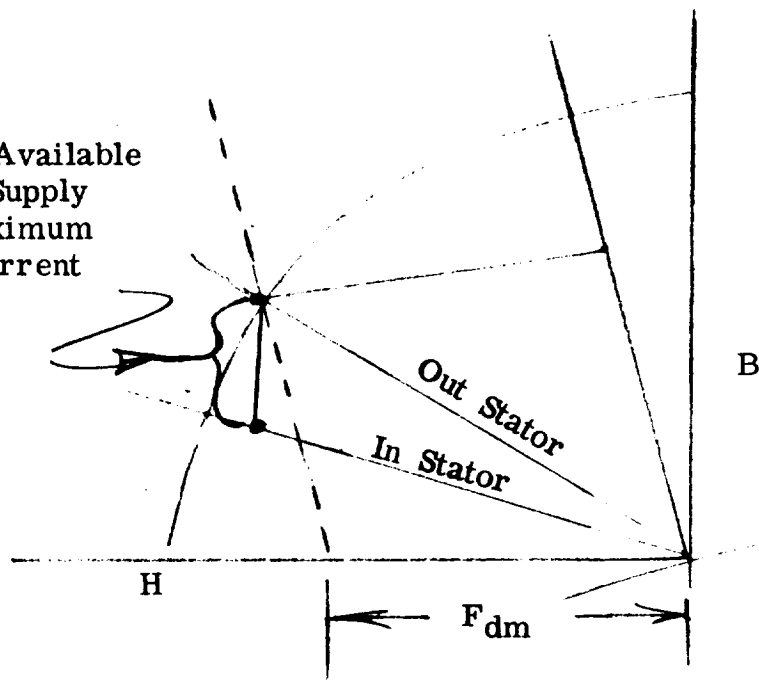
The out-stator permeance establishes the minimum flux level in the magnet and the in-stator permeance establishes the leakage flux level.

The difference between the in-stator flux, which is all leakage, and the maximum flux level determined by the minor hysteresis loop and the air-gap line, gives the value of useful magnet flux that is available to generate voltage.

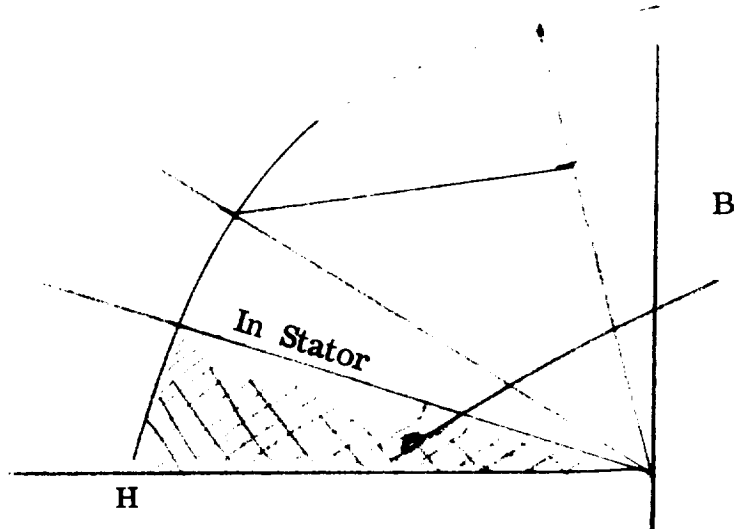
At zero P. F., as the permanent magnet generator is loaded, the demagnetizing mmf has the effect of shifting the air-gap line over and the flux available to generate voltage is decreased.

Flux Available
To Supply
Maximum
Current

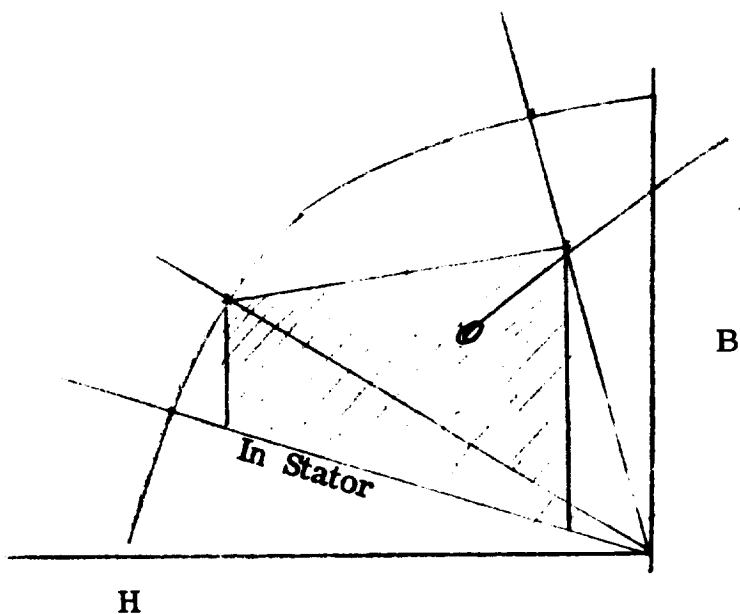
FIGURE A 62



Maximum Load or
short circuit that
can be endured with-
out demagnetizing
magnets.



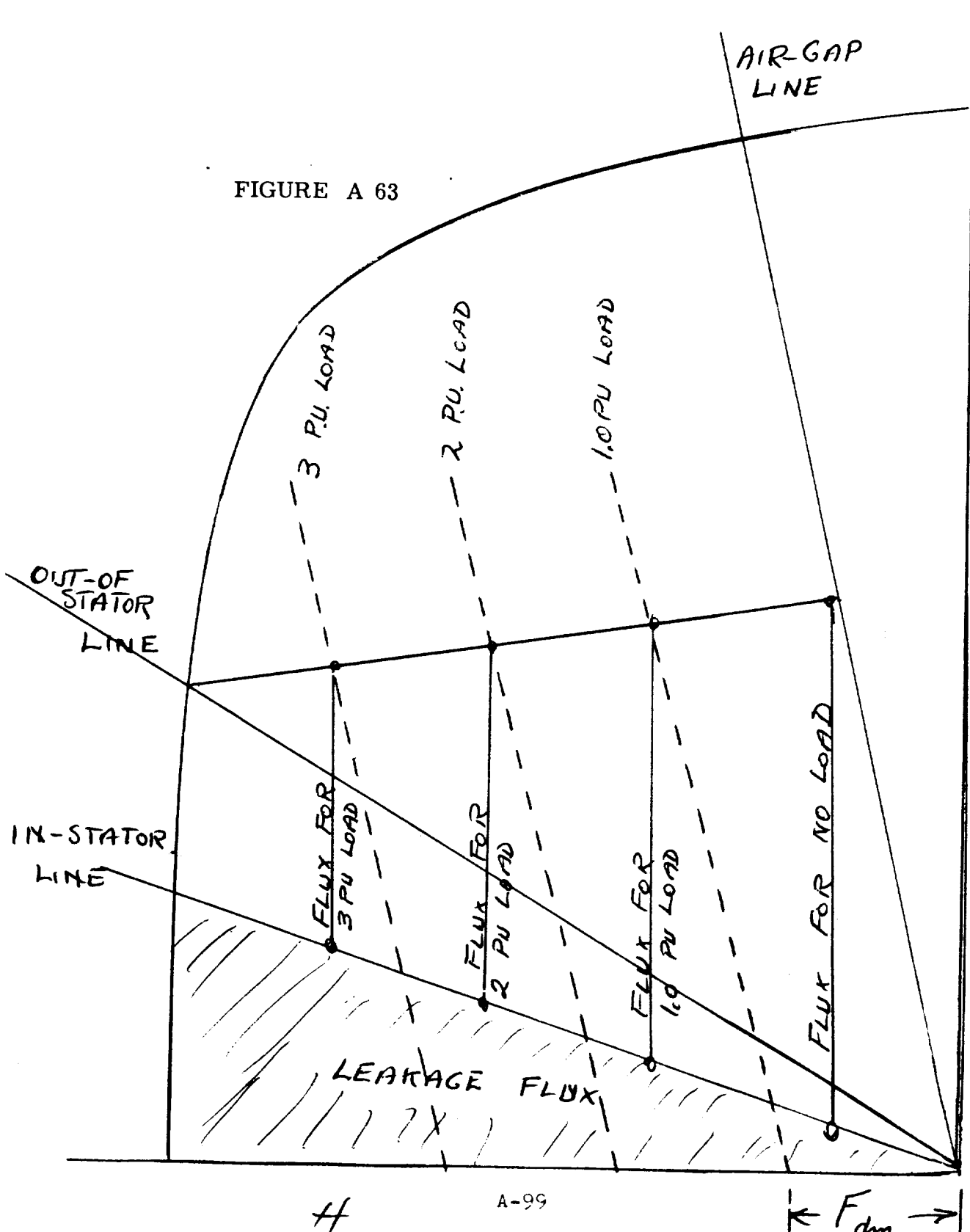
Shaded portion represents
leakage flux that cannot
be utilized.



Shaded portion represents
flux available to generate
voltage.

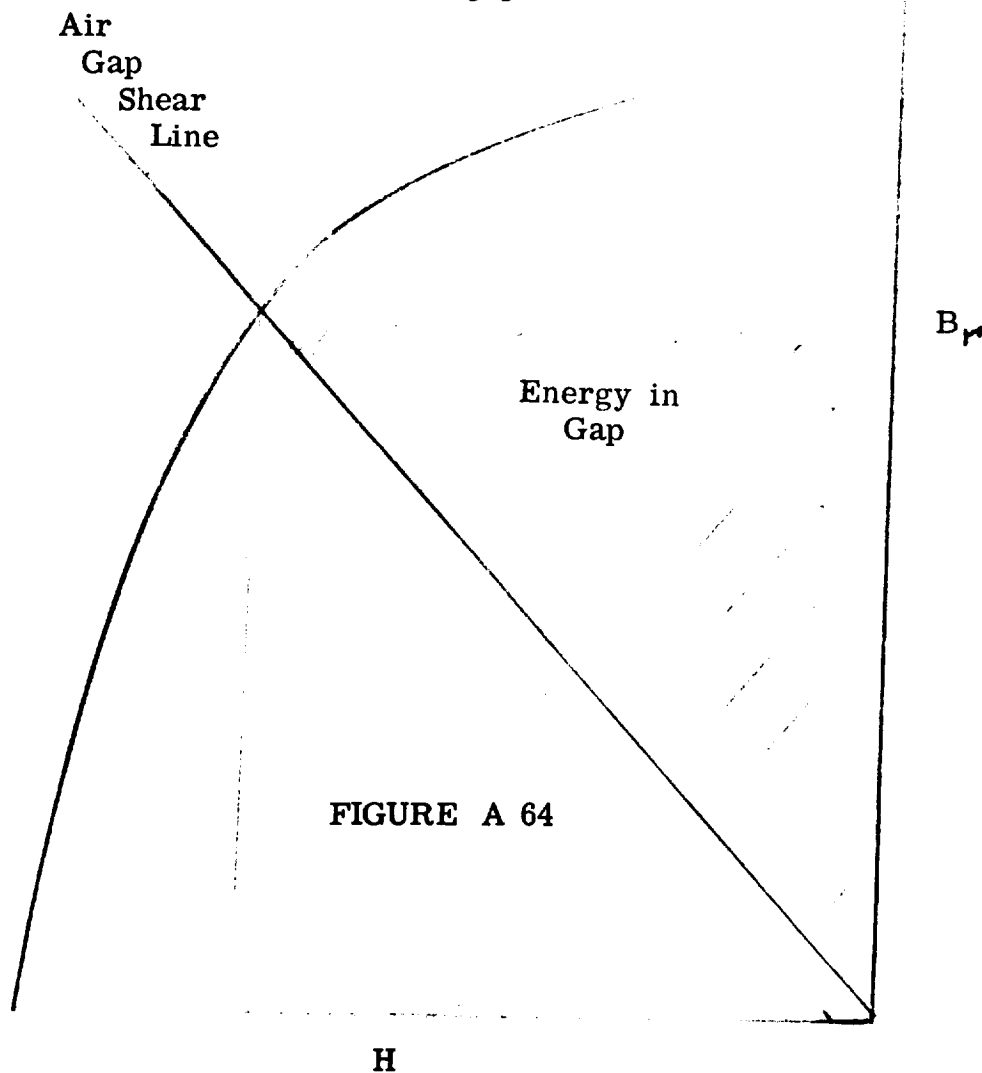
The IZ drop in the windings must be subtracted from the generated voltage and the remaining voltage is the load voltage.

FIGURE A 63



ENERGY STORAGE IN THE AIR-GAP

The maximum energy that a magnet can cause to be stored in an air gap is not the same as the energy product of the magnet. If the air gap permeance corresponds to the maximum BH point on the magnet curve, the energy that can be stored and extracted from the air gap will be the part of the BH rectangle above the air gap line or one-half the energy product of the magnet material. To show this take a closed magnetic circuit with the magnet density at its maximum point B_r . Under this condition, all of the magnetic flux is stored in the magnet and none is stored in an air-gap.



Now introduce a short air gap and gradually open the gap until the permeance line or shear line passes through the point on the hysteresis loop corresponding to the maximum energy product.

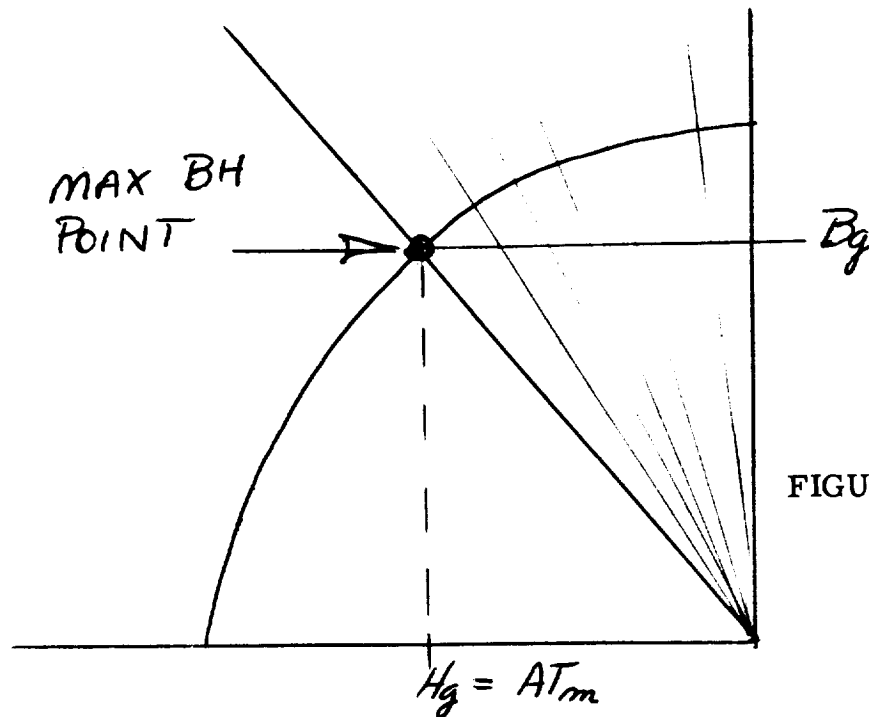


FIGURE A-65

We have gradually added flux to the air gap by increasing the gap.

The gap density, ignoring fringing is B_g and the attractive force between sides of the gap is $F = \frac{B_g^2 (\text{Area})}{2 u}$ Joules per inch where B_g is webers per square inch

A = Area of gap in in^2

u = Permeability of air in webers per ampere turn in an inch cube

or
$$F = \frac{B_g^2 A}{72} \text{ lb.}$$

Where B_g is Kiloline/ in^2

A is in square inches

The permeance of the air gap is $P_g = \frac{\mu A}{l}$ where

A = Area of gap and

l = Length of the gap

The slope of the permeance shear line through the magnet characteristic major hysteresis loop is

$$\frac{P_g}{P_m} = \frac{\frac{\mu A_g}{l_g}}{\frac{A_m}{l_m}}$$

Area gap = area magnet (ignoring fringing) in the special case of the gap in the magnetic circuit $\frac{P_g}{P_m} = \frac{\mu l_m}{l_g}$

$$B_m = B_g = (AT_m)_{\text{magnet}} \frac{\mu l_m}{l_g}$$

When $B_g = B_m$ is approximately fixed at the point of maximum BH or maximum energy product, then $l_g = \frac{\mu l_m}{B_g} (AT)_{\text{max.}}$, and since the representation is in magnet ampere turns per inch, $l_g = \frac{\mu (AT)_{\text{max.}}}{B_g}$

$$F = \frac{B^2 A}{2\mu}$$

Work or energy = $F l_g$

$$\begin{aligned} W &= \frac{B^2 A}{2\mu} \left(\frac{\mu AT_{\text{max}}}{B_g} \right) \\ &= \frac{B_g (AT)_{\text{max}}}{2} \end{aligned}$$

= 1/2 the maximum energy product

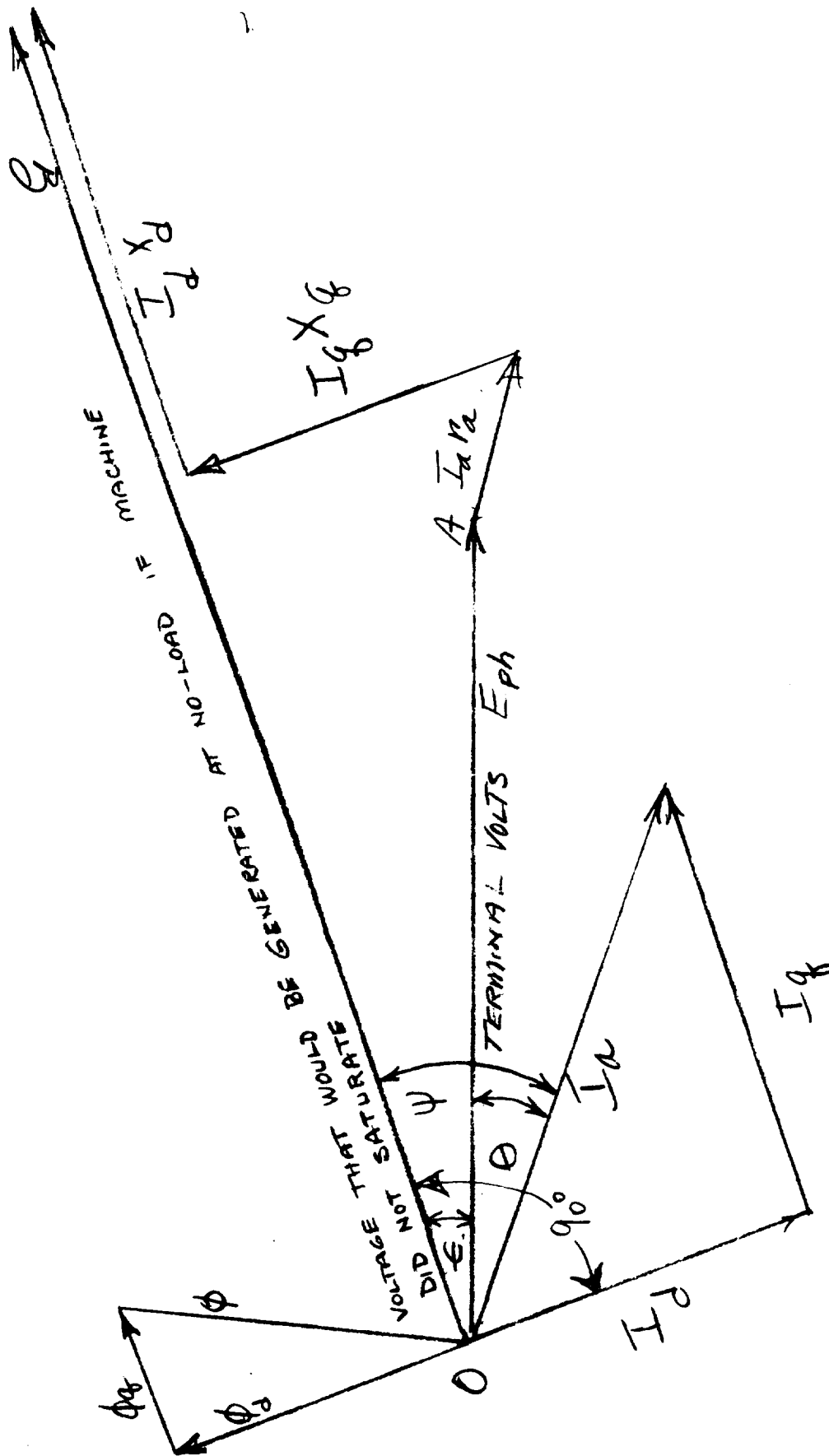
VECTOR DIAGRAMS FOR PERMANENT-MAGNET GENERATORS

A unique peculiarity of the permanent-magnet generator is its low synchronous reactance. The demagnetizing mmf of the stator winding has little effect on the permanent-magnet because of the low permeability of the magnet. The magnet permeability is nearly the same as that of air. As a result, the direct-axis synchronous reactance is slightly lower than the quadrature axis synchronous reactance and with no significant error, the permanent-magnet generator can be regarded as a round-rotor generator with the $X_d = X_q$. This assumption simplifies the voltage vector diagram from that of Figure A-66 to that of Figure A-67, and Figure A-68.

In figures A-67 and A-68, note that the angle a , between the terminal voltage vector and the vector $I(r_a + jX_d)$ is fixed, but angle c is not fixed. To show the locus of the terminal voltage at a given power factor we construct the vector diagrams shown in figures A-69 and A-70. The locus of the voltage vector is shown in dashed lines and the length of the voltage vector is plotted against per-unit line amps.

Figure A-71 is a comparison between the terminal voltage versus ampere output for a machine having a high resistance stator winding and the same machine with a low resistance stator winding.

The comparison shows that a low resistance stator winding is helpful in obtaining low voltage regulation or drop from no-load to full-load.



VECTOR DIAGRAM FOR A SALIENT-POLE, SYNCHRONOUS GENERATOR

FIGURE A-66

1.
VOLTAGE VECTOR DIAGRAMS FOR P.M. GENERATORS
HAVING HIGH STATOR WINDING RESISTANCE

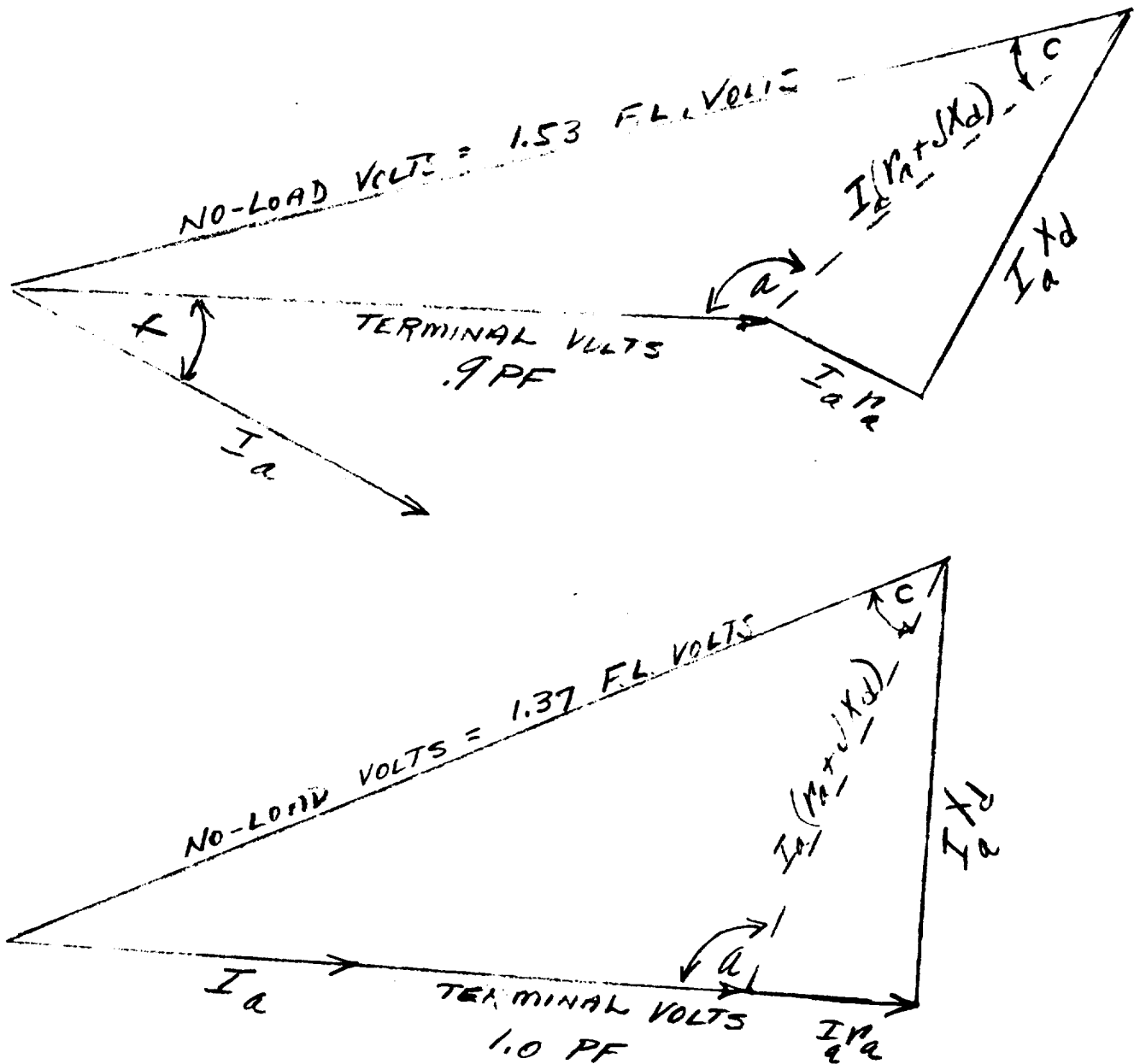
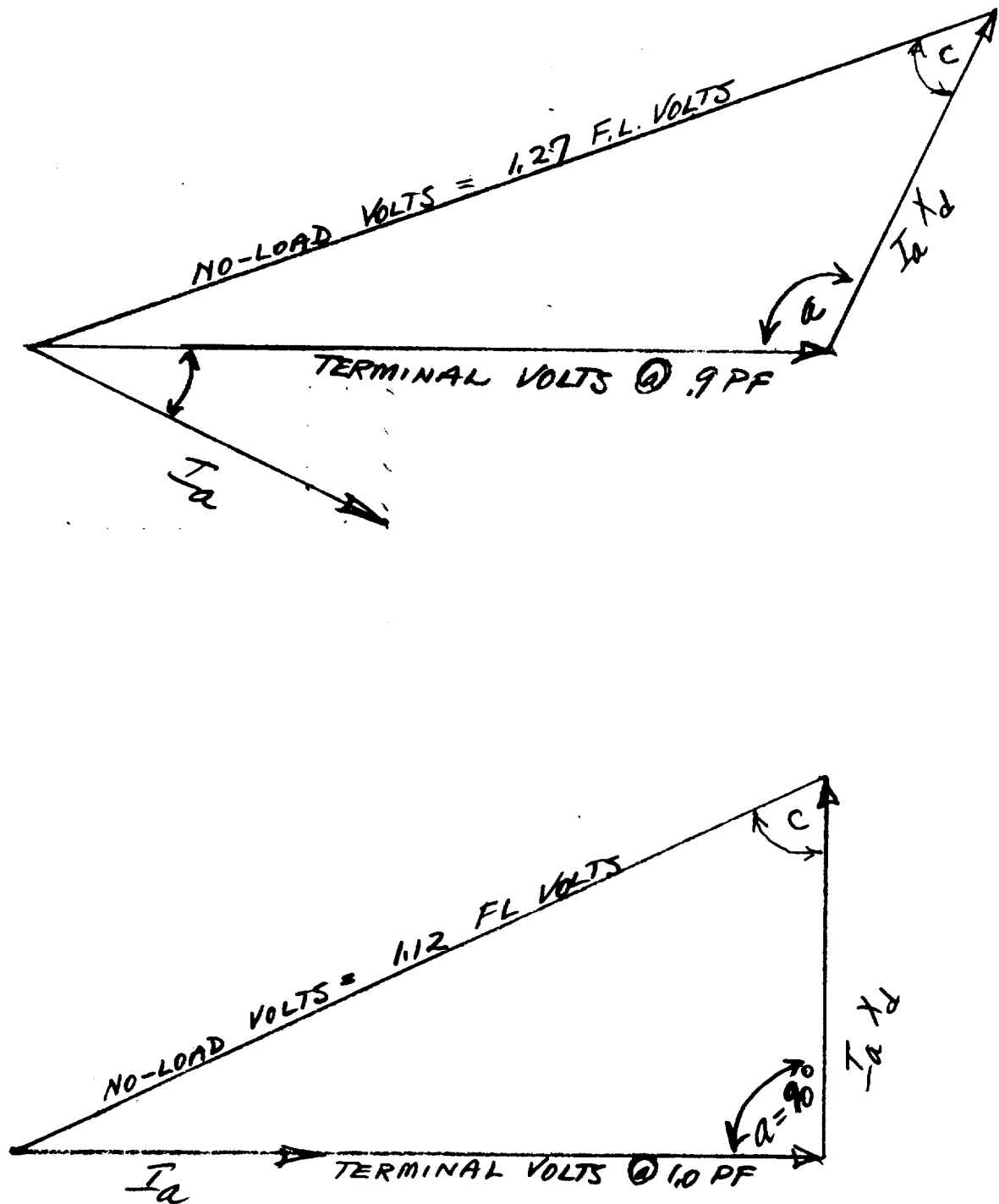
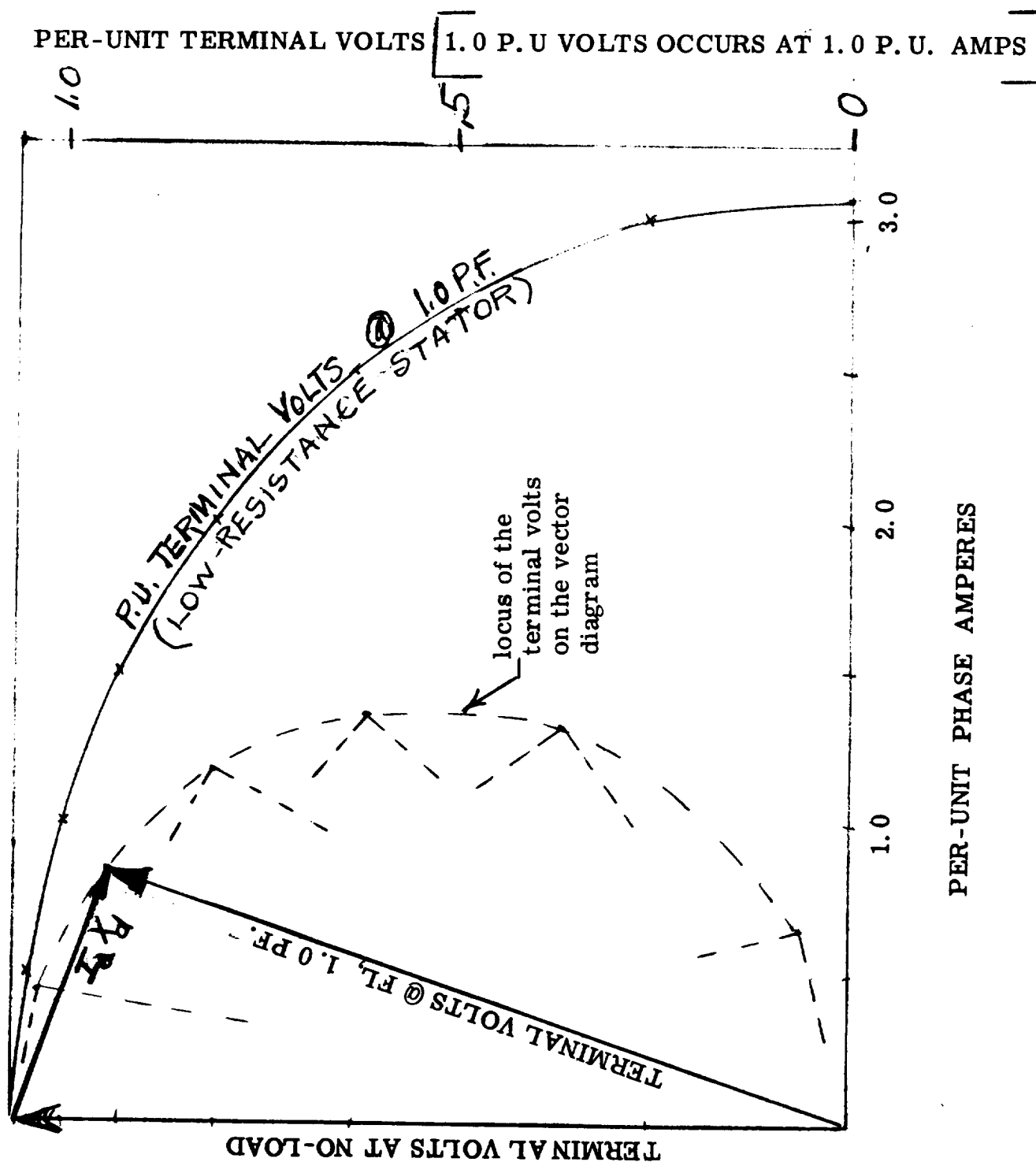


FIGURE A-67

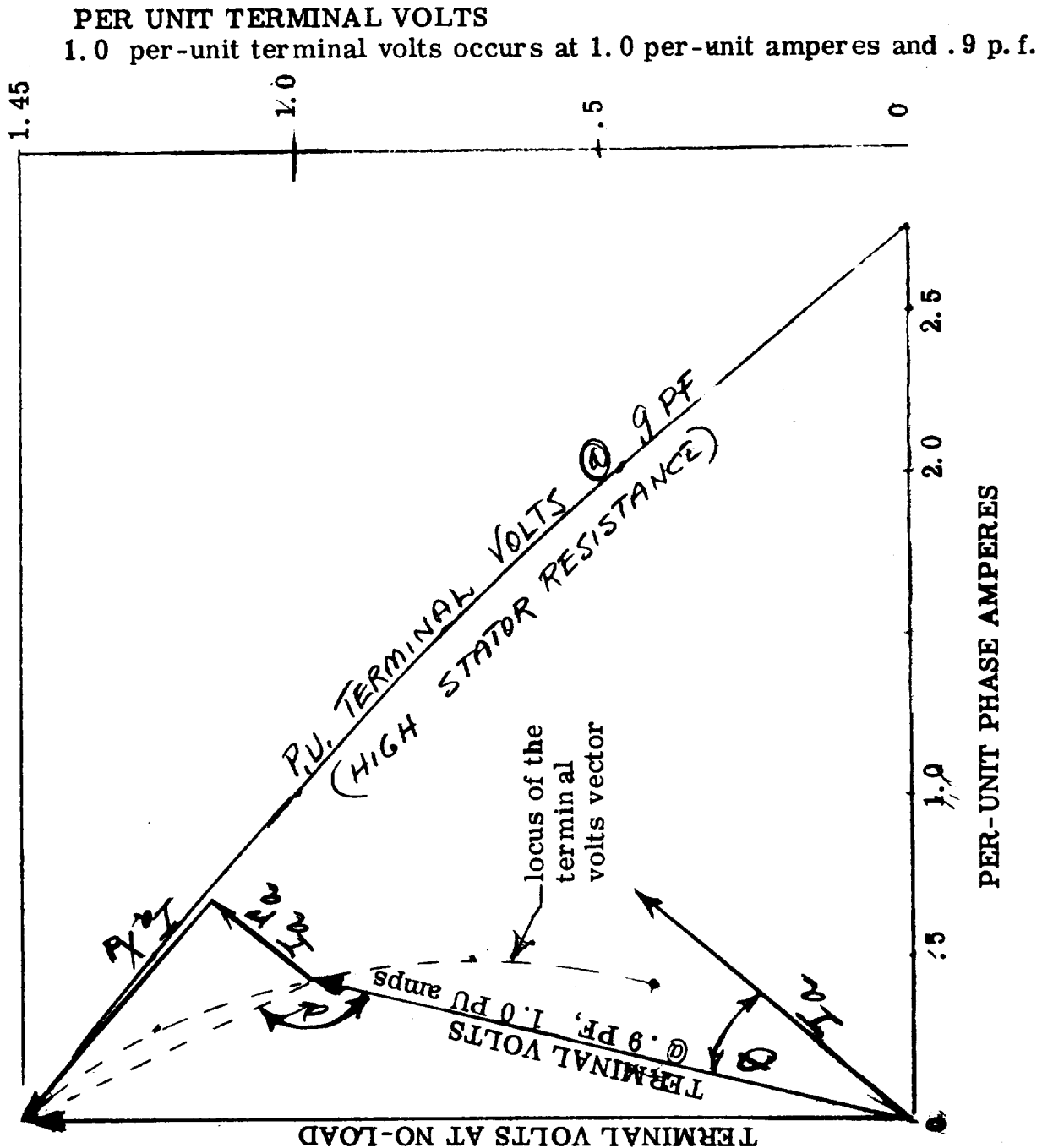
VOLTAGE VECTOR DIAGRAMS FOR P. M. GENERATORS
HAVING LOW (NEGLECTIBLE) STATOR WINDING RESISTANCE



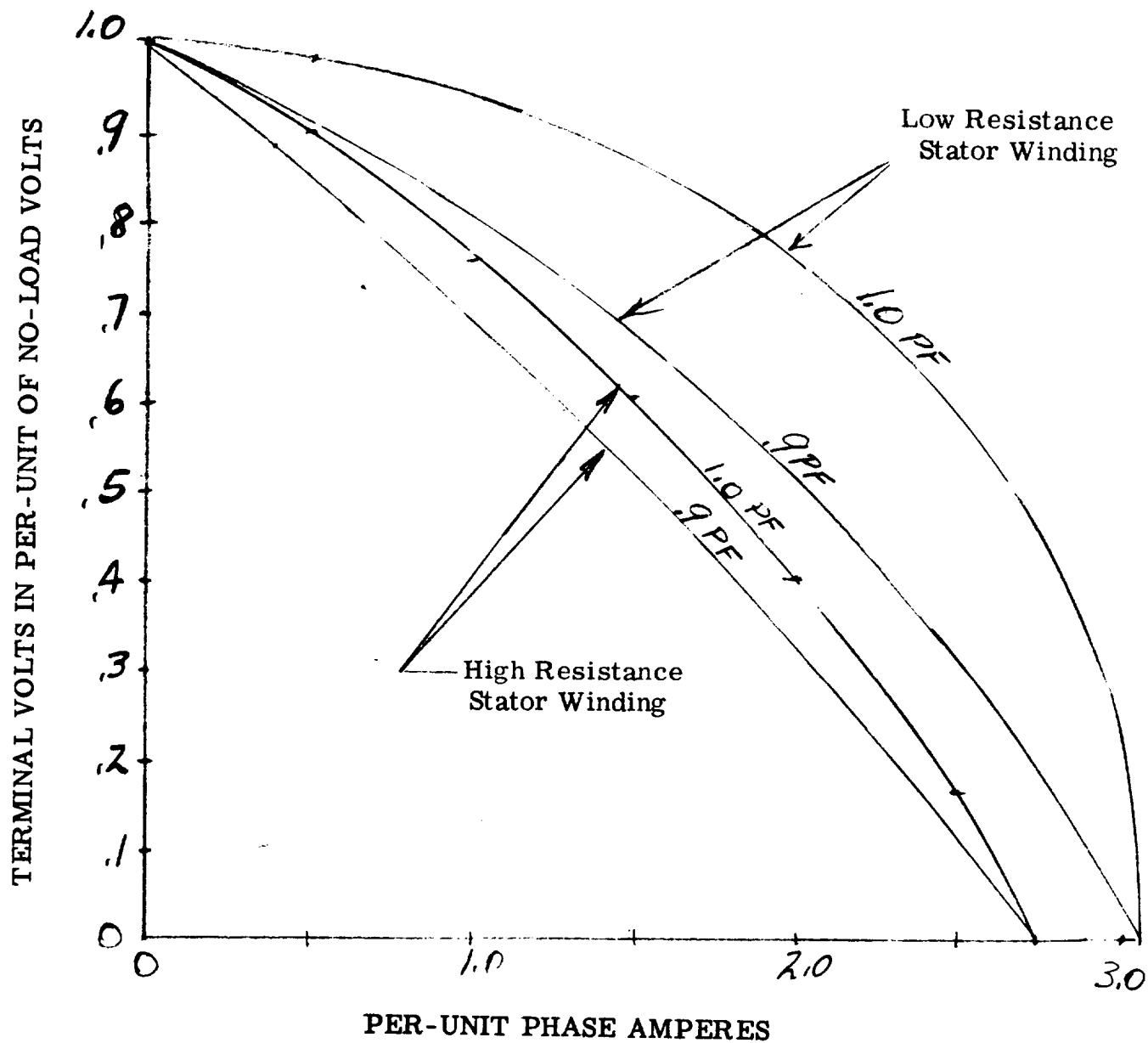
LOCUS OF THE TERMINAL VOLTAGE VECTOR ON THE VECTOR DIAGRAM and THE VOLT-AMPERE CHARACTERISTIC. BOTH THE VECTOR DIAGRAM AND THE V-A CHARACTERISTIC ARE FOR A GENERATOR WITH A LOW RESISTANCE STATOR WINDING (LOW ENOUGH TO BE DISREGARDED)



LOCUS OF THE TERMINAL VOLTAGE VECTOR ON THE VECTOR DIAGRAM and THE VOLT-AMPERE CHARACTERISTIC. BOTH THE VECTOR DIAGRAM AND THE V-A CHARACTERISTIC ARE FOR A GENERATOR WITH HIGH RESISTANCE STATOR WINDINGS.



1.
CURVES SHOWING THE VOLT-AMPERE CHARACTERISTIC
OF A PERMANENT-MAGNET GENERATOR WITH HIGH
RESISTANCE STATOR WINDINGS AND WITH LOW-RESISTANCE
STATOR WINDINGS. THE SAME GENERATOR IN BOTH
CASES, EXCEPT FOR THE WINDING RESISTANCE.



The following list of cobalt steels known as "hard" magnetic steels was taken from Cobalt No. 4 Sept., 1959, the publication of the Cobalt Information Center in Brussels.

<u>Cobalt Steels</u>	<u>Composition</u>	<u>B_r Gauss</u>
2% Cobalt Steel (G. B.)		
Co 040)		
16/120/48) Germany	4 Cr 2 Co 1 C 0.6 W	9800
WH)		
K2)		
3% Cobalt Steel (G. B.)		
Co 045)		
18/97/47) Germany	9 Cr 3 Co 1.5 MO 1 C	7200
Kobalt 100)		
HA 1 (Belgium)		
KS 4 (Japan)		
6% Cobalt Steel (G. B.)		
Co 050)		
20/68/44) Germany	9 Cr 6 Co 1.5 MO 1 C	7800
Kobalt 125)		
K 6)		
HA 2 (Belgium)		
MS 6 (Switzerland)		
9% Cobalt Steel (G. B.)		
Co 160)		
25/51/43) Germany	9 Co 9 Cr 1.5 MO 1 C	8000
KS 3 (Japan)		
11% Cobalt Steel)		
Co 060) Germany	11 Co 8.5 Cr 1.5 MO 1 C	8400
K 11)		
15% Cobalt Steel (G. B.)		
Co 070		
Kobalt 200		
28/46/43	15% Co 9 Cr 1.5 MO 1 C	8500
K 16		
HA 3 (Belgium)		
MS 15 (Switzerland)		
KS 2 (Japan)		

List of Cobalt Steels (Cont)

<u>Cobalt Steels</u>	<u>Composition</u>	<u>B_r Gauss</u>
17% Cobalt Steel (USA)	17 Co 8 W 2.5 Cr 0.175 C	9500
20% Cobalt Steel (G. B.)	20 Co 9 Cr 1.5 MO 1 C	9000
30% Cobalt Steel) Co 090) Germany K 30)	30 Co 4.5 Cr 4.5 W 0.9 C	8600
35% Cobalt Steel (G. B.) KS-1 (Japan) Co 100) Kobalt 300) Germany 40/35/42	35 Co 6 Cr 5 W 0.9 C	9000
Hi-Cobalt (USA) HA-4 (Belgium) MS-35 (Switzerland) Ergit Max 1 (Hungary)		
36% Cobalt Steel (USA)	36 Co 5 W 4 Cr 0.7 C	9500
38% Cobalt Steel (USA)	38 Co 5 W 4 Co 0.7 C	10000

PERMANENT-MAGNET STEELS

TABLE A 1

Material	Materials Alloyed with Iron	* Incremental Permeability	Maximum Stored Energy of Air Gap	Flux Density for Max. Energy
		μ_{Δ}	$(BdHd)_m$	$\leftarrow B_d$
	Per Cent	Relative	joules per cu. in.	kmax. per sq. in.
Carbon steel, oil-quenched	0.011	38
Chromium steel.....	2 Cr, 1C	0.014	41
Chromium steel.....	6 Cr, 1C	0.022	45
Tungsten steel.....	5.5 W, 0.7 C	30	0.017	41
Cobalt-chrome steel.....	15 Co, 11 Cr, 1C	0.040	33
Cobalt steel.....	36 Co, 5W, 2 Cr, 0.8 C	9	0.052	35
Alnico I.....	12 Al, 20 Ni, 5 Co	6.7	0.091	30
Alnico II.....	10 Al, 6 Cu, 17 Ni, 12.5 Co	6.2	0.104	29
Alnico II (sintered).....	10 Al, 6 Cu, 17 Ni, 12.5 Co	0.089	28
Alnico III.....	12 Al, 25 Ni	6.0	0.085	29
Alnico IV.....	12 Al, 28 Ni, 5 Co	3.4	0.085	19
Alnico V.....	8 Al, 3 Cu, 14 Ni, 24 Co	3.1	0.286	62
Nipermag.....	12 Al, 32 Ni, + Ti	0.087	20
Platinum-cobalt alloy.....	77 Pt, 23 Co, 0 Fe	1.1	0.244	16

PERMANENT-MAGNET STEELS

TABLE A 2

Material	Materials Alloyed with Iron	Resistivity	Specific Gravity	Density
		ρ	δ	
		microhm, inches		lb. per cu. in.
Carbon steel, oil-quenched	7.82	0.282
Chromium steel.....	2 Cr, 1C
Chromium steel.....	6 Cr, 1C
Tungsten steel.....	5.5 W, 0.7 C	11.8	8.17	0.295
Cobalt-chrome steel.....	15 Co, 11 Cr, 1C
Cobalt steel.....	36 Co, 5W, 2 Cr, 0.8 C	8.27	0.298
Alnico I.....	12 Al, 20 Ni, 5 Co	31.5	6.9	0.249
Alnico II.....	10 Al, 6 Cu, 17 Ni, 12.5 Co	24.5	7.1	0.256
Alnico II (sintered).....	10 Al, 6 Cu, 17 Ni, 12.5 Co
Alnico III.....	12 Al, 25 Ni	25.6	6.9	0.250
Alnico IV.....	12 Al, 28 Ni, 5 Co	29.5	7.0	0.254
Alnico V.....	8 Al, 3 Cu, 14 Ni, 24 Co	18.5	7.3	0.264
Nipermag.....	12 Al, 32 Ni, + Ti	26.0	7.0	0.254
Platinum-cobalt alloy.....	77 Pt, 23 Co, 0 Fe	19.7	14.6	0.529

TABLE A 3

COMPOSITIONS AND PROPERTIES OF
SOME USEFUL PERMANENT MAGNET MATERIALS

Name	When Used	Typical Composition	H _c	B _r	(BH) _m x 10 ⁻⁷
Tungsten Steel	1885	6 W, 0.7 C, 0.3 Mn	65	10,500	0.3
Low Chrome Steel	1916	0.9 Cr, 0.6 C, 0.4 Mn	50	10,000	0.2
High Chrome Steel	1916	3.5 Cr, 1 C, 0.4 Mn	65	9,500	0.3
KS Magnet Steel	1917	36 Co, 7 W, 3.5 Cr, 0.9 C	230	10,000	0.9
Cobalt Chrome Steel	1921	16 Co, 9 Cr, 1 C, 0.3 Mn	180	8,000	0.6
Remalloy	1931	12 Co, 17 Mo (or W)	250	10,500) 10,000)	1.2) 1.1)
Mishima Alloy	1931	25 Ni, 12 Al	475	7,000	1.4
Alnico 2	1934	12 Co, 17 Ni, 10 Al, 6 Cu	560	7,300	1.7
Magnetoflex	1935	20 Ni, 60 Cu	600	5,800	2.0
Platinum Cobalt Alloy	1936	77 Pt, 23 Co	3000*	5,000	4.5
Vicalloy	1938	52 Co, 10 V	200	11,500	1.5
Alnico 5	1940	24 Co, 14 Ni, 8 Al, 3 Cu	575	12,500	4.5

**A WAY TO START THE DESIGN OF AN ELECTROMAGNETIC
A-C SYNCHRONOUS GENERATOR**

TABLE A 3

COMPOSITIONS AND PROPERTIES OF
SOME USEFUL PERMANENT MAGNET MATERIALS

Name	When Used	Typical Composition	H _c	B _r	(BH) _m x 10 ⁻³
Tungsten Steel	1885	6 W, 0.7 C, 0.3 Mn	65	10,500	0.3
Low Chrome Steel	1916	0.9 Cr, 0.6 C, 0.4 Mn	50	10,000	0.2
High Chrome Steel	1916	3.5 Cr, 1 C, 0.4 Mn	65	9,500	0.3
KS Magnet Steel	1917	36 Co, 7 W, 3.5 Cr, 0.9 C	230	10,000	0.9
Cobalt Chrome Steel	1921	16 Co, 9 Cr, 1 C, 0.3 Mn	180	8,000	0.6
Remalloy	1931	12 Co, 17 Mo (or W)	250	10,500) 10,000)	1.2) 1.1)
Mishima Alloy	1931	25 Ni, 12 Al	475	7,000	1.4
Alnico 2	1934	12 Co, 17 Ni, 10 Al, 6 Cu	560	7,300	1.7
Magnetoflex	1935	20 Ni, 60 Cu	600	5,800	2.0
Platinum Cobalt Alloy	1936	77 Pt, 23 Co	3000*	5,000	4.5
Vicalloy	1938	52 Co, 10 V	200	11,500	1.5
Alnico 5	1940	24 Co, 14 Ni, 8 Al, 3 Cu	575	12,500	4.5

A WAY TO START THE DESIGN OF AN ELECTROMAGNETIC A. C. GENERATOR

To start the design of an electromagnetic A. C. generator:

1. Assume a value of ampere loading. The ampere loading is the ampere wires per inch of stator bore periphery and the symbol used in the design manuals for this value is A. The value of A that is assumed represents the designers estimate of the load-carrying capability of the final generator design. Because of what the value of ampere-loading represents, it is the hardest single parameter chosen by the designer to evaluate without completely calculating the design performance of the generator. It is really a guess!

For Lundell generators that must be capable of supplying an overload, use an ampere-loading of 900 to 1000 at the overload condition. If the overload is 150%, start with an A of 600. If the overload is 200%, start with an A of 450 or 500. Do the same for the Homopolar Inductor. For the wound-pole generator, use a value of about 800 ampere-wires per inch for the rated load value if the overload is to be 200%. (This is a value of 1600 at the 200% overload condition.)

Thermal considerations will limit the continuous load-carrying capabilities of any of the electromagnetic generators and the thermal limit of the wound-pole generator is usually found in the field winding.

2. Assume an air gap density of 40 Kilolines per square inch. The symbol is Bg.
3. The rating and speed are known so, if A = 500 is used

$$\text{KVA} = \frac{d^2 \ell (\text{RPM}) A \text{Bg}}{90 \times 10^7}$$

d = rotor diameter in inches

ℓ = stator stack length in inches

or

$$d^2 \ell = \frac{90 \times 10^7 (\text{KVA})}{\text{RPM} A \text{Bg}}$$

$$= \frac{90 \times 10^7 (\text{KVA})}{\text{RPM}(500) 40}$$

$$d^2 \ell = \frac{45 \times 10^3 (\text{KVA})}{\text{RPM}}$$

4. Assume $\ell = \frac{1}{2}d$ Then $d^2 \ell = \frac{d^3}{2}$

And

$$d = \sqrt[3]{45 \times 10^3 \frac{\text{KVA}}{\text{RPM}}}$$

NOTE: Any value of ℓ can be assumed for a trial design but

$\ell = \frac{1}{2}d$ is a good place to start.

5. The frequency is known and, therefore, the poles are

$$P = \frac{120 f}{N} \quad \text{where}$$

P = No. of poles

f = frequency in CPS

N = RPM

6. A three-phase machine should have at least one (1) slot per phase per pole.

$$\text{Slots} = q P m$$

Where q = slots per phase per pole

P = Poles

m = number of phases

The slots per phase per pole, q can be an integer or can be an improper fraction if when reduced to its lowest terms the denominator can be divided into the number of poles an integral number of times but not three (3) for a three-phase machine.

Usually, if the q is an integer or has 2 in the denominator of the improper fraction the design can be made satisfactorily. As an example, if the machine has 6 poles and three phases, the total slots Q can be written $Q = P m q = 6 \times 3 \times 2\text{-}1/2$

$$= 45 \text{ slots}$$

See the Appendix of this report for information on laying out windings.

7. Machines operating at 400 cps cannot usually have conductors much thicker than .100 inches in depth because of eddy currents at full load. This is an oversimplified general statement but examination of the eddy factor formula in the design manual will show the factors involved.

Since the conductor is usually small and the rotor speeds high in 400 cps and higher frequency generators, it is desirable to use as many slots as can be easily punched and wound. The more slots there are, the less the load factor of pole face loss will be and the less the slot leakage reactance will be.

A good slot pitch to consider in a smaller 400 cps generator is about .30 inch and the minimum slot pitch might be .20 inch or

$$.20 < \tau_s < .35$$

$$\text{Slots} = Q = \frac{\tau d}{.3}$$

If this comes out satisfactorily, proceed. If not, use a smaller or larger slot pitch.

Example: A 6 pole generator with a 3.0" stator bore

$$Q = \frac{\tau (3.0)}{.3} = 10 \tau = 31$$

$6 \times 3 \times 2 = 36$, so either 36 or 45 slots would probably be used.

If the winding could be more simply designed with 27 slots, that number might be used. The possible combinations are:

$$\begin{array}{ll}
6 \times 3 \times 1 = 18 & \tau_s = .523 \\
6 \times 3 \times 1-1/6 = 20 & \tau_s = .47 \\
6 \times 3 \times 1-1/2 = 27 & \tau_s = .349 \\
6 \times 3 \times 1-5/6 = 35 & \tau_s = .269 \\
6 \times 3 \times 2 = 36 & \tau_s = .262 \\
6 \times 3 \times 2-1/6 = 37 & \tau_s = .254 \\
6 \times 3 \times 2-1/2 = 45 & \tau_s = .209
\end{array}$$

8. Now we have the bore area and the flux density so the theoretical total flux is $\phi_T = B_g \times A_{\text{gap}} = B_g \pi d \ell$

Then E_{LL} is known and the only unknown is the number of conductors needed

$$N_e = \text{effective conductors} = NK_p$$

$$N = \text{total conductors}$$

$$K_p = \text{pitch factor}$$

$$N_e = \frac{60 \times 10^5 E_{LL}}{\text{RPM } (C_W) \phi_T}$$

$$N = \frac{N_e}{K_p}$$

$$K_p = .866 \text{ for } 2/3 \text{ pitch and about } .960 \text{ for longer pitches}$$

$$N_s = \frac{N}{Q} = \text{conductors per slot}$$

N_s must be an even number if a series circuit is used because there are two coil sides per slot in a normal winding. To make the winding suitable for the machine, parallel windings can be used or the number of slots can be varied as explained previously. If these efforts do not produce a satisfactory winding combination, the diameter of the generator can be changed and the stack length changed also to give about the same $d^2\ell$.

9. The slot area is a variable that is dependent upon the tooth flux. Enough tooth must be provided to assure mechanical integrity and to keep the flux density to about $100 \frac{KL}{IN^2}$ at 400 cps no load - less at higher frequencies.

Make a preliminary calculation of tooth area as instructed in the design manual and then using the number of conductors calculated previously in step 8, size the conductors so that the current density is acceptable. For air-cooled designs, the current density allowable may be 10,000 amperes per square inch or slightly more. Current densities as low as 2000-3000 amperes per square inch might be used in generators that are poorly cooled or that operate in high ambient temperatures.

10. The slot size and shape is determined by the space available between teeth, and conductor and insulation requirements. Semi-closed slots are often wound through the opening by using small wire,

several strands in-hand or in parallel. If only two wires per slot are necessary push-through windings can be easily managed. The large commercial generators are almost always made with open slots for winding ease. Allow .050" over the bare conductor width for slot cell and conductor insulation and about .100" over the vertical conductor total dimension to allow for insulation, a center stick and a top stick.

11. Most of the information is now provided for the computer program and a trial design calculation can be made.
12. Repeat the above procedure for other ampere loadings and gap densities as indicated by the results of the first trial design.
From an examination of the results of these trials, the proper parameters can be selected.

DESIGNING A PM GENERATOR

To start a permanent magnet generator design:

1. Assume an ampere loading of 250. That is, 250 ampere wires per inch around the bore periphery. The symbol is A.
2. Assume an air gap density of 20 Kilolines per square inch. The symbol is Bg.
3. Follow the procedure explained previously for Electromagnetic generators except keep the tooth and core densities low - 50 to 70 Kl/in².

BIBLIOGRAPHY

- Kilgore, L. A. -- "Calculation of Synchronous Machine Constants -- Reactance and Time Constants Affecting Transient Characteristics." Transactions AIEE 1931, PP 1201-13.
- Barnes, E. C. -- "An Experimental Study of Induction Machine End-Turn Leakage Reactance." Transactions AIEE 1951, PP 671-7.
- Pollard, E. I. -- "Calculation of No-Load Damper Winding Loss in Synchronous Machines." Transactions AIEE 1932, PP 477-81.
- "Load Losses in Salient-Pole Synchronous Machines." Transactions AIEE 1935, PP 1332-40.
- Spooner, Thomas ; Kinnard -- "Surface Iron Losses with Reference to Laminated Materials." Transactions AIEE 1924, PP 262-80.
- Ginsberg, David -- "Design Calculations for A.C. Generators." Transactions AIEE 1950, PP 1274-80.
- Ginsberg, David; Jokl, A. L. ; Blum, L. M. -- "Calculation of No-Load Wave Shape of Salient-Pole A.C. Generators." Transactions AIEE 1953, PP 974-80.
- Ginsberg, David; Misenheimer, L. J. -- "Design Calculations for Permanent-Magnet Generators." Transactions AIEE III, 1953, PP 96-102.
- Strauss, Fritz -- "Synchronous Machines with Rotating Permanent-Magnet Fields". Transactions AIEE 1952 III, PP 887-93.

GENERATOR SELECTION CRITERIA

1. The first part of the document is a list of the names of the persons who were present at the meeting.

2. The second part of the document is a list of the names of the persons who were absent from the meeting.

3. The third part of the document is a list of the names of the persons who were present at the meeting.

4. The fourth part of the document is a list of the names of the persons who were absent from the meeting.

5. The fifth part of the document is a list of the names of the persons who were present at the meeting.

6. The sixth part of the document is a list of the names of the persons who were absent from the meeting.

7. The seventh part of the document is a list of the names of the persons who were present at the meeting.

8. The eighth part of the document is a list of the names of the persons who were absent from the meeting.

9. The ninth part of the document is a list of the names of the persons who were present at the meeting.

10. The tenth part of the document is a list of the names of the persons who were absent from the meeting.

11. The eleventh part of the document is a list of the names of the persons who were present at the meeting.

12. The twelfth part of the document is a list of the names of the persons who were absent from the meeting.

13. The thirteenth part of the document is a list of the names of the persons who were present at the meeting.

14. The fourteenth part of the document is a list of the names of the persons who were absent from the meeting.

15. The fifteenth part of the document is a list of the names of the persons who were present at the meeting.

16. The sixteenth part of the document is a list of the names of the persons who were absent from the meeting.

17. The seventeenth part of the document is a list of the names of the persons who were present at the meeting.

18. The eighteenth part of the document is a list of the names of the persons who were absent from the meeting.

AIDS TO GENERATOR SELECTION

The purpose of this section is to aid the reader in selecting the best generator for a specific application.

For use as preliminary design approximations, curves are given showing a breakdown of the weights of the electromagnetic parts of four generators. These four generators are considered by the investigators to be the generators most likely to be used in the majority of aerospace applications.

The four generators are: 1. The wound-pole, synchronous generators. 2. The two, inside, stationary-coil or Becky-Robinson Lundell generators. 3. The outside-coil Lundell Generators. 4. The homopolar inductor a-c generators.

The investigators evaluate the four generators as follows: For use in mild environments, at low speeds and at low radiation levels, the wound-pole rotating rectifier generators are best. They can have the best waveform, the best overload capabilities, the fastest response and the lowest subtransient reactances, which means that the waveform will be least disturbed by discontinuous loads such as magnetic amplifiers or silicon controlled rectifiers. The maximum

radiation level that the rotating rectifier generator should be subjected to is probably about 10^{12} NVT and the vibration level should be not more than 10 g rms random.

For use in medium environments where the wound-pole generators are eliminated because of temperature or radiation but where minimum weight is desired, the two-coil Becky-Robinson generators are best. Maximum rotor peripheral speed is about 43,000 feet per minute for reliable operation. Coolant temperature can be 400°F. Vibration levels can be higher than the wound-pole generators will stand, but probably should not exceed 15 g rms random for long life. Radiation levels might be 10^{18} NVT as a maximum.

For extreme environments, two generator types are useable, the two-coil or the single-coil, outside-coil, Lundell generator or the A-C Homopolar Inductor generator. The thermal and vibration limits are not firmly established. The weight and reactances of the Lundell-type generator may, in many cases, be lower than those of the Homopolar Inductor.

The Lundell generator has only one stator and the Inductor has two stators. The additional stator doubles the complexity of the Homopolar Inductor for applications where the bore must be sealed to protect the stator from a hostile environment.

The maximum coolant temperature for the outside-coil Lundell and the Homopolar Inductor is about 700°F. At high temperatures, creep, aging and/or oxidation of magnetic steels and electrical conductors, insulation degradation, and bearing life all become severe problems. Maximum radiation levels for these two generators are about 10^{18} NVT.

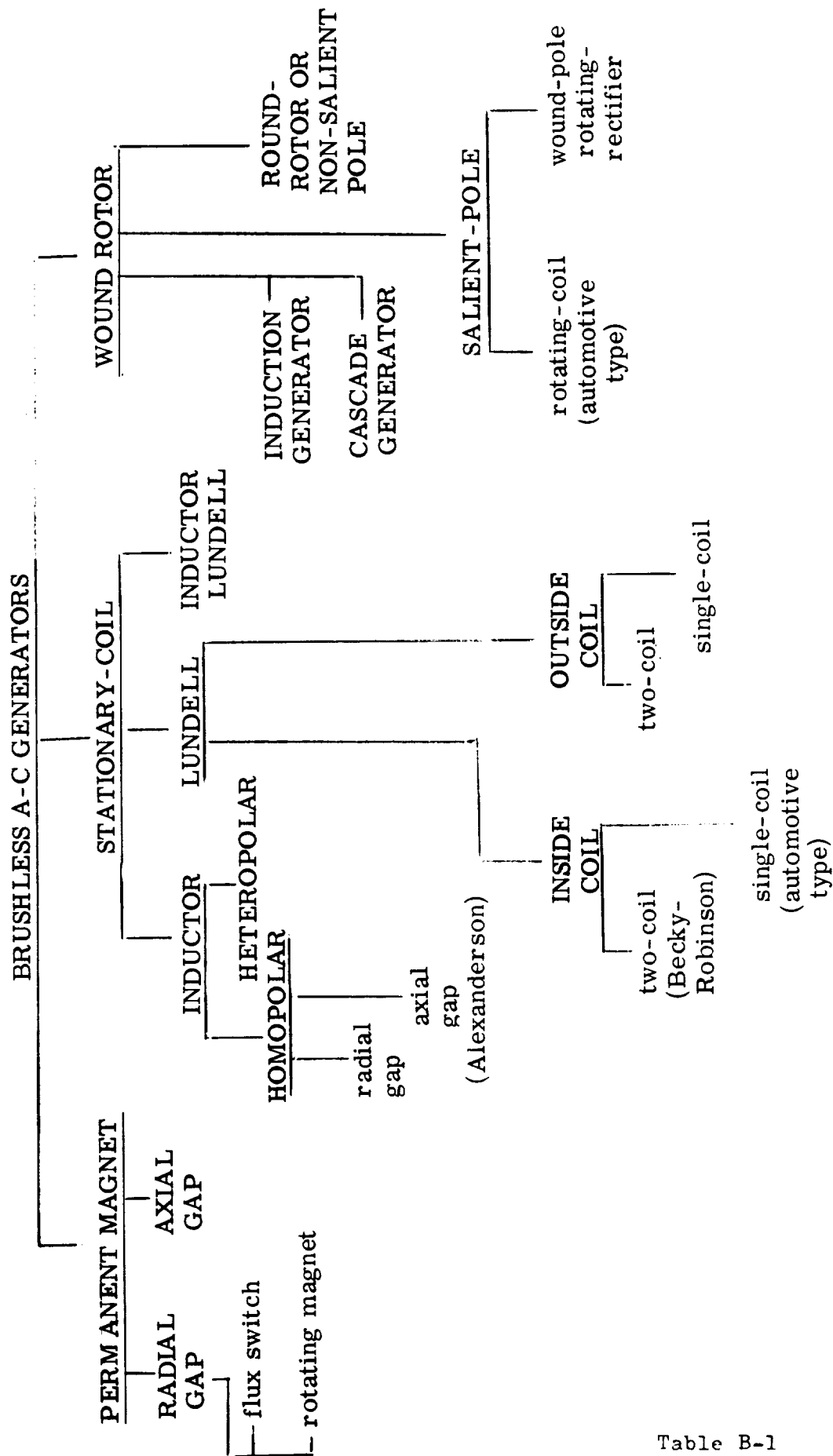


Table B-1

GENERATOR TYPE	MINIMUM NUMBER OF POLES	MAXIMUM ROTOR SPEED, FT. PER MIN.	MAXIMUM LENGTH TO DIAMETER RATIO	COMPARATIVE WEIGHTS AT EQUAL SPEEDS AND RATINGS	OVERLOAD CAPABILITY	VOLTAGE WAVE QUALITY	REACTANCES	SUITABILITY FOR SEVERE ENVIRONMENT			
								RADIATION	HIGH TEMPERATURE	VIBRATION	CRYOGENIC
WOUND-POLE, SALIENT POLE	* 4	20000	NO LIMIT EXCEPT THERMAL	LOWEST 1	BEST	BEST POSSIBLE	LOWEST	POOR	POOR	POOR	POOR
WOUND-POLE, NON-SALIENT POLE	2	24000	NO LIMIT EXCEPT THERMAL	NEXT LOWEST 2	NEXT BEST	2nd BEST POSSIBLE	NEXT LOWEST	POOR	POOR	POOR	POOR
OUTSIDE-COIL, STATIONARY COIL, LUNDELL, 1 & 2 COIL	2	50000	.5	4th LOWEST IN LARGE RATINGS	4th	GOOD	MEDIUM	GOOD	BEST	GOOD	GOOD
2-COIL, INSIDE-COIL, STATIONARY COIL LUNDELL, BECKY-ROBINSON	* 4	43000	.5	3rd LOWEST	3rd BEST	GOOD	MEDIUM	GOOD	GOOD TO FAIR	GOOD TO FAIR	FAIR
1-COIL, INSIDE, STATIONARY COIL, LUNDELL	* 4	35000	.3	HIGH	GOOD	FAIR	MEDIUM	GOOD	FAIR	FAIR	FAIR TO POOR
ROTATING-COIL LUNDELL (AUTOMOTIVE TYPE)	2	15000	.3	HIGH	GOOD	FAIR	MEDIUM	POOR	POOR	FAIR	POOR
DISK-TYPE LUNDELL, STATIONARY-COIL	* 4	43000	—	HIGH	POOR	FAIR	HIGH	GOOD	FAIR	FAIR	FAIR TO POOR
HOMOPOLAR INDUCTOR	4	60000	.5	HIGHEST	POOR	FAIR	HIGHEST	GOOD	GOOD	GOOD	GOOD
PERMANENT-MAGNET	2	15000	NO ELECTRICAL LIMIT	HIGH EXCEPT IN SMALL RATINGS	POOR	FAIR	LOW **	GOOD	LIMIT AT 800°F	FAIR	POOR


* x x x APPROXIMATE ONLY

* TWO-POLES ARE POSSIBLE BUT NOT DESIRABLE. 4 POLES SHOULD BE THE MINIMUM.


** IN SMALL RATINGS WHERE PM GENERATORS ARE PRACTICAL, THE PM GEN. SYN. REACTANCES ARE SMALLER THAN THOSE OF ANY OTHER GENERATOR.

APPROXIMATE DIMENSIONS FOR HOMOPOLAR
INDUCTORS AND TWO, OUTSIDE-COIL LUNDELL GENERATORS

Two, Outside-Coil Lundell AC Generator

<u>Poles</u>	<u>B_g</u>	<u>A</u>	<u>ℓ</u>	<u>d³</u>	<u>D</u>	<u>ty</u>
4	35	600	$\frac{d}{2}$	7.15 x KVA	1.32d	.072d
4	50	600		5 x KVA	1.42d	.095d
6	35	700		9.2 x KVA	1.25d	.076d
6	50	700		6.45 KVA	1.31d	.103d
8	35	800		10.7 KVA	1.2d	.079d
8	50	800		7.5 KVA	1.26d	.1075d

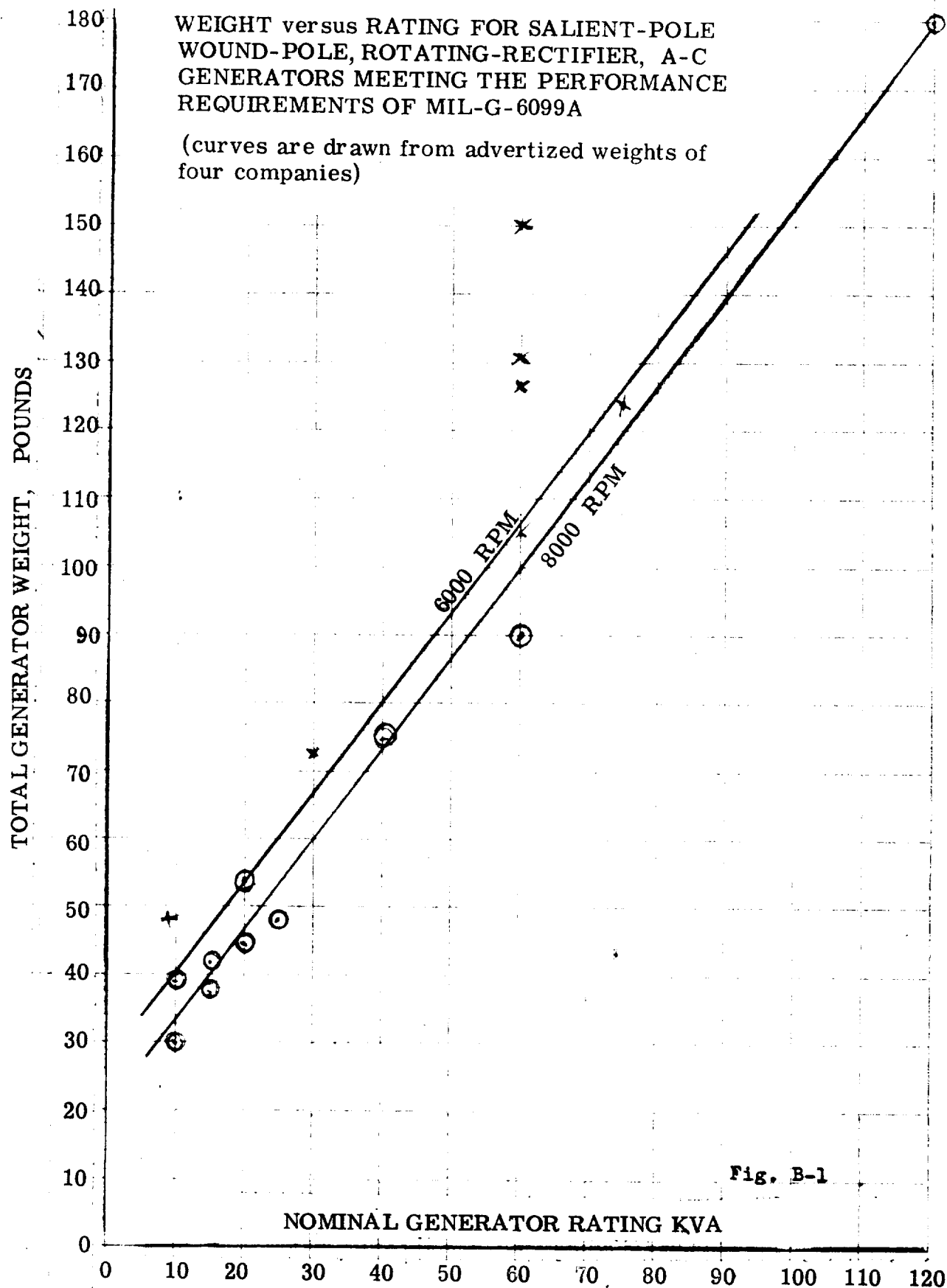
Homopolar Inductor AC Generator

<u>Poles</u>	<u>B_g</u>	<u>A</u>	<u>ℓ</u>	<u>d³</u>	<u>D</u>	<u>ty</u>
4	35	600	$\frac{d}{2}$	7.15 x KVA	1.32d	.061d
4	50	600		5 x KVA	1.42d	.082d
6	35	700		9.2 x KVA	1.25d	.065d
6	50	700		6.45 x KVA	1.31d	.089d
8	35	800		10.7 x KVA	1.2d	.0675d
8	50	800		7.5 x KVA	1.26d	.092d

NOTES: 1) Depth of slot is assumed .05d in all cases.

2) $h_c = D - (1.1)d$

Table B-3



VOLUME versus RATING, FOR SALIENT-POLE,
WOUND-POLE, ROTATING-RECTIFIER, A-C
GENERATORS MEETING THE PERFORMANCE
REQUIREMENTS OF MIL-G-6099A

(points are taken from the overall dimensions of
the machines used for the weight versus rating curve)

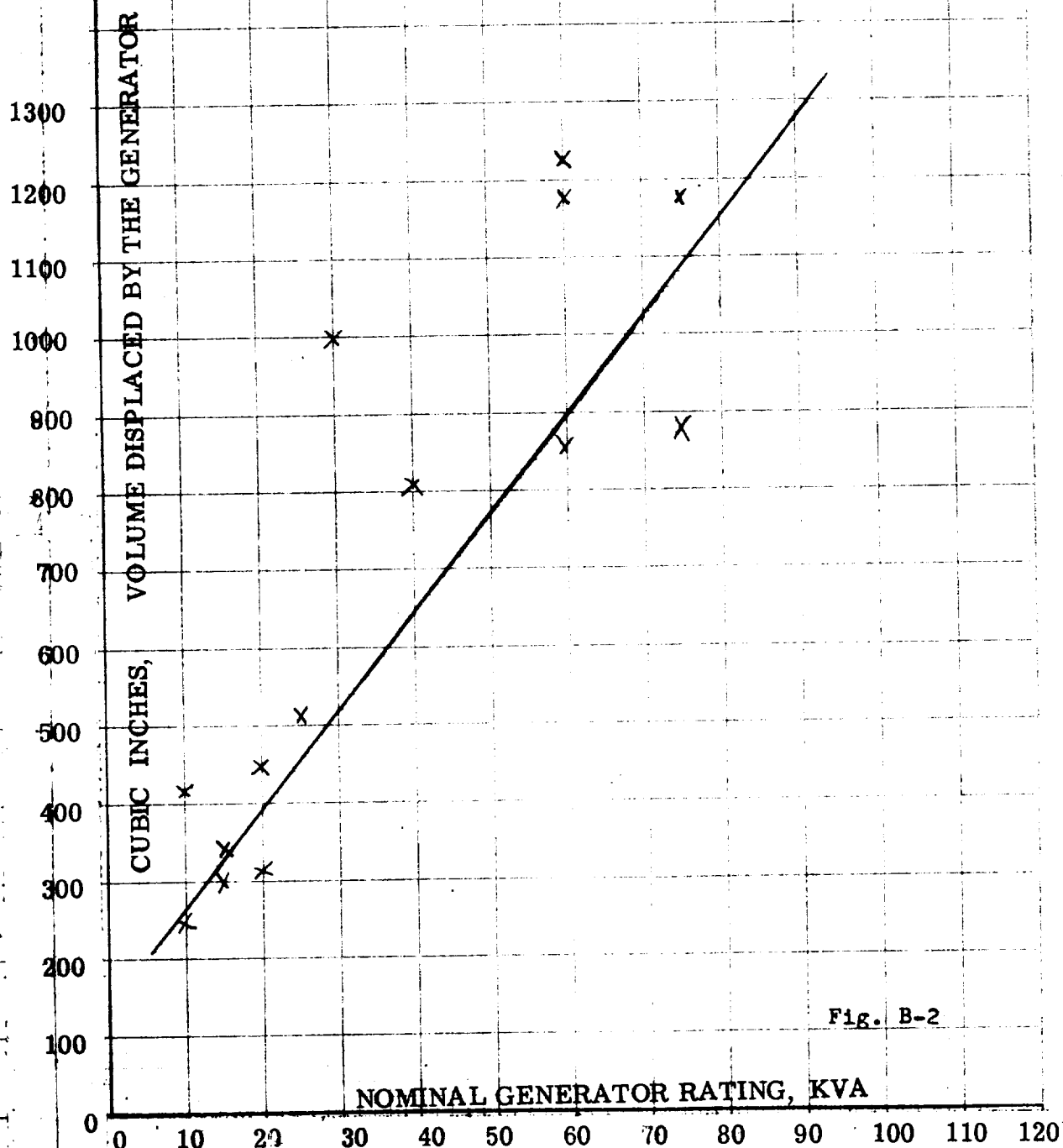
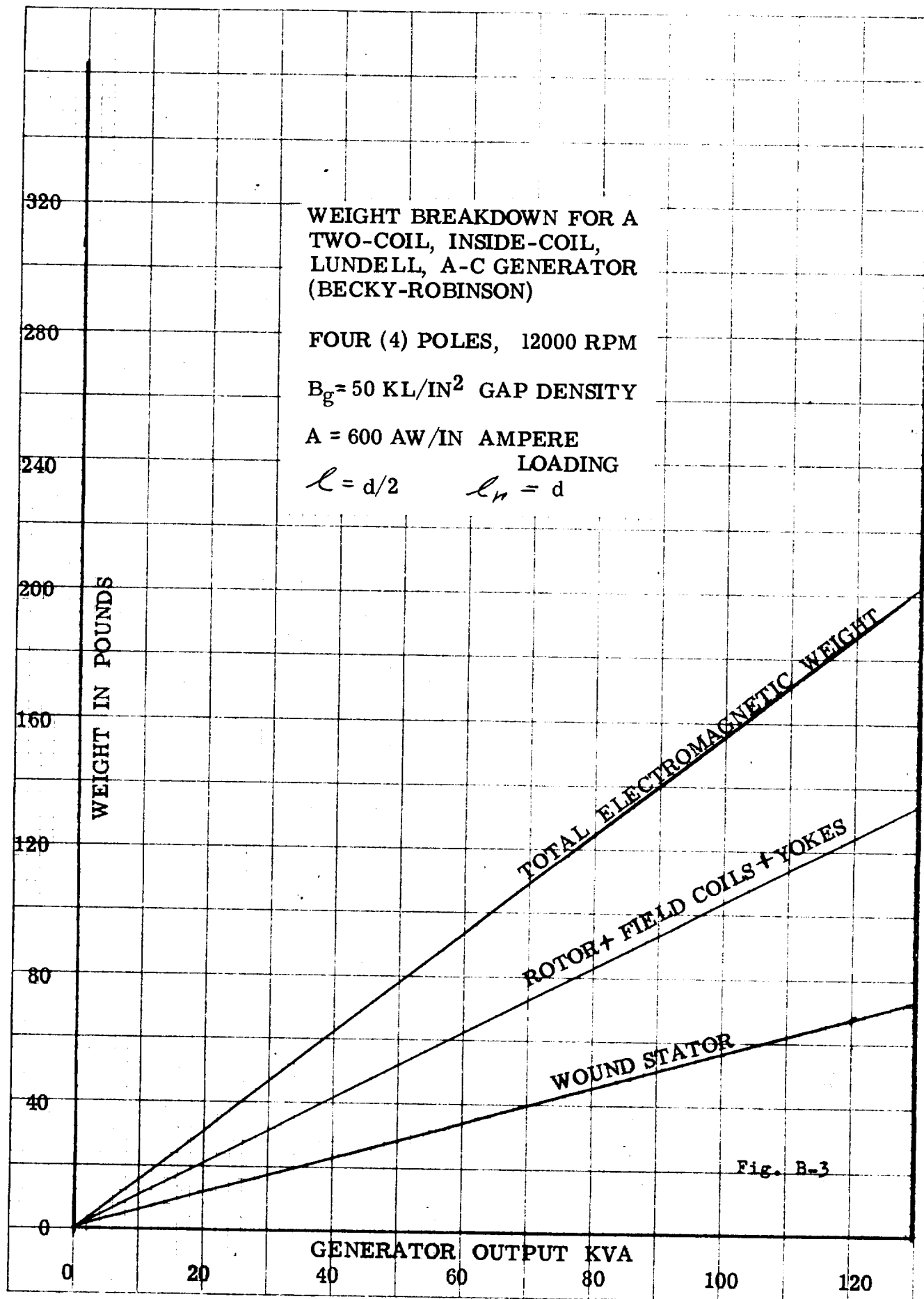


Fig. B-2



WEIGHT BREAKDOWN FOR A
TWO-COIL, INSIDE-COIL,
LUNDELL, A-C GENERATOR
(BECKY-ROBINSON)

SIX (6) POLES, 8000 RPM

$B_g = 50 \text{ KL/IN}^2$ GAP DENSITY

$A = 700 \text{ AW/IN}$ AMPERE
LOADING
 $\ell = d/2$ $\ell_p = d$

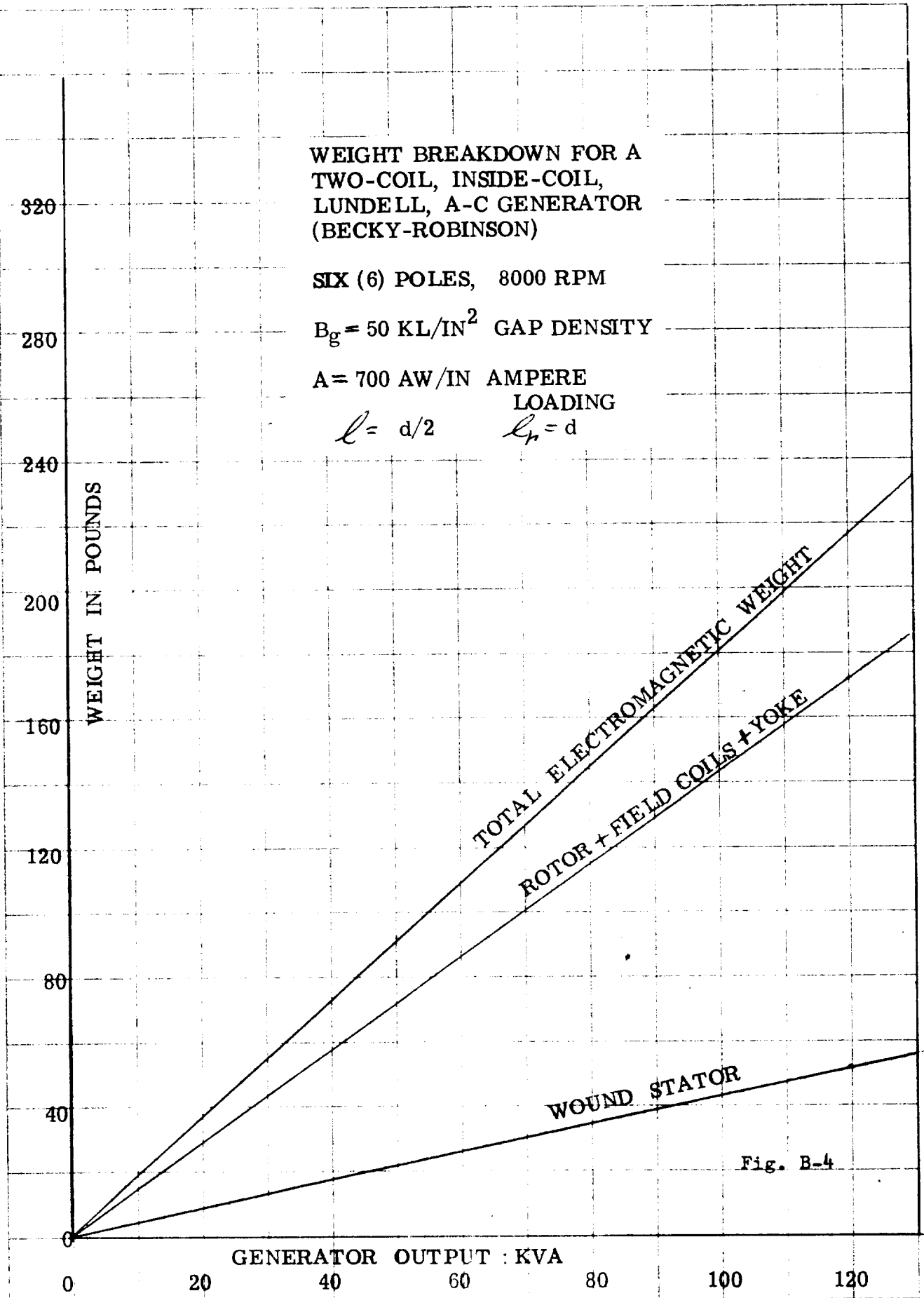
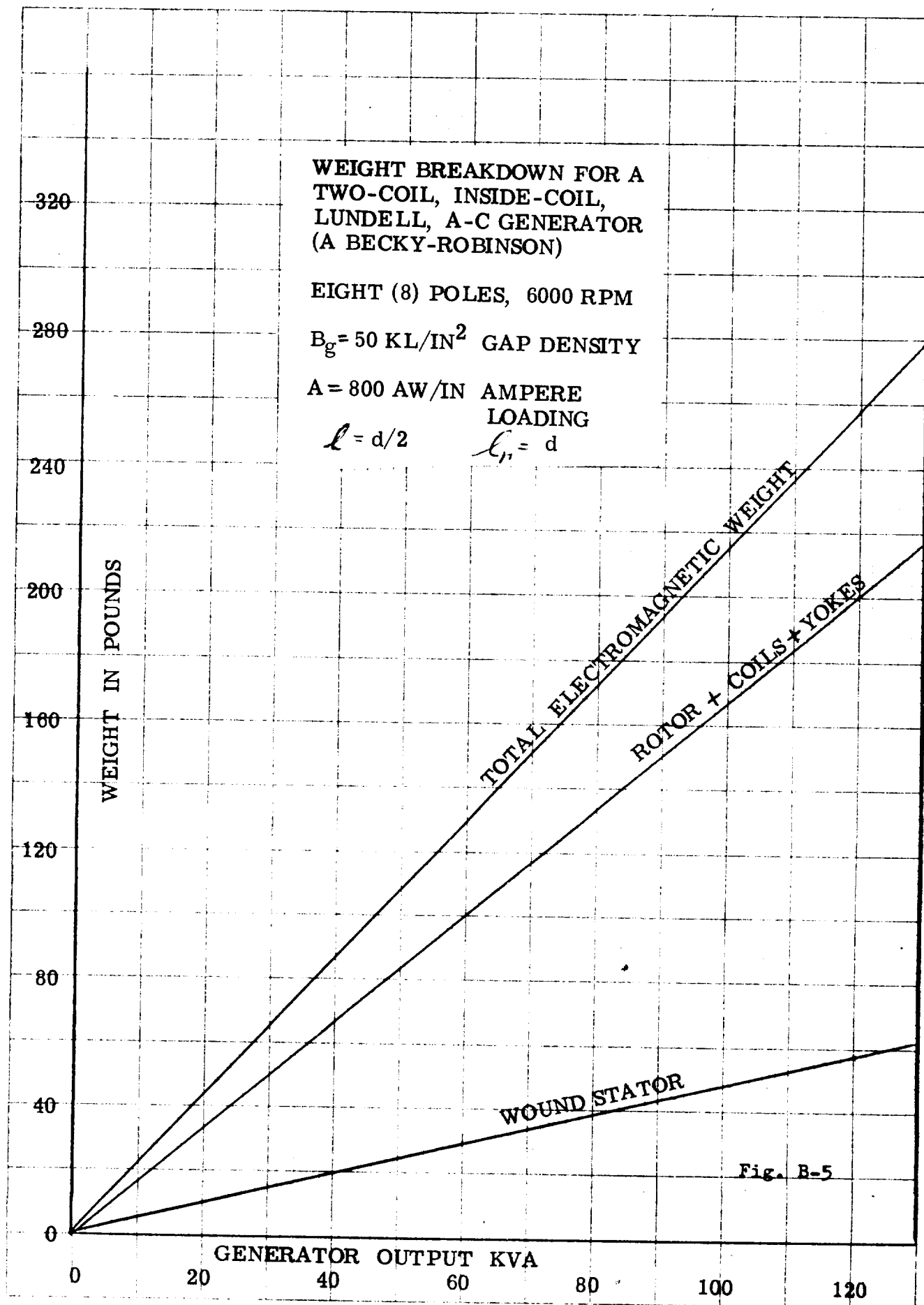
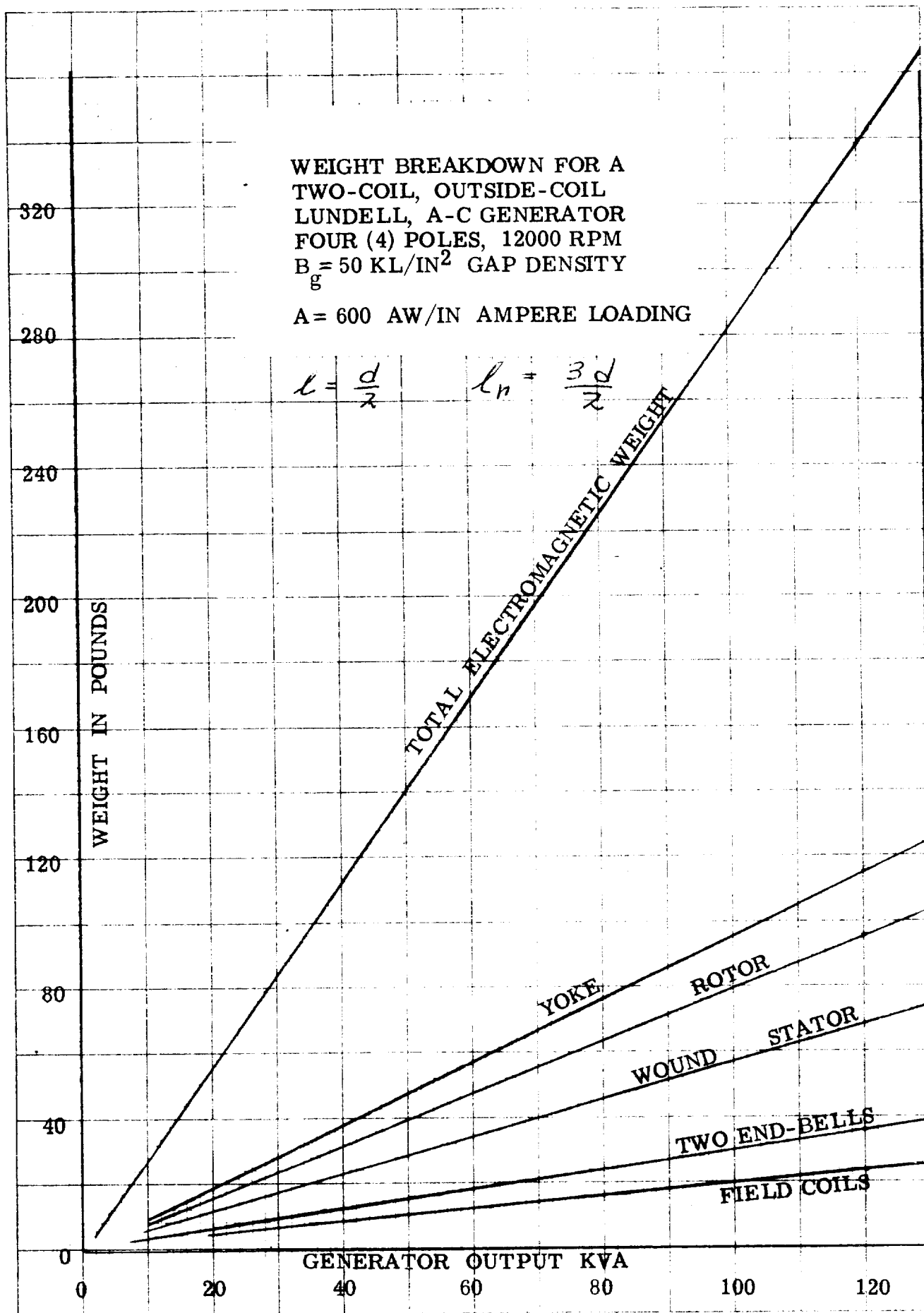


Fig. B-4



46 ORGO
46 ORGO
46 ORGO

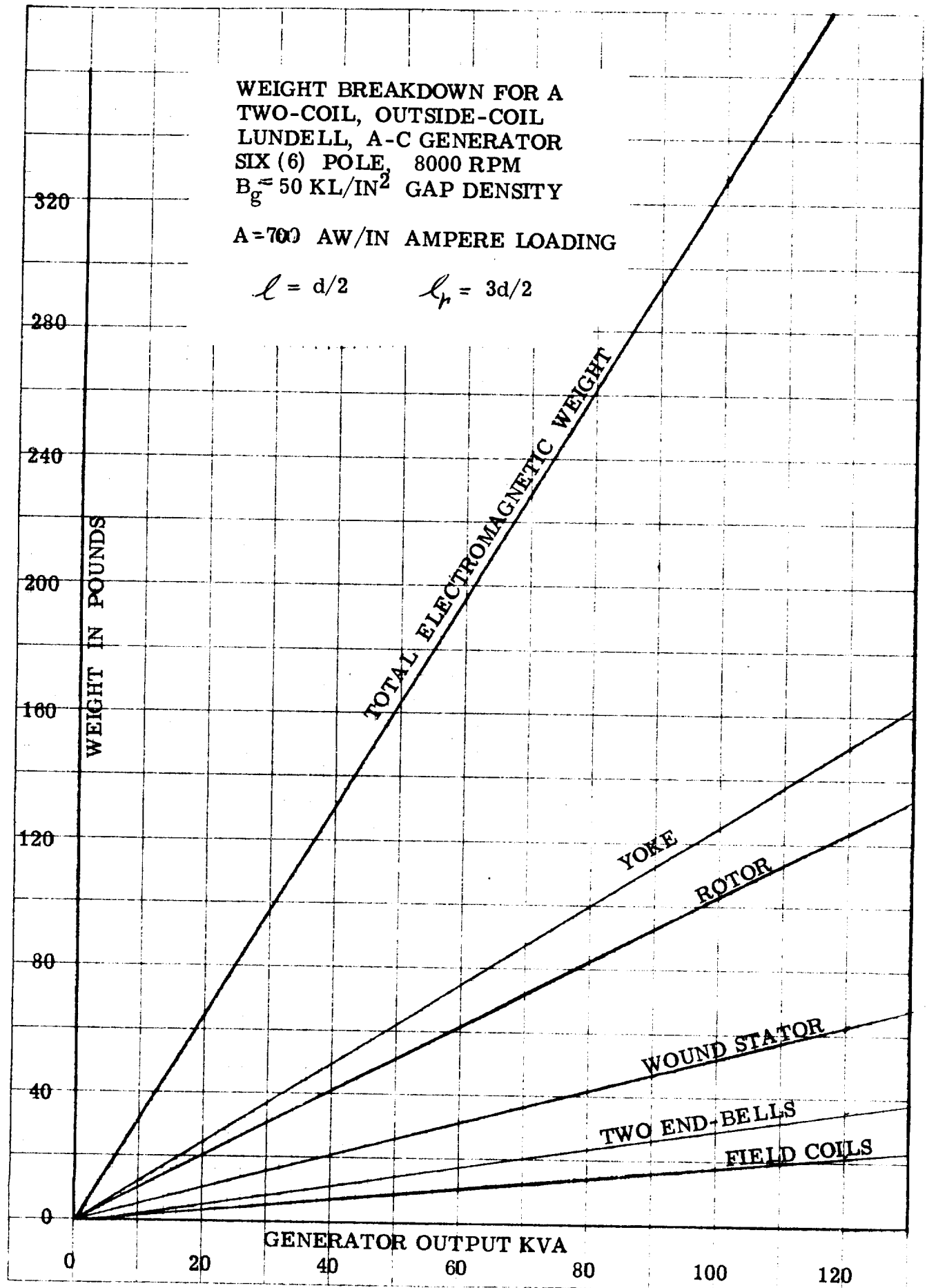


WEIGHT BREAKDOWN FOR A
TWO-COIL, OUTSIDE-COIL
LUNDELL, A-C GENERATOR
SIX (6) POLE, 8000 RPM
 $B_g = 50 \text{ KL/IN}^2$ GAP DENSITY

$A = 700 \text{ AW/IN}$ AMPERE LOADING

$$l = d/2$$

$$l_r = 3d/2$$



WEIGHT BREAKDOWN FOR A
TWO-COIL, OUTSIDE-COIL
LUNDELL, A-C GENERATOR

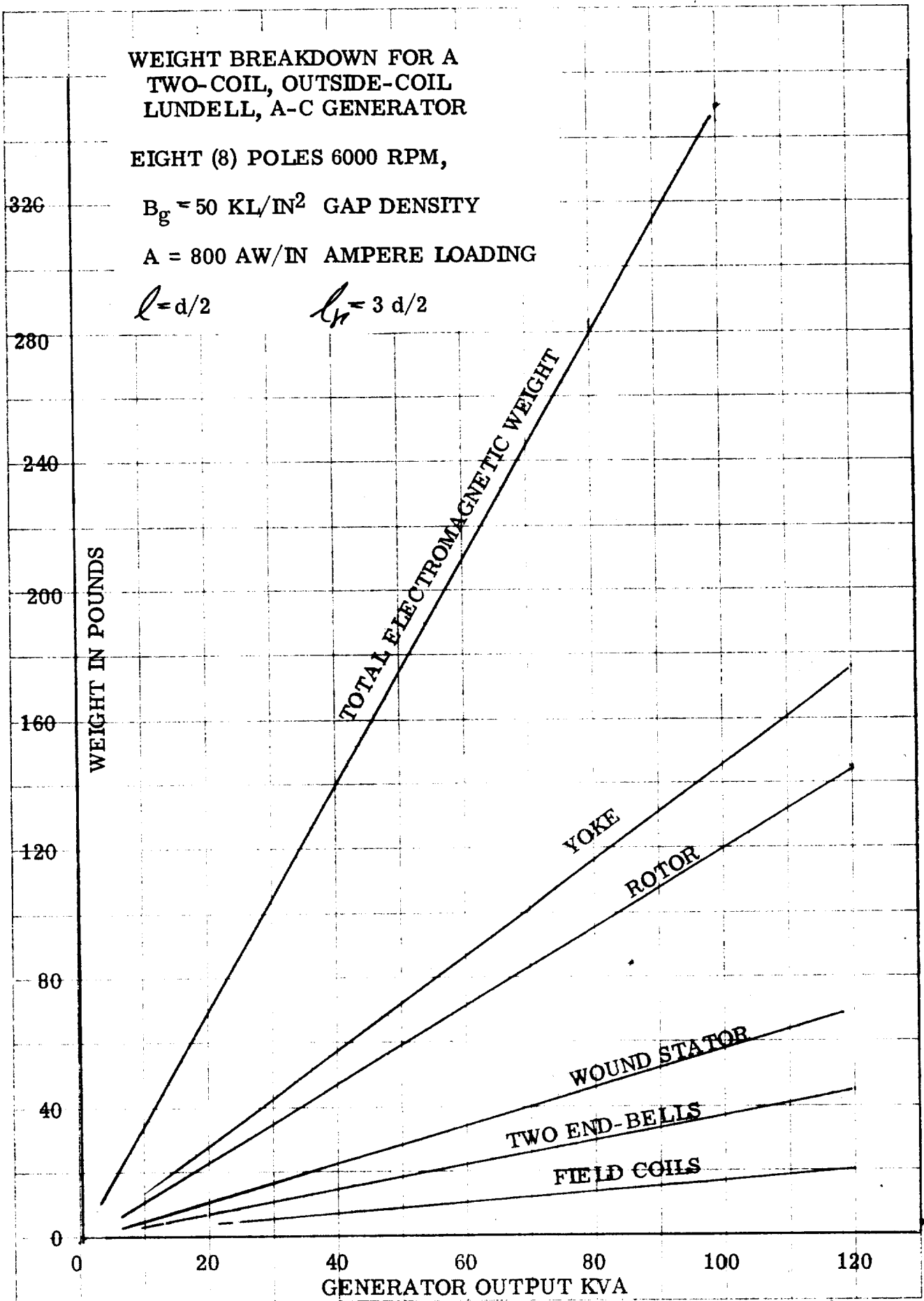
EIGHT (8) POLES 6000 RPM,

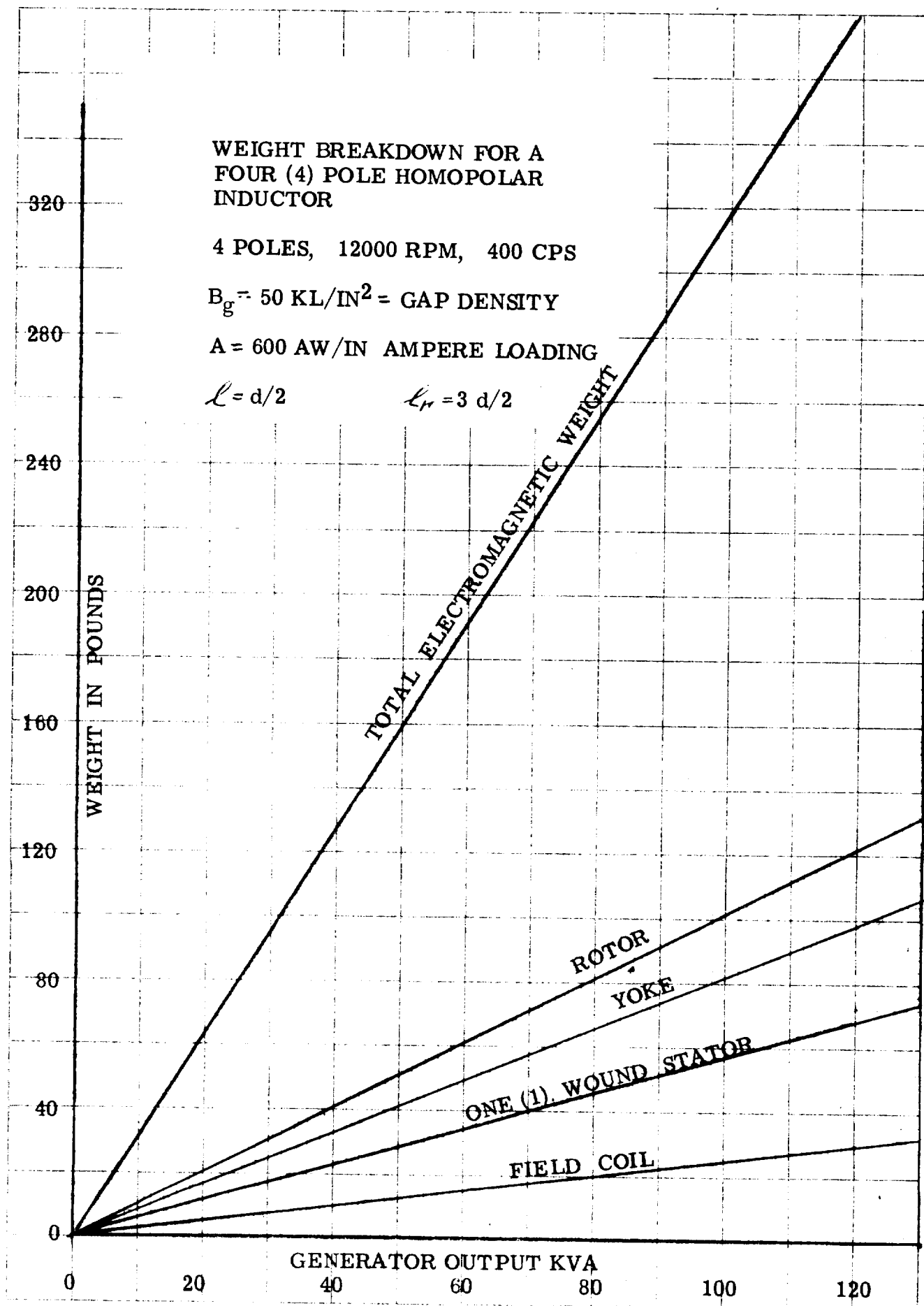
$B_g = 50 \text{ KL/IN}^2$ GAP DENSITY

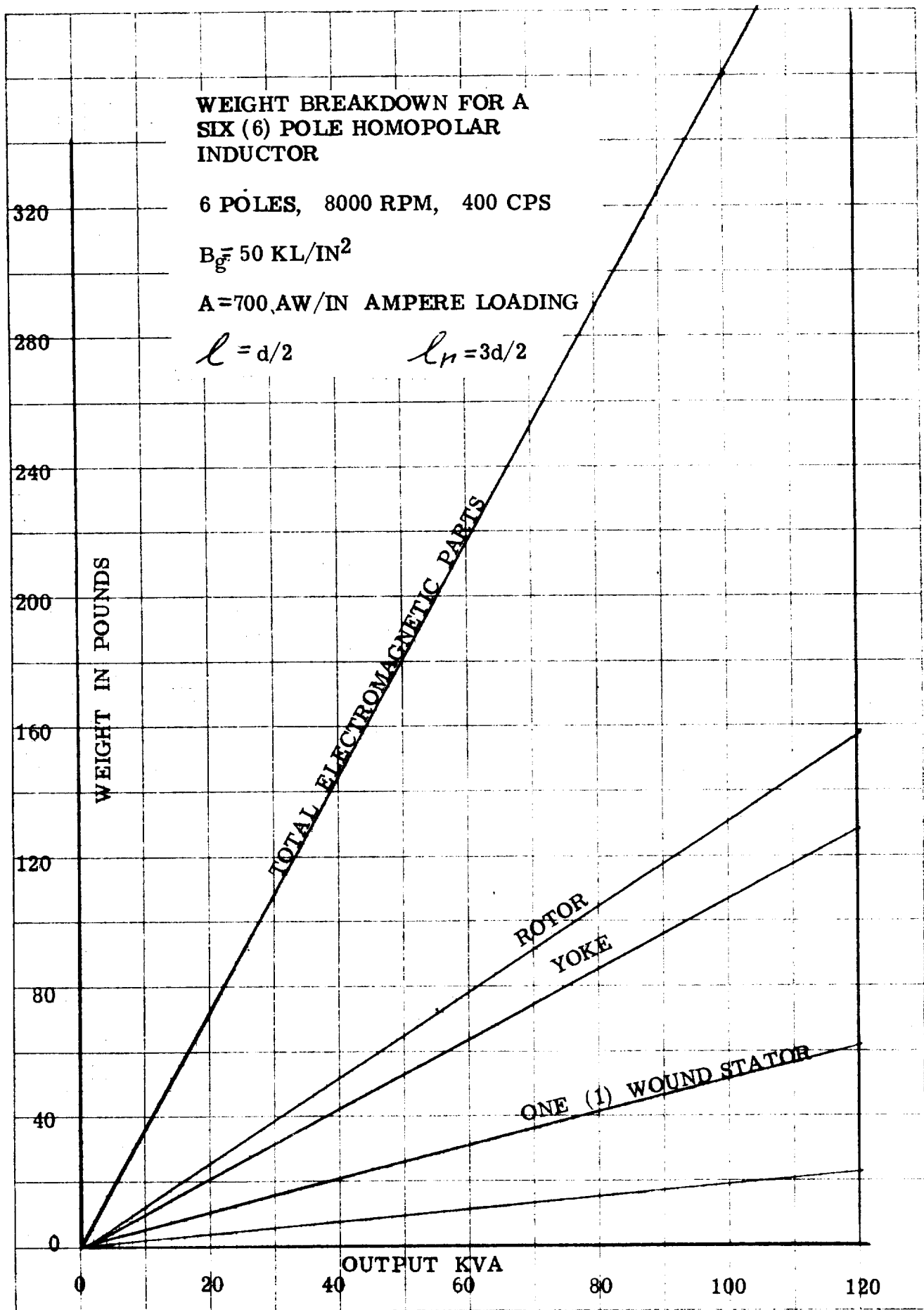
$A = 800 \text{ AW/IN}$ AMPERE LOADING

$$l = d/2$$

$$l_r = 3 d/2$$







WEIGHT BREAKDOWN FOR AN EIGHT (8) POLE HOMOPOLAR INDUCTOR

8 POLES, 6000 RPM, 400 CPS

$B_g = 50 \text{ KL/IN}^2$ GAP DENSITY

$A = 800 \text{ AW/IN}$ AMPERE LOADING

$l = d/2$

$l_p = 3 d/2$

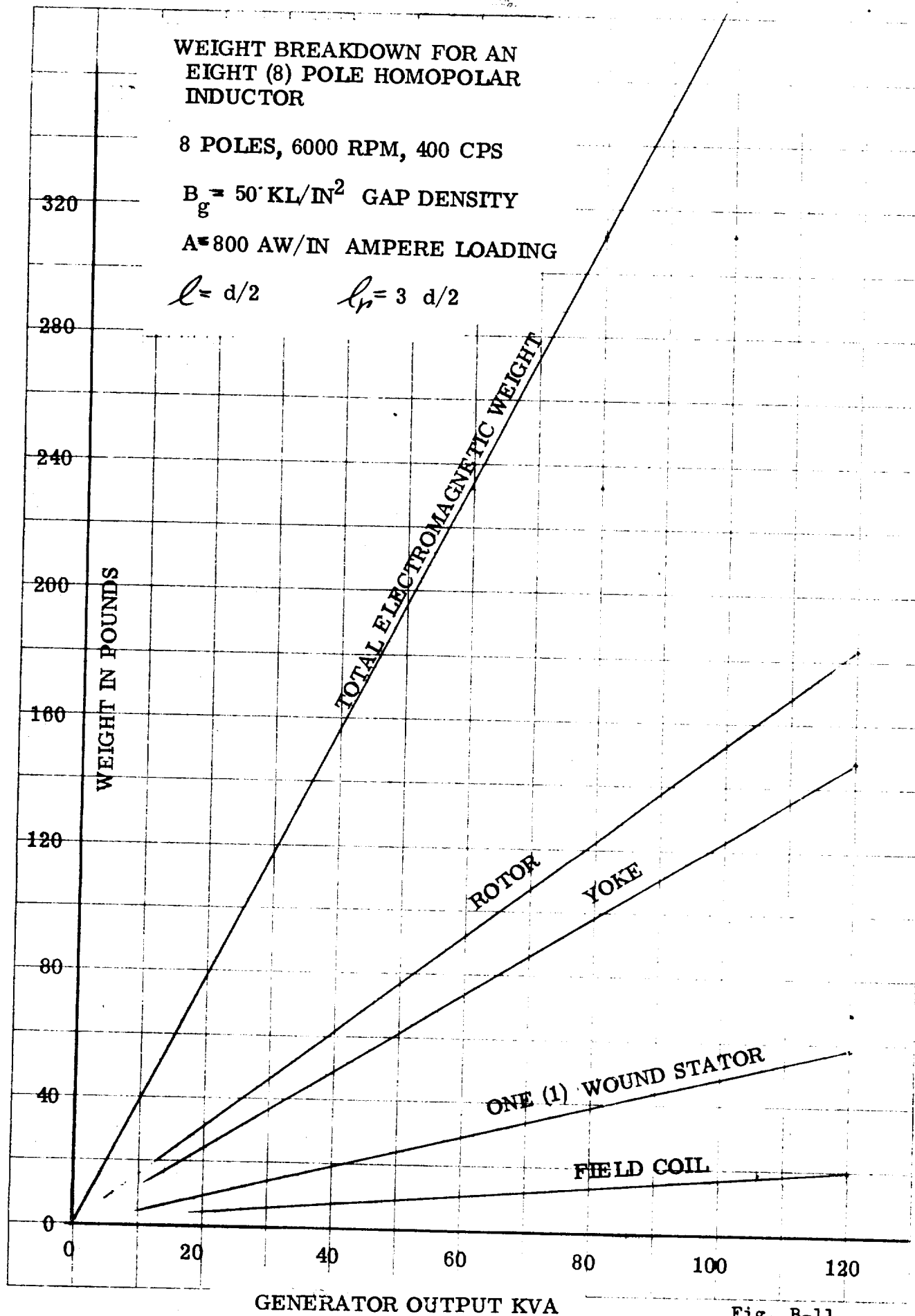


Fig. B-11

**WEIGHT versus OUTPUT RATING FOR WOUND, LAMINATED
STATORS OF A-C ELECTROMAGNETIC GENERATORS**

Use as approximate for 4-pole, 6-pole, 8-pole,
400 cps generators, wound-pole, salient-pole,
and non-salient-pole.

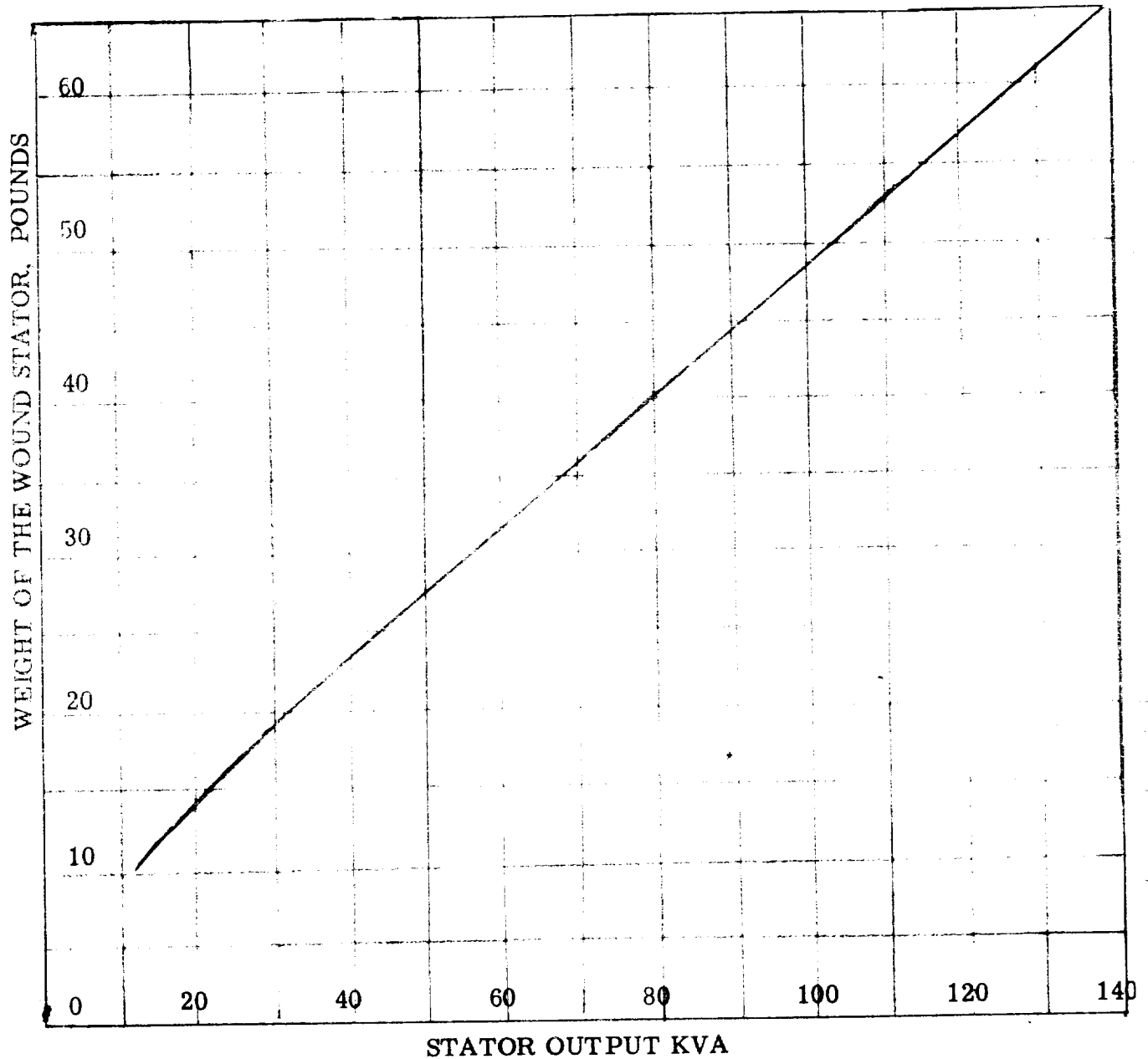
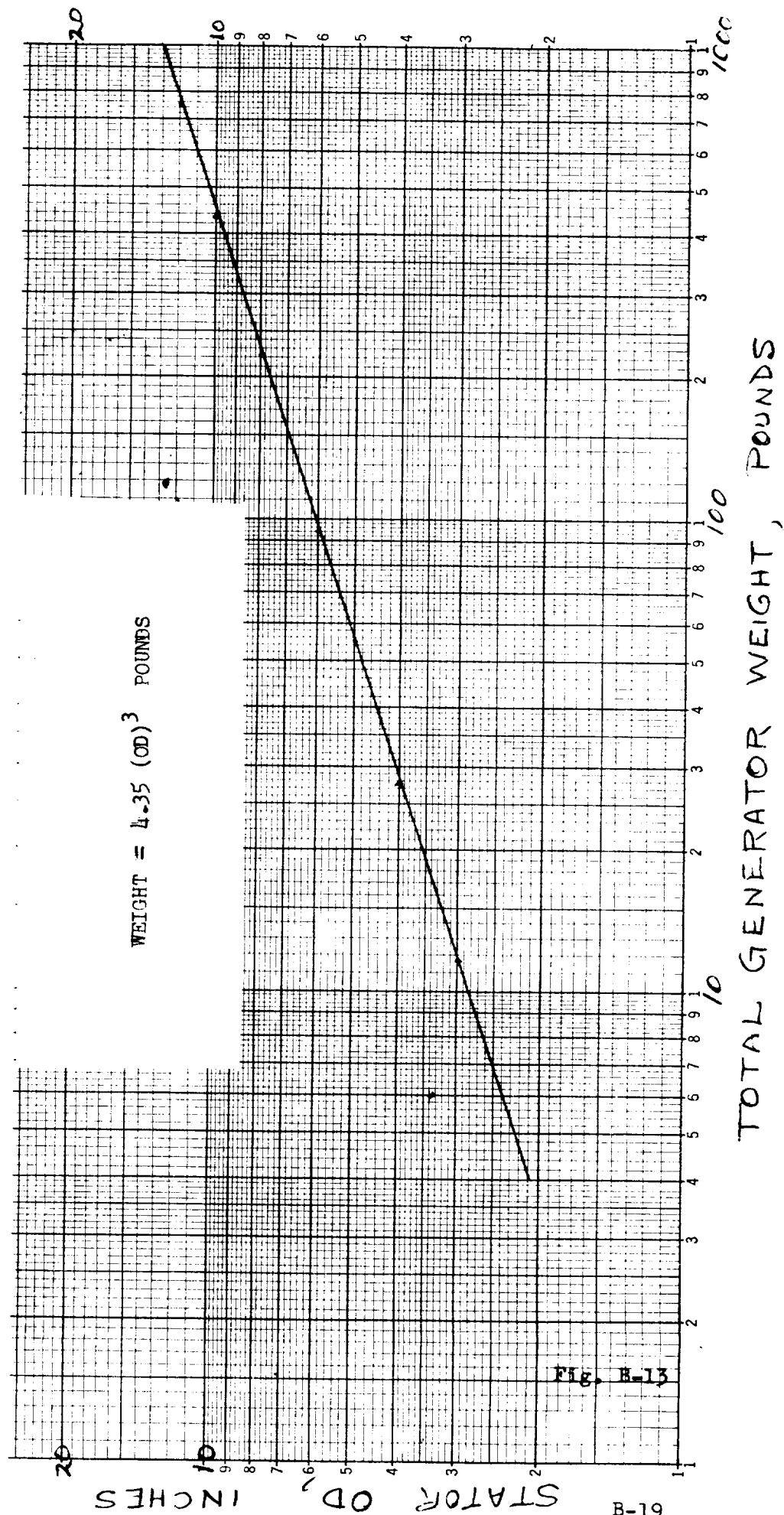


Fig. B-12

WEIGHT VS STATOR OD, FOR DISK-TYPE LUNDELL GENERATORS HAVING ONE STATOR



KVA OUTPUT VS STATOR O.D. FOR DISK-TYPE GENERATORS HAVING A SINGLE STATOR

The assumed parameters are: $B_p = 30$ kilolines per square inch
The stator ampere loading A , is 700 amperes per inch of
stator periphery (taken at the average stator diameter).

$$\text{The formula } KVA = \frac{P_g A (RPM) D^2 L}{90 (10^3)}$$

$$\text{becomes } KVA = \frac{5.55 \text{ RPM (OD)}^3}{10^6}$$

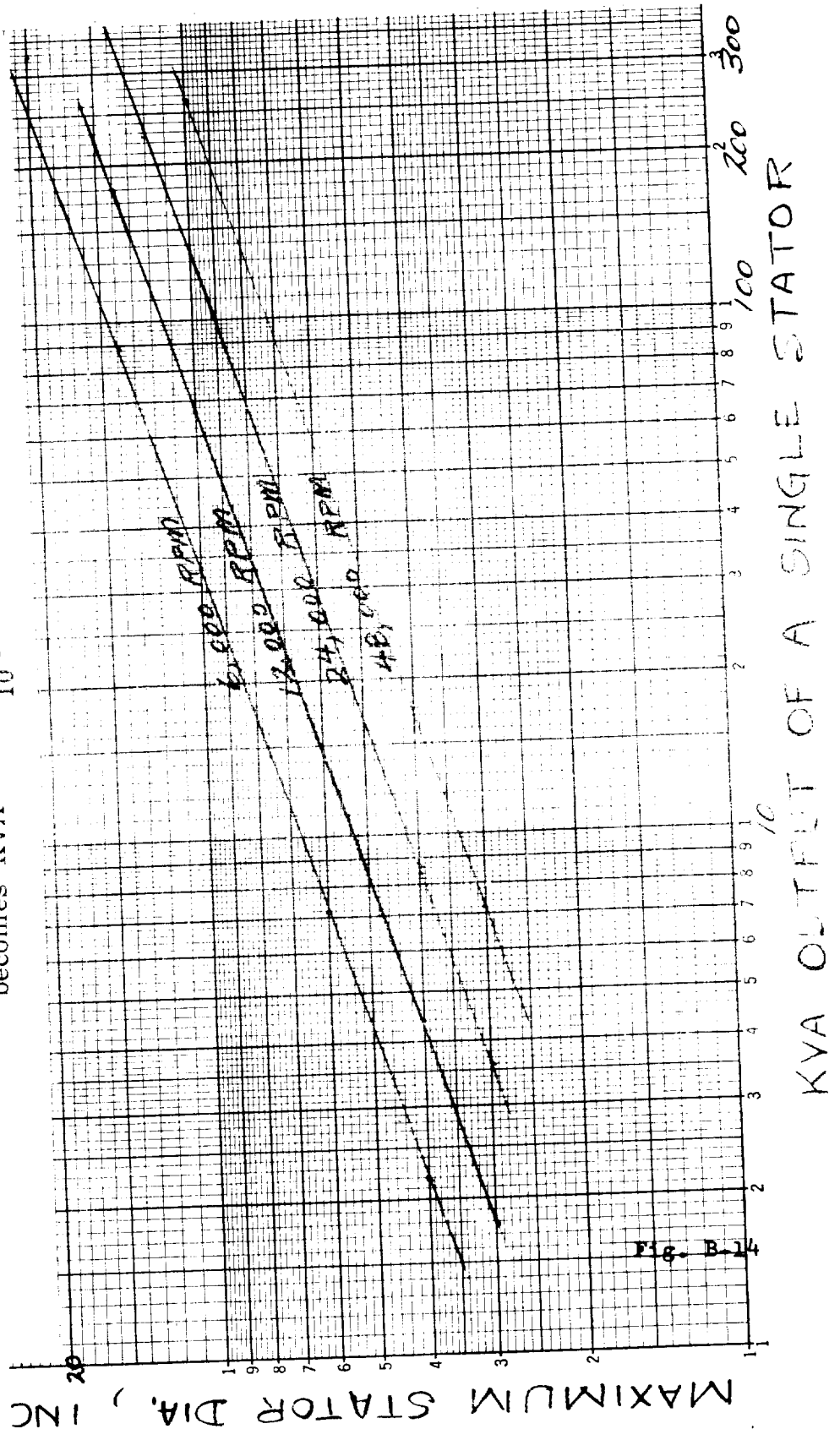


Fig. B-14

POLE FACE LOSSES

The pole-face losses given on pages B-22 through B-25 should be used as the approximations they are. The curves are inserted here to call attention to a limiting condition and a problem. The source of the formulae and derivation of the curves are both given in the Appendix.

The output of a solid rotor generator is limited by the amount of pole-face loss that can be tolerated thermally so more work needs to be done both on ways to limit the pole face loss and on more exact methods of calculating the losses.

Two methods considered for reducing pole-face losses have been:

1) Rotor surface treatment to increase the resistivity of the steel and 2) grooving the rotor to approximate a laminated condition at the pole surface. The first method has given inadequate results for the materials tried. The losses for a solid pole face are from 5 to 6 times as great as for a properly laminated pole face.

POLEFACE LOSSES AT NO LOAD AND AT FULL LOAD
 FOR ROTORS OF VARIOUS DIAMETERS $B_g = 30 \text{ KL/IN}^2$
 $A = 900 \text{ AW/IN}$ SLOT PITCH = .4 $b/g = 20$

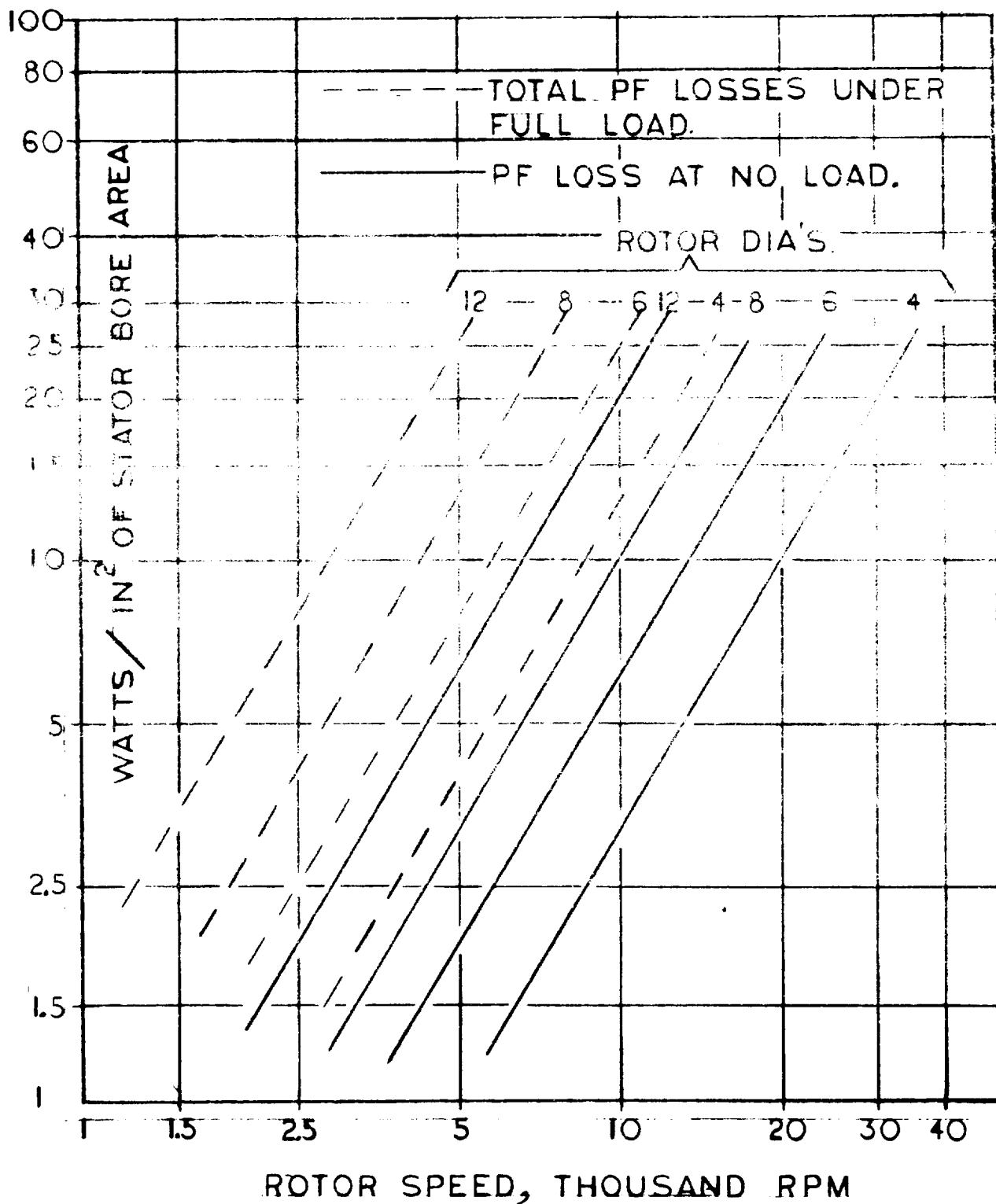
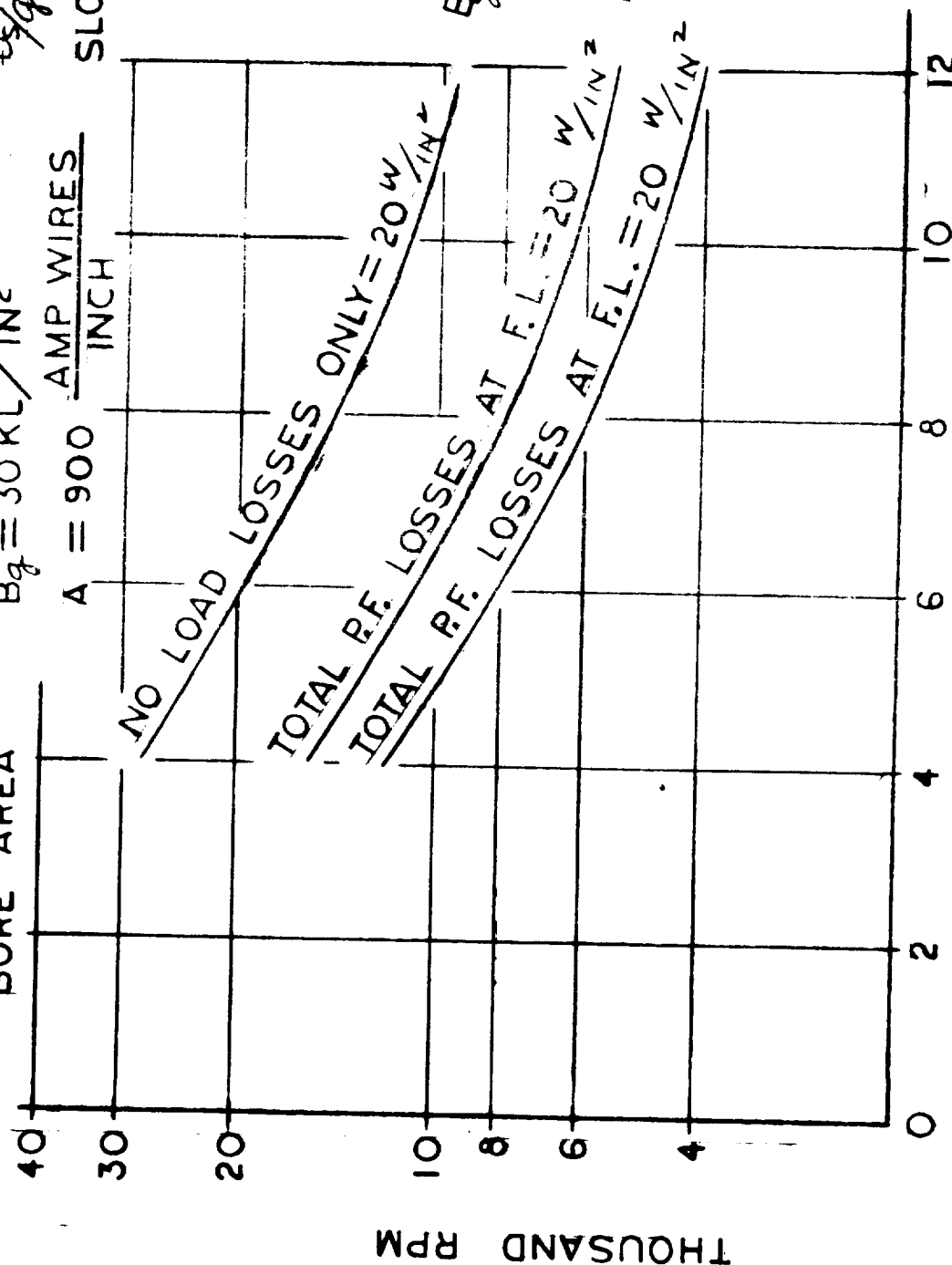


Fig. B-15

ROTOR DIA. VS ROTOR SPEED FOR SOLID POLE FACE ALTERNATORS
 LIMITED TO 20 WATTS / IN² POLE FACE LOSSES BASED ON STATOR
 BORE AREA $B_g = 30 \text{ KL} / \text{IN}^2$ $C_1 = 1.0$

SLOT PITCH = .30

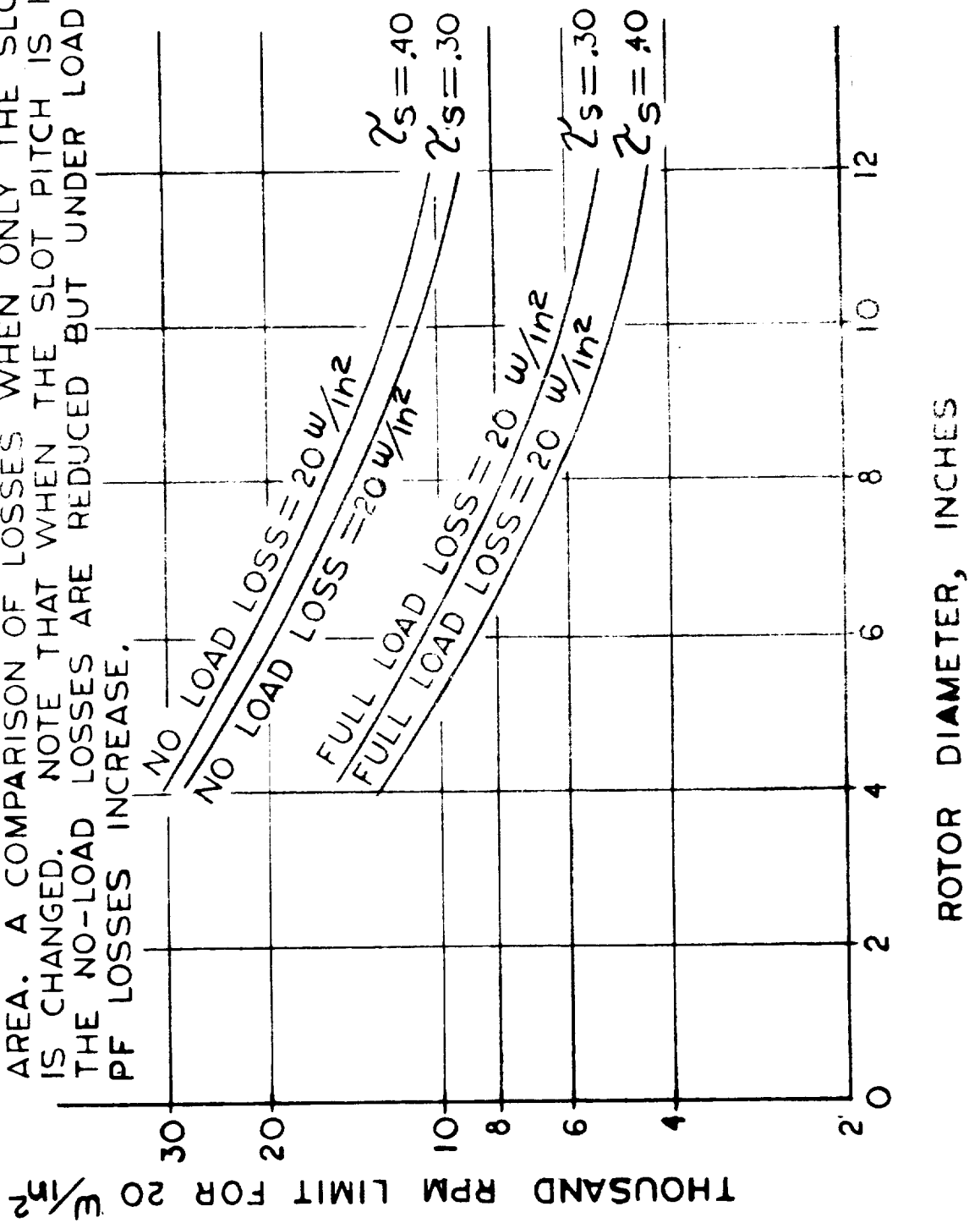
A = 900 AMP WIRES
 INCH



ROTOR DIAMETER, INCHES

CURVE

ROTOR DIA. VS ROTOR SPEED FOR SOLID POLE FACE ALTERNATORS LIMITED TO 20 WATTS PER SQ. INCH BASED ON THE STATOR BORE AREA. A COMPARISON OF LOSSES WHEN ONLY THE SLOT PITCH IS CHANGED. NOTE THAT WHEN THE SLOT PITCH IS INCREASED THE NO-LOAD LOSSES ARE REDUCED BUT UNDER LOAD THE TOTAL PF LOSSES INCREASE.



POLEFACE LOSSES IN A SOLID POLEFACE AT
 NO LOAD AS A FUNCTION OF SPEED WHEN
 THE GAP DENSITY $B_g = 45 \text{ KL/IN}^2$
 $b_g = 2.0$ SLOT PITCH $\gamma_s = .30$

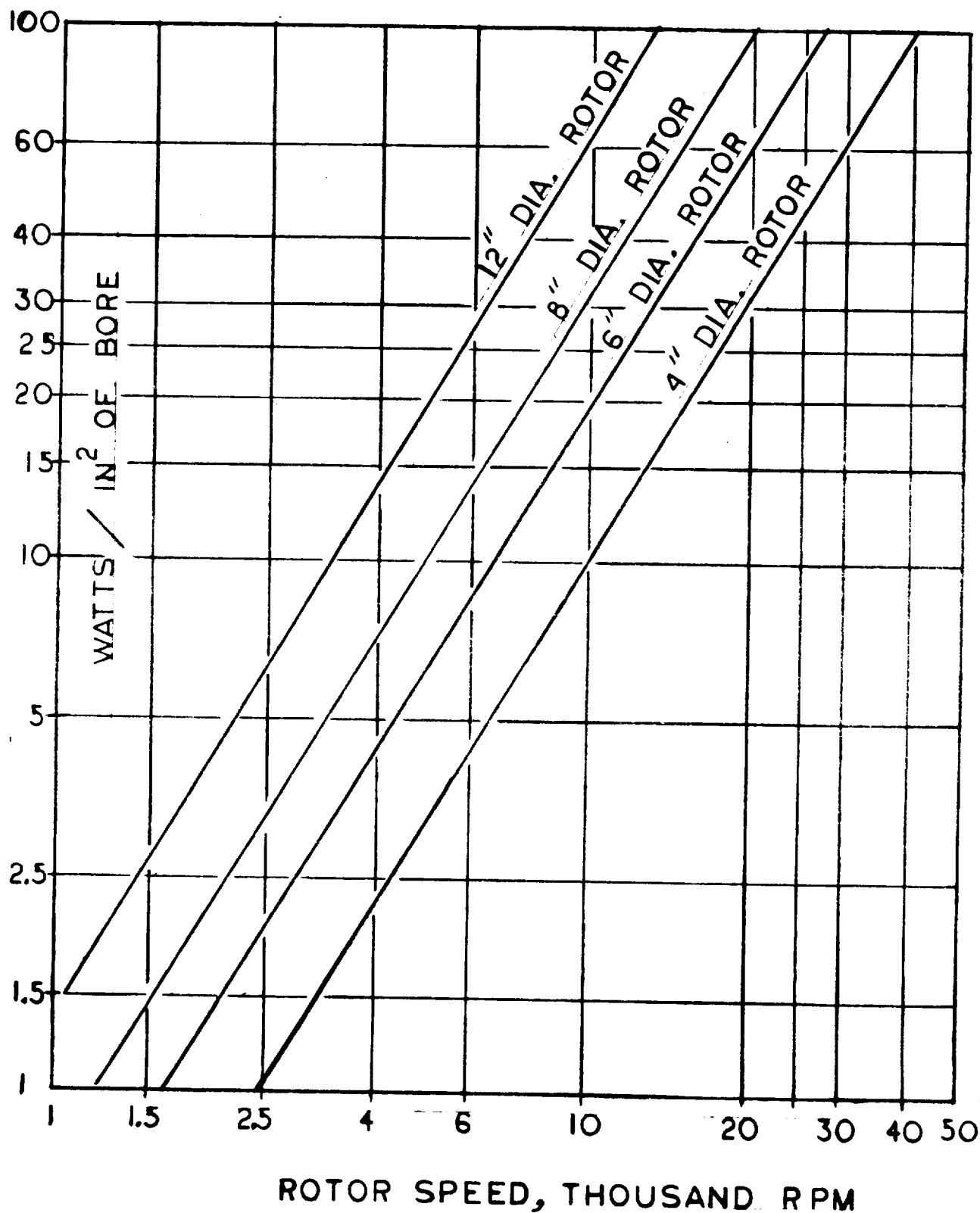
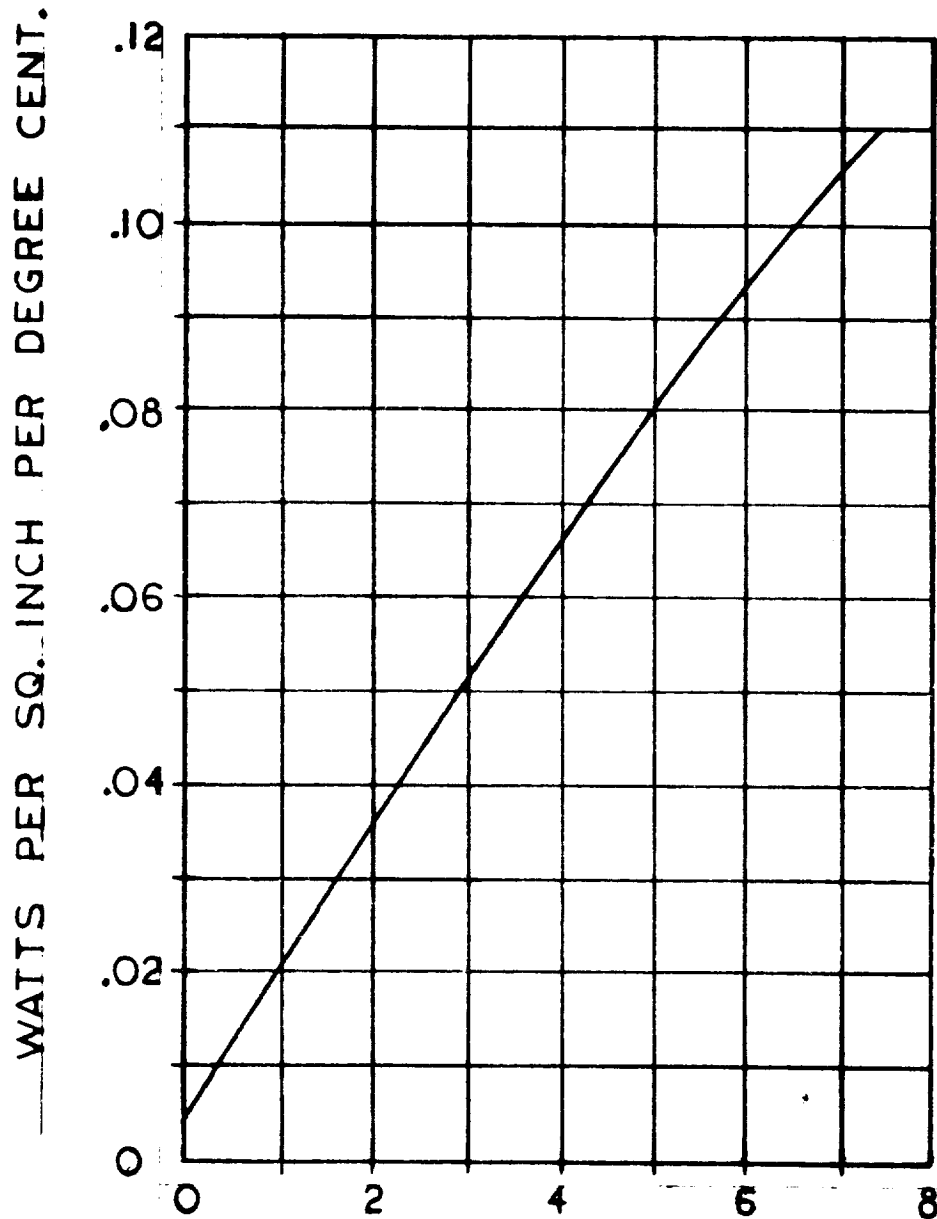


Fig. B-18

SURFACE HEAT DISSIPATION FROM
A GENERATOR ROTOR.



AVERAGE AIR VELOCITY THROUGH
MACHINE IN THOUSANDS OF FEET
PER MINUTE.

FROM LUKE: HEATING OF RAILWAY
MOTORS. AIEE TRANS 1922 VOL 41
PP 165-173.

USING SYNCHRONOUS GENERATORS AS MOTORS

IN BRIEF

Synchronous generators can be started as induction motors and operated as synchronous motors. The following discussion explains motor operation of the two types of synchronous generators; wound-pole and solid-rotor.

DISCUSSION

General

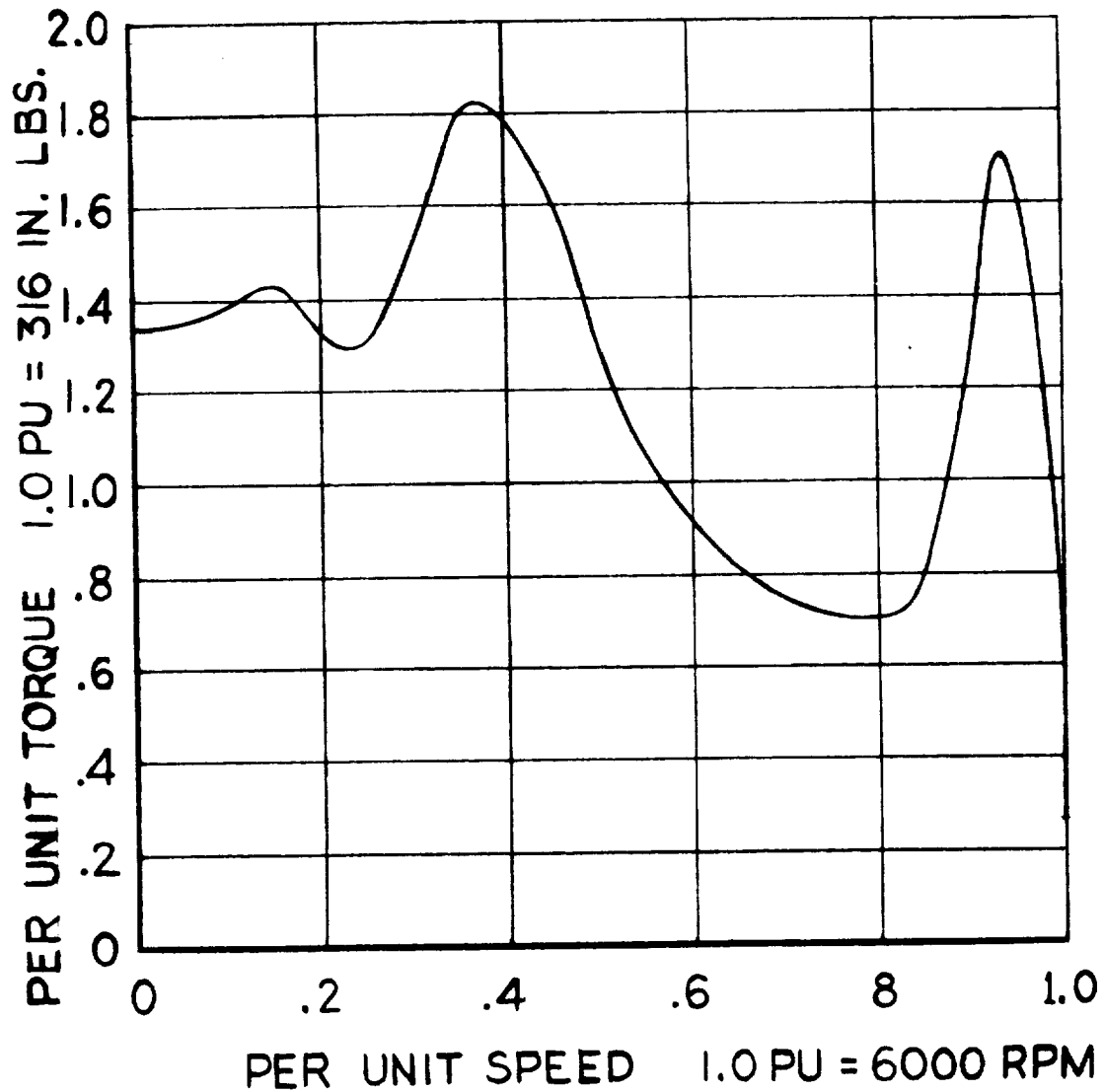
The rotating electrical generator converts mechanical energy to electrical energy. Electric motors convert electrical energy to mechanical energy. There is no basic difference in the two classes of machines as one machine can be designed to operate reversibly - as a motor or as a generator.

If the synchronous generator is used as a motor, it can operate either as a synchronous motor or as an induction motor. An induction generator can be motored only as an induction motor. The two modes of electrical motor operation are, then, synchronous and induction.

When the synchronous generator operates as a synchronous motor, it can be brought into synchronism by starting it as an induction motor until its speed is near synchronism and then applying field current to the d-c fields to accelerate the rotor to synchronous speed. It can also be started in synchronism by slowly varying the voltage and frequency from a low voltage level and low frequency to the rated values. This latter method is called a full synchronous start and throughout this kind of start, the synchronous motor can produce rated torque at rated current. Since the full synchronous start requires special supply equipment, it is not often used.

A salient-pole wound-field synchronous generator can be, and usually is, made with a pole face winding that is essentially an induction motor cage winding. This winding is called an amortisseur or damper winding. Its primary purpose

SPEED-TORQUE CHARACTERISTIC OF A
WOUND-POLE, SALIENT-POLE, SYNCHRONOUS,
GENERATOR HAVING A COPPER CAGE
WINDING. FIELD WINDINGS ARE SHORTED.
NO SKEW IN STATOR OR ROTOR



GENERATOR IS 30 KVA, .75 PF, 400 CPS,
6,000 RPM. P.U. BASE IS 22.5 KW.

FIGURE B-20

in a generator is to damp out rotor oscillations and negative sequence flux waves. The same cage winding is well suited for induction motor operation and can sometimes be made as a double cage winding for higher starting torque combined with low slip.

The synchronous motor with the damper winding (or squirrel cage pole face winding) can have about the same speed-torque characteristics as an induction motor. The important difference is that the cage winding is much smaller than it would be if the motor were a normal induction motor, and the operating cycle must be short because of the small cage bars. Large synchronous motors are frequently limited to two successive starts after which the rotor cage must be allowed to cool for about 30 minutes before another start is attempted. They cannot be continuously operated out of synchronism.

Speed-Torque Characteristic of Salient-Pole Machine

The speed-torque characteristics of a 30 KVA salient-pole, synchronous generator operating as an induction motor is shown in Fig. B-20. This generator shows cusps in the speed torque curve that can be removed by skewing the stator one slot pitch.

Per-Unit Base

The speed-torque curves in this discussion are plotted on a per-unit scale with the generator nameplate kilowatt rating used as the 1.0 P. U. base. The 30 KVA, .75 PF machine tested has a KW rating of 22.4 KW.

$$1.0 \text{ P. U. torque is then } T = \frac{(84300) (22.5)}{6000} = 316 \text{ in. lb.}$$

$$\text{Torque in inch pounds} = \frac{84300 (\text{Kilowatts})}{\text{RPM}}$$

Such a base is meaningful. A machine designed for low power-factor loads has lower reactances than a machine designed for the same output at a high power factor. The per unit torque of a low reactance motor is higher than that of a high reactance motor.

Induction Motor Characteristics

The starting and speed-torque characteristics of an induction motor can be varied over a wide range by changing the resistance of the rotor winding. Wound-rotor induction motors are made with insulated polyphase rotor windings. These windings connect to slip rings on the shaft and variable external resistance can be added to the rotor windings. By varying these resistances, the maximum torque point on the speed-torque curve can be varied from zero speed to around 98% speed. Synchronous motors have been made with insulated, pole face windings connected through slip rings to external starting resistances. Such motors are special and seldom used.

When the rotor resistance of a polyphase induction motor is changed, the speed torque characteristic curve retains its basic shape but changes scale. The maximum torque remains the same but moves to a new slip point that is proportional to the change in resistance. If the resistance of the rotor is doubled, all of the points of the speed-torque curve shift to new slip values twice that of the original. Figure B-21 illustrates this change.

The characteristic curve shown for rotor resistance $R = 1$ is approximately that of a normal low-slip motor. The characteristic curve shown for $R = 4$ is for a high slip motor and could represent a torque motor.

A motor designed to give high torque against a load driving it in the reverse direction might have the characteristic shown for $R = 8$.

TORQUE - SLIP CURVES OF AN INDUCTION MOTOR SHOWING THE EFFECT OF VARYING THE RESISTANCE OF THE ROTOR WINDING.

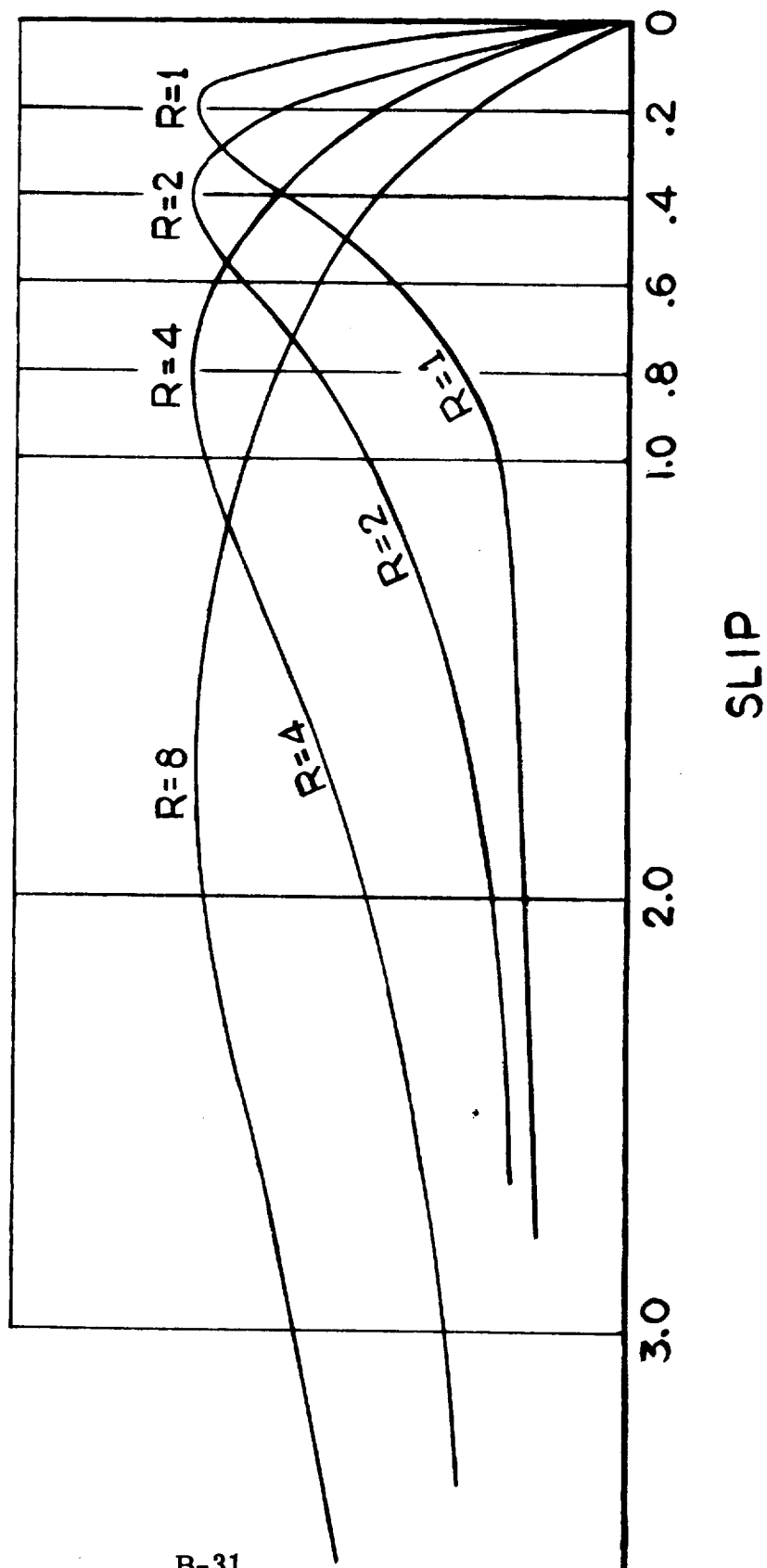


FIGURE B-21

If a synchronous motor having a cage winding is to start under load and synchronize, it may be required to have high starting torque and low slip. A low slip motor will produce its maximum torque at 95% to 98% of synchronous speed.

To pull into synchronism, the usual synchronous motor must be operating at 95% speed or more when the field current is applied. The torque resulting from the attraction between the moving stator flux wave and the flux from the wound rotor pole must be sufficient to accelerate the rotor from the 95% speed to synchronous speed.

If the slip is too great, (the speed too low) at the time field current is applied in an attempt to synchronize, the rotor will slip poles, the speed will decrease and the starting attempt must be discontinued before the rotor overheats. To have high starting torque, the damper or cage winding should have high resistance and the maximum speed as an induction motor may be well below 95% of synchronous speed, so that the machine cannot be synchronized. To obtain the combination of high starting torque and low slip, a double cage winding can be used in larger machines. The high slip frequency at standstill and the high reactance of the combination cage winding forces the rotor current into the top winding which has high resistance. At lower slip frequencies, the rotor current flows in the bottom cage winding also and the winding then has low resistance. This double cage winding was invented and first used by Dolivo Dobrowolsky in 1889.

Solid-Rotor Machines

If a synchronous machine has a solid pole face, a damper circuit is difficult to install and its effect is not pronounced. The characteristics of a solid-pole, Lundell generator starting at no-load, rated voltage, are shown on Figure B-22.

The no-load starting characteristics of the solid rotor are shown with and without a copper cage winding. Both rotors pulled into synchronism quickly (i.e., without hesitation or any evidence of marginal operation) without field excitation. The test curves show that the copper cage does increase torque near synchronism.

The solid rotor synchronous motor is usually impossible to synchronize under load and some designs cannot be relied upon to synchronize at no load unless special steps are taken. Such special steps may be operating at a frequency higher than rated during the start so that the terminal speed of the rotor is above rated synchronous speed, then reducing the frequency of the supply current faster than the rotor speed can drop. The rotor will then easily synchronize with the supply.

SPEED-TORQUE CHARACTERISTIC OF A TWO-COIL LUNDELL
GENERATOR WITH SOLID POLE FACES.

TWO ROTORS WERE TESTED -- ONE WITH COPPER CAGE
AND ONE WITHOUT.

GENERATOR RATING 30 KVA, .75 PF, 400 CPS, 8000 RPM.

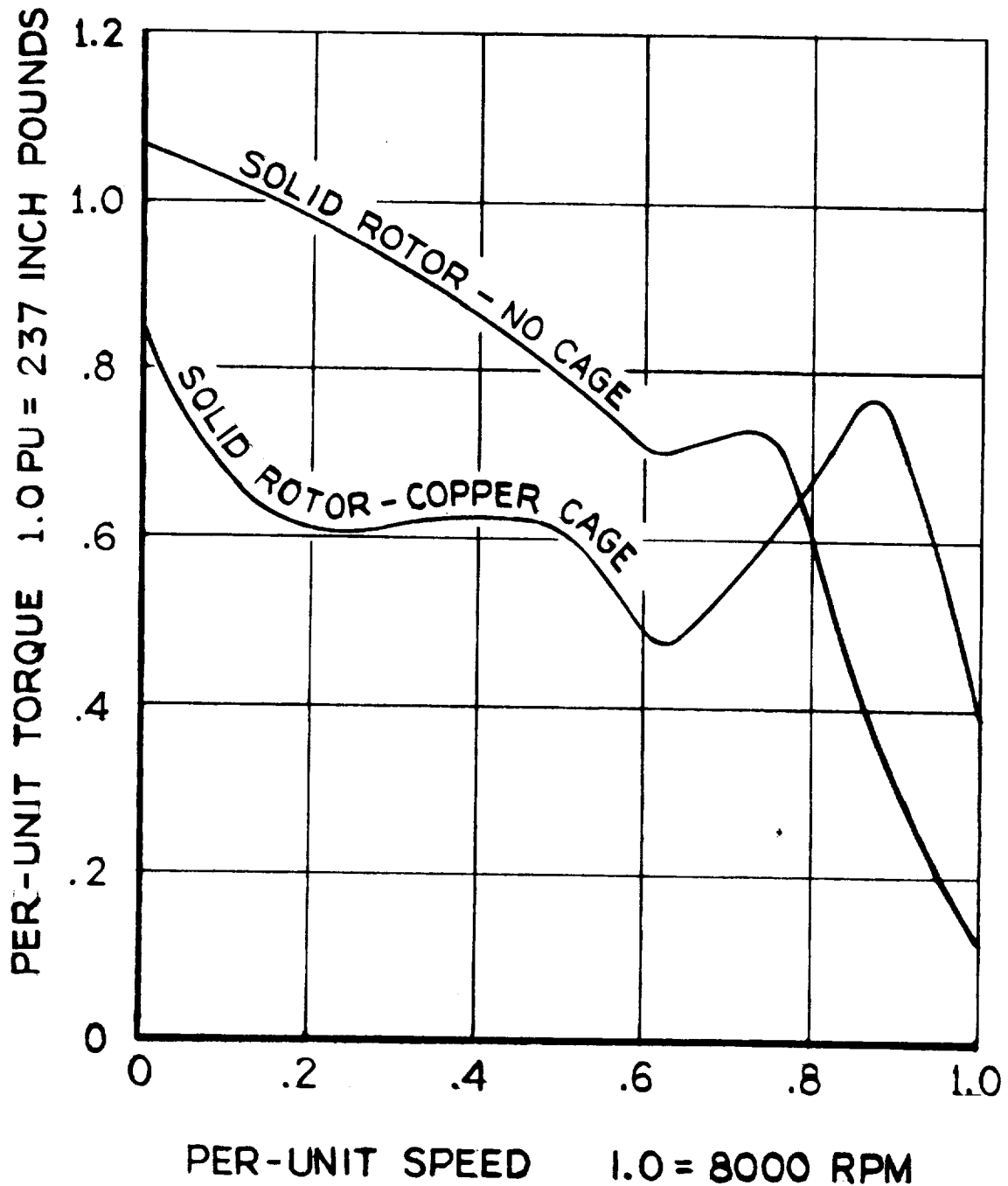
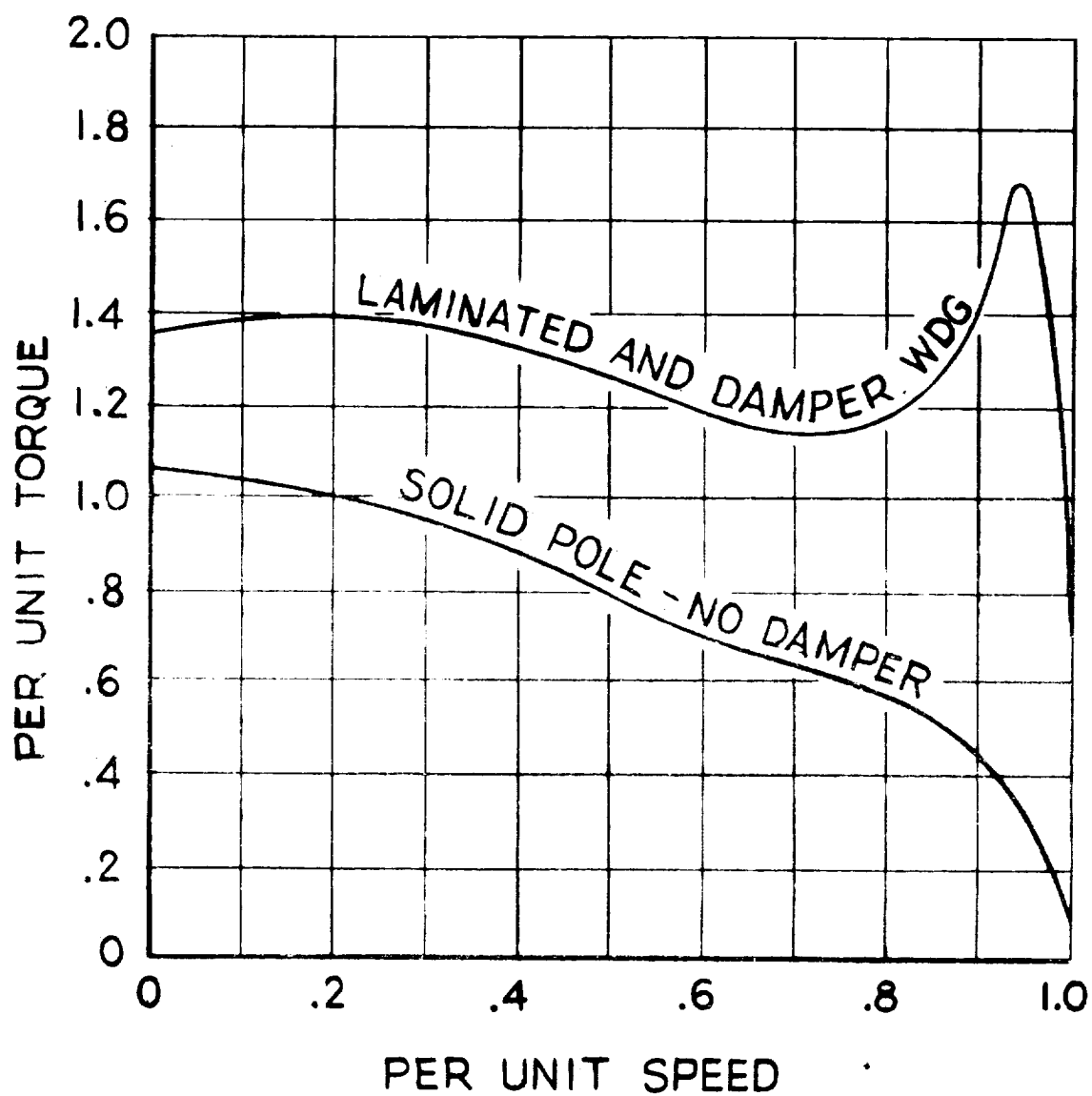


Fig. B-22



Comparison of speed torque characteristics to be expected from conventional salient-pole generators with damper windings and solid-pole Lundell generators without damper windings ($X_d = 160\%$ approx.).

Fig. B-23

Another procedure that can sometimes be resorted to is to use a small induction motor having a higher synchronous speed and mounted on the same shaft as the large machine. The small machine will assist the large machine enough to drive it up to synchronous speed. Starting motors are sometimes used on large synchronous condensers where normal starting currents in the large machine would cause a severe voltage dip on the utility distribution system.

Some of the brushless generators have rotors that can easily be laminated and some do not. If the rotor speed is not too great, the homopolar inductor generator can have laminated rotors and also cage windings. The Lundell generators are difficult to make with laminated rotor poles. The heteropolar inductor cannot have a cage winding at all and we do not know how to use it as a motor. The cascade machine has its cage winding on the d-c poles for generator operation.

Of the synchronous generators, the solid rotor machines can operate longest as induction motors. The losses in the solid rotor are not concentrated in small bars but are distributed well over the entire rotor surface. The heat transfer is fast and the entire rotor stores the heat. The laminated rotor with a small cage winding has its losses concentrated in the bars and heat transfer from the bars to the steel laminations is poor.

Continuous Operation

When some significant load is to be carried by a synchronous machine for any appreciable time such as 20 HP motor load on a 20 KVA generator, the machine must be in synchronism - both to carry the load and to survive for more than a few minutes (of the order of 5 minutes).

If the load and speed are both reduced enough, the generator can operate continuously as an induction motor because the rotor has some continuous load capability as an induction motor.

Rotating Rectifier Machine

The wound-pole synchronous generators with rotating rectifiers on or in the shaft have a special starting problem that usually prevents their being considered for motor duty.

When a wound-pole synchronous machine is started as a motor, the fields are shorted through a starting resistance that can be zero or some finite value. If the fields are open, the induced voltage in the field is dangerous to the field insulation. Fig B-24 shows the field voltage of a 30 KVA, 6000 rpm wound-pole synchronous generator during a motor start. The fields were open circuited during one start and shorted through a 15 ohm resistor during another start. The resulting curves demonstrate that the maximum current induced was 12-1/2 amperes and that the induced voltage on open circuit was 1800 volts RMS at standstill and 300 volts RMS at 90% speed.

When rectifiers are used in the excitation supply circuit, they block on one half cycle so that the resistance presented by them is, for practical purposes, infinite. Since obtainable rectifiers cannot withstand 2000 (+) volts or even 650 (+) volts in the reverse direction, the fields must still be shorted during the start cycle and then energized to pull the machine into synchronism.

To short the fields during the start, three methods that have been tried are:

1. Short the fields by using slip rings, brushes, and a relay. Open the relay at end of induction motor start.
2. Use a centrifugal switch that shorts the fields at standstill and opens them at 90% or more of synchronous speed.
3. Use controlled diodes with the rectifier bridge and apply them in such a way that they short the motor field automatically during the start cycle.

Stationary coil, brushless machines do not have a comparable starting problem.

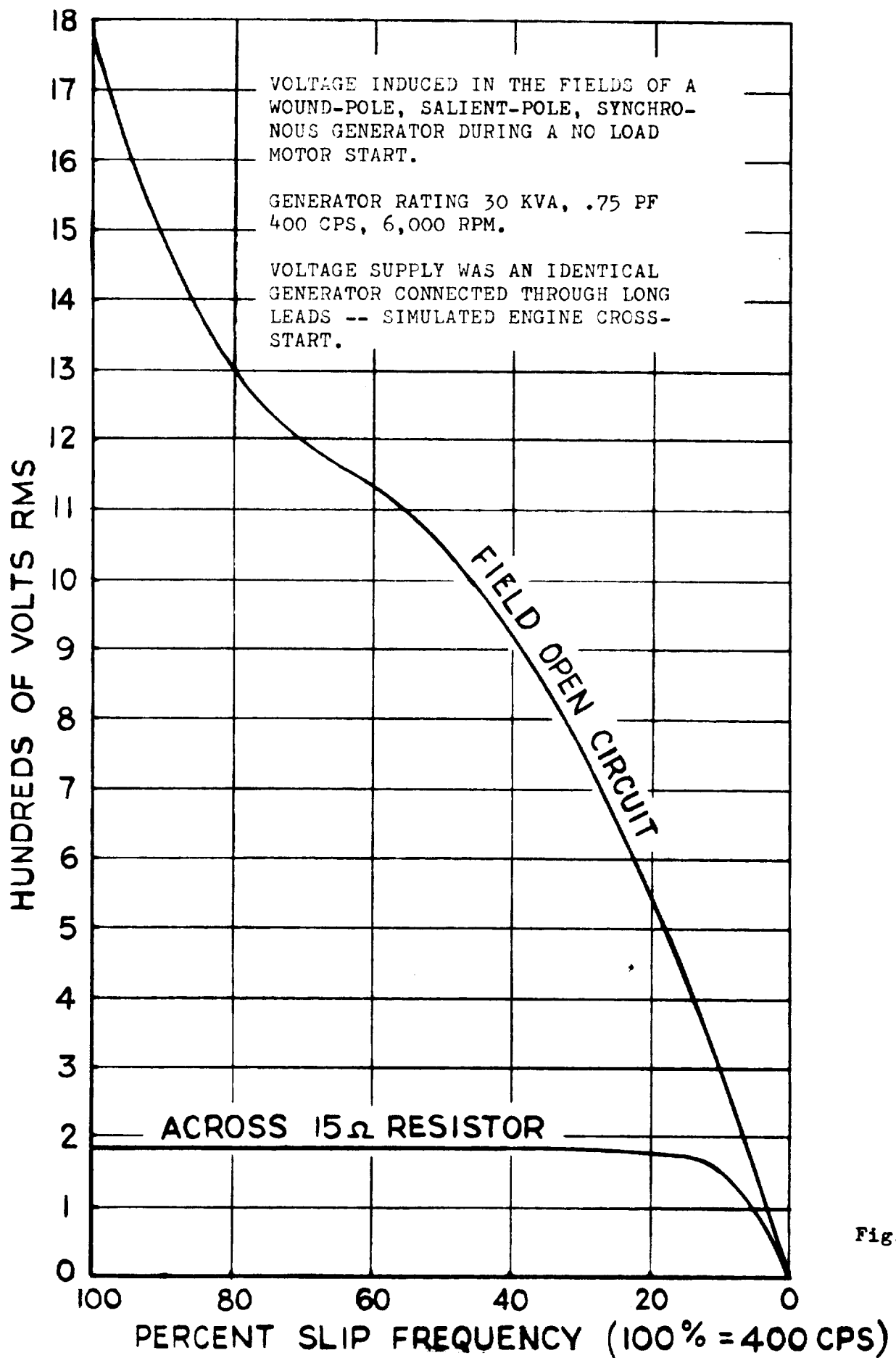


Fig. B-24

GENERATOR THERMAL ANALYSIS

TABLE OF CONTENTS

	Page
A. INTRODUCTION	C-1
B. PROBLEM STATEMENT	C-2
C. RESULTS	C-3
D. ANALYSIS	C-4
1. Calculation of Thermal Resistances	C-6
a. Rotor Shaft and Bearing	C-7
b. Stator and End Turns	C-11
2. Nodal Equations	C-17
a. General Description	C-17
b. Equations in Index Notation	C-18
c. Definition of Matrix Coefficients	C-22
3. Description of Computer Program	C-38
a. Input Preparation	C-38
b. Method of Operation	C-41
4. Sample Calculation Illustrating Use of Computer Program	C-43
a. Preparation of Input	C-43
b. Program Output	C-46
c. Discussion of Sample Calculation	C-46
E. CONCLUSIONS AND RECOMMENDATIONS	C-50
FIGURES	C-51
APPENDICES	C-53
- Rotor Friction Analysis	C-54
- Computer Program Listing (See Computer Appendix SECTION CA)	
NOMENCLATURE	C-65

A. INTRODUCTION

In recent years, electrical alternators have found increasing use in applications which emphasize reliability, compactness and high specific power output. The most demanding of these applications has been auxiliary space power generation.

Space equipment must necessarily be highly reliable and yet as compact as possible. These two requirements are similar in demands they place on the heat transfer characteristics of an alternator. Reliability decreased with increasing temperature because of the adverse effects of higher temperatures on the life of electrical insulation. Increasing compactness which results in higher specific power, causes higher internal temperatures because the losses per unit volume of material are higher. Thus, the achievement of both high reliability and greater compactness depends on the designer's ability to predict and control internal temperatures.

The objective of this study is to develop an analytical model which will enable the design engineer to quickly determine the steady-state temperature distribution of several alternator designs. The analytical model is then reduced to a design tool in the form of a computer program.

The work reported here was performed by Mechanical Technology, Inc. for Lear Siegler, Inc., as a part of their study for NASA of brushless rotating electrical alternators. The alternator configurations of particular interest are the homopolar, Lundel, and wound-rotor designs.

B. PROBLEM STATEMENT

The objective of this study is to provide a tool for making engineering comparisons of the steady-state heat transfer characteristics of compact alternators.

The tool is to be a FORTRAN language computer program which will calculate general heat flow and temperature distributions in brushless alternators. Program input should include alternator geometry, thermal properties of the construction materials, appropriate thermal boundary conditions and internal heat generation rates.

C. RESULTS

The basic objective of this study was met. An analysis of the steady-state temperature distribution in a typical alternator was completed and reduced to a working tool in the form of a computer program.

The assumptions in the analysis make it applicable to alternators with steady-state temperatures, axisymmetric geometry and internal heat generation, and constant current density in the stator windings. The effect of temperature on the electrical resistivity of the windings and laminations has been included.

The analytical approach involved writing a heat balance for each internal temperature node in terms of the nodal temperatures, thermal resistances, heat input and boundary conditions. The resulting set of equations was represented by a matrix of coefficients multiplied by a matrix of unknown temperatures. The temperatures were then obtained by inverting the coefficient matrix.

A sample problem representing a known electric motor was used to test the computer program. The resulting temperatures appear reasonable both in magnitude and distribution. Furthermore, the calculated winding temperatures would lead to a predicted motor life that is compatible with the 2500 hours of operation the motor has logged to date.

D. ANALYSIS

Analysis of the temperature distribution in an alternator requires a mathematical model describing the internal heat flow paths, the heat transfer boundary conditions, and material properties. In the model selected, the generator geometry is represented by a grid of temperature nodes connected by heat flow paths described as thermal resistances. At selected internal nodes, provision is made for heat input representing internal heat generation. Thermal boundary conditions are described by a sink temperature or a cooling-gas stream temperature. The program also takes into account the effect of increased temperature on the electrical resistivity of the materials of construction.

The analytical approach has four basic steps:

1. The equations for the thermal resistances between nodes are developed.
2. A heat balance is written for each node in terms of the nodal temperature, thermal resistances, heat input, and boundary conditions.
3. The nodal equations are represented as a matrix of coefficients where each coefficient is a composite of thermal resistances and heat inputs.
4. The matrix of coefficients is solved for the unknown temperatures using a matrix inversion technique.

The following parts of this section describe each of the above steps in detail along with the programming of the analysis for the IBM 1620 Computer. Since the program was written in the widely used FORTRAN computer language, it is not limited to the 1620 alone. It can readily be recompiled for any computer equipped with a FORTRAN compiler.

The major assumptions in the analysis were:

1. Temperature distributions are steady-state.
2. Geometry is axisymmetric and symmetrical about the mid-plane perpendicular to the axis of revolution.
3. Internal heat generation is two-dimensional but axisymmetric.

4. Current density in the stator windings is constant. The temperature coefficient of resistivity is applied to the product I^2R .

The types of internal heat generation which are accounted for are as follows:

1. I^2R heating in the copper windings in the stator.
2. Eddy current losses in the stator laminations.
3. Stray-load losses in the stator core due to armature current.
4. Rotor losses.
5. Iron losses (hysteresis loss).
6. Bearing friction and rotor windage loss.

The losses appear in the analysis as heat inputs at appropriate nodes.

A separate section of this report, Appendix CA, is devoted to formulae for calculation of friction and windage losses.

1. Calculation of the Thermal Resistances

The thermal resistances used in describing the alternator are composites of two basic types of resistance, conduction and convection. The resistances can be obtained from the basic law of heat transfer, i.e.,

$$q = \frac{\Delta T}{R}, \text{ where } \Delta T = \text{temperature differential}$$

R = thermal resistance

q = rate of heat flow

Conduction

For conduction in a solid, the thermal resistance is given by

$$(1) \quad R = \frac{12\ell}{kA}, \frac{^{\circ}\text{F-hr}}{\text{Btu}} \quad \text{where } \ell = \text{length of conduction path in direction of heat flow, inches.}$$

A = cross sectional area perpendicular to heat flow path, in.²

k = thermal conductivity of material, Btu/hr.-ft.-[°]F

For the particular case of a circular cylinder with conduction in the radial direction:

r_2 = outer radius, in.

r_1 = inner radius, in.

L = axial length, in.

$\ell = r_2 - r_1$, in.

$$A = \text{mean area} = 2\pi L \bar{r}_{\text{mean}} = 2\pi L \frac{r_2 - r_1}{\log_e \frac{r_2}{r_1}}, \text{ in.}^2$$

$$(2) \quad R_{\text{cyl.}} = \frac{6}{\pi k L} \log_e \frac{r_2}{r_1}, \frac{^{\circ}\text{F-hr.}}{\text{Btu}}$$

Convection

For convection from the outside surface of an area A_s :

$$(3) \quad R = \frac{144}{h_s A_s}, \text{ where } h_s = \text{surface heat transfer coefficient, Btu/hr.-ft.}^2\text{-}^{\circ}\text{F.}$$
$$A_s = \text{surface area, in.}^2$$

The various thermal resistances used in the analysis are composites of one or more of equations (1), (2), and (3).

The following equations describe the method of calculating the thermal resistances shown in Fig. C1. Details of the thermal resistances in the stator are shown in Fig. C2 for clarification.

a. Rotor Shaft and Bearing

Resistance 1 - Axial resistance of shaft beneath half of the axial length of the bearing plus any external resistance (if any) to an ultimate sink.

$$R_1 = \frac{6b}{\pi k_s (r_2^2 - r_1^2)} + R_{\text{SHAFT}} \quad (1)$$

Resistance 2 - Combination resistance of radial conduction through the shaft and half the thickness of the bearing film.*

$$R_2 = \frac{6 \ln \frac{r_2}{r_1}}{\pi k_s b} + \frac{3t_p}{\pi k_g r_2 b} \quad (2)$$

Resistance 3 - Combination resistance of radial conduction through half the thickness of the bearing film* and bearing to ultimate sink.

$$R_3 = \frac{3t_p}{\pi k_g r_2 b} + R_{\text{Bearing}} \quad (3)$$

Resistance 4 - Combination of axial resistance along a length of shaft equal to $d/3$ plus $b/2$.

$$R_4 = \frac{12}{\pi k_s (r_2^2 - r_1^2)} \left(\frac{b}{2} + \frac{d}{3} \right) \quad (4)$$

* The expression for heat transfer across the bearing film, $\frac{3t_p}{\pi k_g r_2 b}$, applies to laminar films which are the most common. For turbulent bearings, heat transfer will be governed by the surface heat transfer coefficient, h .

Resistance 5 - Combination of radial conduction and convection from an axial length of shaft of $2/3 d$.

$$R_5 = \frac{108}{\pi r_2^2 h_s} + \frac{9}{\pi k_s d} \ln \left(\frac{r_2}{r_1} \right) \quad (5)$$

Resistance 6 - Axial conduction along a shaft length of $d/2$.

$$R_6 = \frac{6d}{\pi k_s (r_2^2 - r_1^2)} \quad (6)$$

Resistance 7 - Combination of radial conduction and convection from an axial length of shaft of $d/3$.

$$R_7 = \frac{216}{\pi r_2^2 h_s} + \frac{18}{\pi k_s d} \ln \left(\frac{r_2}{r_1} \right) \quad (7)$$

Resistance 8 - Combination of axial conduction along a length of shaft of $d/6$ and a length of rotor of $\frac{\ell}{6}$.

$$R_8 = \frac{2d}{k_s \pi (r_2^2 - r_1^2)} + \frac{2\ell}{\pi k_{ri} (r_2^2 - r_1^2)} \quad (8)$$

Resistance 9 - Radial conduction in rotor along a length of $\frac{\ell}{3}$.

$$R_9 = \frac{18}{\pi k_r \ell} \ln \left(\frac{r_2}{r_1} \right) \quad (9)$$

Resistance 10 - Combination of radial conduction and convection in a gap over a length of $\frac{\ell}{3}$.

$$R_{10} = \frac{216}{\pi r_3^2 h_g \ell} + \frac{18}{\pi k_r \ell} \ln \left(\frac{r_3}{r_2} \right) \quad (10)$$

Resistance 11 - Axial conduction in rotor along a length of $\frac{\ell}{2}$.

$$R_{11} = \frac{6\ell}{k_{ro} \pi (r_3^2 - r_2^2)}$$

Resistance 12 - Axial conduction in rotor along a length of $\frac{\ell}{3}$.

$$R_{12} = \frac{4\ell}{k_{ri} \pi (r_2^2 - r_1^2)}$$

Resistance 13 - Equal to R_9 .

Resistance 14 - Equal to R_{12} .

Resistance 15 - Equal to R_{11} .

Resistance 16 - Equal to R_{13} .

Resistance 17 - Equal to R_8 .

Resistance 18 - Equal to R_7 .

Resistance 19 - Equal to R_6 .

Resistance 20 - Equal to R_5 .

Resistance 21 - Equal to R_4 .

Resistance 22 - Equal to R_2 .

Resistance 23 - Equal to R_1 .

Resistance 24 - Equal to R_3 .

Resistance 25 - Equal to R_{10} .

Resistance 26 - Equal to R_{10} .

b. Stator and End Turns

Resistance 27 - Combination resistance of convection and radial conduction into stator iron (Typical of R_i in Fig. C-2).

$$R_{27} = \frac{216}{\pi r_4 \ell h_g} + \frac{18}{\pi k_{lam} \ell} \ln \left(\frac{r_8 + r_4}{2r_4} \right)$$

Resistance 28 - Equal to R_{27} .

Resistance 29 - Equal to R_{27} .

Resistance 30 - Radial conduction in stator lamination (Typical of R_{zy} in Fig. C-2.

$$R_{30} = \frac{12 \left(\frac{R_9 + R_8}{2} - \frac{R_8 + R_4}{2} \right)}{k_{lam} \frac{\ell}{3} \frac{w}{2} 2K_s} = \frac{18 (R_9 - R_4)}{k_{lam} \ell w K_s}$$

Resistance 31 - Equal to R_{30} .

Resistance 32 - Equal to R_{30} .

Resistance 33 - Radial conduction in stator lamination (Typical of R_{xy} in Fig. C-2.)

$$R_{33} = \frac{12}{k_{lam}} \frac{\frac{R_5 - R_8}{2}}{\frac{\ell}{3} \frac{w}{2} 2K_s} = \frac{18 (R_5 - R_8)}{k_{lam} \ell w K_s}$$

Resistance 34 - Radial conduction from copper coil to stator lamination (Typical of R_z , in Fig. C-2).

$$R_{34} = \frac{18v}{k_u \ell K_s} + \frac{36 t_{ins}}{k_{ins} u \ell K_s} + \frac{18}{\pi k_{lam} \ell} \ln \left(\frac{2r_8}{r_8 + r_4} \right)$$

Resistance 35 - Equal to R_{33} .

Resistance 36 - Equal to R_{34} .

Resistance 37 - Equal to R_{33} .

Resistance 38 - Equal to R_{34} .

Resistance 39 - Axial conduction along copper coil from stack ends of motor to end turn.

$$R_{39} = \frac{2\ell}{k_c u v K_s F_{area}} + \frac{3\ell e}{\pi k_c F_{area} (r_7^2 - r_6^2)}$$

Resistance 40 - Axial conduction along copper stator coils.

$$R_{40} = \frac{4\ell}{k_c u v F_{area} K_s}$$

Resistance 41 - Equal to R_{40} .

Resistance 42 - Equal to R_{39} .

Resistance 43 - Radial conduction from coil to back iron of stator (Typical of R_x in Fig. C-2).

$$R_{43} = \frac{18v}{k * K_s u \ell} + \frac{36 t_{ins}}{k_{ins} u \ell K_s} + \frac{18}{\pi k_{lam}} \ln \left(\frac{r_5 + r_9}{2r_9} \right)$$

Resistance 44 - Equal to R_{43} .

Resistance 45 - Equal to R_{43} .

Resistance 46 - Surface heat transfer from end turns.

$$R_{46} = \frac{144}{\pi r_6 h_e d \ell_e}$$

Resistance 47 - Equal to R_{46} .

Resistance 48 - Radial conduction from end turn.

$$R_{48} = \frac{12}{\pi k * \ell_e} \ln \left(\frac{r_7 + r_6}{2r_6} \right)$$

Resistance 49 - Equal to R_{48} .

Resistance 50 - Axial conduction in end turns.

$$R_{50} = \frac{6\ell_e}{\pi k_{cop} F_{area} (r_7^2 - r_6^2)}$$

Resistance 51 - Radial conduction in end turns.

$$R_{51} = \frac{12}{\pi k * \ell_e} \ln \left(\frac{2r_7}{r_7 + r_6} \right)$$

Resistance 52 - Equal to R_{51} .

Resistance 53 - Surface heat transfer from end turns.

$$R_{53} = \frac{144}{\pi r_7 h_e \ell_e}$$

Resistance 54 - Equal to R_{53} .

Resistance 55 - Equal to R_{46} .

Resistance 56 - Equal to R_{46} .

Resistance 57 - Equal to R_{48} .

Resistance 58 - Equal to R_{48} .

Resistance 59 - Equal to R_{51} .

Resistance 60 - Equal to R_{51} .

Resistance 61 - Equal to R_{53} .

Resistance 62 - Equal to R_{54} .

Resistance 63 - Radial conduction in stator near stator outside surface.

$$R_{63} = \frac{18}{\pi k \ell} \ln \left(\frac{2r_5}{r_5 + r_9} \right)$$

Resistance 64 - Equal to R_{63} .

Resistance 65 - Equal to R_{63} .

Resistance 66 - Surface heat transfer at back iron surface.

$$R_{66} = \frac{216}{\pi r_5 \ell h_o}$$

Resistance 67 - Equal to R_{66} .

Resistance 68 - Equal to R_{66} .

Resistance 69 -

$$R_{69} = \frac{216}{\pi r_5 \ell h_o} \left(1 + \frac{h_o}{h_w}\right)$$

Resistance 70 - Equal to R_{69} .

Resistance 71 - Equal to R_{69} .

Resistance 72 - Conduction axially along stator iron.

$$R_{72} = \frac{4\ell}{k'_{lam} w v K_s}$$

Resistance 73 - Equal to R_{72} .

Resistance 74 - Axial conduction along stator iron.

$$R_{74} = \frac{4\ell}{k'_{lam} (r_5 - r_9) (u + w) K_s}$$

Resistance 75 - Equal to R_{74} .

Resistance 76 - Equal to R_{50} .

Resistance 77 - Conduction radially from stator coil to stator lamination.
(Typical of R_y in Fig. C-2).

$$R_{77} = \frac{18u}{k^*v\ell K_s} + \frac{18 t_{ins}}{k_{ins} v\ell K_s} + \frac{9w}{k_{lam} v\ell K_s}$$

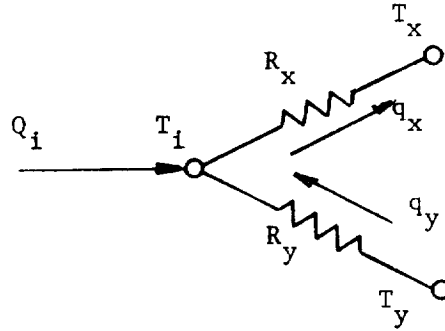
Resistance 78 - Equal to R_{77} .

Resistance 79 - Equal to R_{77} .

2. Nodal Equations

a. General Description

The nodal equations are determined by writing the equation of the heat flows toward and away from a particular node and setting it equal to zero. The heat flow at each node is caused either by internal heating or by a temperature gradient. Consistent directions of heat flow at each node are assumed throughout the entire mesh. Typically, a heat flow diagram will appear as the following:



The steady-state heat balance (which implies no heat storage at the node) for the diagram is:

$$\Sigma Q = 0$$

$$Q_i + q_y - q_x = 0$$

But

$$q_y = \frac{T_y - T_i}{R_y}$$

$$q_x = \frac{T_i - T_x}{R_x}$$

From this the nodal equation is obtained.

$$Q_i + \frac{T_y}{R_y} + \frac{T_x}{R_x} - T_i \left(\frac{1}{R_x} + \frac{1}{R_y} \right) = 0$$

The coefficients of the unknown temperatures are evaluated in a systematic way in terms of the coefficients of a non-singular matrix A_i^j .

b. Equations in Index Notation

At each unknown temperature node in Figure 1, the heat flows are summed and set equal to zero. This procedure is used for internal rotor temperatures as well as coolant environmental temperatures. The nodes involved in the calculations are denoted by \otimes . The nodes which are gas are denoted as \boxtimes . The equations which result can be written in index notation i.e., $(A_i^j X_j = B_i)$

$$A_1^1 X_1 + A_1^2 X_2 = B_1 \quad (1)$$

$$A_2^1 X_1 + A_2^2 X_2 + A_2^3 X_3 = B_2 \quad (2)$$

$$A_3^2 X_2 + A_3^3 X_3 + A_3^4 X_4 + A_3^{43} X_{43} = B_3 \quad (3)$$

$$A_4^3 X_3 + A_4^4 X_4 + A_4^5 X_5 + A_4^{44} X_{44} = B_4 \quad (4)$$

$$A_5^4 X_4 + A_5^5 X_5 + A_5^6 X_6 + A_5^7 X_7 = B_5 \quad (5)$$

$$A_6^5 X_5 + A_6^6 X_6 + A_6^8 X_8 + A_6^{15} X_{15} = B_6 \quad (6)$$

$$A_7^5 X_5 + A_7^7 X_7 + A_7^8 X_8 + A_7^{10} X_{10} = B_7 \quad (7)$$

$$A_8^6 X_6 + A_8^7 X_7 + A_8^8 X_8 + A_8^9 X_9 + A_8^{16} X_{16} = B_8 \quad (8)$$

$$A_9^8 X_8 + A_9^9 X_9 + A_9^{10} X_{10} + A_9^{17} X_{17} = B_9 \quad (9)$$

$$A_{10}^7 X_7 + A_{10}^9 X_9 + A_{10}^{10} X_{10} + A_{10}^{11} X_{11} = B_{10} \quad (10)$$

$$A_{11}^{10} X_{10} + A_{11}^{11} X_{11} + A_{11}^{12} X_{12} + A_{11}^{41} X_{41} = B_{11} \quad (11)$$

$$A_{12}^{11} X_{11} + A_{12}^{12} X_{12} + A_{12}^{13} X_{13} + A_{12}^{42} X_{42} = B_{12} \quad (12)$$

$$A_{13}^{12} X_{12} + A_{13}^{13} X_{13} + A_{13}^{14} X_{14} = B_{13} \quad (13)$$

$$A_{14}^{13} X_{13} + A_{14}^{14} X_{14} = B_{14} \quad (14)$$

$$A_{15}^6 X_6 + A_{15}^{15} X_{15} + A_{15}^{20} X_{20} + A_{15}^{44} X_{44} = B_{15} \quad (15)$$

$$A_{16}^8 X_8 + A_{16}^{15} X_{15} + A_{16}^{16} X_{16} + A_{16}^{19} X_{19} = B_{16} \quad (16)$$

$$A_{17}^9 X_9 + A_{17}^{16} X_{16} + A_{17}^{17} X_{17} + A_{17}^{18} X_{18} = B_{17} \quad (17)$$

$$A_{18}^{17} X_{17} + A_{18}^{18} X_{18} + A_{18}^{23} X_{23} + A_{18}^{24} X_{24} = B_{18} \quad (18)$$

$$A_{19}^{16} X_{16} + A_{19}^{19} X_{19} + A_{19}^{22} X_{22} + A_{19}^{25} X_{25} = B_{19} \quad (19)$$

$$A_{20}^{15} X_{15} + A_{20}^{20} X_{20} + A_{20}^{21} X_{21} + A_{20}^{26} X_{26} = B_{20} \quad (20)$$

$$A_{21}^{20} X_{20} + A_{21}^{21} X_{21} + A_{21}^{22} X_{22} + A_{21}^{26} X_{26} + A_{21}^{33} X_{33} = B_{21} \quad (21)$$

$$A_{22}^{19} X_{19} + A_{22}^{21} X_{21} + A_{22}^{22} X_{22} + A_{22}^{23} X_{23} + A_{22}^{25} X_{25} + A_{22}^{32} X_{32} = B_{22} \quad (22)$$

$$A_{23}^{18} X_{18} + A_{23}^{22} X_{22} + A_{23}^{23} X_{23} + A_{23}^{24} X_{24} + A_{23}^{31} X_{31} = B_{23} \quad (23)$$

$$A_{24}^{18} X_{18} + A_{24}^{23} X_{23} + A_{24}^{24} X_{24} + A_{24}^{25} X_{25} + A_{24}^{30} X_{30} + A_{24}^{31} X_{31} = B_{24} \quad (24)$$

$$A_{25}^{19} x_{19} + A_{25}^{22} x_{22} + A_{25}^{24} x_{24} + A_{25}^{25} x_{25} + A_{25}^{26} x_{26} + A_{25}^{32} x_{32} = B_{25} \quad (25)$$

$$A_{26}^{20} x_{20} + A_{26}^{21} x_{21} + A_{26}^{25} x_{25} + A_{26}^{26} x_{26} + A_{26}^{27} x_{27} + A_{26}^{33} x_{33} = B_{26} \quad (26)$$

$$A_{27}^{26} x_{26} + A_{27}^{27} x_{27} + A_{27}^{28} x_{28} + A_{27}^{38} x_{38} + A_{27}^{44} x_{44} = B_{27} \quad (27)$$

$$A_{28}^{27} x_{27} + A_{28}^{28} x_{28} + A_{28}^{37} x_{37} + A_{28}^{43} x_{43} = B_{28} \quad (28)$$

$$A_{29}^{29} x_{29} + A_{29}^{30} x_{30} + A_{29}^{42} x_{42} + A_{29}^{39} x_{39} = B_{29} \quad (29)$$

$$A_{30}^{24} x_{24} + A_{30}^{29} x_{29} + A_{30}^{30} x_{30} + A_{30}^{41} x_{41} + A_{30}^{40} x_{40} = B_{30} \quad (30)$$

$$A_{31}^{23} x_{23} + A_{31}^{24} x_{24} + A_{31}^{31} x_{31} + A_{31}^{32} x_{32} + A_{31}^{34} x_{34} = B_{31} \quad (31)$$

$$A_{32}^{22} x_{22} + A_{32}^{25} x_{25} + A_{32}^{31} x_{31} + A_{32}^{32} x_{32} + A_{32}^{33} x_{33} + A_{32}^{35} x_{35} = B_{32} \quad (32)$$

$$A_{33}^{21} x_{21} + A_{33}^{26} x_{26} + A_{33}^{32} x_{32} + A_{33}^{33} x_{33} + A_{33}^{36} x_{36} = B_{33} \quad (33)$$

$$A_{34}^{33} x_{33} + A_{34}^{36} x_{36} + A_{34}^{38} x_{38} = B_{34} \quad (34)$$

$$A_{35}^{32} x_{32} + A_{35}^{35} x_{35} + A_{35}^{36} x_{36} = B_{35} \quad (35)$$

$$A_{36}^{31} x_{31} + A_{36}^{34} x_{34} + A_{36}^{35} x_{35} = B_{36} \quad (36)$$

$$A_{37}^{27} x_{27} + A_{37}^{37} x_{37} + A_{37}^{38} x_{38} = 0 \quad (37)$$

$$A_{38}^{28} x_{28} + A_{38}^{37} x_{37} = B_{38} \quad (38)$$

$$A_{39}^{30} X_{30} + A_{39}^{34} X_{34} + A_{39}^{40} X_{40} = 0 \quad (39)$$

$$A_{40}^{29} X_{29} + A_{40}^{39} X_{39} + A_{40}^{40} X_{40} = 0 \quad (40)$$

$$A_{41}^{11} X_{11} + A_{41}^{17} X_{17} + A_{41}^{30} X_{30} + A_{41}^{41} X_{41} = 0 \quad (41)$$

$$A_{42}^{12} X_{12} + A_{42}^{29} X_{29} + A_{42}^{41} X_{41} + A_{42}^{42} X_{42} = 0 \quad (42)$$

$$A_{43}^3 X_3 + A_{43}^{28} X_{28} + A_{43}^{43} = B_{43} \quad (43)$$

$$A_{44}^4 X_4 + A_{44}^{27} X_{27} + A_{44}^{43} X_{43} + A_{44}^{44} X_{44} = 0 \quad (44)$$

c. Definition of Matrix Coefficients

The matrix coefficients A, B and the unknown X are equivalent to composite thermal resistances, heat generation and temperatures. The equivalent values are tabulated as follows:

Coefficients A_i^j . All values of A_i^j are zero except those listed below:

$$A_1^1 = 1/R_2 + 1/R_3$$

$$A_1^2 = -1/R_2$$

$$A_2^1 = -1/R_2$$

$$A_2^2 = 1/R_1 + 1/R_2 + 1/R_4$$

$$A_2^3 = -1/R_4$$

$$A_3^2 = -1/R_4$$

$$A_3^3 = 1/R_4 + 1/R_5 + 1/R_6$$

$$A_3^4 = -1/R_6$$

$$A_3^{43} = -1/R_5$$

$$A_4^3 = -1/R_6$$

$$A_4^4 = 1/R_6 + 1/R_7 + 1/R_8$$

$$A_4^5 = -1/R_8$$

$$A_4^{44} = -1/R_7$$

$$A_5^4 = -1/R_8$$

$$A_5^5 = 1/R_8 + 1/R_9 + 1/R_{12}$$

$$A_5^6 = -1/R_9$$

$$A_5^7 = -1/R_{12}$$

$$A_6^5 = -1/R_9$$

$$A_6^6 = 1/R_9 + 1/R_{10} + 1/R_{11} - \beta_r Q_8$$

$$A_6^8 = -1/R_{11}$$

$$A_6^{15} = -1/R_{10}$$

$$A_7^5 = -1/R_{12}$$

$$A_7^7 = 1/R_{12} + 1/R_{13} + 1/R_{14}$$

$$A_7^8 = -1/R_{13}$$

$$A_7^{10} = -1/R_{14}$$

$$A_8^6 = -1/R_{11}$$

$$A_8^7 = -1/R_{13}$$

$$A_8^8 = 1/R_{11} + 1/R_{13} + 1/R_{15} + 1/R_{26} - \beta_r Q_{10}$$

$$A_8^9 = -1/R_{15}$$

$$A_8^{16} = -1/R_{26}$$

$$A_9^8 = -1/R_{15}$$

$$A_9^9 = 1/R_{15} + 1/R_{16} + 1/R_{25} - \beta_r Q_{11}$$

$$A_9^{10} = -1/R_{16}$$

$$A_9^{17} = -1/R_{25}$$

$$A_{10}^7 = -1/R_{14}$$

$$A_{10}^9 = -1/R_{16}$$

$$A_{10}^{10} = 1/R_{14} + 1/R_{16} + 1/R_{17}$$

$$A_{10}^{11} = -1/R_{17}$$

$$A_{11}^{10} = -1/R_{17}$$

$$A_{11}^{11} = 1/R_{17} + 1/R_{18} + 1/R_{19}$$

$$A_{11}^{12} = -1/R_{19}$$

$$A_{11}^{41} = -1/R_{18}$$

$$A_{12}^{11} = -1/R_{19}$$

$$A_{12}^{12} = 1/R_{19} + 1/R_{20} + 1/R_{21}$$

$$A_{12}^{13} = -1/R_{21}$$

$$A_{12}^{42} = -1/R_{20}$$

$$A_{13}^{12} = -1/R_{21}$$

$$A_{13}^{13} = 1/R_{21} + 1/R_{22} + 1/R_{23}$$

$$A_{13}^{14} = -1/R_{22}$$

$$A_{14}^{13} = -1/R_{22}$$

$$A_{14}^{14} = 1/R_{22} + 1/R_{24}$$

$$A_{15}^6 = -1/R_{10}$$

$$A_{15}^{15} = W_1 C + 1/R_{27} + 1/R_{10}$$

$$A_{15}^{20} = -1/R_{27}$$

$$A_{15}^{44} = -W_1 C$$

$$A_{16}^8 = -1/R_{26}$$

$$A_{16}^{15} = -W_1 C$$

$$A_{16}^{16} = W_1 C + 1/R_{26} + 1/R_{28}$$

$$A_{16}^{19} = - 1/R_{28}$$

$$A_{17}^9 = - 1/R_{25}$$

$$A_{17}^{16} = - W_1 C$$

$$A_{17}^{17} = W_1 C + 1/R_{25} + 1/R_{29}$$

$$A_{17}^{18} = - 1/R_{29}$$

$$A_{18}^{17} = - 1/R_{29}$$

$$A_{18}^{18} = 1/R_{29} + 1/R_{30} + 1/R_{34}$$

$$A_{18}^{23} = - 1/R_{30}$$

$$A_{18}^{24} = - 1/R_{34}$$

$$A_{19}^{16} = - 1/R_{28}$$

$$A_{19}^{19} = 1/R_{28} + 1/R_{31} + 1/R_{36}$$

$$A_{19}^{22} = - 1/R_{31}$$

$$A_{19}^{25} = - 1/R_{36}$$

$$A_{20}^{15} = -1/R_{27}$$

$$A_{20}^{20} = 1/R_{27} + 1/R_{32} + 1/R_{38}$$

$$A_{20}^{21} = -1/R_{32}$$

$$A_{20}^{26} = -1/R_{38}$$

$$A_{21}^{20} = -1/R_{32}$$

$$A_{21}^{21} = 1/R_{32} + 1/R_{37} + 1/R_{73} + 1/R_{79} - \beta_l Q_{25}$$

$$A_{21}^{22} = -1/R_{73}$$

$$A_{21}^{26} = -1/R_{79}$$

$$A_{21}^{33} = -1/R_{37}$$

$$A_{22}^{19} = -1/R_{31}$$

$$A_{22}^{21} = -1/R_{73}$$

$$A_{22}^{22} = 1/R_{31} + 1/R_{35} + 1/R_{72} + 1/R_{73} + 1/R_{78} - \beta_l Q_{26}$$

$$A_{22}^{23} = -1/R_{72}$$

$$A_{22}^{25} = -1/R_{78}$$

$$A_{22}^{32} = -1/R_{35}$$

$$A_{23}^{18} = -1/R_{30}$$

$$A_{23}^{22} = -1/R_{72}$$

$$A_{23}^{23} = 1/R_{72} + 1/R_{30} + 1/R_{33} + 1/R_{77} - \beta_l Q_{27}$$

$$A_{23}^{24} = -1/R_{77}$$

$$A_{23}^{31} = -1/R_{33}$$

$$A_{24}^{18} = -1/R_{34}$$

$$A_{24}^{23} = -1/R_{77}$$

$$A_{24}^{24} = 1/R_{34} + 1/R_{39} + 1/R_{40} + 1/R_{45} + 1/R_{77} - \beta_c Q_{28}$$

$$A_{24}^{25} = -1/R_{40}$$

$$A_{24}^{30} = -1/R_{39}$$

$$A_{24}^{31} = -1/R_{45}$$

$$A_{25}^{19} = -1/R_{36}$$

$$A_{25}^{22} = -1/R_{78}$$

$$A_{25}^{24} = -1/R_{40}$$

$$A_{25}^{25} = 1/R_{36} + 1/R_{40} + 1/R_{41} + 1/R_{44} + 1/R_{78} - \beta_c Q_{29}$$

$$A_{25}^{26} = -1/R_{41}$$

$$A_{25}^{32} = -1/R_{44}$$

$$A_{26}^{20} = -1/R_{38}$$

$$A_{26}^{21} = -1/R_{79}$$

$$A_{26}^{25} = -1/R_{41}$$

$$A_{26}^{26} = 1/R_{38} + 1/R_{41} + 1/R_{42} + 1/R_{43} + 1/R_{79} - \beta_c Q_{30}$$

$$A_{26}^{27} = -1/R_{42}$$

$$A_{26}^{33} = -1/R_{43}$$

$$A_{27}^{26} = -1/R_{42}$$

$$A_{27}^{27} = 1/R_{50} + 1/R_{42} + 1/(R_{51} + R_{53}) + 1/(R_{46} + R_{48}) - \beta_c Q_{33}$$

$$A_{27}^{28} = -1/R_{50}$$

$$A_{27}^{38} = -1/(R_{51} + R_{53})$$

$$A_{27}^{44} = -1/(R_{46} + R_{48})$$

$$A_{28}^{27} = -1/R_{50}$$

$$A_{28}^{28} = 1/R_{50} + 1/(R_{52} + R_{54}) + 1/(R_{47} + R_{49}) - \beta_c Q_{34}$$

$$A_{28}^{37} = -1/(R_{52} + R_{54})$$

$$A_{28}^{43} = -1/(R_{47} + R_{49})$$

$$A_{29}^{29} = 1/R_{76} + 1/(R_{55} + R_{57}) + 1/(R_{59} + R_{61}) - \beta_c Q_{39}$$

$$A_{29}^{30} = -1/R_{76}$$

$$A_{29}^{42} = -1/(R_{55} + R_{57})$$

$$A_{29}^{39} = -1/(R_{59} + R_{61})$$

$$A_{30}^{24} = -1/R_{39}$$

$$A_{30}^{29} = -1/R_{76}$$

$$A_{30}^{30} = 1/R_{39} + 1/R_{76} + 1/(R_{60} + R_{62}) + 1/(R_{56} + R_{58}) - \beta_c Q_{40}$$

$$A_{30}^{41} = -1/(R_{56} + R_{58})$$

$$A_{30}^{40} = -1/(R_{60} + R_{62})$$

$$A_{31}^{23} = -1/R_{33}$$

$$A_{31}^{24} = -1/R_{45}$$

$$A_{31}^{31} = 1/R_{33} + 1/R_{45} + 1/R_{74} + 1/(R_{63} + R_{66}) - \beta_l Q_{43}$$

$$A_{31}^{32} = -1/R_{74}$$

$$A_{31}^{34} = -1/(R_{63} + R_{66})$$

$$A_{32}^{22} = -1/R_{35}$$

$$A_{32}^{25} = -1/R_{44}$$

$$A_{32}^{31} = -1/R_{74}$$

$$A_{32}^{32} = 1/R_{35} + 1/R_{44} + 1/R_{74} + 1/(R_{64} + R_{67}) - \beta_l Q_{44} + 1/R_{75}$$

$$A_{32}^{33} = -1/R_{75}$$

$$A_{32}^{35} = -1/(R_{64} + R_{67})$$

$$A_{33}^{21} = -1/R_{37}$$

$$A_{33}^{26} = -1/R_{43}$$

$$A_{33}^{32} = -1/R_{75}$$

$$A_{33}^{33} = 1/R_{37} + 1/R_{43} + 1/R_{75} + 1/(R_{65} + R_{68}) - \beta_l Q_{45}$$

$$A_{33}^{36} = -1/(R_{65} + R_{68})$$

$$A_{34}^{33} = -1/(R_{65} + R_{68})$$

$$A_{34}^{36} = W_2 C + 1/R_{71} + 1/(R_{65} + R_{68})$$

$$A_{34}^{38} = -W_2 C$$

$$A_{35}^{32} = -1/(R_{64} + R_{67})$$

$$A_{35}^{35} = W_2 C + 1/R_{70} + 1/(R_{64} + R_{67})$$

$$A_{35}^{36} = -W_2 C$$

$$A_{36}^{31} = -1/(R_{63} + R_{66})$$

$$A_{36}^{34} = W_2 C + 1/R_{69} + 1/(R_{63} + R_{66})$$

$$A_{36}^{35} = -W_2 C$$

$$A_{37}^{27} = -1/(R_{51} + R_{53})$$

$$A_{37}^{38} = W_2 C + 1/(R_{51} + R_{53})$$

$$A_{37}^{37} = -W_2 C$$

$$A_{38}^{28} = -1/(R_{52} + R_{54})$$

$$A_{38}^{37} = W_2 C + 1/(R_{52} + R_{54})$$

$$A_{39}^{30} = - 1/(R_{60} + R_{62})$$

$$A_{39}^{34} = - W_2 C$$

$$A_{39}^{40} = W_2 C + 1/(R_{60} + R_{62})$$

$$A_{40}^{29} = - 1/(R_{59} + R_{61})$$

$$A_{40}^{39} = W_2 C + 1/(R_{59} + R_{61})$$

$$A_{40}^{40} = - W_2 C$$

$$A_{41}^{11} = - 1/R_{18}$$

$$A_{41}^{17} = - W_1 C$$

$$A_{41}^{30} = - 1/(R_{56} + R_{58})$$

$$A_{41}^{41} = W_1 C + 1/R_{18} + 1/(R_{56} + R_{58})$$

$$A_{42}^{12} = - 1/R_{20}$$

$$A_{42}^{29} = - 1/(R_{57} + R_{55})$$

$$A_{42}^{41} = -W_1 C$$

$$A_{42}^{42} = W_1 C + 1/R_{20} + 1/(R_{57} + R_{55})$$

$$A_{43}^3 = -1/R_5$$

$$A_{43}^{28} = -1/(R_{47} + R_{49})$$

$$A_{43}^{43} = 1/R_5 + W_1 C + 1/(R_{47} + R_{49})$$

$$A_{44}^4 = -1/R_7$$

$$A_{44}^{27} = -1/(R_{46} + R_{48})$$

$$A_{44}^{43} = -W_1 C$$

$$A_{44}^{44} = 1/R_7 + W_1 C + 1/(R_{46} + R_{48})$$

B_i Vector:

$$B_1 = Q_1 + T_{53}/R_3$$

$$B_2 = T_{52}/R_1$$

$$B_3 = Q_4$$

$$B_4 = Q_6$$

$$B_5 = Q_7$$

$$B_6 = Q_8(1-\beta_r T^*)$$

$$B_7 = Q_9$$

$$B_8 = Q_{10}(1-\beta_r T^*)$$

$$B_9 = Q_{11}(1-\beta_r T^*)$$

$$B_{10} = Q_{12}$$

$$B_{11} = Q_{14}$$

$$B_{12} = Q_{16}$$

$$B_{13} = T_{54}/R_{23}$$

$$B_{14} = Q_{18} + T_{55}/R_{24}$$

$$B_{15} = Q_{19}$$

$$B_{16} = Q_{20}$$

$$B_{17} = Q_{21}$$

$$B_{18} = Q_{22}$$

$$B_{19} = Q_{23}$$

$$B_{20} = Q_{24}$$

$$B_{21} = Q_{25}(1-\beta_{\ell}T^*)$$

$$B_{22} = Q_{26}(1-\beta_{\ell}T^*)$$

$$B_{23} = Q_{27}(1-\beta_{\ell}T^*)$$

$$B_{24} = Q_{28}(1-\beta_cT^*)$$

$$B_{25} = Q_{29}(1-\beta_cT^*)$$

$$B_{26} = Q_{30}(1-\beta_cT^*)$$

$$B_{27} = Q_{33}(1-\beta_cT^*)$$

$$B_{28} = Q_{34}(1-\beta_cT^*)$$

$$B_{29} = Q_{39}(1-\beta_cT^*)$$

$$B_{30} = Q_{40}(1-\beta_cT^*)$$

$$B_{31} = Q_{43}(1-\beta_{\ell}T^*)$$

$$B_{32} = Q_{44}(1-\beta_{\ell}T^*)$$

$$B_{33} = Q_{45}(1-\beta_{\ell}T^*)$$

$$B_{34} = T_{66}/R_{71}$$

$$B_{35} = T_{65}/R_{70}$$

$$B_{36} = T_{64}/R_{69}$$

$$B_{37} = 0$$

$$B_{38} = W_{2}^{CT} \text{inlet}$$

$$B_{39} = 0$$

$$B_{40} = 0$$

$$B_{41} = 0$$

$$B_{42} = 0$$

$$B_{43} = W_{1}^{CT} \text{inlet}$$

$$B_{44} = 0$$

3. Description of Computer Program

The analysis has been prepared for solution on the IBM 1620 as program number PNO 183. PNO 183 is divided into three parts. The first calculates resistances, the second calculates the coefficient matrix, A_{ij} and the third part solves the system of 44 simultaneous equations for the nodal temperatures. The system can be represented by the matrix equation

$$A \cdot X = B$$

Using a standard matrix inversion technique, the temperatures are then given by

$$X = A^{-1} \cdot B$$

The three parts are actually separate FORTRAN programs which are run in sequence and linked together by COMMON storage allocations. Further, the second segment which calculates A_{ij} 's had to be split into three subsections because of memory limitations on the 1620.

a. Input Preparation - Units are the Same as Those Given in the Nomenclature

Part 1 - Input

Card 1 Radial Dimensions

Columns	1-10	inner radius of shaft, S1
	11-20	outer radius of shaft, S2
	21-30	outer radius of rotor, S3
	31-40	inner radius of stator, S4
	41-50	outer radius of stator, S5
	51-60	inner radius of end turn, S6

Card 2

Columns	1-10	outer radius of end turn, S7
	11-20	inner radius of stator slot, S8
	21-30	outer radius of stator slot, S9

Card 3 Thermal Conductivity Coefficients

Columns	1-10	shaft coefficient,	AKSH
	11-20	gas coefficient	AKGAS
	21-30	radial rotor coefficient	AKR
	31-40	axial rotor coefficient (inner)	AKRP
	41-50	radial stator lamination coefficient	AKL

Card 4 Thermal Conductivity Coefficients

Columns	1-10	axial stator lamination coefficients	AKSTL
	11-20	slot insulation coefficients	AKINS
	21-30	radial stator winding coefficient	AKSTAR
	31-40	axial stator winding coefficient	AKCOP
	41-50	axial rotor coefficient (outer)	AKROP

Card 5 Heat Transfer Coefficients

Columns	1-10	copper area/slot area	FAREA
	11-20	heat transfer at end turns	HEND
	21-30	heat transfer in gap	HGAP
	31-40	heat transfer back surface	HOUT
	41-50	heat transfer at O. D. of stator	HSINK
	51-60	heat transfer shaft surface	HSH

Card 6 Geometric Factors

Columns	1-10	width of stator slot (Fig. C-2).	U
	11-20	height of stator slot (Fig. C-2).	V
	21-30	distance between stator slots (Fig. C-2).	W
	31-40	length of motor	AL
	41-50	end turn length	ALE
	51-60	length of bearing	B
	61-65	no. of stator slats	KS*

*Fixed point number -- no decimal point.

Card 7 Geometric and Resistivity Factors

Columns 1-10	length of shaft	D
11-20	dimensions of stator (Fig. C-1).	TINS
21-30	radial thickness journal bearing	TP
31-40	resistivity of shaft	RSHAFT
41-50	resistivity of bearing	RBRG

Part 2 - Input

Card 1 Counters and Resistivities

Columns 1-5	number of resistances	NR*
6-10	number of heat flow parameters	NQ*
11-20	rotor resistivity coefficient	BR
21-30	lamination resistivity coefficient	BL
31-40	coil resistivity coefficient	BC
41-50	reference temperature	TSTAR

Card 2 Heat Flow Numbers -- Q(I)

6 items per card in 10 column fields -- as many cards as needed for NQ numbers.

Card n Boundary Temperatures

Columns 1-10	See Fig. C-1.	TINLET
11-20	See Fig. C-1.	T52
21-30	See Fig. C-1.	T53
31-40	See Fig. C-1.	T54
41-50	See Fig. C-1.	T55

*Fixed point number -- no decimal point.

Card n + 1 Boundary Temperatures

Columns 1-10	See Fig. C-1	T64
11-20	See Fig. C-1	T65
21-30	See Fig. C-1	T66

Card n + 2 Flow Parameters

Columns 1-10	gas flow rate in gap	W1
11-20	gas flow rate outside of stator	W2
21-30	specific heat	C

Card n + 3 Resistances, R(I)

6 items per cards in 10 column fields -- as many cards as needed for NR numbers. If sense switch #1 is off, these cards are not needed.

Part 3 - Input

The first card contains the size (N) of the coefficient matrix, present $N = 44$. This card must be loaded whether matrix input is taken from COMMON storage or from cards. Next the coefficient matrix, $A(I,J)$, is loaded rowwise, followed by the constant vector, $B(I)$. The format here is the same as the output format from Part 2C.

b. Method of Operation

This describes the input setup for operating the program on a 60K, card IBM 1620 with FL.PT. hardware. The program can easily be modified and combined into one segment for a 7090,94. Running time on the 1620 is approximately 2 hours, 1.7 hours being required for the matrix inversion.

The deck is set up as follows:

- | | |
|---|------------------|
| 1 | Part 1 |
| 2 | Data for Part 1 |
| 3 | Part 2A |
| 4 | Data for Part 2A |
| 5 | Part 2B |
| 6 | Part 2C |
| 7 | Part 3 |
| 8 | Data for Part 3 |

When running the program then, if sense switch #1 is on for Part 1, the resistances will be punched on cards. If sense switch #1 is on for Part 2A, the resistances will be read from cards but if it is off they will be used as left in COMMON storage from Part 1. If S.S. #1 is on for Part 2C, the coefficient matrix and constant vector will be punched on cards. With S.S. #1 on during Part 3, the coefficient matrix and constant vector are read in from cards but if it is off, they will be used as left in memory from Part 2C.

4. Sample Calculation Illustrating Use of Computer Program

A sample calculation was made to test the validity of the analysis and to illustrate the use of the computer program. The calculation represented a squirrel cage induction motor mounted on gas bearings, which has been in use for over 2500 hours driving a gas circulator. The motor is sealed in a helium loop and uses the loop gas both as a bearing lubricant and motor coolant. Running at 50 horsepower and 11,800 RPM, this unit offered a difficult cooling problem well suited to test the analysis.

Calculation of temperatures in the motor was expected to provide three checks on the analysis and program.

1. A gross check would be obtained if the calculated temperature distribution satisfied the boundary conditions and the basic laws of heat transfer.
2. Calculated winding temperatures should lead to a prediction of insulation life at least equal to the 2500 hours seen by the motor to date.
3. The mathematical stability of the analysis with various temperature coefficients of electrical resistivity could be examined.

a. Preparation of Input

The program input for the sample problem is presented in Table C-3. Input to Part 1, which calculates the thermal resistances, is broken down as follows:

The data on cards 1 and 2 describe the motor geometry. Cards 3 and 4 contain thermal conductivities of the shaft, lamination, winding and insulation materials, and the bearing gas. These values can be obtained from any standard reference on the physical properties of materials. Card 5 lists the film coefficients for heat transfer to the cooling gas at various locations around the motor. The coefficients for the rotor were calculated from the equations in an MTI report^{*} which summarized data from several published references. The coefficients for

* MTI 63TM1 "Survey of Convection Heat Transfer Coefficients Relating to Gas Turbine Geometry," by J. S. Meacher.

TABLE C-3
SAMPLE INPUT

Part 1

$S_1 = 1.4$		FAREA = 0.5	
$S_2 = 1.70$		HEND = 100	
$S_3 = 1.75$	Card 1	HGAP = 200	Card 5
$S_4 = 1.795$		HOUT = 100	
$S_5 = 3.375$		HSINK = .001	
$S_6 = 2.187$		HSH = 150	
$S_7 = 2.625$		AL = 5.0	
$S_8 = 2.1$	Card 2	ALE = 2.0	
$S_9 = 2.8$		B = 2.75	
AKSH = 8.0		KS = 48	Card 6
AKGAS = 0.12		U = .16	
AKR = 12.0	Card 3	V = .70	
AKRP = 12.0		W = .20	
AKL = 18.0		TP = .0004	
AKSTL = 1.0		D = 4.5	
AKINS = 0.1		TINS = .03	Card 7
AKSTAR = 0.9	Card 4	RSHAFT = 0.1	
AKCOP = 200		RBRG = 0.1	
AKROP = 12.0			

Part 2A

BR = BL = 0	$Q_{25} = Q_{26} = Q_{27} = 840$
BC = .003	$Q_{28} = Q_{29} = Q_{30} = Q_{33} = Q_{34} = Q_{39} = Q_{40} = 800$
T INLET = 220	$Q_7 = Q_9 = Q_{12} = 1100$
T STAR = 150	$Q_{19} = Q_{20} = Q_{21} = 430$
W1 = 500	$Q_8 = Q_{10} = Q_{11} = 430$
W2 = 1100	$Q_1 = Q_{18} = 230$
C = 1.20	$Q_4 = Q_6 = Q_{14} = Q_{16} = 0$
T64 = 200	
T65 = 200	
T66 = 200	
T52 = 230	
T53 = 220	
T54 = 230	
T55 = 230	

the stator and end turns were estimated from information obtained from the motor manufacturer. HSINK, the heat transfer coefficient at the sink surrounding the motor was very low because the outer casing of the motor was insulated. Card 6 contains more geometric data as does Card 7. In addition, card 7 contains the estimated composite resistances, RSHAFT and RBRG, between the shaft and the bearing shoe and their respective sinks.

The input for Part 2 requires some discussion regarding the calculation of the various heat inputs (Q_i). The Q_i values represent the various electrical and windage losses in the motor distributed over an appropriate number of nodal points.

The windage Q 's were calculated using the equations of Appendix A of this report. Q_1 and Q_{18} represent the bearing friction loss which was found to be 230 Btu/hr per bearing. The windage loss of the exposed shaft between the bearing and the rotor laminations was negligible compared to the other losses so Q_4 , Q_6 , Q_{14} and Q_{16} were zero. If this loss had been appreciable it would have been divided equally among the four nodes. The friction loss in the gap between rotor and stator was also negligible, as was the loss on the shoulder face. Had they been significant, these losses would have been incorporated in Q_{19} , Q_{20} , Q_{21} and in Q_{19} and Q_{21} respectively.

Electrical losses were divided into four basic categories. Each category was assumed to be equally distributed among the nodes where it occurred. The basic categories and applicable heat input designations were:

<u>Category</u>	<u>Type of Loss</u>	<u>Q_i</u>
Stator Copper	I^2R	$Q_{28}, Q_{29}, Q_{30}, Q_{33}, Q_{34},$ Q_{39}, Q_{40}
Stator Iron	Hysteresis and eddy current	Q_{25}, Q_{26}, Q_{27}
Rotor Iron	Hysteresis and eddy current	Q_7, Q_9, Q_{12}
Stray Gap Loss	Miscellaneous electrical	$Q_{19}, Q_{20}, Q_{21}, Q_8, Q_{10}, Q_{11}$

The distribution of losses other than the stator copper loss is not usually well known. For the sample calculation, the motor rated horsepower, efficiency, and stator copper loss at rated power, and distribution of the remaining losses were obtained from manufacturers' data. Since the operating power was less than rated power, the I^2R loss for the operating case was scaled down by the square of the load. The remaining losses, which were proportional only to frequency (speed) did not change from the full load case. The resulting losses for the sample motor were as follows:

Rated Horsepower 75
 Efficiency 89%
 Total losses $(1-.89)(75)(2540) = 21,000 \text{ Btu/hr.}$
 Loss Distribution:

<u>Type of Loss</u>	<u>Dependency</u>	<u>Percent of Full Load Loss</u>	<u>Amount of Loss</u>	
			<u>At 75 HP</u>	<u>At 50 HP</u>
Stator Copper	$(\text{Load})^2$	60%	12,600 Btu/hr.	5600 Btu/hr.
Stator Iron	Frequency	12%	2,520 Btu/hr.	2520 Btu/hr.
Rotor Iron	Frequency	15.7%	3,300 Btu/hr.	3300 Btu/hr.
Stray Load Loss	Frequency	12.3%	2,580 But/hr.	2580 Btu/hr.

The remaining input for Part 2A is self-explanatory since it involves boundary temperatures, cooling gas flows and temperature coefficients of resistivity.

b. Program Output

The result of the calculation was the output sheet, Table C-4, in which the 44 unknown temperatures are denoted X_i .

c. Discussion of Sample Calculation

The sample calculation output showed that the program passed the first gross check. The distribution of temperatures follows a logical pattern. For example, highest temperatures are internal where heat is being generated, cooling gas temperature increases as it passes through the motor, and the boundary conditions are satisfied.

TABLE C-4

SAMPLE OUTPUT

X(1)=	24.060E+01
X(2)=	24.016E+01
X(3)=	22.136E+01
X(4)=	23.047E+01
X(5)=	30.585E+01
X(6)=	28.720E+01
X(7)=	31.605E+01
X(8)=	29.597E+01
X(9)=	29.791E+01
X(10)=	31.638E+01
X(11)=	24.716E+01
X(12)=	23.939E+01
X(13)=	24.948E+01
X(14)=	25.003E+01
X(15)=	22.667E+01
X(16)=	23.233E+01
X(17)=	23.787E+01
X(18)=	30.144E+01
X(19)=	29.543E+01
X(20)=	29.406E+01
X(21)=	32.475E+01
X(22)=	32.415E+01
X(23)=	33.034E+01
X(24)=	45.078E+01
X(25)=	43.948E+01
X(26)=	44.736E+01
X(27)=	47.051E+01
X(28)=	47.791E+01
X(29)=	48.303E+01
X(30)=	47.517E+01
X(31)=	29.306E+01
X(32)=	28.874E+01
X(33)=	28.875E+01
X(34)=	22.467E+01
X(35)=	22.355E+01
X(36)=	22.249E+01
X(37)=	22.071E+01
X(38)=	22.140E+01
X(39)=	22.608E+01
X(40)=	22.536E+01
X(41)=	23.839E+01
X(42)=	23.878E+01
X(43)=	22.042E+01
X(44)=	22.097E+01

The second check was also met. The highest calculated winding temperature of 483 F would lead to a life estimate of about 10,000 hours for class H insulation. This is compatible with the 2500 hours running time logged by the motor to date.

Finally, the third check, the examination of mathematical stability, was completed. It was found that an unstable calculation could be produced with a non-zero copper resistivity coefficient by decreasing the value of AKSTAR and decreasing the gas flow. The physical significance of these changes was that heat could not be removed from the windings as fast as it was generated. The rising temperature caused an increase in resistivity which in turn led to higher heat generation and still higher temperatures until the cycle became unstable. The clue given by the program that such instability exists is the appearance of some negative temperatures in the output. In all stable problems, output temperatures must always be positive and higher than the boundary values. The instability was due to the presence of a non-zero temperature coefficient of resistivity. When the coefficient was set equal to zero, the problem became stable.

A final item which was observed in making the stability check concerned the value of AKSTAR, the thermal conductivity of the stator winding in the radial direction. Lear-Siegler currently uses a value of 0.3 in their temperature calculations (which do not include the resistivity coefficient) although they feel that 0.9 or 1.0 may be a more realistic value. In the sample calculation made here, 0.9 produced best correlation with observed motor performance with the resistivity coefficient included. The value of 0.3 led to calculated winding temperatures of well over 1000 F which would indicate a very short motor life. Thus it appears that 0.9 is a realistic value when the effect of temperature on resistivity is included.

In summary, the program and analysis have passed the checks inherent in the sample problem. The program represents a working tool which the designer can use to evaluate steady-state temperatures, and subsequently life, of compact alternators. Through the incorporation of the temperature coefficient of resistivity, designs which are thermally unstable can be detected. However, it has been shown that the winding temperatures which are usually the most critical, are sensitive to the value of both the resistivity coefficient and the radial

thermal conductivity of the windings. An experimental program to measure these quantities accurately would help the designer realize the full potential of the analysis. It is recommended that such a program be undertaken. Another area in which accurate input data is essential is the distribution of losses. While the copper loss is the most important single item, the distribution of the eddy current and stray gap losses is very important in high performance designs where cooling requirements must be determined exactly.

E. CONCLUSIONS AND RECOMMENDATIONS

1. The analysis presented in this report satisfies the requirements of the problem statement. It provides the steady-state temperature distribution in an alternator given the geometry, thermal characteristics, internal heat generation rates and thermal boundary conditions. The analysis is also applicable to motors.
2. The analysis has been programmed in FORTRAN for digital computer solution. The program has been carefully checked, first by section and then in total. A sample problem, based on a known motor application, has been used as a final program check.
3. The accuracy of the temperature distributions that can be obtained with this analysis is limited at the present time by the lack of accurate heat transfer coefficients and thermal conductivities in certain key areas such as the end turns and coil core. It is recommended that a program be undertaken to measure these quantities under conditions closely approximating those of alternators in service.
4. The computer program allows the design engineer to rapidly determine the effect of alternator loss distribution on steady-state alternator temperatures. This is accomplished by specifying the local heat generation rates at internal nodes. It must be remembered, however, that the accuracy of the calculated temperatures will be a direct function of the accuracy with which the loss distribution is specified.
5. It is recommended that designers who expect to use the computer program extensively recompile it for a larger, faster computer. The running time, which is about two hours per case on the IBM 1620, could be reduced to about 1.2 minutes on an IBM 7094 with an accompanying reduction in costs of about 90% per case. Similar savings in time and money could be obtained with other large computers. The only requirement is that they be equipped with a FORTRAN compiler.

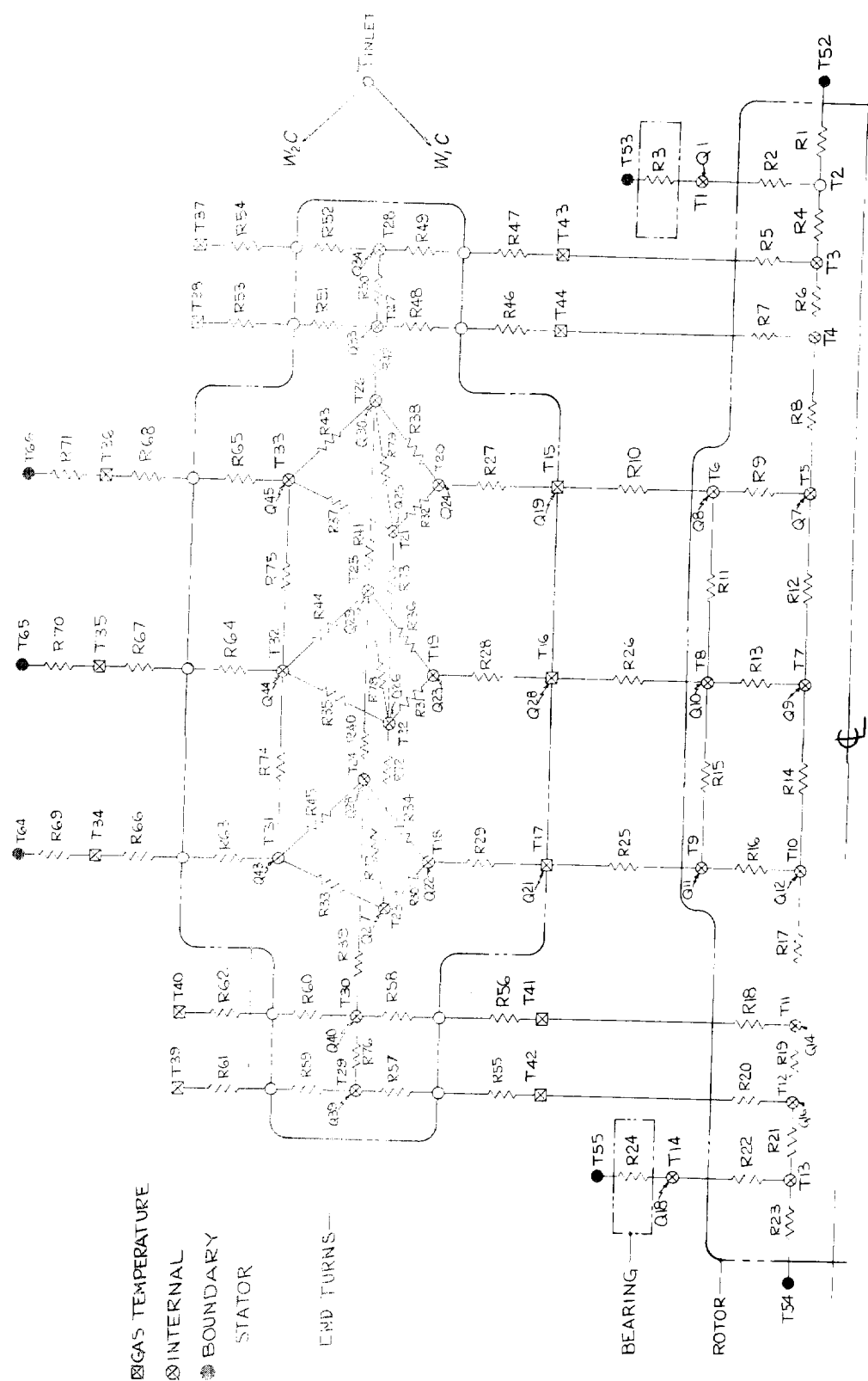


Fig. C-1 Schematic of Alternator Temperature Nodes and Heat Flow Paths

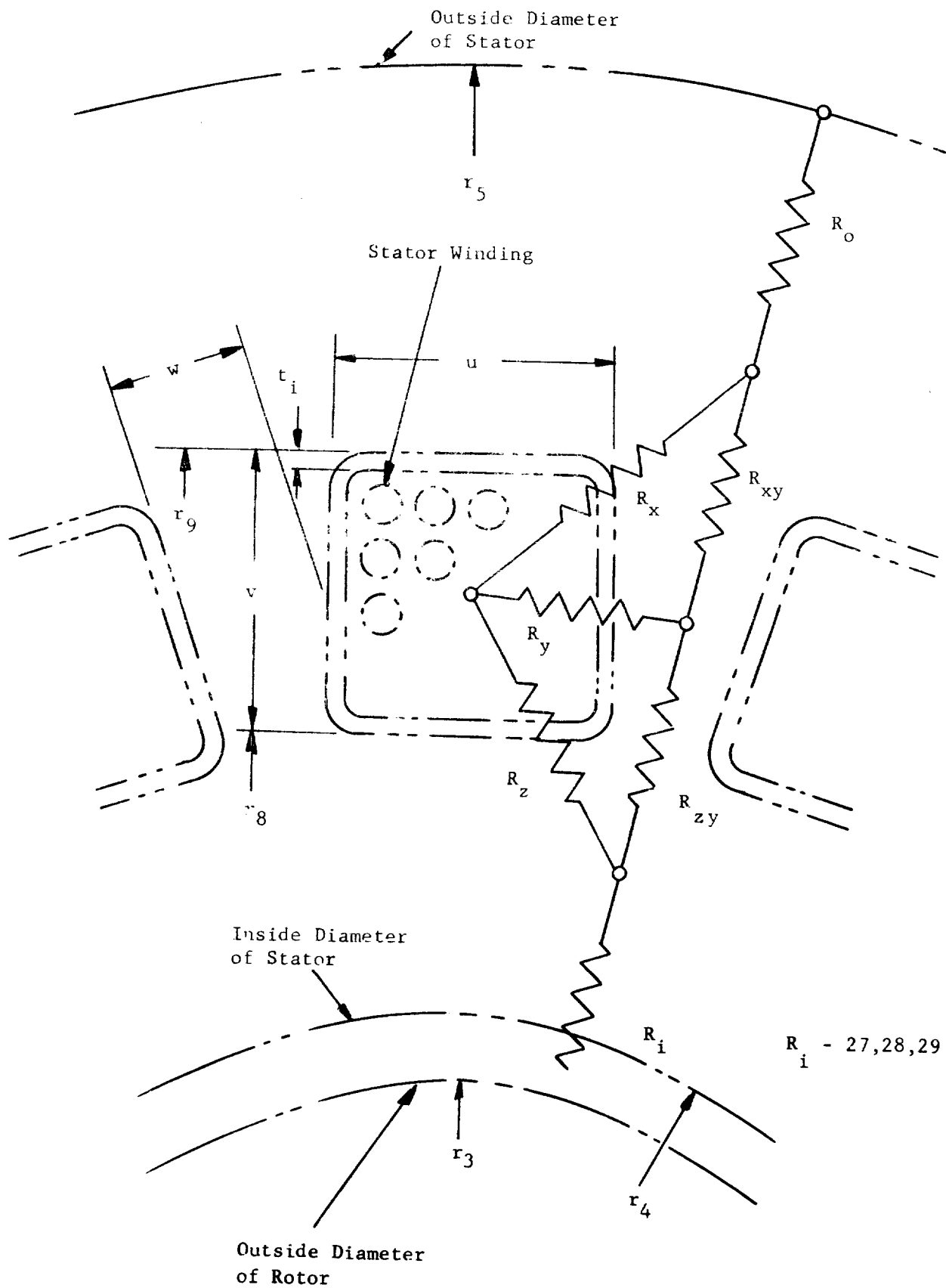


Fig. C-2 Schematic of Thermal Resistances in Stator Winding Region

APPENDICES

APPENDIX
ROTOR FRICTION ANALYSIS

by
Dr. J. H. Vohr

ROTOR FRICTION ANALYSIS

The power loss, ΔP , due to frictional drag on a rotating shaft of radius R and rotational speed ω is given by

$$(1) \quad \Delta P = \omega R F$$

where F is the frictional force acting on the shaft. Recommended expressions and procedures for determining F for various sections of the typical rotor shaft shown in Figure A-1 will be discussed below. The calculation of power loss for the various sections of the rotor will be accomplished by substituting the appropriate values for F and R in Eq. (1).

Bearing Friction

It is recommended that the friction force F for gas-lubricated full-circular journal bearings be determined from curves presented by Raimondi (Ref. 1). These curves are shown in Figure C-4 (a) through (d).

For preloaded tilting-pad bearings it is recommended that F be calculated from

$$(2) \quad F = \frac{n\mu r_2 \omega}{h_m} (r_2 \Delta\theta b)$$

where*

n = no. of pads

$\Delta\theta$ = arc length of each pad

h_m = minimum clearance in pad

b = width of each pad (See Fig. C-3)

The use of the minimum clearance in expression (2) makes this calculation of F slightly conservative.

*See nomenclature for undefined symbols on Page C-65

Windage Loss in Gap Between Rotor and Stator

A typical clearance between the stator and the rotor is .03 inches. A typical surface speed for the rotor is 300 ft./sec. Assuming air at atmospheric pressure in the rotor gap, the Reynolds number corresponding to the above typical data would be

$$\begin{aligned} N_{RE} &= \frac{\omega r_3 (r_4 - r_3)}{v} \quad (\text{where } v = \mu/\rho) \\ &= \frac{300(.03/12)}{16.88 \times 10^{-5}} \\ &= 4450 \end{aligned}$$

Assuming a three inch diameter for the shaft, the Taylor number for the flow in the rotor gap would be

$$\begin{aligned} T_a &= N_{Re} \sqrt{\frac{r_4 - r_3}{r_3}} \\ &= 4450 \sqrt{\frac{.03}{1.5}} \\ &= 1780 \end{aligned}$$

Thus, we see that the typical Reynolds and Taylor numbers for the flow in the rotor gap are sufficiently high such that the flow pattern should be characterized by the presence of both turbulence and Taylor vortices (critical value of Taylor number for development of vortices is 41.2). The friction factor, λ , for flow in this mixed flow regime can be predicted with quite good accuracy by the following empirical expressions suggested by Wendt (Ref. 2).

$$(3) \quad \lambda = 0.46 \left[\frac{(r_4 - r_3)r_4}{r_3^2} \right]^{1/4} N_{Re}^{-0.5}, \quad (4 \times 10^2 < N_{Re} < 10^4)$$

$$(4) \quad \lambda = 0.073 \left[\frac{(r_4 - r_3)r_4}{r_3^2} \right]^{1/4} N_{Re}^{-0.3}, \quad (N_{Re} > 10^4)$$

where

$$(5) \quad N_{Re} = \frac{\omega r_3 (r_4 - r_3)}{\nu}$$

$$(6) \quad \lambda = F / \pi \rho \omega^2 r_3^3 \ell$$

Concerning the effect on λ of flowing cooling air axially through the rotor gap, it is difficult to say whether this will increase or decrease λ . Generally speaking, an axial flow tends to inhibit the development of vortices which would tend to decrease λ . On the other hand, axial flow would tend to increase the level of turbulence which would increase λ . The net effect of axial flow might very well be negligible. Since there are no experimental data on this question, it is recommended that expressions (3) and (4) be used regardless of whether or not there is axial flow.

Equations (3) and (4) strictly apply only to the situation where both the surface of the rotor and the stator are smooth. Should the stator be grooved axially, then the term $(r_4 - r_3)$ should be taken to be the minimum clearance between the stator and the rotor.

Windage Losses Over Length d of Rotor Between Stator Gap and Bearing

Let us first consider the situation shown in Fig. C-3 in which the end turns extend more than half the distance from the stator to the bearing, i.e.

$$\ell_e / d > 1/2$$

For this case, the friction factor λ' for the drag on the length d of the rotor could best be estimated by Equations (3) or (4) with r_2 and r_6 substituted for r_3 and r_4 respectively and with the Reynolds number defined by

$$(7) \quad N_{Re} = \frac{r_2 \omega (r_6 - r_2)}{\nu}$$

The friction factor F on the length d of the shaft would be given by

$$(8) \quad F = \lambda' \pi \rho \omega^2 r_2^3 d$$

When $\ell_e/d < 1/2$, it will probably be more accurate to treat the length d of the rotor as a shaft rotating in free space. The friction factor λ' in this case would be given by the following equation from Reference 4.

$$(9) \quad 1/\sqrt{\lambda'} = -0.6 + 4.07 \log N'_{Re} \sqrt{\lambda'}$$

where

$$(10) \quad N'_{Re} = \frac{\omega r_2^2}{\nu}$$

Should one wish to be conservative in the calculation of λ' , one can evaluate λ' by both Equation (9) and Equations (3) or (4) (with r_2 and r_6 in place of r_3 and r_4) and use the larger value.

Windage Loss on End Face A Shown in Figure C-3

In calculating the windage loss on the end face A at the shoulder of the rotor it is recommended that one use the same friction factor, λ' , that one uses along the cylindrical length d of the shaft. The local differential friction force df on the end face A would then be given by

$$(11) \quad df = \lambda' \left[\pi \rho \omega^2 r^3 dr \right]$$

The differential power loss dP on the end face A would be given by

$$(12) \quad dP = \lambda' \left[\pi \rho \omega^3 r^4 dr \right]$$

Total power loss ΔP_A on one end face A would be given by

$$(13) \quad \Delta P_A = \int_{r_2}^{r_3} dP = \frac{\lambda'}{5} \left[\pi \rho \omega^3 (r_3^5 - r_2^5) \right]$$

SUMMARY OF RECOMMENDED RELATIONSHIPS FOR CALCULATING FRICTION POWER LOSSES FOR
TYPICAL ROTOR SHAFT

(1) Bearing (Gas-Lubricated)

(a) Full Journal Bearing

$$\Delta P_B = \omega r_2 F$$

where F is obtained from the curves in Figs. C-4 (a) through (d).

(b) Tilting Pad Bearings

$$\Delta P_B = \frac{\omega^2 r_2^3 n \mu \Delta \theta b}{h_m}$$

(2) Gap Between Rotor and Stator

$$\Delta P_G = (\omega^3 r_3^4 \ell \pi \rho) 0.46 \left[\frac{(r_4 - r_3) r_4}{r_3^2} \right]^{1/4} N_{Re}^{-0.5}, \quad (4 \times 10^2 < N_{Re} < 10^4)$$

$$\Delta P_G = (\omega^3 r_3^4 \ell \pi \rho) 0.073 \left[\frac{(r_4 - r_3) r_4}{r_3^2} \right]^{1/4} N_{Re}^{-0.3}, \quad (N_{Re} > 10^4)$$

where

$$N_{Re} = \frac{\omega r_3 (r_4 - r_3)}{\nu}$$

(3) Shaft Between Stator and Bearing

(a) $\ell_e / d > 1/2$

$$\Delta P_e = (\omega^3 r_2^4 d \pi \rho) 0.46 \left[\frac{(r_6 - r_2) r_6}{r_2^2} \right]^{1/4} N_{Re}^{-0.5}, \quad (4 \times 10^2 < N_{Re} < 10^4)$$

$$\Delta P_e = (\omega^3 r_2^4 d \pi \rho) 0.073 \left[\frac{(r_6 - r_2) r_6}{r_2^2} \right]^{1/4} N_{Re}^{-0.3}, \quad (N_{Re} > 10^4)$$

where

$$N_{Re} = \frac{\omega r_2 (r_6 - r_2)}{\nu}$$

$$(b) \ell_e / d < 1/2$$

$$\Delta P_e = \omega^3 r_2^4 d \pi \rho \lambda'$$

$$\text{where } 1/\sqrt{\lambda'} = -0.6 + 4.07 \log N_{Re}' \sqrt{\lambda'}$$

$$N_{Re}' = \frac{\omega r_2^2}{\nu}$$

(4) Shoulder Face (End Face A in Figure C-3)

$$\Delta P_A = \omega^3 \pi \rho (r_3^5 - r_2^5) \frac{\lambda'}{5}$$

where λ' is given by

$$(a) \ell_e / d > 1/2$$

$$\lambda' = 0.46 \left[\frac{(r_6 - r_2 - r_6)}{r_2^2} \right]^{1/4} N_{Re}^{-0.5}, \quad (4 \times 10^2 < N_{Re} < 10^4)$$

$$\lambda' = 0.073 \left[\frac{(r_6 - r_2) r_6}{r_2^2} \right]^{1/4} N_{Re}^{-0.3}, \quad (N_{Re} > 10^4)$$

$$\text{where } N_{Re} = \frac{\omega r_2 (r_6 - r_2)}{\nu}$$

or

$$(b) \ell_e / d < 1/2$$

$$1/\sqrt{\lambda'} = -0.6 + 4.07 \log N_{Re}' \sqrt{\lambda'}$$

$$\text{where } N_{Re}' = \frac{\omega r_2^2}{\nu}$$

$$(5) \text{ Total Power Loss} = 2\Delta P_B + \Delta P_G + 2\Delta P_e + 2\Delta P_A$$

REFERENCES

1. Raimondi, A. A., "A Numerical Solution for the Gas Lubricated Full Journal Bearing of Finite Length," ASLE Transactions 4, pp. 131-155, (1961).
2. Wendt, F., 1933 Ingenieur-Archiv, 4, p. 577, as reported in Reference 3.
3. Donnelly, R. J. and Simon, N. J., "An Empirical Torque Relation for Supercritical Flow Between Rotating Cylinders," Journal of Fluid Mechanics 7, p. 401, (1959).
4. Theodorsen, T. and Regier, A., "Experiments on Drag of Rotating Discs, Cylinders and Streamline Rods at High Speeds," NACA Report 793, pp. 1-18, (1944), as reported in Reference 5.
5. Dorfman, L. A., "Hydrodynamic Resistance and the Heat Loss of Rotating Solids," Translated by N. Kemmer, Oliver and Boyd Ltd., Edinburgh and London, 1963.

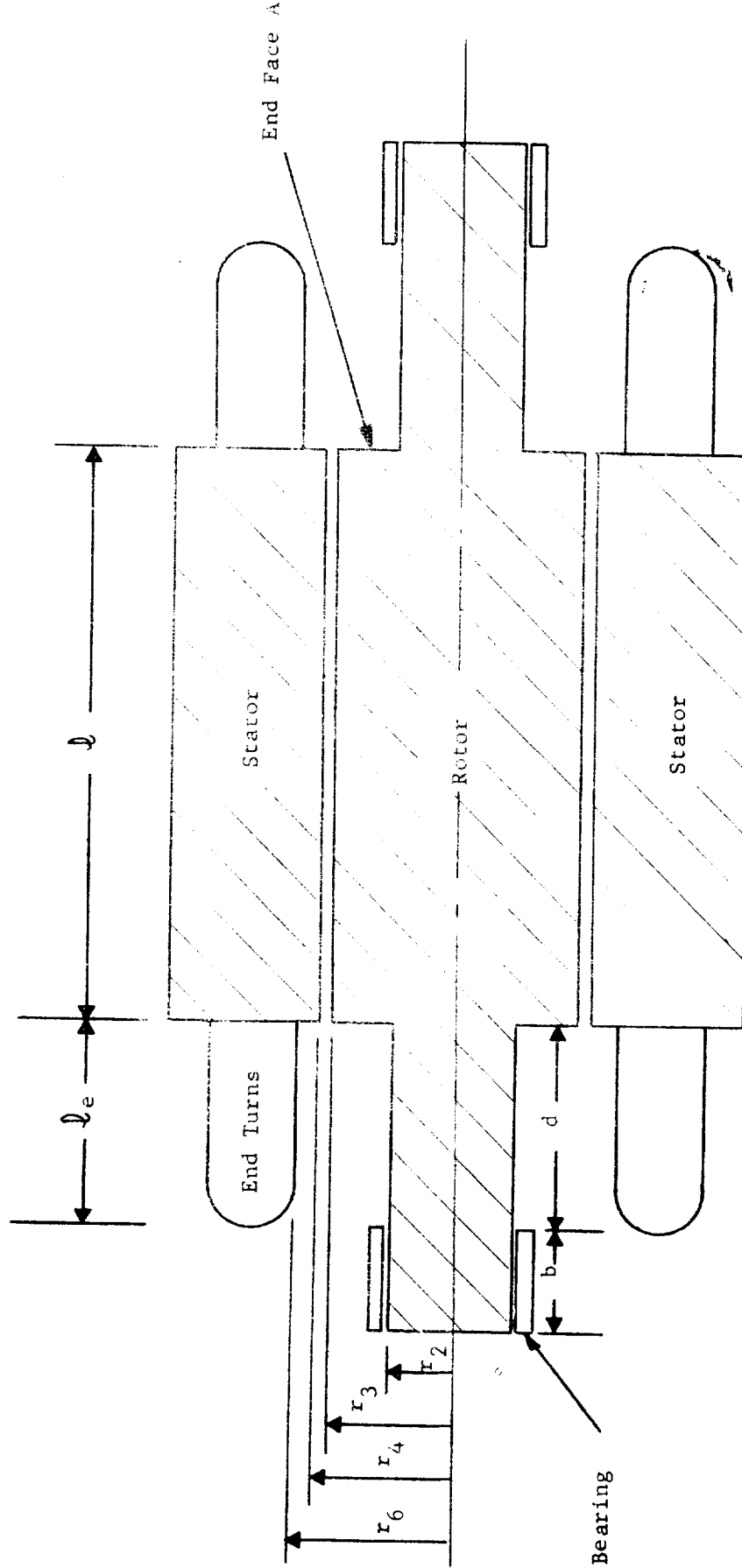


Fig. C-3 Alternator Configuration and Dimensions

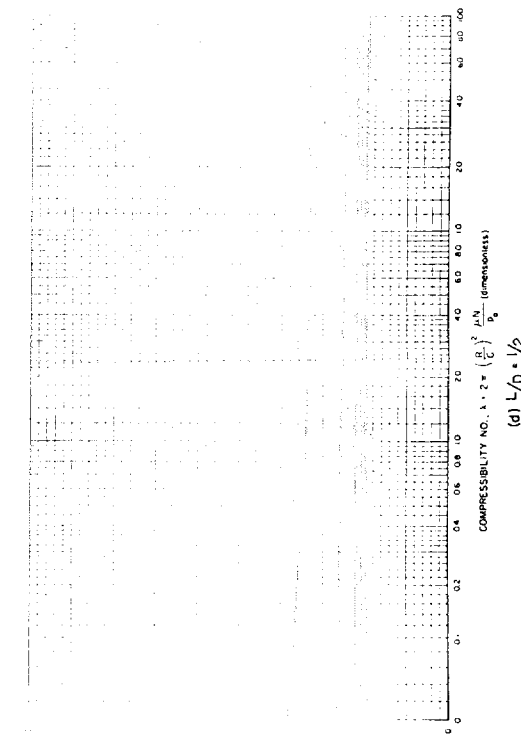
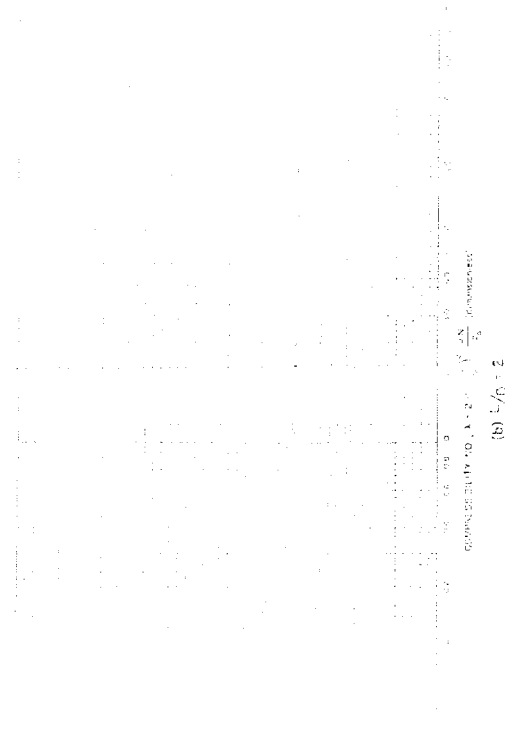
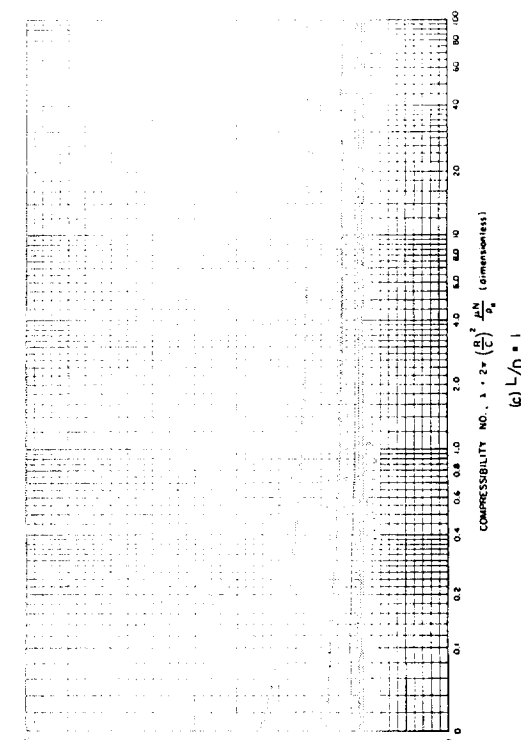
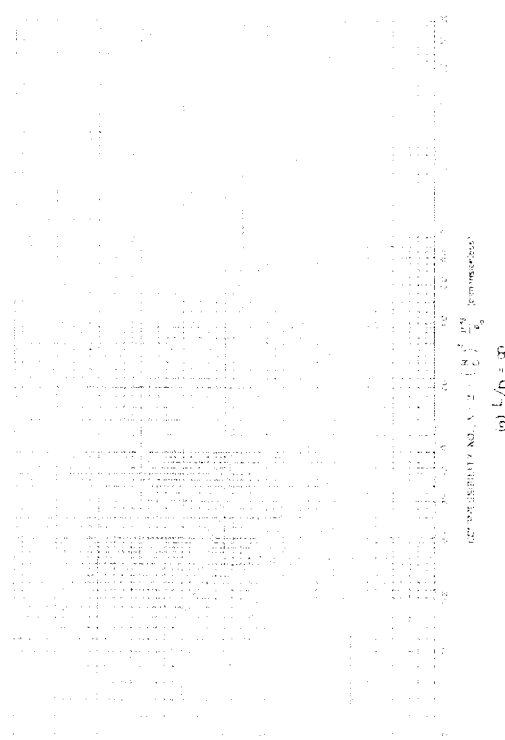


Fig. C-4 Design Charts for Friction

NOMENCLATURE

<u>Variable</u>	<u>Description</u>	<u>Units</u>	<u>Computer Language</u>
r_1	inner radius of shaft	inches	S1
r_2	outer radius of shaft	inches	S2
r_3	outer radius of rotor	inches	S3
r_4	inner radius of stator	inches	S4
r_5	outer radius of stator	inches	S5
r_6	inner radius of end turn	inches	S6
r_7	outer radius of end turn	inches	S7
r_8	inner radius of stator slot	inches	S8
r_9	outer radius of stator slot	inches	S9
u	width of stator slot	inches	U
v	height of stator slot	inches	V
w	distance between stator slots	inches	W
t_i	thickness of slot insulation	inches	TINS
k_s	thermal conductivity of shaft	Btu/hr-ft-°F	AKSH
k_g	thermal conductivity of gas	Btu/hr-ft-°F	AKGAS
k_r	thermal conductivity of rotor (radially)	Btu/hr-ft-°F	AKR
k'_{ri}	thermal conductivity of rotor (axially, inner surface)	Btu/hr-ft-°F	AKRP
k'_{ro}	thermal conductivity of rotor (axially, outer surface)	Btu/hr-ft-°F	AKROP
k_{lam}	thermal conductivity of lamination of stator, radially	Btu/hr-ft-°F	AKL
k'_{lam}	thermal conductivity of lamination of stator, axially	Btu/hr-ft-°F	AKCTL

NOMENCLATURE
(Contd)

<u>Variable</u>	<u>Description</u>	<u>Units</u>	<u>Computer Language</u>
k_{ins}	thermal conductivity of slot insulation	Btu/hr-ft-°F	AKINS
k^*	thermal conductivity of stator winding, radially	Btu/hr-ft-°F	AKSTAR
k_{cop}	thermal conductivity of stator winding, axially	Btu/hr-ft-°F	AKCCP
F_{area}	ratio of copper area/slot area	-----	FAREA
h_e	heat transfer coefficient at end turns	Btu/hr-ft ² -°F	HEND
h_g	heat transfer coefficient in gap	Btu/hr-ft ² -°F	HGAF
h_o	heat transfer coefficient at back iron surface	Btu/hr-ft ² -°F	HOUT
h_w	heat transfer coefficient of ultimate sink at O.D. of stator	Btu/hr-ft ² -°F	HSINK
h_s	heat transfer coefficient of shaft surface	Btu/hr-ft ² -°F	HSH
K_s	number of stator slots	-----	KS
ℓ	stack length	inches	AL
ℓ_e	end ℓ_x tension length	inches	ALE
b	length of bearing	inches	B
d	length of shaft between rotor and bearing	inches	D
t_p	radial clearance of journal bearing	inches	TP
R_{shaft}	thermal resistance between end of shaft and ultimate sink	$\frac{°F-hr}{BTU}$	RSHAFT
$R_{bearing}$	thermal resistance between bearing and ultimate sink	$\frac{°F-hr}{BTU}$	RBRG
β_r	temperature coefficient of resistivity of rotor material	°F ⁻¹	PR

NOMENCLATURE (Contd)

<u>Variable</u>	<u>Description</u>	<u>Units</u>	<u>Computer language</u>
β_c	temperature coefficient of resistivity of stator windings	$^{\circ}\text{F}^{-1}$	BC
β_l	temperature coefficient of resistivity of rotor lamination	$^{\circ}\text{F}^{-1}$	BL
T^*	reference temperature for $\beta_r, \beta_c, \beta_l$	$^{\circ}\text{F}$	TCTAR
T64	boundary temperature, see Figure 1	$^{\circ}\text{F}$	T64
T65	boundary temperature, see Figure 1	$^{\circ}\text{F}$	T65
T66	boundary temperature, see Figure 1	$^{\circ}\text{F}$	T66
T52	boundary temperature, see Figure 1	$^{\circ}\text{F}$	T52
T53	boundary temperature, see Figure 1	$^{\circ}\text{F}$	T53
T54	boundary temperature, see Figure 1	$^{\circ}\text{F}$	T54
T55	boundary temperature, see Figure 1	$^{\circ}\text{F}$	T55
C	specific heat at constant pressure	Btu/lb- $^{\circ}\text{F}$	C
w_1	flow rate of gas in gap	lbs/hr	w1
w_2	flow rate of gas outside stator	lbs/hr	w2
TINLET	inlet gas temperature	$^{\circ}\text{F}$	TINLET
Q_i	heat generation at node, See Figure 1	Btu/hr	Q(I)

GENERATOR ROTOR DYNAMICS



ROTOR DYNAMICS

TABLE OF CONTENTS

	Page
A. INTRODUCTION-----	D-1
B. CRITICAL SPEEDS-----	D-3
C. ROTOR RESPONSE TO SYNCHRONOUS EXCITATION-----	D-6
FIGURES -----	D-8a

A. INTRODUCTION

The following discussion pertains to the subject of rotor dynamics, with specific emphasis on the problems associated with high-speed, solid rotor, brushless electrical alternators supported on gas bearings, such as are being studied for use in space power systems.

The term "rotor dynamics" is a general term which covers dynamic motion of a mechanical system composed of a rotating assembly, its bearings, and the bearing support structures (sometimes referred to as bearing pedestals). There are many facets to the rotor dynamics problems. The most commonly considered aspects are the rotor system resonant frequencies (more commonly called critical speeds) and the dynamic shaft displacements due to rotating mechanical unbalance or other imposed dynamic loads (e.g., aerodynamic, electromagnetic, vibratory and / or shock loads). Other aspects of the rotor dynamics problem which, though less familiar, are very critical in gas-bearing supported equipments are:

- a) half frequency whirl,
- b) resonant whip,
- c) other self-excited vibration phenomena of the coupled bearing-rotor system (e.g., thrust bearing - rotor instabilities).

In the case of gas-bearing supported electrical alternators, there is the possibility of additional rotor system stability phenomena. Journal bearing whirl has already been observed in certain motor driven gas-bearing machinery and has been positively identified as being excited by the electromagnetic fields of the motor. There is good reason to suspect that similar phenomena may occur in alternator systems. Considerable research and experimentation is needed in this area.

The rotor dynamics problem is of major importance because of the very small clearances and limited damping capabilities of gas bearings. Certain of the self-excited vibration phenomena are unstable and rotor displacements can quickly build up to destructive amplitudes once the instability mode is

excited. Operation in the vicinity of rotor system critical speeds, while of a stable nature, can also lead to destructive amplitudes if the rotor is not mechanically balanced to a very high degree. With good balance, it is usually possible to drive gas-bearing machines through the first two system criticals, i.e., the damping capabilities of the bearings are usually sufficient to limit the resonant amplitudes to safe values. The first two system criticals can be referred to as rigid body criticals (this is discussed more fully in the following section). The energy levels associated with these rigid body criticals are usually low enough that the bearings can damp the resonant displacements to acceptable amplitudes. In general, it has not been possible to drive gas-bearing machines through the third system critical, which is a flexural (or bending) critical. The energy levels associated with the higher frequency flexural criticals cannot be absorbed within the bearings, with the net result that resonant shaft displacements become destructively high. Therefore, unless an additional damping mechanism can be built into the rotor system, it is generally necessary to restrict operating speeds to approximately 80% of the third system critical.

Many of the rotor system instability phenomena are directly associated with the type of bearing used. Consequently, such phenomena are usually analyzed as a bearing design problem. However, instabilities which can be attributed to electromagnetic alternator or motor effects may be independent of bearing type. Since very little is known about the dynamic electromagnetic characteristics of high-speed alternators, the remainder of this discussion will be limited to critical speeds and synchronous whirl.

B. CRITICAL SPEEDS

A computer study has been made to determine the critical speed characteristics of three solid-rotor, brushless alternator types supported on gas bearings.

The alternator types are:

- a) the inside coil Lundell,
- b) the outside coil Lundell,
- c) the homopolar.

The objective of the study was to determine, on a relative basis, which type of alternator, if any, would be best suited to high speed applications. Accordingly, rotor dimensions and weights were obtained for each type of alternator on the basis of a 10 KVA, 12,000 rpm rating. The rotor configurations, as used for the critical speed evaluation, are shown in Figures D-1, D-2, & D-3.

Critical speed calculations were initially made for each of the alternator rotor types supported by a 1 1/2 inch diameter bearing at each end of the rotor. Flexural criticals were not encountered up to speeds of 100,000 rpm. Thus, each rotor by itself is a quite stiff structure.

In an actual power system, the alternator rotor does not exist by itself, but is intimately connected to some type of drive turbine at one end and some type of thrust bearing, usually located at the opposite end. On the basis of several 10 KVA space system design studies made by MTI, it is known that the turbine would weigh approximately 10 pounds and the thrust bearing about 5 pounds. Using two inch diameter journal bearings, a 10 pound turbine, and a 5 pound thrust bearing, a critical speed model was set up for each of the alternator types.

Based on the model of Figure D-4, critical speed maps have been computed as a function of journal bearing stiffness for each of the alternator designs. These maps are shown in Figures D-5, D-6, & D-7. Only the first three critical speeds are shown. The lower two curves on each map may be termed the

"rigid body" criticals in the range of

$$0 \leq K \leq K_1$$

where K is journal bearing stiffness, and K_1 is dependent upon the flexural characteristics of the rotor system. For instance, K_1 would be about 5×10^5 lb./in. for both the homopolar and the outside coil Lundell, while for the inside coil Lundell the value would be about 2×10^5 lb./in. Above these values of K_1 , the term "rigid body" is no longer applicable since the critical speeds are beginning to approach the criticals of a simply supported rotor, as represented by the case of $K \rightarrow \infty$.

At stiffness values of

$$0 \leq K \leq K_1, \quad \text{Where } K_1 \text{ is a special limiting value}$$

the highest critical speed curve plotted on the maps (which is really the third system critical) is essentially the free-free flexural frequency of the rotor. As $K \rightarrow \infty$, this third critical approaches the third flexural frequency of a simply supported rotor. This effect is illustrated by Figure D-7.

Stiffness values for hydrodynamic gas journal bearings typically range from 25,000 lb./in. to 150,000 lb./in. Values for hydrostatic gas journal bearings can reach 1,000,000 lb./in.

It is seen from Figures D-5, D-6 & D-7 that the rigid body criticals have about the same speed vs. stiffness characteristics. This is an expected result since the weights of the three alternator rotors are about the same, and each rotor, by itself, is very stiff. The rigid body criticals are essentially functions of only bearing spring rate and rotor system mass.

The third critical speed, i.e., the "free-free bending" (or flexural) mode, is about the same for both the outside coil Lundell and the homopolar. The free-free flexural frequency for the inside coil Lundell, however, is only 1/3 of the comparable values for the other two alternators.

The reason for this is quite clear from a comparison of the rotor geometries shown in Figures D-1, D-2 & D-3. The homopolar and outside coil Lundell are essentially solid rotors of appreciable diameter. The rotor of the inside coil Lundell, however, looks more like a fairly large mass supported on a relatively small diameter shaft. This latter condition inherently leads to lower critical speeds as a result of the increased flexibility of the shaft sections.

It may be concluded that the homopolar and outside coil Lundell alternators are inherently better suited to high speed operation from a critical speed standpoint. However, the actual critical speed values given in Figures D-5, D-6, & D-7 should only be considered on a relative basis since the actual rotating system of turbine, journals, and thrust bearing has been rather arbitrarily defined. In addition, the dimensions and weights of the alternator rotors are based on a 10 KVA, 12,000 rpm rating.

C. ROTOR RESPONSE TO SYNCHRONOUS EXCITATION

In addition to knowing the critical speed characteristics of a rotor system, it is also important to know the dynamic amplitudes of rotor vibration which will occur during operation. This data is necessary in order to determine if the bearing design is able to accommodate the dynamic amplitudes without exceeding the minimum film thickness criterion.

Studies of rotor response can be made if the nature of the dynamic forces acting on the rotor are known as a function of power level and speed (rotor displacements can also be excited by vibratory motions of the bearing pedestals). In the case of electrical alternators, the effects of the electromagnetic forces on the rotor response can, and should, be theoretically investigated, particularly since it is suspected that certain components of these forces can lead to rotor instabilities. However, such investigations have not yet been made and it is beyond the scope of this discussion to undertake such an analysis here.

It has been suggested that the major electromagnetic force which would excite an alternator rotor would occur when the rotor is eccentric to the stator, in which case there would be pole-face forces which would rotate at running speed. While this may be an oversimplified or incomplete accounting of the force components, it is a type of excitation which, like mechanical unbalance, can be evaluated with existing computer programs.

To illustrate the influences of synchronous excitation forces, the rotor system shown in Figure D-4 using a homopolar alternator rotor, has been studied for several unbalance conditions. The first condition is the influence of a mechanical unbalance force in the plane of the drive turbine. Unbalance at this location can reasonably be expected, over a period of time, as a result of material creep. The rotor response to 1.0 ounce-inch of unbalance in the turbine plane (station 1) at 12,000 rpm is shown in Figure D-8. The value of 1.0 ounce-inch has been picked for computational ease. The plotted values of response amplitudes can be ratioed directly for other values of unbalance moment.

Three response curves are shown in Figure D-8 corresponding to bearing stiffness values of 300,000 lb./in., 100,000 lb./in. and 50,000 lb./in. The response amplitudes for the 100,000 lb./in. case are seen to be considerably greater than for the other two stiffness values. By referring to Figure D-5 it is seen that the first rotor critical speed for a stiffness of 100,000 lb./in. is about 10,800 rpm. Since rotor speed was taken as 12,000 rpm in Figure D-8, the large amplitudes result from a near resonance condition. It is also seen that the response amplitudes for $K = 300,000$ lb./in. are 180 degrees out of phase with the other two response curves. This is a result of the well known phase shift characteristic of vibration responses which occurs as rotor speed passes through the rigid body criticals, which happens in this case as K decreases from 300,000 lb./in. to 50,000 lb./in.

A reasonable standard of balance, on a balancing machine, for an alternator system similar to Figure D-4 is 0.002 oz.-in. The amplitudes plotted in Fig. D-8 would thus be divided by 500 to obtain actual expected amplitudes.

The influence of pole-face forces on rotor response can be estimated from Figure D-9. In this case, running speed was again taken at 12,000 rpm and 1.0 ounce-inch of unbalance was placed at each end of the rotor (stations 4 and 8) with a phase angle of 90 degrees. The responses are again plotted for three values of bearing stiffness, the same as in Figure D-8. In this case the maximum rotor amplitudes occur at the 50,000 lb./in. bearing stiffness. Reference to Fig. D-5 indicates that this type of unbalance excitation results in a larger contribution by the second critical mode than is the case for a turbine unbalance.

The influence of combined turbine unbalance and alternator pole-face forces can be obtained by superposition of Figures D-8 and D-9.

Fig. D-10 shows the affect of both turbine unbalance and pole-face forces for the same rotor system at a much higher speed of 50,000 rpm. Bearing stiffness of 100,000 lb./in. is used. It is seen from Fig. D-5 that 50,000 rpm falls approximately midway between the second and third system criticals. The resulting response amplitudes, for both the turbine unbalance and the pole-face

forces, are considerably smaller than were obtained at 12,000 rpm.

The significance of the above result is quite apparent. A value of 1 ounce-inch was used for the turbine and pole-face unbalance forces in both the 12,000 and 50,000 rpm calculations. Thus the actual dynamic forces were 17.3 times larger at the 50,000 rpm speed. The resulting rotor amplitudes, however, were considerably lower. The conclusion is quite clear. To obtain minimum dynamic response amplitudes at a given design speed, the critical speed characteristics of the rotor system should be designed such that design speed is as far removed from the system criticals as is physically possible. In most gas bearing applications this will mean that design speed should fall approximately midway between the second and third system criticals.

It is once again emphasized that the numerical results shown on Figures D-8, D-9, & D-10 apply to an arbitrarily defined system, and should not be extrapolated to another design. Each design must be analyzed separately to obtain actual amplitude data.

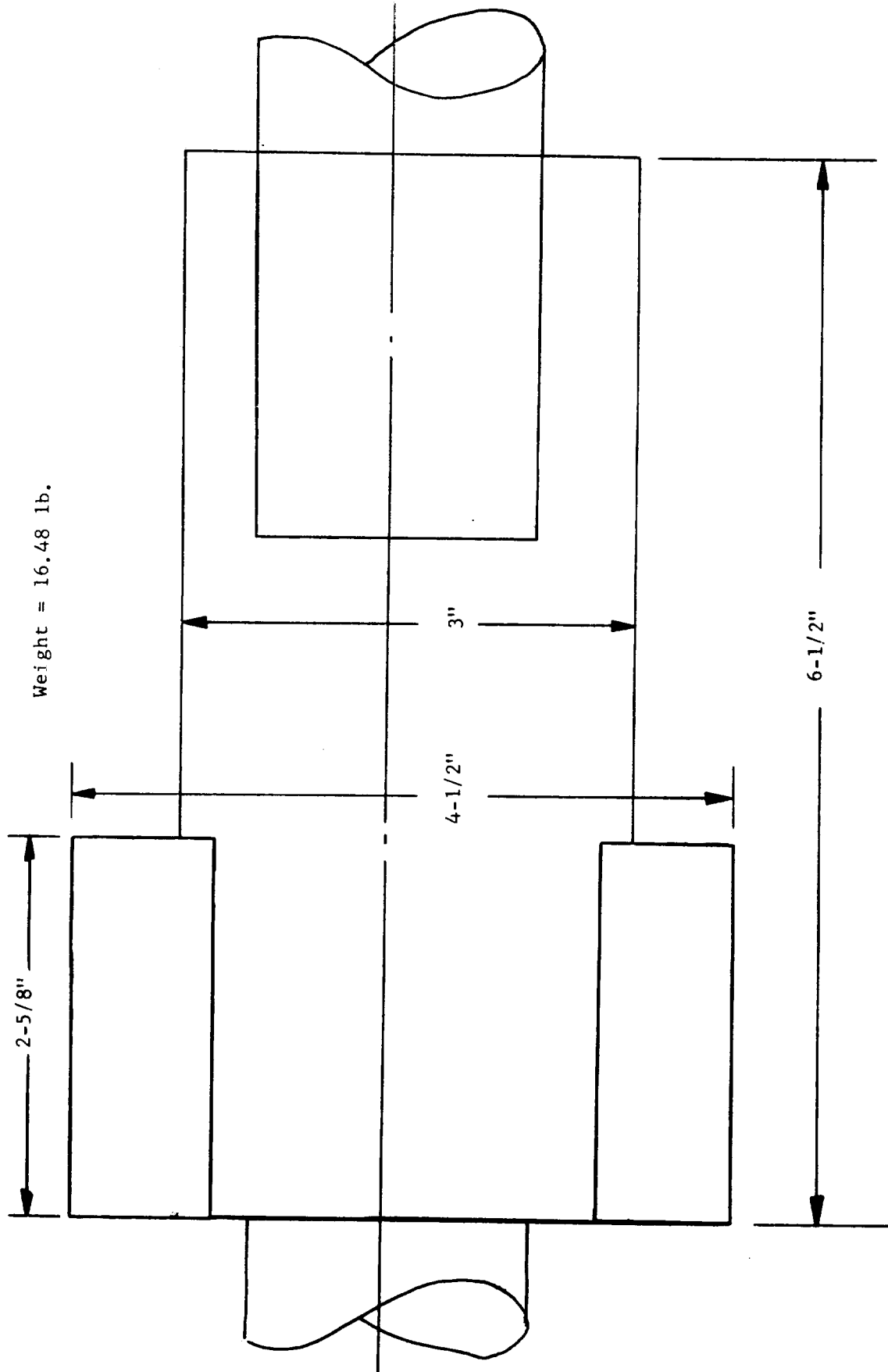


Fig. D-1 Configuration of 10 KVA, 12,000 rpm Homopolar Alternator Rotor

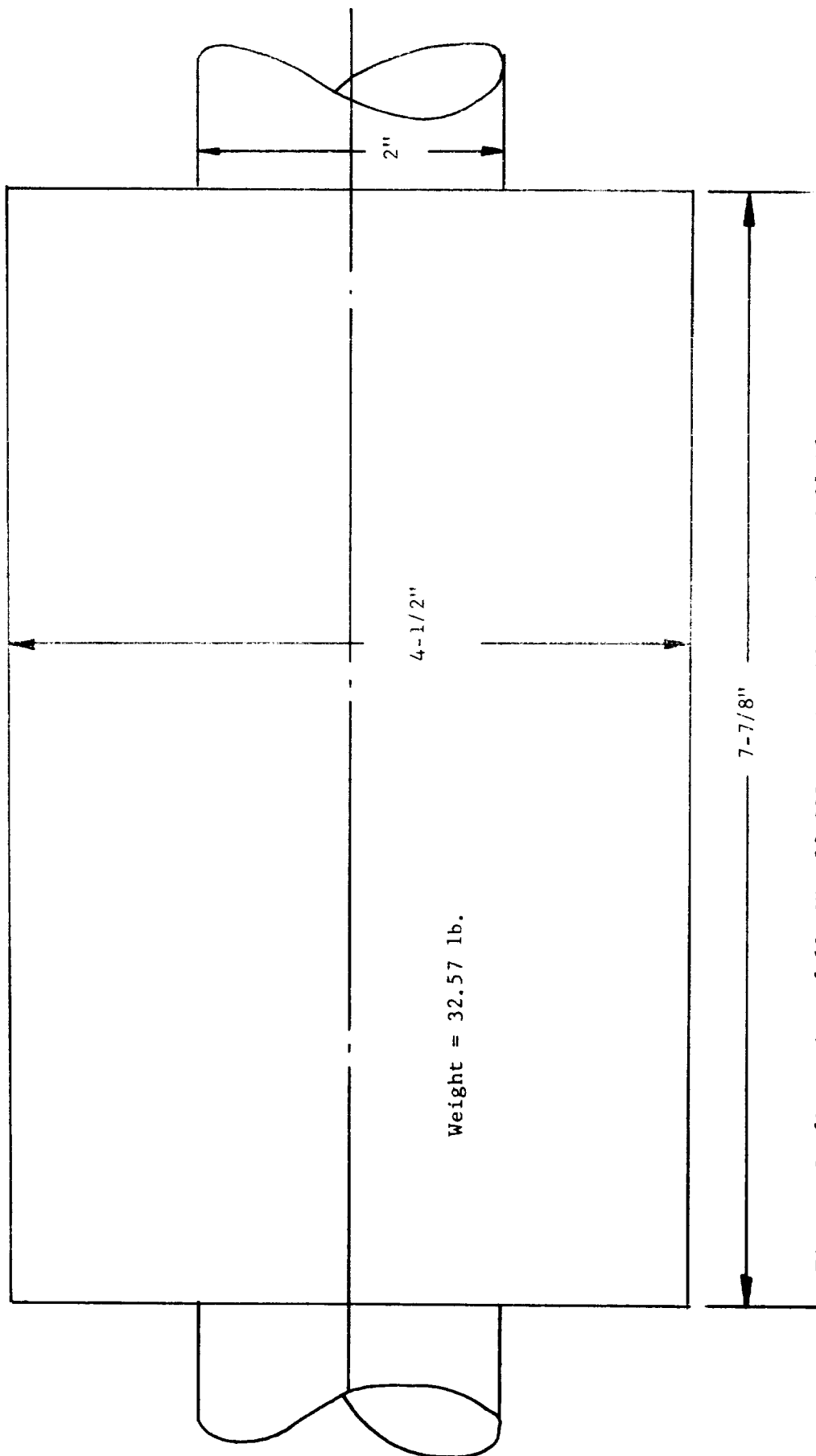


Fig.D-2 Configuration of 10 KVA, 12,000 rpm Outside Conf. Lyndell Alternator Rotor

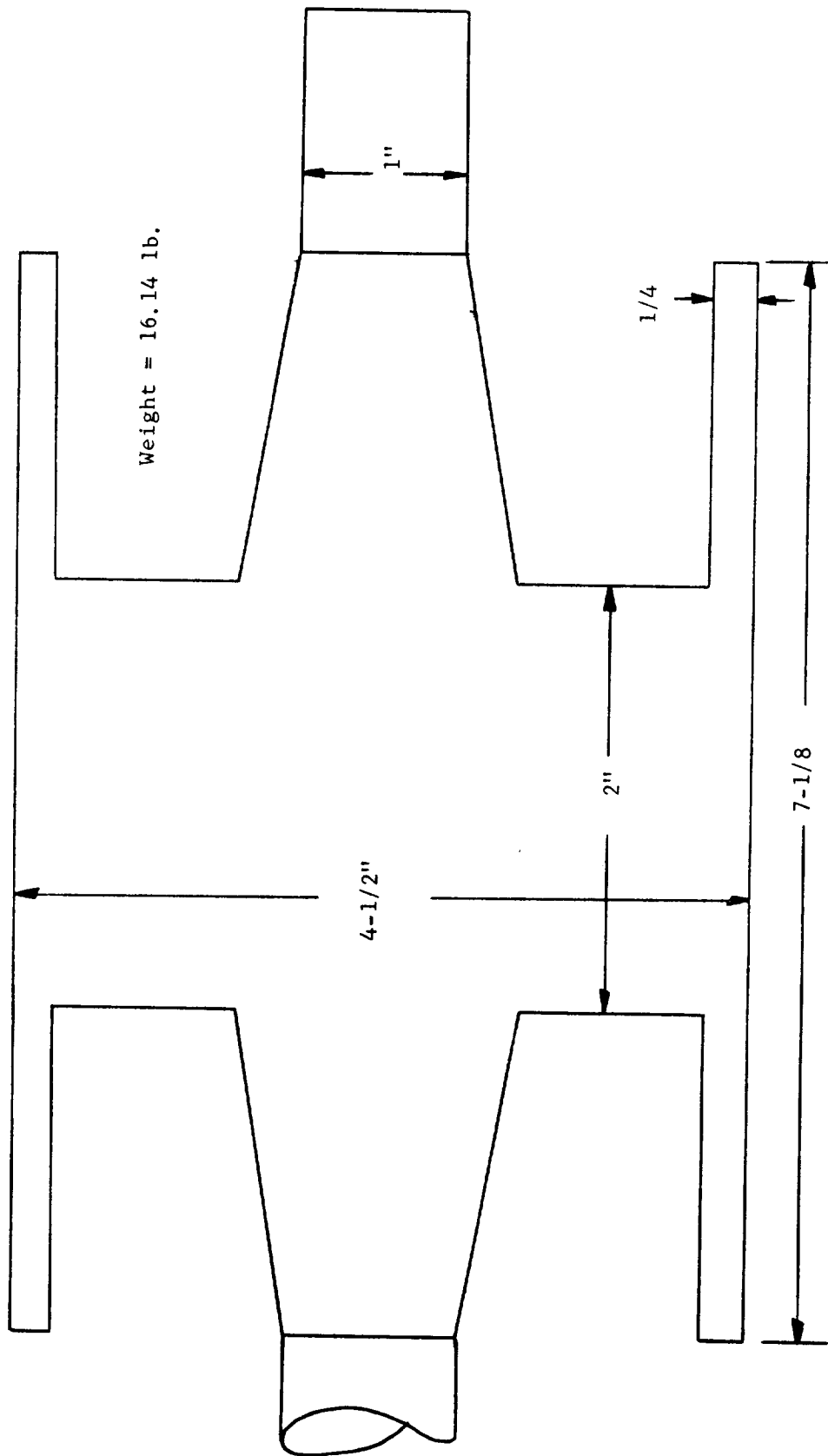


Fig. D-3 Configuration of 10 KVA, 12,000 rpm Inside Coil Lundell Alternator Rotor

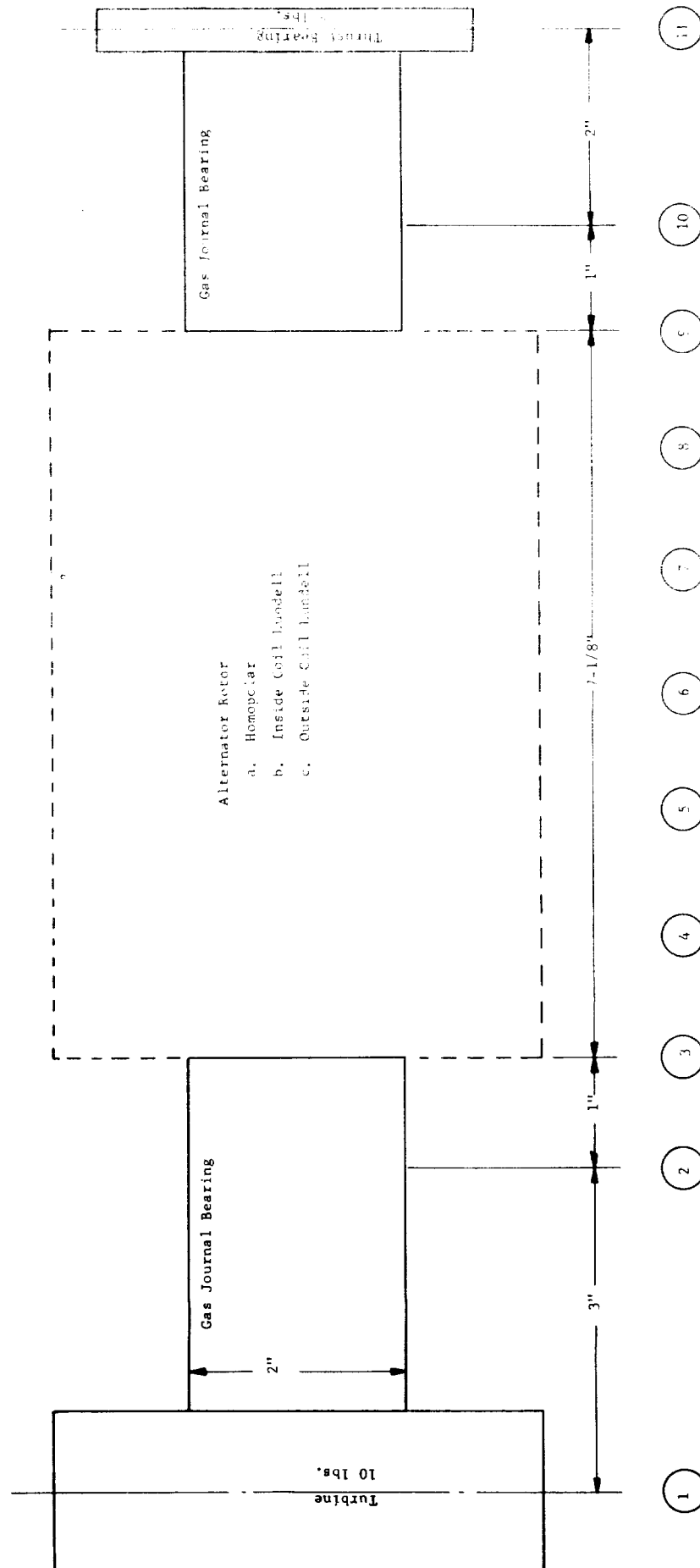


Fig. D-4 Model Used For Comparison of Critical Speed Characteristics of Three Alternator Systems.

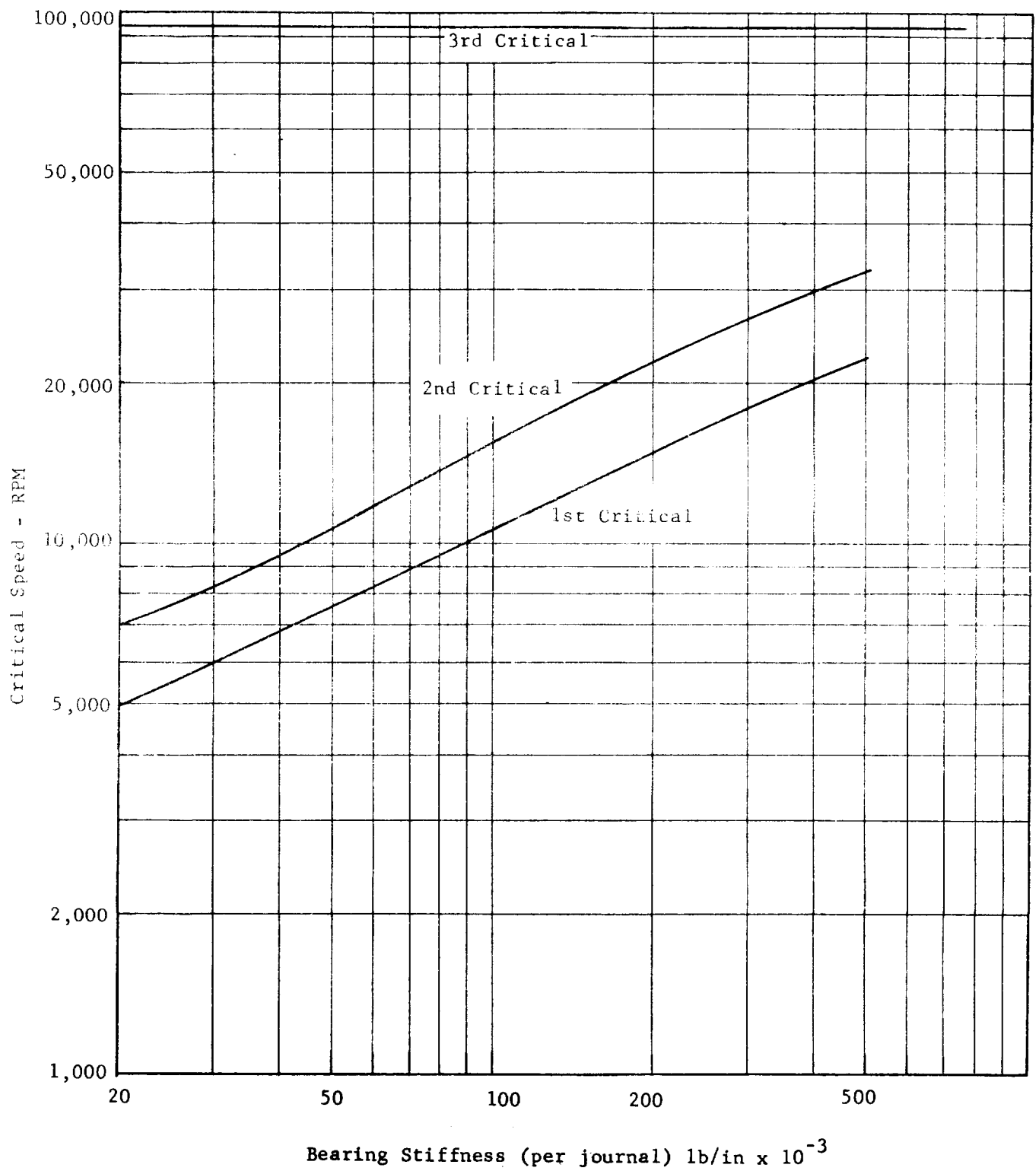


Fig. D-5 Critical Speed Map for Homopolar Alternator System

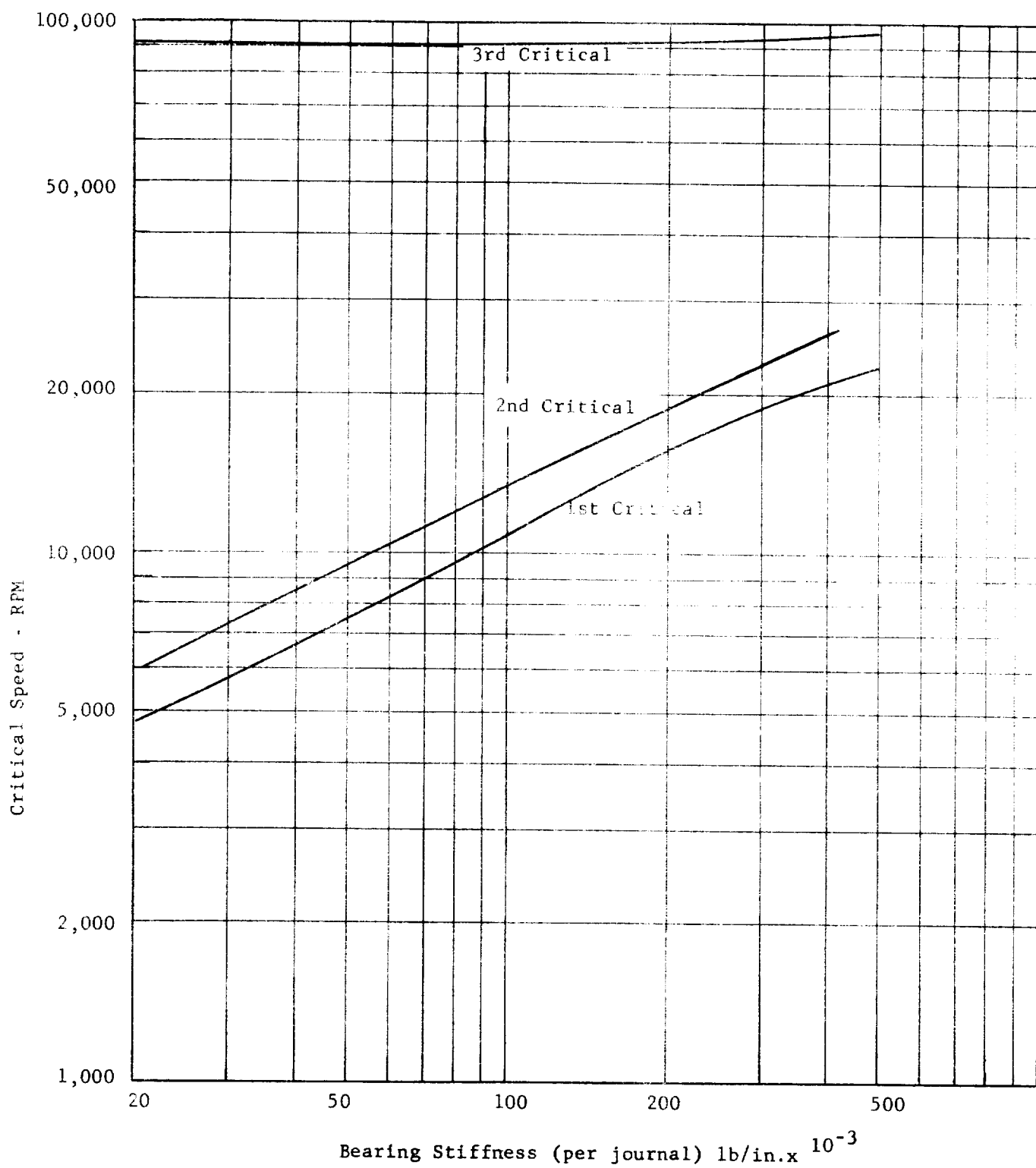


Fig.D-6, Critical Speed Map for Outside Coil Lundell Alternator

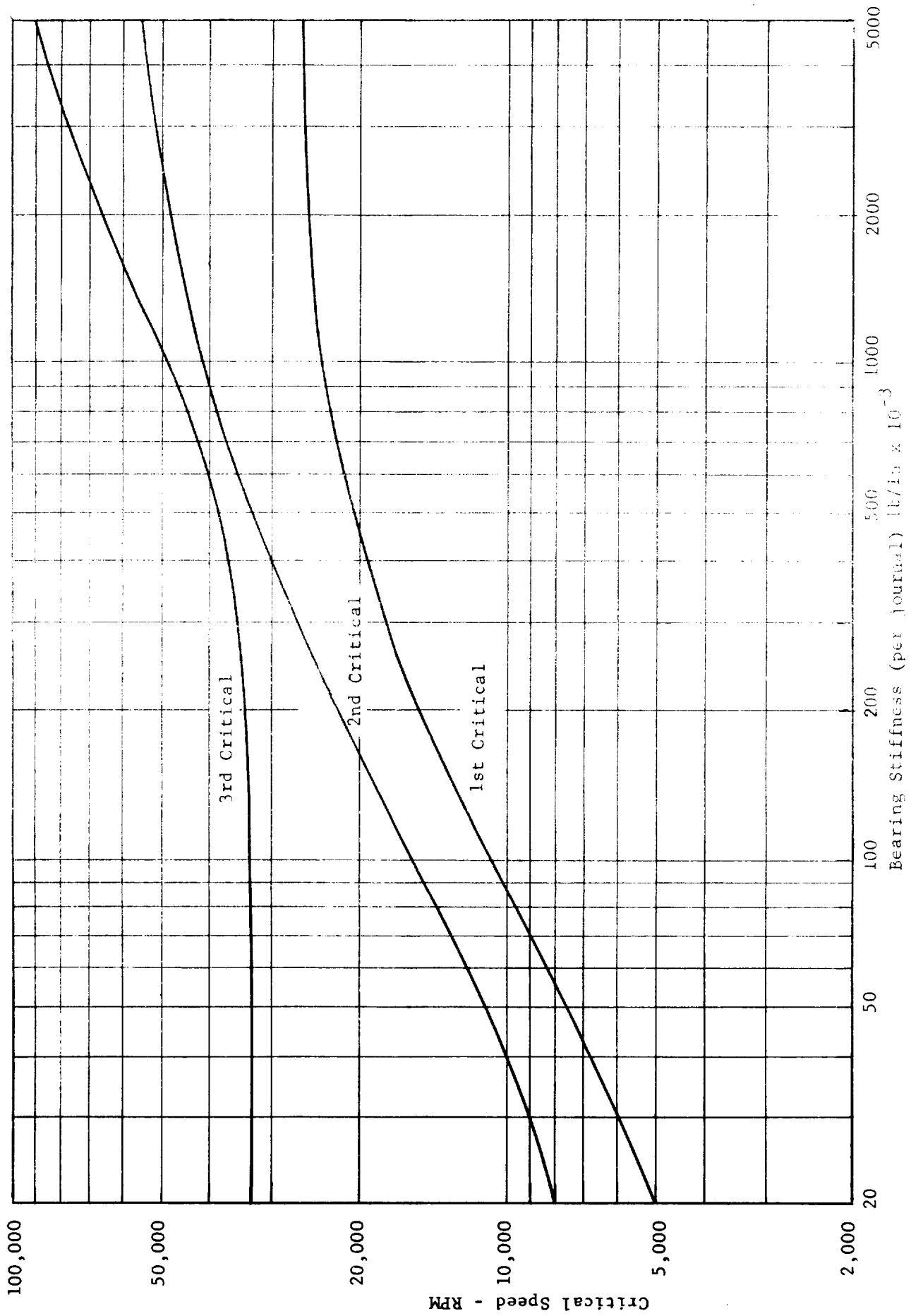


Fig.D-7 Critical Speed Map For Inside Coil Lundell Alternator System

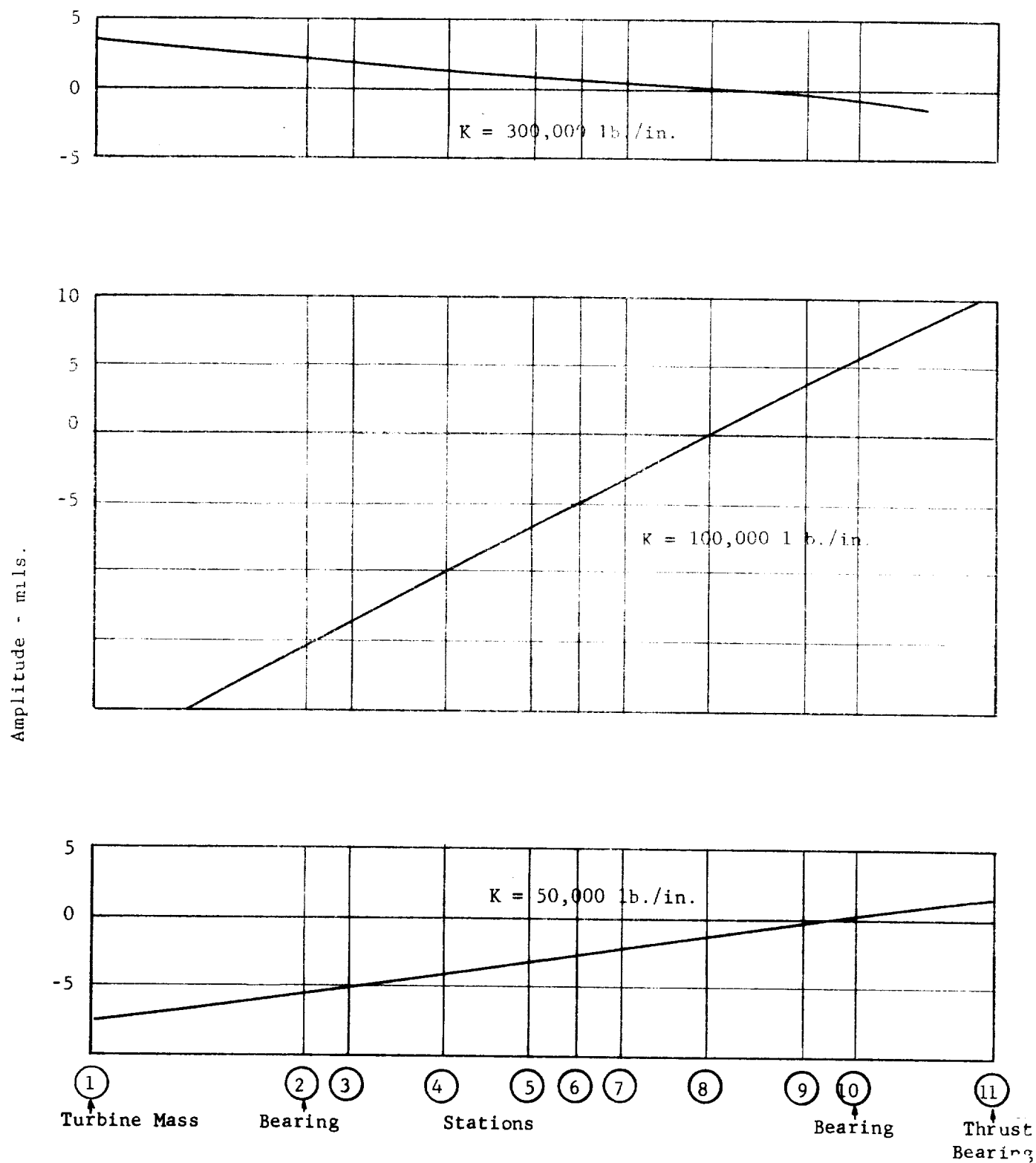


Fig. D-8 Dynamic Response Amplitudes of Homopolar Alternator System Due to 1.0 oz.in. of Turbine Unbalance.

Rotor Speed - 12,000 RPM

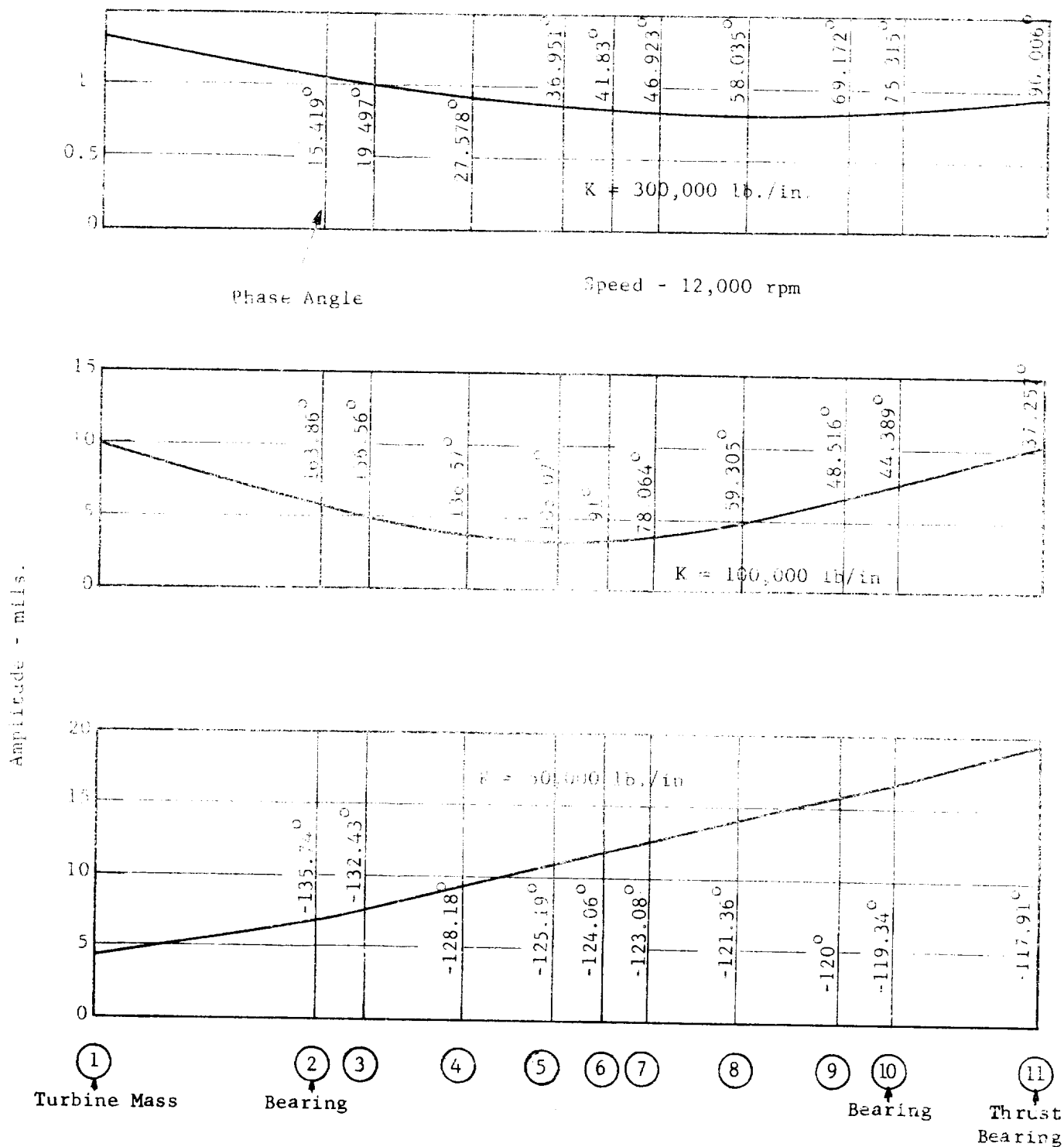


Fig. D-9 Dynamic Response Amplitudes of Homopolar Alternator System Due to 1.0 oz.in. of Unbalance of Each Pole Face (stations 4 and 8), 90 Degrees Apart.

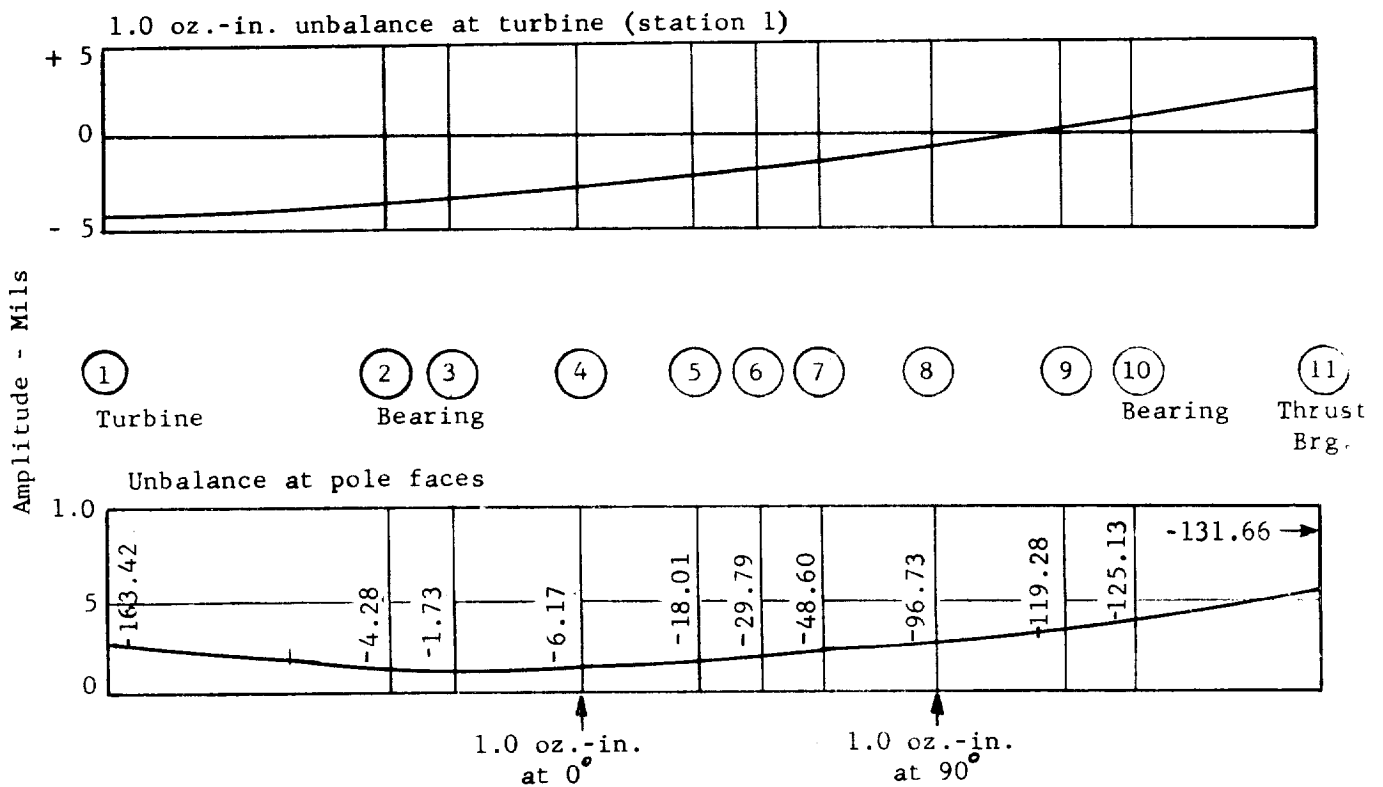


Fig. D-10 - Dynamic Response Amplitudes of Homopolar Alternator System
at 50,000 RPM

Bearing stiffness - 100,000 lb./in.

DISCUSSION OF GAS BEARINGS AND
ROLLING CONTACT BEARINGS



TABLE OF CONTENTS

	<u>Page</u>
A. FOREWORD	E-1
B. INTRODUCTION TO GAS BEARINGS	E-1
1. Advantages and Uses of Gas Bearings	E-2
2. Gas Bearing Terminology	E-3
3. Classification of Gas Bearing Types	E-5
4. Design Information	E-5
Tables	E-7
Figure	E-11a
C. SELF-ACTING JOURNAL BEARINGS	E-12
1. Preliminary Discussion	E-12
2. Design Calculations for the Plain Circular Bearings	E-15
3. Design Calculations for the Tilting-Pad Bearings	E-18
Nomenclature	E-22
Figures	E-22a
D. SELF-ACTING THRUST BEARINGS	E-23
1. Introduction	E-23
2. General Descriptions of Spiral-Grooved Thrust Bearings	E-24
3. Design Considerations	E-26
4. Example	E-32
5. Dynamic Considerations	E-37
References	E-39
Nomenclature	E-40
Tables	E-41
Figures	E-43a
E. EXTERNALLY-PRESSURIZED JOURNAL BEARINGS	E-44
1. Introduction	E-44
2. Selection of the Hydrostatic Bearings	E-45
3. Design for Steady-State Operation, Non-Rotating Rotor	E-46
4. Design for Dynamical Operation, Rotating Rotor	E-51
Nomenclature	E-53
Figures	E-54a

Table of Contents (Cont'd)

F. EXTERNALLY-PRESSURIZED THRUST BEARINGS	E-55
1. Introduction	E-55
2. Selection of the Hydrostatic Bearings	E-56
Nomenclature	E-63
G. GAS BEARING MATERIALS	E-64
1. Summary	E-64
2. Materials for Gas-Lubricated Bearing Applications	E-64
References	E-75
Tables	E-76
H. SPECIAL CONSIDERATIONS IN GAS BEARING DESIGN	E-79
Rolling Contact Bearings	E-81

A. FOREWORD

The following is a brief review of gas bearing selection and design procedures. Mathematical derivation of the compressible lubrication equation or the solution of this equation is not included in this discussion since they are well-covered in existing literature. Instead, the emphasis is placed on the different types of gas bearings which have been developed for the various ranges of operating conditions. Examples of gas-bearing design calculations are given for many such bearing types. The important materials considerations in gas bearing design and selection are also summarized, based on our experience in this area. In all cases, special emphasis is laid on dynamic operation (rather than steady-state load capacity) since this is generally a very critical problem and it governs the selection of particular bearing types.

B. INTRODUCTION TO GAS BEARINGS

1. Advantages and Uses of Gas Bearings

Any bearing system must possess definite advantages before it is considered for a specific application. The advantages that gas bearings offer are:

- a. No contamination of the system by the lubricant
- b. Chemical stability over a very wide temperature range
- c. Resistance to damage by radio activity
- d. Favorable viscosity-temperature characteristics
- e. High reliability and long operating life
- f. Low and uniform friction

The viscosity of gases, unlike that of liquids, increases with temperature. This, combined with the chemical stability of gases, removes inherent limitations on high temperature operation that are found with other lubrication systems. The same is true of systems that operate in a radio-active environment.

The absolute viscosity of gases is low, as shown in Fig. E-1. Thus, unless the load capacity of gas bearings is enhanced by external pressurization, they are limited to light loads as compared to the oil-lubricated slider or rolling element bearings. Within present state-of-the-art, self-acting gas bearings are used to carry loads ranging from about 1 to 15 psi, depending on speed, geometry and other factors as shown later in this discussion. The low viscosity, however, permits them to tolerate high shear rates with relatively low heat generation, so that they are ideally suited for high-speed operation.

Perhaps the greatest stimulus to the increased use of gas bearings has been increased acceptance of the concept of process fluid lubrication. By using the system fluid as the system lubricant, an auxiliary fluid (and potential contaminant) is removed. Sealing problems are also greatly reduced and such auxiliaries as lube pumps, filters, coolers, pipes and others are eliminated. Finally, gas lubrication shares with other forms of full, fluid film lubrication the property of high reliability and long operating life since, except for starts and stops,

the mating surfaces of the bearings are always separated by a fluid film. Table E-2 summarizes some of the important applications of gas bearings and the specific advantages of gas bearings in such applications.

2. Gas Bearing Terminology

The terminology of gas lubrication has grown as increasingly critical applications have shown that the dynamic characteristics of the bearings and of the coupled rotor-bearings system can determine the success or failure of any particular application. To aid in later discussion, the terminology used in discussion of steady-state and dynamic performance of gas bearing is summarized below:

Self-Acting (or Hydrodynamic) Gas Bearing - one in which the surfaces are separated by gas film pressures generated by the relative motion of the surfaces.

Externally-Pressurized (or Hydrostatic) Gas Bearing - one in which the surfaces are separated mainly by the introduction of pressurized gas into the clearance space.

Hybrid Bearings - bearings which combine the self-acting and externally-pressurized features.

Composite Bearings - bearing geometries which are capable of supporting radial and thrust loads, e.g., spherical, conical, etc.

Steady-State Performance of Bearings - under this condition, the gas film pressure distribution is independent of time. This means a stationary journal axis or thrust collar axis.

Dynamic Performance - under this condition the axis of the journal or the thrust collar moves so that the local, gas film pressure varies with time. Examples of dynamic operation are:

- a. start-up and shut-down transients
- b. motion excited by a rotating load
- c. motion excited by a reciprocating load
- d. bearing instability as described below

Bearing Instability - dynamic operation of excessive amplitude caused by self-excited, time dependent fluid film pressures.

Threshold of Instability - corresponds to journal speed at which instability is initiated.

Critical Speed - this is the rotating speed of a journal which corresponds to the resonance frequency of the system. (The system's critical speeds include rigid body as well as bending or torsional critical speeds).

Synchronous Whirl - this is a whirling, orbital motion of the journal or bearing at a frequency equal to the rotational frequency. The motion of the journal or bearing center is in the same direction as the direction of the journal rotation.

An example of the synchronous whirl is the case of an unbalanced rotating load. (If unidirectional loads are absent in a plain, cylindrical journal bearing, the whirling locus is a circle. If, however, a unidirectional load is also present in a plain cylindrical journal bearing, the whirling locus is an ellipse.)

Synchronous Wobble - this is a wobbling motion of a thrust runner or thrust bearing at a frequency equal to the rotational frequency and in the same direction as the rotating member. An example of the synchronous wobble is the case of an angularly misaligned collar (thrust runner).

Half-Frequency Whirl - a special case of instability generally associated with self-acting journal bearings. This instability occurs when the journal speed reaches a critical value. The journal axis whirls at a frequency of one-half or nearly one-half of the journal speed in the same

direction as the journal rotation. The motion of the journal axis can be either conical or translatory.

Resonant Whip-(Often called "Resonant Fluid Film Whirl") - A resonant vibration of a journal in a fluid film journal bearing which occurs at approximately twice the actual first system critical and persists at higher speeds. The frequency of vibration is approximately equal to the first system critical regardless of running speed. The motion of the journal axis is in the same direction as the shaft rotation. This condition is caused in part, by a flexible rotor. In self-acting gas-lubricated systems, the rotor is generally very stiff as compared to the gas film; thus, up to now, this condition has not really been positively identified. A similar condition has, however, been observed with a rigid rotor supported on externally-pressurized journal bearings.

Pneumatic Hammer - this is a self-excited oscillation in the flow system of an externally-pressurized bearing. This oscillation does not necessarily require the relative motion of the bearing surfaces.

3. Classification of Gas Bearing Types

In order to meet a wide variety of applications, self-acting, externally-pressurized and hybrid bearings have been developed. A summary of the characteristics of these bearing types is given in Table E-3.

In addition, numerous geometries for each type have been suggested, as indicated in Tables E-4 and E-5. Of these, the ones that have been used most extensively have been: (a) the plain circular and the tilting-pad, self-acting journal bearings, (b) the helical-grooved and the tilting-pad, self-acting thrust bearing, (c) the orifice compensated, journal and thrust, externally-pressurized bearings. The main discussion will therefore be limited to these particular types and the reasons for their general usage.

4. Design Information

Gas bearings have generally low damping, due to the low viscosity of gases. In

addition, due to the compressibility of gases, the damping decays rapidly at very high speeds. For these reasons, as well as the absence of boundary lubrication safeguards, the selection and design of gas bearings is much more critical than is the case with conventional, oil lubrication. Experience has shown that careful analysis is required of:

- a. steady-state performance
- b. dynamic performance and rotor-bearing coupling
- c. removal of heat generated to prevent serious distortions
and loss of clearance
- d. Mechanical design for minimal unbalance and shifting

These will be considered further in this review. For the present, we have summarized in Table E-6 the data that has to be obtained in the design phase.

TABLE E-2

GAS BEARING APPLICATIONS

	<u>Industry</u>	<u>Applications</u>
<u>No Contamination</u>	Nuclear	Pumps, compressors, blowers, circulators, turbines, motors
	Chemical	Compressors, turbines, expanders
	Food	Compressors, blowers, circulators, motors
	Pharmaceutical	Compressors, blowers, circulators, motors
	Refrigeration	Compressors, expanders
	Medical	Dental drills
<u>Low-High Temperature</u>	Refrigeration	Cryogenic compressors, expanders
	Space	Turbines, compressors, generators
	Utility	Turbines, compressors, generators
	Nuclear	Pumps, compressors, turbines, motors
<u>Radiation</u>	Nuclear	Compressors, turbines
	Space	Compressors, turbines, generators
<u>High Reliability and Long Life</u>	Nuclear	Compressors, blowers, circulators, turbines, motors, generators
	Space	Compressors, turbines, motors, generators, gyros, disks, drums
	Textile	Spindles
	Consumer	Motor, generators, compressors, blowers, circulators, fans, recorders, computers
<u>Low and Constant Friction</u>	Electrical	Dynamometers
	Military	Gyros, accelerometers, turn tables, optical scanners
<u>Close Position Control and Low Vibration</u>	Machine Tool	Grinders, turn tables
	Consumer	Recorders, computers, dental drills

TABLE E-3

OPERATING CHARACTERISTICS OF DIFFERENT GAS BEARING TYPES

Bearing system	Operating Characteristics				
	Load-carrying capacity	Max. stable speed	Starting torque	Materials compatibility	Auxiliary equipment needed
Externally pressurized (hydrostatic)	Depends on supply pressure and bearing geometry	Very high	Very low Small torque due to assembly of orifices & Flow paths.	Minimum problem	Separate comp. or other cont. high press. supply
Self-acting (hydrodynamic) with dry starting	Limited by speed, bearing geometry and fluid properties	Depends mainly on bearing and rotor geometry, fluid properties	Depends on choice of materials	Carefully select materials for minimum wear during starting & stopping	None
Self-acting with hydrostatic starting and stopping	Limited by speed, bearing geometry, and fluid properties	Depends mainly on bearing and rotor geometry, fluid properties	Very low	Minimum problem	Reservoir of fluid for starting, stopping
Hybrid (combined externally pressurized and self-acting)	Depends on supply pressure, bearing geometry, speed, and fluid properties	Depends mainly on bearing and rotor geometry, fluid properties	Very low	Minimum problem	Separate comp. or other cont. high-pressure supply

TABLE E-4

GAS-LUBRICATED JOURNAL BEARINGS

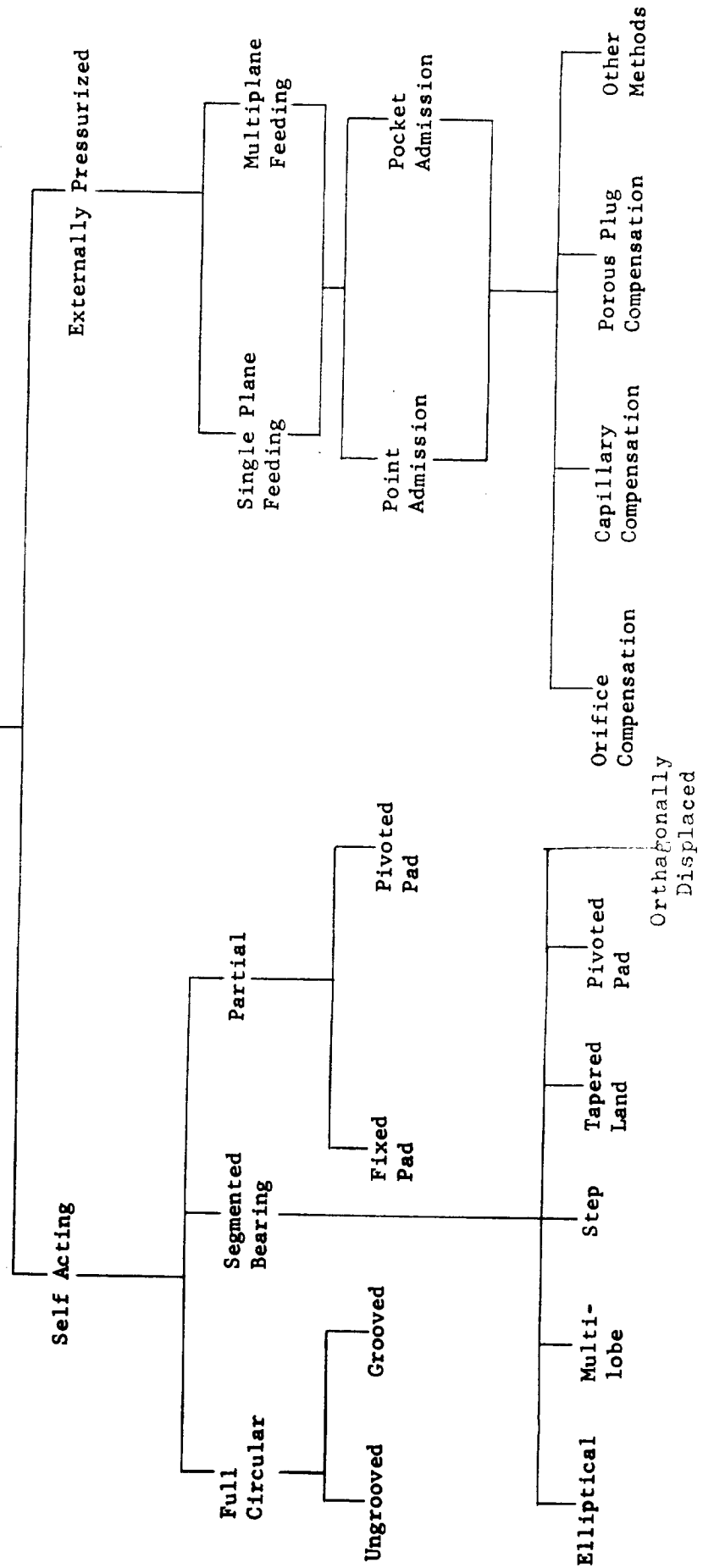


TABLE E-5

GAS-LUBRICATED THRUST BEARINGS

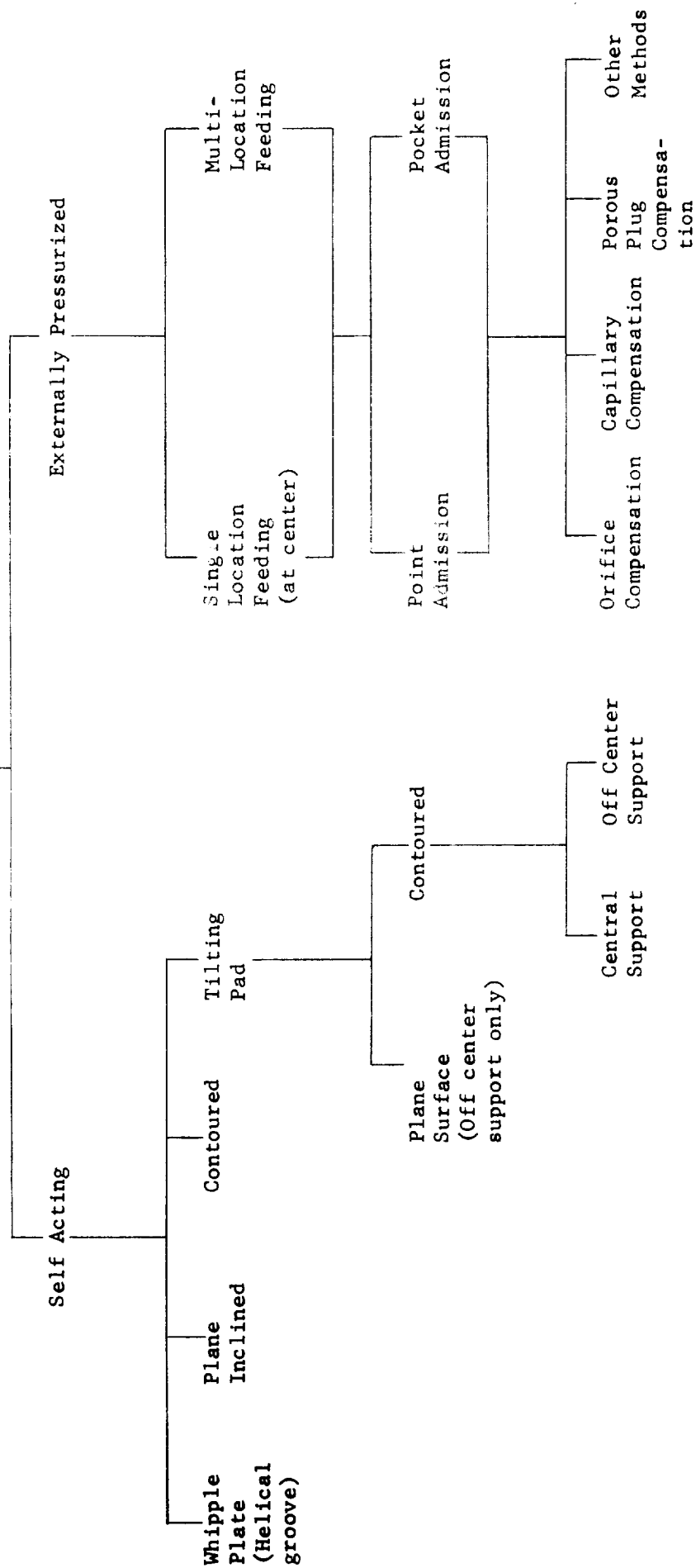


TABLE E-6

REQUIRED DESIGN INFORMATION

Steady State Performance

<u>Type</u>	<u>Needed Data</u>	<u>Design Parameters</u>
Self-Acting	Load carrying capacity Bearing or journal friction Attitude angle Minimum film thickness Thermal map	Bearing geometry (Including tolerance effects) Speed Fluid characteristics Ambient pressure
Externally Pressurized	Load carrying capacity Bearing or journal friction Attitude angle Minimum film thickness Supply flow requirement Thermal map	Bearing geometry (Including tolerance effects) Speed Fluid characteristics Ambient pressure Supply pressure External flow resistance

Dynamic Performance Information

<u>Type</u>	<u>Needed Data</u>	<u>Design Parameters</u>
Self-Acting	Region of stable operation Stiffness characteristics Damping characteristics Other film force characteristics Bearing influences on rotor criticals Thermal map for transient conditions	Bearing geometry (Including tolerance effects) Speed Fluid characteristics Ambient pressure Rotor flexibility Time varying loads
Externally Pressurized	Region of stable operation Stiffness characteristics Damping characteristics Other film force characteristics Bearing influences on rotor criticals Thermal map for transient conditions	Bearing geometry (Including tolerance effects) Speed Fluid characteristics Ambient pressure Rotor flexibility Time varying loads Supply pressure External flow impedance

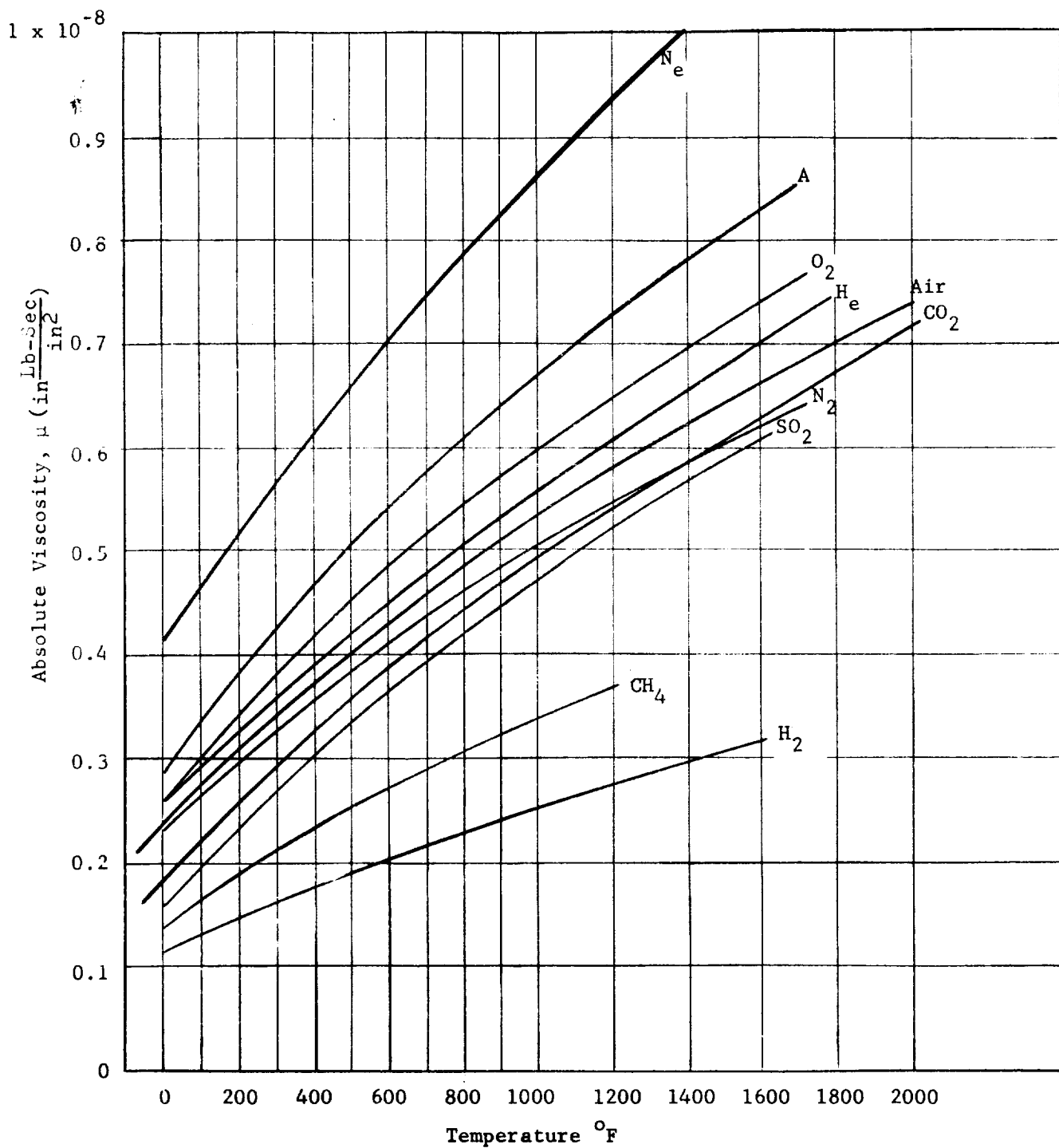


Fig. E-1 Absolute Viscosity of Various Gases

C. SELF-ACTING JOURNAL BEARINGS

1. Preliminary Discussion

The simplest type of self-acting, gas-lubricated journal bearing is the plain, cylindrical bearing. As such, it has been more extensively analyzed than any other and it is frequently used — at least in moderate speed applications (say $\leq 10^5$ RPM). The operation of the plain, cylindrical bearing is shown schematically in Fig. E-7. Under a steady-state load, W , and speed, N , the shaft center will assume a position in the bearing cavity at distance, e , from the bearing center and at an angle, ϕ , from the load line. The ratio $e = \frac{e}{C}$ is called the eccentricity ratio and angle, ϕ , is the attitude angle. Here, C is the radial clearance of the bearing so that the limiting values of e are $e = 0$ when the shaft and bearing centers coincide (i.e., $e = 0$) and $e = 1$ when the shaft is in contact with the bearing surface, (i.e., $e = C$).

For plain circular bearings, the attitude angle is quite large, approaching 90 degrees at low values of e . For static equilibrium, the resultant of the fluid film pressures must be equal and opposite to the applied load, W . Since the attitude angle is not zero, this resultant has components both along and normal to the line that passes between the bearing and shaft centers. The presence of the force component normal to the line of centers provides a force that tends to induce an orbital motion of the journal center. In certain regions of operation, which will be quantitatively defined later, small perturbations in the load, which result in corresponding perturbations of the tangential force component, induce a whirling motion of the shaft center. The whirl occurs at a frequency that is about one-half the operating speed and it is accompanied by a collapse of the fluid film pressures and subsequent failure. This is the condition known as "half-frequency" whirl. It is essential in selecting and designing gas bearings to compute the threshold of instability and to ensure that it is outside the required operating range.

Returning now to Fig. E-7, it is seen that the bearing clearance is divided into two regions by the line of centers. One of these is the converging zone, in

which positive (i.e., higher than ambient) pressures are generated by viscous shear. The other is the diverging (or "diffuser") region in which negative (i.e., lower than ambient) pressures are developed. The load capacity of the bearing is the resultant of these pressures which, as noted above, must be equal and opposite to W . A continuous interchange is made with the ambient gas, as gas is forced out of the ends of the bearing in the converging (positive pressure) region and drawn into the diverging (negative pressure) region.

The principal merits of the plain, cylindrical bearings are:

- (a) simplicity
- (b) ease of manufacture
- (c) relatively high load capacity as compared to most other geometries.

As opposed to this, its principal disadvantage is its low threshold of instability. It also has poor tolerance to misalignment so that, in many applications, it should be flexibly mounted in a diaphragm or in struts, of lower angular stiffness than the fluid film, in order to permit the bearing to align itself with the shaft.

It can be shown theoretically, and it has been demonstrated experimentally, that the threshold of instability can be raised by a number of methods which are based on:

- (a) increasing the operating eccentricity ratio
- (b) eliminating the negative pressure region of the bearing.

Thus, in cases where the load is unidirectional, some improvement in the threshold of instability can be achieved by undercutting the portion of the bearing above the point of application of the load, i.e., by using a partial-arc bearing in place of a full circular one. Other schemes that have been used include:

- (a) fabrication of steps or grooves in the upper part of the bearing. These generate positive pressures in the diverging regions of the bearing and result in increased eccentricity ratio and reduced attitude angle and, hence, a higher threshold of instability.

- (b) Introduction of pressurized gas into the upper part of the bearing to provide additional bearing load and, hence, higher eccentricity ratios and instability threshold.

Alternately, for high-speed applications, a much greater increase in the threshold of instability can be achieved by utilizing pivoted or flexibly supported pads, or by resorting to a fully flexible bearing surface, such as a foil bearing. Of these, the one that has been most commonly used and the one which has been furthest analyzed and developed is the tilting-pad bearing, shown schematically in Fig. E-8.

The gas-lubricated, tilting-pad bearing is an outgrowth of similar bearings that are sometimes used with oil lubrication to overcome instability problems. The tilting-pad bearing consists of a number of pads (most commonly, 3 or 4) each of which is supported in a theoretically frictionless pivot. A line pivot may be used, so that the pads can freely adjust to any desired inclination in the circumferential direction, but have no freedom of motion in the axial direction. Preferably, however, point pivots are used, so that the pads can incline both in the circumferential and axial directions. This latter method makes the bearing self-aligning.

Tilting-pad bearings are inherently stable, provided the moments of inertia of the pads are small enough that they will track motions of the shaft without phase lag. This is achieved if the inertia-angular stiffness system comprising the moment of inertia of each pad and the angular stiffness of the fluid film between the pad and the shaft has a critical speed that is much higher than the frequency of any dynamic loads to which the rotor-bearing system is subjected. In general design practice, the pads are designed so that their critical speeds in both pitch (i.e., angular motions about the shaft axis) and roll (i.e., angular motions about an axis tangent to the shaft surface and perpendicular to the shaft axis) are no less than twice the running speed. This may be called pad resonance in pitch, roll and yaw or sometimes flutter.

It can be shown that when these conditions are satisfied, the bearing load and the shaft center displacement in a tilting-pad bearing are co-linear (i.e., the attitude angle is zero) if the bearing load vector passes through one of the

pivots or mid-way between the pivots of adjacent pads. The attitude angle is non-zero, but it is very small, if the bearing load vector has some other orientation. Thus, the tangential component of force ($W \sin \phi$) which is normal to the line of centers, is also either zero or very small in a well-designed, tilting-pad bearing so that half-frequency whirl instability should not develop. It must be cautioned, however, that if the pivot friction is significant or if the moments of inertia of the pads are too large to permit the pads to track shaft motions, half-frequency whirl may be encountered. The procedure for calculating the tracking capability of tilting-pad bearings is therefore an important part of the design and it is described here in the section dealing with design calculations.

2. Design Calculations for the Plain Circular Bearing

Design data for plain, circular journal bearings is generally presented in the literature in terms of the three independent parameters:

Compressibility number: $\Lambda = \frac{6\mu\omega}{P_a} \left(\frac{R}{C}\right)^2^*$

Eccentricity ratios: ϵ

Slenderness ratio: L/D .

When these parameters are defined, it is possible to calculate the steady-state and dynamic performance characteristics of a bearing. These are:

Load Capacity: $\frac{1}{S} = \frac{W}{\mu NLD} \left(\frac{C}{R}\right)^2$

(Alternately, the load parameter $\frac{W}{P_a LD}$ is used)

Attitude angle: ϕ

Friction Force: $\frac{FC}{2\pi\mu\omega R^2 L}$

Threshold Speed: $\omega_T \left(\frac{MC}{W}\right)^{1/2}$

As an example, the design charts for plain, circular bearings are shown in Fig. E-9, for bearings having $L/D = 1/2, 1$ and 2 . They are calculated from numerical

* see nomenclature at the end of this section.

integrations of the Reynolds' Equation. Digital computer programs for this purpose have been prepared by several contributors to gas-bearing technology both in this country and abroad. Much of the work in this country has been achieved as a result of a continuing program sponsored by several government agencies and administered by the Fluid Mechanics Branch of the Office of Naval Research, Washington, D.C.

The following is an example of the use of the design charts for sizing of a gas bearing:

Given: A horizontal symmetrical shaft weighing 12 lbs. is to be supported in two plain cylindrical journal bearings. The operating speed is 12,000 RPM and the preferred journal bearing size is two inches in diameter by two inches long. At its operating speed, the bearings will be subjected to a load of 14 lbs. each, in addition to the dead weight load. The ambient gas is air at 14.7 psia and 100 F ($\mu = 2.8 \times 10^{-9}$ lbs.sec/in²).

It is desired to investigate the performance of the bearing for a range of clearances.

The calculations would proceed about as follows:

C/R	0.0005	0.00075	0.001	0.00125	0.0015
C (inches)	0.0005	0.00075	0.001	0.00125	0.0015
W (lbs.)	20	20	20	20	20
Λ	5.74	2.55	1.44	0.92	0.638
1/S	2.23	5.02	8.93	13.9	20.1
ϵ	0.3	0.4	0.52	0.64	0.72
ϕ (degrees)	28	43	51	49	46
$h_{\min} = C(1 - \epsilon)$, inches	0.00035	0.00045	0.00048	0.00045	0.00042
$\frac{FC}{2\pi\mu\omega R^2 L}$	1.04	1.12	1.3	1.6	1.7
F (lbs.)	0.092	0.066	0.059	0.056	0.050
$(\frac{MC}{W})^{1/2} \omega_{\text{threshold}}$	1.7	2.0	2.0	2.3	3.0
Threshold speed (RPM)	26,000	25,000	21,000	22,000	26,000

The calculations show that the bearing has acceptable values of eccentricity ratio and minimum film thickness throughout the range of clearances that was investigated. Furthermore, the stability thresholds are much higher than the operating speed. In such an application, therefore, the plain, circular bearing would be satisfactory. The actual value of clearance that would finally be selected would depend on the desired value of bearing stiffness.

It should be noted, however, that the bearing in the above example is stable at its operating speed because of the relatively high load it carries in addition to the weight of the rotor. If, however, the bearings had carried only the dead weight of the shaft, then, repeating the above calculations for $W = 6$ lbs. and $C = 0.001$ ", shows that:

$$\epsilon = 0.2$$

$$\text{Threshold speed} = 7100 \text{ RPM} .$$

Thus, the bearings would be unstable at 12,000 RPM.

The bearing stiffness is an important parameter since it affects the critical speeds of the rotor-bearing system. Generally, in such calculations, each bearing is treated as a spring having the value of the radial stiffness of the fluid film at the operating, steady-state eccentricity ratio.

The radial stiffness is then:

$$K_r = \left. \frac{\partial(W \cos \phi)}{\partial(h_{\min})} \right|_{\epsilon = \text{steady-state eccentricity ratio}}$$

For small values of Λ , this can be evaluated approximately by a numerical differentiation of the plot of $W \cos \phi$ vs h_{\min} .

In critical applications, a more exact approach is needed. In such cases, each bearing is represented by a set of eight stiffness and damping coefficients obtained as follows:

$$K_{xx} = \frac{\partial W}{\partial x} x$$

$$C_{xx} = \frac{\partial W}{\partial \dot{x}} x$$

$$K_{xy} = \frac{\partial W}{\partial y} x$$

$$C_{xy} = \frac{\partial W}{\partial \dot{y}} x$$

$$K_{yx} = \frac{\partial W}{\partial x} y$$

$$C_{yx} = \frac{\partial W}{\partial \dot{x}} y$$

$$K_{yy} = \frac{\partial W}{\partial y} y$$

$$C_{yy} = \frac{\partial W}{\partial \dot{y}} y$$

where: x, y are the vertical and horizontal components of motion of the shaft center

\dot{x}, \dot{y} are the vertical and horizontal components of the velocity of the shaft center.

K_{xx}, K_{xy}, K_{yx} and K_{yy} are the stiffness coefficients.

C_{xx}, C_{xy}, C_{yx} and C_{yy} are the damping coefficients.

Eight stiffness and damping coefficients are required because of cross coupling effects since the force and displacement are not co-linear.

3. Design Calculations for the Tilting-Pad Bearing

The tilting-pad bearing has the following geometrical parameters:

- a) No. of shoes
- b) Pad arc length
- c) Slenderness ratio (L/D)
- d) Pivot location
- e) Geometrical preload

The new geometrical parameters introduced here are d and e listed above. Since each pad is pivoted, it will seek an inclination such that the resultant of the fluid film forces passes through the pivot point. The inclination of the pad and the magnitude of the fluid film pressures will therefore depend on the location of the pivot. This is generally selected to provide maximum load capacity in the operating range. At low values of Λ , (say up to $\Lambda = 3$), the optimum pivot

position is in the range:

$$\frac{\theta_p}{\beta} = 0.55 \text{ to } 0.6$$

where θ_p is the angular distance between the pad inlet and the pivot location and β is the angular extent of the pad.

At higher values of Λ , larger values of $\frac{\theta_p}{\beta}$ are used up to a maximum value of 0.7 as $\Lambda \rightarrow \infty$.

Geometrical preloading is recommended in order to assure high values of bearing stiffness (even at small values of eccentricity ratio) and in order to prevent or at least minimize flutter of the pads which are located opposite to the direction of bearing load vector. Geometrical preloading is achieved by moving the pads in, so that the bearing clearance is smaller than the ground clearance of the pads. The geometrical preload coefficient is defined as:

$$m = 1 - \frac{C_B}{C_P}$$

where C_B is the bearing clearance and C_P is the ground clearance of the pads.

In tilting-pad bearing calculations, the compressibility number is referred to the ground clearance of the pads, i.e.,

$$\Lambda = \frac{6\mu\omega}{P_a} \left(\frac{R}{C_P}\right)^2$$

The two eccentricity ratios of interest are:

$$\text{Pad eccentricity} = \frac{e_1}{C_P} = \epsilon_P$$

$$\text{and Bearing eccentricity} = \frac{e_2}{C_B} = \epsilon_B$$

where, e_1 is the distance between the shaft center and the center of curvature of the pad and e_2 is the distance between the shaft center and the geometrical center of the bearing.

Design charts can be obtained for tilting-pad bearings. However, the procedure is considerably more complex than is the case for plain, circular bearings. This is due to the much larger number of parameters. An example of such design charts is given in Fig. E-10. This summarizes all the necessary bearing data for four-pad bearings with:

$$L/D = 0.7$$

$$\beta = 80^\circ$$

$$\theta_p = 0.7$$

$$m = 1/2$$

$$\Lambda \rightarrow \infty$$

(The load capacity, stiffness and friction torque of tilting-pad gas bearings approach asymptotic values as $\Lambda \rightarrow \infty$. Figure E-10 can be used with good accuracy down to values of $\Lambda \geq 30$. For values of $\Lambda < 30$, other curves calculated for the smaller values of Λ should be used).

Following is an example in the use of the curves:

Given: A symmetrical, two pound rotor is to be carried on two tilting-pad bearings. The bearing data is as follows:

$$\text{No. of Pads} = 4$$

$$\beta = 80^\circ$$

$$\frac{\theta_p}{\beta} = 0.7$$

$$m = 1/2$$

$$D = 0.75 \text{ in.}$$

$$L/D = 0.7$$

$$C_p = 0.375 \times 10^{-3} \text{ in.}$$

$$M_{\text{pad}} = J_{\text{pitch}}/R_p^2 = 2.63 \times 10^{-6} \text{ lb. sec./in.}$$

$$J_{\text{roll}} = 0.382 \times 10^{-6} \text{ lb. in. sec}^2, \text{ each pad.}$$

The operating conditions are:

$$N = 2500 \text{ RPS}$$

$$P_a = 10 \text{ psia}$$

$$\text{Gas is Helium at } 300^\circ\text{F } (\mu = 3.6 \times 10^{-9} \text{ lbs. sec/in}^2)$$

It is desired to calculate the bearing performance under the steady-state, dead weight load and to check whether the pads will track shaft motions.

The calculations would proceed as follows:

$\Lambda =$	34
$W/P_a LD =$	0.244
$\epsilon_B =$	0.23
$h_{pivot}/C_P =$	0.42
$h_{pivot} =$	0.157×10^{-3} inches
$C_P K/P_a LD =$	3.8
$K =$	40,000 lbs.
$C_P T/\pi \mu LDR^2 N =$	9.3
$T =$	0.041 lb/inches
$16 C_P K_{roll}/P_a L^2 =$	1.7
$K_{roll} =$	355 in.lbs/rad.
$N_{crit.roll} = (1/2\pi \sqrt{K_{roll}/J_{roll}})^{1/2}$	4850 R.P.S.
$N_{crit.roll}/N =$	1.94
$C_P N^2 M_{crit}/P_a LD =$	0.037
$M_{crit} =$	65×10^{-6} lb.sec ² /in.
$M_{crit}/M_{pad} =$	24.7

The pivot film thickness friction torque and bearing stiffness are shown above. It is noted that the ratio of the critical mass of the pad to the actual mass of the pad is 24.7 to 1, so that the pad will track motions of the shaft in the pitch direction. Also, the ratio of the critical frequency of the pad in the roll direction of the running speed is 1.94 to 1.

This is very nearly equal to the requirement that the ratio of pad critical speed by operating speed should be 2 to 1, so that the pads will also track shaft motions in the roll direction. Thus, the above bearings are satisfactory from these standpoints.

NOMENCLATURE FOR SECTION C: Self-Acting Journal Bearings

C	Radial Clearance, inches (Also used to denote damping coefficient, $\frac{\text{lb. sec}}{\text{in.}}$)
D	Diameter, inches
e	Eccentricity, inches
F	Force, lbs.
h	Film Thickness, inches
J	Moment of Inertia, lb. in. sec^2
K	Stiffness Coefficient lbs/in.
L	Length, inches
M	Mass, $\text{lb. sec}^2/\text{in.}$
m	Geometrical Preload Coefficient
N	Speed, R.P.S.
P_a	Ambient Pressure, psia
R	Radius, inches
R_p	Radius to Pivot Point, inches
S	Sommerfeld Number
T	Friction Torque, lb. in.
W	Load, lbs.
β	Angular Extent of Pad, degrees
ϵ	Eccentricity Ratio
θ_p	Angle between leading edge of pad & pivot point, degrees
Λ	Compressibility Number
μ	Absolute Viscosity, lbs. sec/in^2
ω	Angular Velocity, radians/sec.

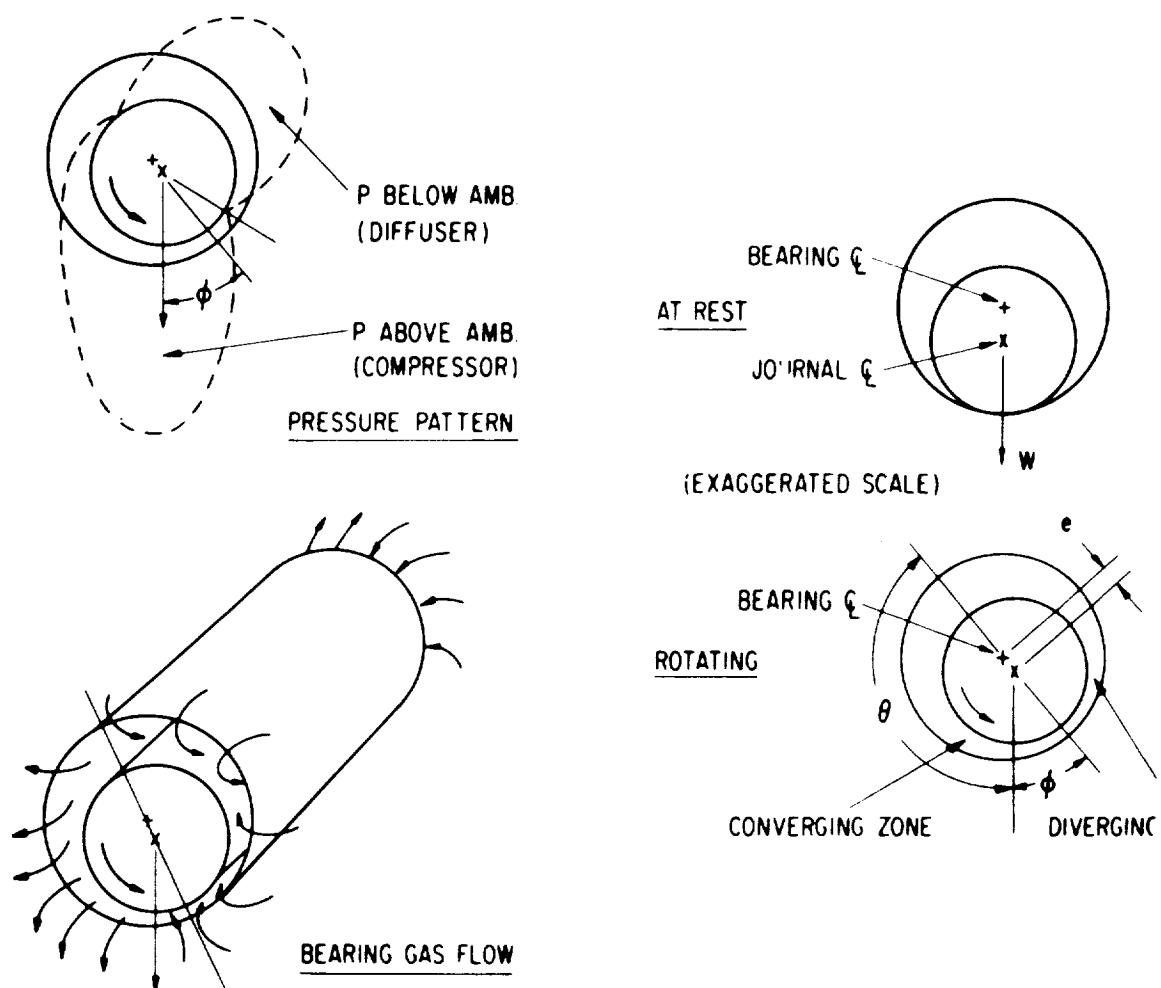


Fig. E-7 Self-Acting Gas Bearings

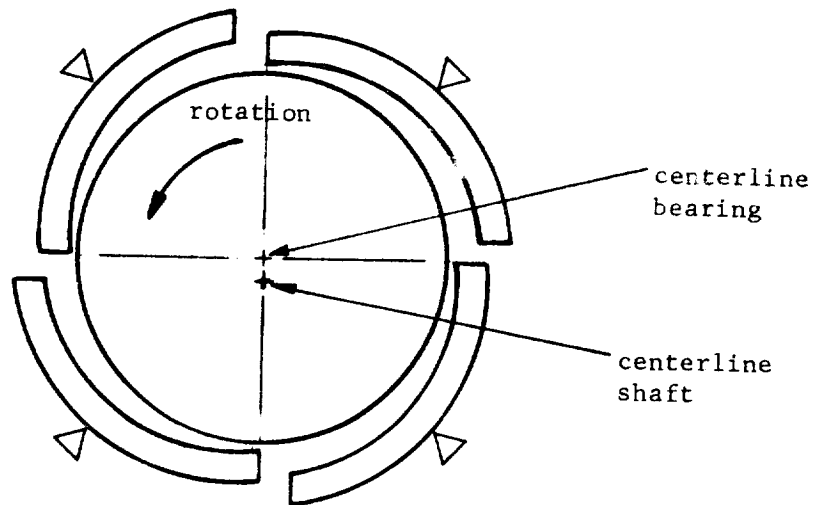


Fig. E-8 Schematic of Tilting Pad Bearing.

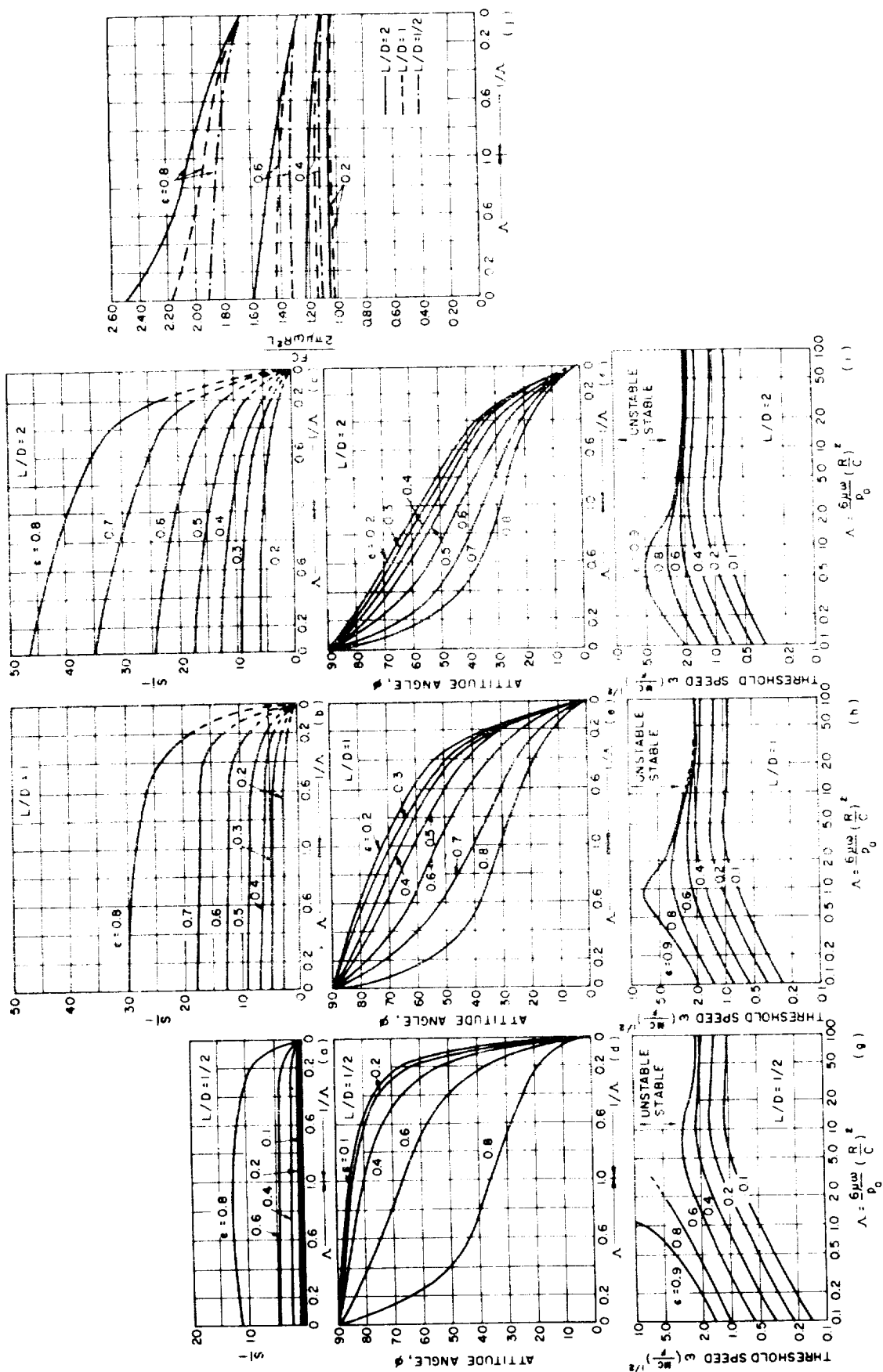
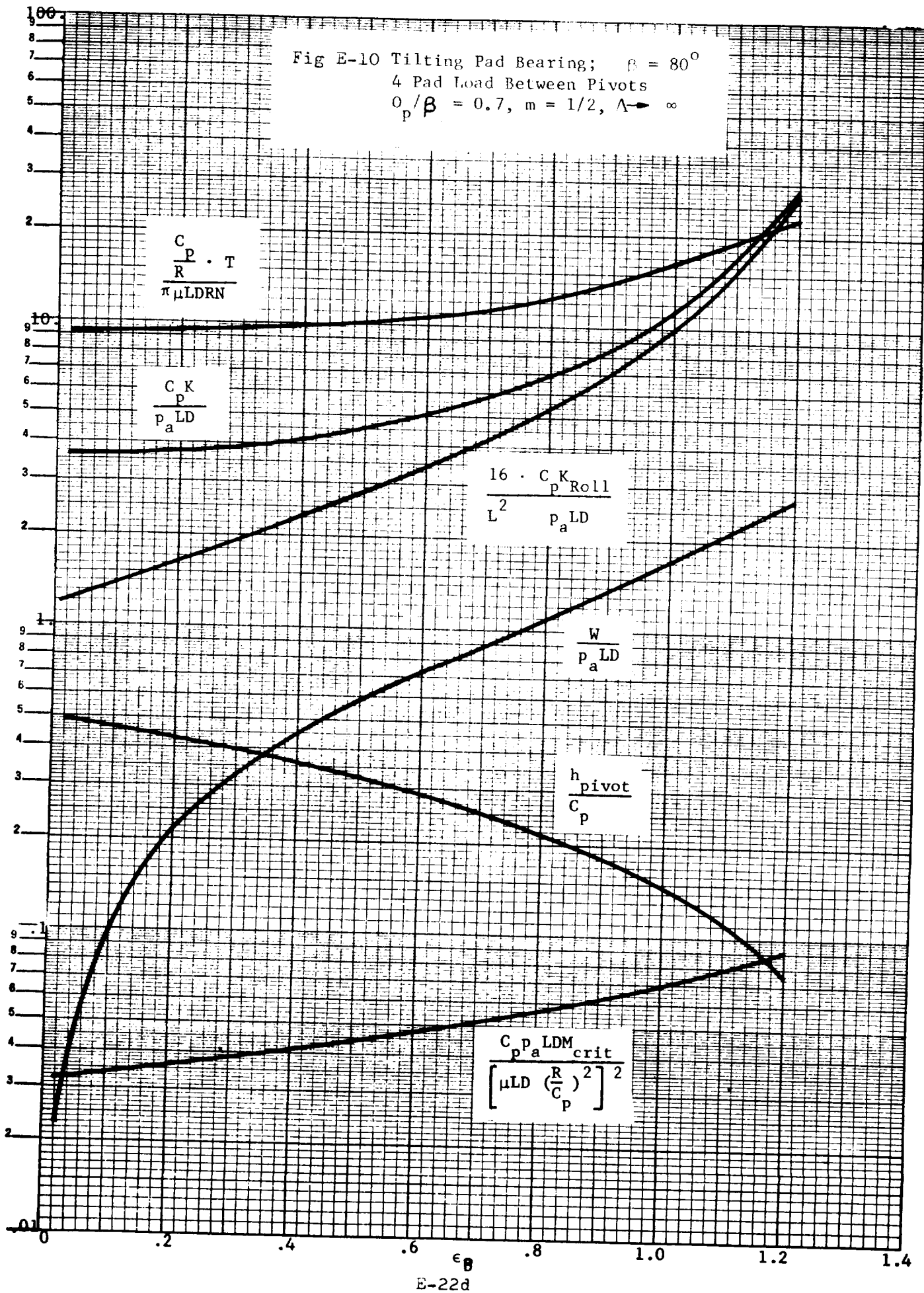


Fig. E-9 Charts for Calculating Load, Attitude Angle, Friction and Threshold of Stability for Self-Acting, Plain Cylindrical Journal Bearings

Fig E-10 Tilting Pad Bearing; $\beta = 80^\circ$
 4 Pad Load Between Pivots
 $O_p/\beta = 0.7, m = 1/2, \Lambda \rightarrow \infty$



D. SELF-ACTING THRUST BEARINGS

1. Introduction

Self-acting fluid film bearings carry load because pressure is built up in the fluid film when the moving surface drags the fluid film through the varying gap between the rotating and stationary surfaces. A variable gap viewed in the direction of the velocity of the moving surface is a necessary feature of all self-acting bearings. For self-acting thrust bearings, the required gap variation is formed by engraved pattern on the face of either the runner (rotor) or the thrust collar (stator).

Various types of self-acting thrust bearings are named according to the geometry of the engraved pattern. The most popular ones are illustrated in Figure E-11. Shearing action of the bearing surfaces acts on the engraved pattern to cause the pressure in the bearing gap to rise above the ambient. This pressure rise leads to the load carrying capability of the bearing. Typical pressure rise distributions in bearing gaps are illustrated in Figure E-12.

Closed form analytical solutions for various types of self-acting thrust bearings do not exist. If one were willing to neglect the end leakage effects as well as the curvature of the annulus, then the solutions due to Harrison, Archibold, and Kochi (Ref. 1) of tapers and steps could be used to estimate the performance of a number of the above mentioned thrust bearings. Unfortunately, the assumptions involved often lead to over-optimistic designs, and since the labor required to apply these results would still be quite formidable, these data have very limited practical value to designers.

Ausman, after imposing a number of fairly reasonable assumptions, was able to obtain solutions for the step, annular, thrust bearing. The data has been compiled into a conveniently usable form and a step-by-step example is provided to help the designer to select an optimum configuration for his application. This information is given in Ref. 2.

The spiral-grooved thrust bearing is theoretically the best among self-acting thrust bearings (its load capacity is about twice that of the step thrust bearing). Its practical application has been limited by lack of analytical data, difficulty in fabrication, and sensitivity to tolerances and distortions. Most of these difficulties have been removed in recent years. In the present section, an up-to-date assessment of this type of bearing, from the designer's point of view will be reviewed.

2. General Descriptions of Spiral-Grooved Thrust Bearings

The principal element in a spiral-grooved thrust bearing consists of a series of uniformly-spaced shallow grooves on one of the opposing bearing surfaces. The depth of each groove is up to three times the bearing clearance. The sides of the grooves are spiral lines.

An explanation of the physical role played by the shallow grooves will now be given with reference to Figure E-13. Because hydraulic resistance along the grooves is smaller than that across the grooves, a relative sliding motion between the surfaces, in a direction inclined to the grooves, tends to induce flow along the grooves. This flow, again because of the inclination of the grooves, has a component normal to the sliding direction. In this manner, the shallow inclined grooves function as a viscous pump. Capillary blockage of the induced flow causes pressure in the gap to rise above ambient and thereby enables the bearing to carry load. Pressure gradient in the gap of this type of bearing is primarily in the direction normal to that of sliding.

Also shown in Figure E-13 are definitions of the geometrical parameters of the grooving. They are the angle of inclination β , groove and ridge widths, and gaps at the groove and ridge regions. It is customary to use ratios to describe the widths and gaps; i.e.,

$$\text{Width Ratio} = a_g/a_r ;$$

$$\text{Gap Ratio} = h_g/h_r ;$$

These three parameters are assumed to be invariant with respect to the radial position in all known theoretical treatments of the subject. Thus, the depth of the grooves is constant and the sides of the grooves are logarithmic spirals.

Three major variations of annular, spiral-grooved, thrust bearings are shown in Figure E-14. In the "pump-in" design, the viscous pump is communicated to the ambient at the outer radius, while the capillary is communicated to the ambient at the inner radius. In this configuration, the induced flow is radially inward. In the "pump-out" design, the relative locations of the viscous pump and the capillary seal are interchanged, and the induced flow is radially outward. In the "herring-bone" design, two viscous pumps oppose each other and, theoretically, the total radial flow can be reduced to zero. From the standpoint of steady-state bearing performance, the "pump-in" design is much superior to the other two. For example, with the ratio of outer to inner radii equal to 2.0, an optimized "pump-in" design can carry 1.5 and 1.2 times as much load as the optimized versions of the "pump-out" and "herring-bone" designs respectively.

To define the bearing configuration completely, it is necessary to specify the number of grooves around the periphery, n_g ; the bearing gap, C , which is the same as that at the capillary seal and at the ridge region, h_r ; and the fractional radial extent of grooving, which is $(R_1 - R_m)/(R_1 - R_2)$ for the "pump-in" design. The bearing gap is also contained in the compression number

$$\Lambda_c = \frac{6\pi\mu N(R_1^2 - R_2^2)}{p_a C^2} ; \quad (D-1)$$

where:

- μ = viscosity
- N = revolutions per second
- p_a = ambient pressure

3. Design Considerations

The most essential merits and disadvantages of the spiral-grooved, thrust bearing as compared to other types of thrust bearings are indicated as follows:

Merits Relative to

1. Tilting-Pads
 - a. Mechanical Simplicity
 - b. Larger Load Capacity -- particularly at a low ambient pressure
2. Externally Pressurized Bearing -- no pressurized gas supply is needed.

Disadvantages Relative to

1. Tilting-Pads
 - a. More Sensitive to Tolerances and Distortions
 - b. Higher Lift-Off Speed
2. Externally Pressurized Bearing -- subject to wears at starts and stops

The performance of a spiral-grooved, thrust bearing can be described in terms of its load capacity W , stiffness K , and friction torque T . These can be expressed non-dimensionally as

$$\bar{W} = \frac{W}{p_a \pi (R_1^2 - R_2^2) \Lambda_c} \quad (D-2)$$

$$\bar{K} = \frac{KC}{p_a \pi (R_1^2 - R_2^2) \Lambda_c} \quad (D-3)$$

$$\bar{T} = \frac{TC}{\pi^2 \mu N (R_1^4 - R_2^4)}$$

$$\bar{T} = \frac{6T}{p_a \pi (R_1^2 + R_2^2) C \Lambda_c} \quad (D-4)$$

Each of these performance parameters depends on the six dimensionless configuration parameters Λ_c , a_g/a_r , h_g/h_r , β , (R_1-R_2) , and n_g . The influence of n_g is relatively insignificant so long as n_g is large enough, say more than 20. More will be said about this point later. Both \bar{W} and \bar{K} decreases very slightly with increasing Λ_c . For the "pump-in" design \bar{W} and \bar{K} drop less than 2 percent and 4 percent respectively at $\Lambda_c = 100$. The other four parameters can be varied to obtain maximum \bar{W} or maximum \bar{K} .

For making preliminary estimates, the following numbers are suggested:

$$\bar{W}_{\text{first estimate}} = 0.020$$

$$\bar{K}_{\text{first estimate}} = 0.044$$

$$\bar{T}_{\text{first estimate}} = 1.0$$

Neglecting the effect of n_g for the moment, the available design information will be briefly reviewed. Whitley and Williams (Ref. 3), neglecting curvature and assuming small Λ_c , found the combinations of geometrical parameters for maximum \bar{W} and maximum \bar{K} as given below:

	<u>Max. \bar{W}</u>	<u>Max. \bar{K}</u>
β	18.8°	17.8°
a_g/a_r	1.93	1.90
h_g/h_r	4.05	3.25
$(R_1 - R_m)/(R_1 - R_2)^*$	0.73	0.723
\bar{W}	0.0219	0.0204
\bar{K}	0.0438	0.0495

Arwas and Chow (Ref. 4) and independently Wildmann (Ref. 5), still neglecting curvature, re-examined influence of Λ_c on the optimum combination of geometrical parameters on \bar{W} . Their findings are summarized in Table E-18, Wildmann also examined tolerance effects of each variable by varying it to cause 10 percent

*For "pump-in" design only.

decrease in \bar{W} while holding the other three at the optimum values. This data is listed in Table E-19. Although there are some disparities between the results of Arwas-Chow and those of Wildman, the amounts of discrepancy are well within the 10 percent tolerance band for load. It is also apparent that, at least for Λ_c up to 100, the optimum combination of parameters determined from small Λ_c analysis is quite satisfactory, and that \bar{W} is nearly independent of Λ_c .

Malanoski and Pan (Ref. 6) consider effects of both curvature and Λ_c , using the parameters for maximum load given above. They found that the "pump-in" design has larger \bar{W} and \bar{K} than the "pump-out" design. Using the parameter

$$R = \frac{\text{Outlet Radius}}{\text{Inlet Radius}}$$

which combines the effects of curvature and flow direction, their conclusion is graphically shown in Figure E-15. They also found that \bar{W} and \bar{K} are nearly independent of Λ_c for Λ_c up to about 150 for the "pump-in" design, whereas they both deteriorate considerably when Λ_c exceeds 50.

Thus far, all information discussed are subject to the assumption that there are innumerable number of grooves on the bearing face ($n_g \rightarrow \infty$). While the desired role of the grooves is to induce flow and pressure gradient in the radial direction, the pressure necessarily also fluctuate in the circumferential direction periodically from groove to groove. In fact, it is appropriate to consider that circumferential zig-zags of the pressure must be present for the bearing to be able to carry load. At the entrance edge of each groove, the ambient condition permit the pressure to have the zig-zags. Consequently, there is an "end leakage" phenomenon causing a region, which extends from the entrance edge approximately as far as a groove width in the radial direction, to be ineffective as illustrated in Figure E-16. When the number of grooves become fewer, other parameters remaining unchanged, the width of each groove becomes wider. Thus, the edge leakage effect also becomes more dominant.

From simple geometrical considerations, it can be shown that, for the "end-leakage" to be small, the number of grooves should be more than $20/(1-R_2/R_1)$. Muijderman (Ref. 7) consider both the effects of curvature and n_g for small Λ_c . He found the optimum parameters for maximum \bar{W} as well as \bar{W} itself are somewhat dependent on n_g . His results for the "pump-in" design are converted into the present nomenclature as shown in Table E-20. It is seen, that Muijderman's results are consistent with the simple rule given above. Furthermore, the dependence of various parameters on n_g is well within the 10 percent \bar{W} tolerance band.

There is another effect when the number of grooves is too few. The slopes associated with the zig-zags in the circumferential direction are relatively unchanged, while the groove width and the spacing between grooves would increase with decrease in the number of grooves. Consequently, the amount of circumferential pressure fluctuation would be correspondingly larger. If this amount of pressure fluctuation becomes significant as compared to the absolute pressure level, each segment of the zig-zags in the pressure profile would become curved. A measure of this phenomenon is $\Lambda_c / [n_g (1-R_2/R_1)]$. Malanoski and Pan examined this question by comparing their result based on the assumption $n_g \rightarrow \infty$ at $\Lambda_c = 25$ with the calculation and experiment performed by Cooper for a bearing with eighteen grooves. Cooper's calculation was a finite difference procedure which treated the circumferential pressure zig-zags in detail. The comparison of \bar{W} is as follows:

\bar{W}	Malanoski and Pan	Cooper (Ref. 8)	
		Calc.	Experiment
	0.0188	0.0204	0.0183

The comparison of pressure profiles along two radial lines is shown in Figure E-17. On the basis of these comparisons, it appears that

$$\frac{\Lambda_c}{n_g(1-R_2/R_1)} < \frac{25}{18 \times 0.58} \approx 2.4 \quad (D-5)$$

along with the purely geometrical argument

$$n_g(1-R_2/R_1) > 20 \quad (D-6)$$

would be sufficient assurance that there are enough grooves in the bearing.

It is also possible to have too many grooves. For instance, it is intuitively obvious that narrow deep grooves would not be effective in promoting viscous pumping. In order that viscous pumping be effective, each groove width must be considerably larger than the gap at the groove. This criterion can be expressed as

$$\frac{n_g h_g}{(R_1 + R_2)} < \text{some number} \approx 0.2 \quad (D-7)$$

If both faces of the thrust bearing are smooth, the friction torque would be exactly that due to shearing of the fluid in the gap and \bar{T} would be unity. With shallow spiral grooves on one of the faces, the shear stress is reduced because the gap is intermittently relieved. Also, because of the circumferential zig-zags in the pressure, the shear would be somewhat less in the ridge region and somewhat more in the groove region than those due to shear of parallel surfaces with the corresponding gaps. Consequently, \bar{T} is always less than 1.0. The values of \bar{T} based on Muijderman's calculations are given in Table E-20. It is seen that \bar{T} is insensitive to either R_2/R_1 or n_g .

Although the thrust bearing generally is not required to provide angular stiffness to support the rotor, in order to minimize the effect of non-perpendicularity, it is a good practice to mount the thrust plate on a flexure. For the flexure mount to be effective, the angular stiffness of the thrust bearing should be substantially higher than that of the flexure. Unfortunately, in the published literature, there is no genuine analysis for the angular stiffness of spiral-grooved thrust bearings. However, a reasonable first estimate can be made by

assuming that under angular misalignment, the thrust bearing reacts with a torque equivalent to having the local axial displacement distributed around its mean radius. With this approximation, the angular stiffness in units of moment/radian is numerically equal to $K(R_1+R_2)^2/8$.

4. Example

Suppose a spiral-grooved bearing design is sought with the following given data:

Thrust Load	5 lbs.
Speed	18,000 rpm
Gas	Air ($\mu = 2.7 \times 10^{-9}$ Reyn)
Ambient Pressure	14.7 psia
Minimum Inner Dia.	1 in.

Step 1 - Assume $R_1/R_2 = 0.5$, and allow 2 lbs. extra load as margin.

From Fig. E-17

$$\bar{W} = 0.0272$$

$$= \frac{7.0}{\pi \times 14.7 \times R_1^2 \times (1-0.5^2) \times \Lambda_c}$$

$$= \frac{0.202}{R_1^2 \Lambda_c}$$

$$\therefore R_1^2 \Lambda_c = 0.202/0.0272 = 7.43$$

By definition,

$$\begin{aligned} \Lambda_c &= \frac{6\pi\mu N(R_1^2 - R_2^2)}{P_a C^2} \\ &= \frac{6 \times \pi \times 2.7 \times 10^{-9} \times 300 \times R_1^2 \times 0.75}{14.7 \times C^2} \end{aligned}$$

$$= 0.78 \times 10^{-6} (R_1/C)^2$$

$$R_1^2 \Lambda_c = 0.78 \times 10^{-6} (R_1^2/C)^2 = 7.43$$

$$R_1^2/C = 9.53 \times 10^{-6} = 3.08 \times 10^3$$

It is a standard practice in fluid film bearings to operate with a bearing gap about equal to 1/1000 of the outer radius. Considering a range in the neighborhood of this value we can have the following combinations.

$R_1/C \times 10^{-3}$	1.00	1.25	1.50	1.75	2.00
R_1 (in)	3.08	2.46	2.05	1.76	1.54
C (mil)	3.08	1.97	1.37	1.01	0.77

The choice depends mostly on the available room and whatever effects the bearing size might have on the rotor dynamics. For the moment, assume our choice should be

$$R_1 = 1.500 \text{ in.}$$

Then

$$C = 0.73 \text{ mil}$$

$$\Lambda_c = 3.29$$

$$R_2 = 0.750 \text{ in.}$$

Step 2 - To determine the geometrical parameters of grooving, assume for the present $n_g = 30$. Then, from Table E-20 using $R_2/R_1 = 0.5$, we find

$$\beta = 14.2^\circ$$

$$a_g/a_r = 1.43$$

$$h_g/h_r = 4.44$$

$$(R_1 - R_m)/(R_1 - R_2) = 0.720$$

$$\bar{W} = .0251$$

Thus

$$h_g = 4.44 \times 0.73 \text{ mil}$$

$$= 3.21 \text{ mil}$$

$$R_m = R_1 - 0.72 \times (R_1 - R_2)$$

$$= 1.5 \times (1.0 - 0.72 \times 0.5)$$

$$= 0.960 \text{ in.}$$

Step 3 - The number of grooves will be chosen to meet the criteria discussed above. There are three in-equalities; they are Eqs. (D-5, D-6, D-7)

$$\left[\frac{\Lambda_c}{n_g (1 - R_2/R_1)} \right] < 2.4$$

$$n_g (1 - R_2/R_1) > 20$$

$$n_g h_g (R_1 + R_2) < 0.2$$

Using previously found numbers,

$$n_g > \frac{3.29}{0.5 \times 2.4} = 2.74$$

$$n_g > \frac{20}{0.5} = 40$$

$$n_g < \frac{0.2}{3.21 \times 10^{-3} \times 2.25} = 27.7$$

We see the second and third requirements are inconsistent. However, the data in Table E-20 already allows for the effect of the second inequality, therefore, we shall waive the second requirement and choose

$$n_g = 25$$

Go back to Table E-20, interpolating, we obtain the revised grooving geometry

$$\beta = 13.5^\circ$$

$$a_g/a_r = 1.40$$

$$h_g/h_r = 4.52$$

$$(R_1 - R_m)/(R_1 - R_2) = 0.72$$

$$\bar{W} = 0.0247$$

$$\bar{T} = 0.69$$

Therefore, the revised groove gap is

$$h_g \approx 4.52 \times 0.73 \text{ mil} = 3.30 \text{ mil}$$

Check the third inequality for n_g once more:

$$n_g < \frac{0.2}{3.3 \times 10^{-3} \times 2.25} = 26.9$$

This is seen to be satisfied.

The groove depth is

$$h_g - C = 2.57 \text{ mil}$$

R_m is still 0.960 in.

The ridge width at R_m is

$$\frac{2\pi \times 0.960}{25} \times \frac{1}{(1.0 + 1.4)} = 0.1005 \text{ in.}$$

Measured perpendicular to the spiral, we have

$$0.1005 \times \sin 13.5^\circ = 0.0235 \text{ in.}$$

This dimension should be kept in mind when the manufacturing method is considered.

The revised load capacity is

$$W = 7.0 \times \frac{0.0247}{0.0272} = 6.36 \text{ lb.}$$

The friction torque is, from Eq. (D-4),

$$\begin{aligned} T &= \frac{p_a \pi (R_1^2 + R_2^2) C \Lambda_c \bar{T}}{6} \\ &= \frac{14.7 \times \pi \times 15^2 \times (1 + 0.25) \times 0.73 \times 10^{-3} \times 3.29 \times 0.69}{6} \\ &= 0.036 \text{ in.-lb.} \end{aligned}$$

The required friction power is, therefore,

$$\frac{0.036}{12} \times \frac{300 \times 2\pi}{550} = .0103 \text{ hp.}$$

Step 4 - Assume the ratio between \bar{S} and \bar{W} given by Figure E-16 is not affected by end-leakage. Then, from Eqs. (D-2) and (D-3)

$$K = \frac{W}{C} \times \frac{\bar{K}}{\bar{W}}$$

$$= \frac{6.36}{0.73 \times 10^{-3}} \times \frac{0.0519}{0.0272}$$

$$= 16,600 \text{ lb./in.}$$

The angular stiffness is

$$\frac{16,600 \times 2.25^2}{8} = 10,500 \text{ in.lb./rad.}$$

The mounting flexure should have a smaller angular stiffness, say, 4,000 in.lb./rad.

5. Dynamic Considerations

Although the thrust bearing does not play an important role in the critical speed of the rotor, there are two dynamic conditions which should be considered. One of these is the excitation of a wobbling motion of the thrust plate due to non-perpendicularity of the thrust runner. For a flexure mounted thrust plate; assuming the transverse moment of inertia of the thrust plate is much smaller than that of the rotor, coupling between thrust plate and rotor motions can be neglected. The natural frequency of the wobbling motion of the thrust plate can be determined from conventional formula using the angular stiffnesses of the thrust bearing and the flexure in series (reciprocal of the sum of reciprocals).

Strictly speaking, the estimate of the angular stiffness of the thrust bearing is based on a static condition while a dynamic stiffness should be used to calculate the resonant frequency. This is a peculiarity common to all gas bearings. Malanoski and Pan considered the problem of the axial oscillation of the spiral-grooved thrust bearing. They found that at the frequency equal to rotational frequency, the dynamic stiffness is quite close to the static stiffness for Λ_c

up to about 6.0. For Λ_c exceeding 6.0, the dynamic stiffness (at rotational frequency) can be considerably less than the static stiffness. They also found that, for $\Lambda_c > 6.0$, a form of self-excited pneumatic hammer can exist. The danger of pneumatic hammer worsens as the inertia of the system increases. Although this study only concerns translational motion, it is reasonable to assume that a similar phenomenon in the angular mode can occur. Therefore, design of the spiral-grooved thrust bearing at a large Λ_c should be done with caution. In the example cited, $\Lambda_c > 6.0$ occurs when $p_a < 8.06$ psia. In the absence of analytic data, the qualitative directions for eliminating pneumatic hammer are enumerated below. They are:

reduced a_g/a_r ,

reduced h_g/h_r ,

reduced radial extent of grooves,

reduced transverse moment of inertia of the thrust plate, and
incorporation of external damping to the thrust plate mounting.

REFERENCES FOR SECTION E: Self-Acting Thrust Bearings

1. W. A. Gross, Gas Film Lubrication, John Wiley & Sons, 1962.
2. E. E. Bisson and W. J. Anderson, Advanced Bearing Technology, NASA SP-38, 1964.
3. S. Whitley and L. G. Williams, "The Gas-Lubricated Spiral-Groove Thrust Bearing", I. G. Report 28, (RD/CA), Risley, Warrington, Lancashire, 1959.
4. E. B. Arwas and C. Chow, "The Performance of Helical-Grooved Thrust Bearings with Compressible Lubricants", MTI Report 62TR39, December 1962. PROPRIETARY.
5. M. Wildmann, "Grooved Plate Gas-Lubricated Thrust Bearings, with Special Reference to the Spiral Groove Bearing", Ampex Corporation Report RR 64-1, January 1964.
6. S. B. Malanoski and C. H. T. Pan, "The Static and Dynamic Characteristics of the Spiral-Grooved Thrust Bearing", ASME Paper No. 64-Lub-9.
7. E. A. Muijderman, Spiral Groove Bearings, Doctoral Thesis, University of Delft, March 18, 1964.
8. S. Cooper, Private Communication; Rolls-Royce Limited, Old Hall, Littleover, Derby, England.

NOMENCLATURE FOR SECTION E: Self-Acting Thrust Bearings

a_g	Groove Width
a_r	Ridge Width
β	Angle of inclination to the circumference of the spiral
C	Bearing Gap, same as h_r
h_g	Gap at Groove
h_r	Gap at Ridge
K	Thrust Stiffness
\bar{K}	Dimensionless Thrust Stiffness, Eq. (D-3)
Λ_c	Compression Number, Eq. (D-1)
μ	Viscosity
N	rps of Rotor
n_g	Number of Grooves
p_a	Ambient Pressure
\mathcal{R}	R_2/R_1 for "pump-in" design, R_1/R_2 for "pump-out" design
R_1	Inner Radius
R_2	Outer Radius
R_m	Radius at Interior Ends of Grooves
T	Friction Torque
\bar{T}	Dimensionless Friction Torque, Eq. (D-4)
W	Thrust Load
\bar{W}	Dimensionless Thrust Load, Eq. (D-2)

TABLE E-18

Optimum Parameters for Max. Load Capacity

Λ_c		<u><10</u>	<u>50</u>	<u>100</u>	<u>200</u>	<u>300</u>
Arvas-Chow	β	19.6°	20.2°	21.3°	23.0°	
	a_g/a_r	1.95	2.05	2.15	2.80	
	h_g/h_r	4.15	4.30	4.30	4.10	
	$(R_1 - R_m)/(R_1 - R_2)^*$	0.725	0.68	0.66	0.63	
	\bar{W}		.0214	.0204	.0188	
Wildman	β	18.2°	18.5°	18.7°		20.0°
	a_g/a_r	1.86	1.93	2.01		2.28
	h_g/h_r	4.05	4.18	4.22		4.40
	$(R_1 - R_m)/(R_1 - R_2)^*$	0.725	0.68	0.64		0.57
	\bar{W}		.0212	.0203		.0183

*For "pump-in" design only.

TABLE E-19

Permissible Tolerance Ranges to Cause 10% Load Decrease

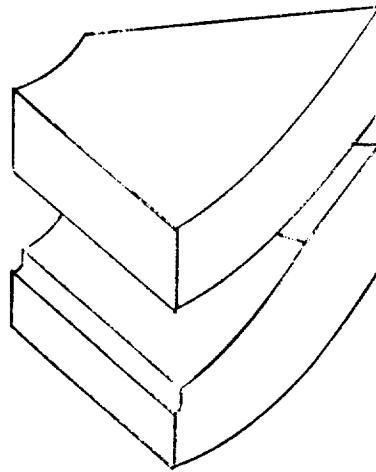
Λ_c	0		100		300	
	<u>min.</u>	<u>max.</u>	<u>min.</u>	<u>max.</u>	<u>min.</u>	<u>max.</u>
β	11.6°	27.5°	12.0°	28.0°	13.0°	28.6°
a_g/a_r	0.77	4.72	.812	5.03	0.903	5.67
h_g/h_r	3.15	5.64	3.23	5.54	3.45	5.56
$(R_1 - R_m)/(R_1 - R_2)^*$.565	.84	.474	.753	.433	.670

*For "pump-in" design only.

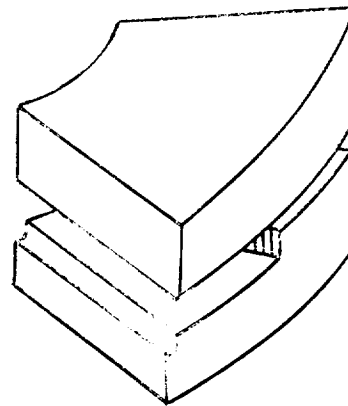
TABLE E-20

Effects of Number of Grooves on the "Pump-In" Design

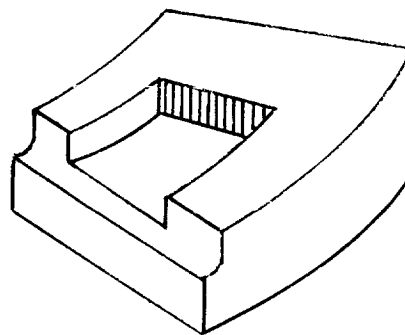
R_2/R_1	n_g	∞	50	30	15
0.4	β	17.2°	15.4°	14.4°	12.2°
	a_g/a_r	1.51	1.43	1.37	1.27
	h_g/h_r	3.94	4.22	4.33	4.70
	$(R_1-R_m)/(R_1-R_2)$.732	.732	.732	.732
	\bar{W}	.0290	.0277	.0269	.0253
	\bar{T}	0.71	--	--	0.68
0.5	β	17.5°	15.4°	14.2°	12.1°
	a_g/a_r	1.59	1.47	1.43	1.32
	h_g/h_r	4.03	4.22	4.44	5.00
	$(R_1-R_m)/(R_1-R_2)$	0.720	0.720	0.720	0.720
	\bar{W}	.0773	.0259	.0251	.0234
	\bar{T}	0.72	--	--	0.68
0.6	β	17.7°	15.1°	13.8°	11.1°
	a_g/a_r	1.67	1.52	1.45	1.33
	h_g/h_r	4.03	4.33	4.57	5.16
	$(R_1-R_m)/(R_1-R_2)$	0.725	0.725	0.725	0.725
	\bar{W}	.0259	.0243	.0235	.0217
	\bar{T}	0.73	--	--	0.68
0.7	β	18.1°	14.7°	13.1°	9.9°
	a_g/a_r	1.79	1.59	1.49	1.41
	h_g/h_r	4.03	4.44	4.70	5.55
	$(R_1-R_m)/(R_1-R_2)$	0.733	0.733	0.733	0.733
	\bar{W}	.0247	.0228	.0218	.0199
	\bar{T}	0.74	--	--	0.65



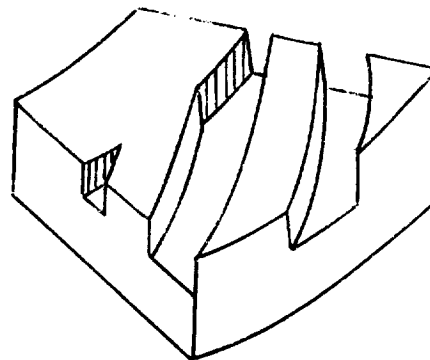
Taper-Land



Step



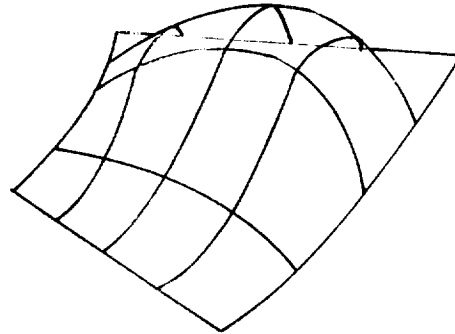
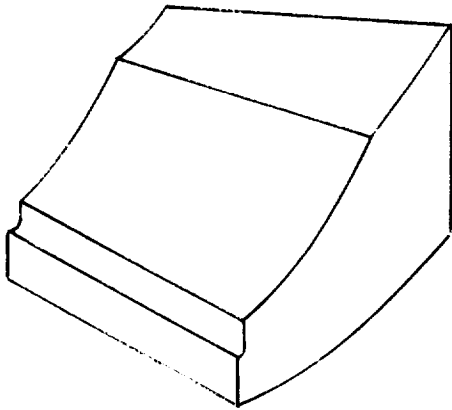
Pocket



Spiral-Groove

Fig. E-11 Examples of
Self-Acting
Thrust Bearings

Taper-Land



Pocket

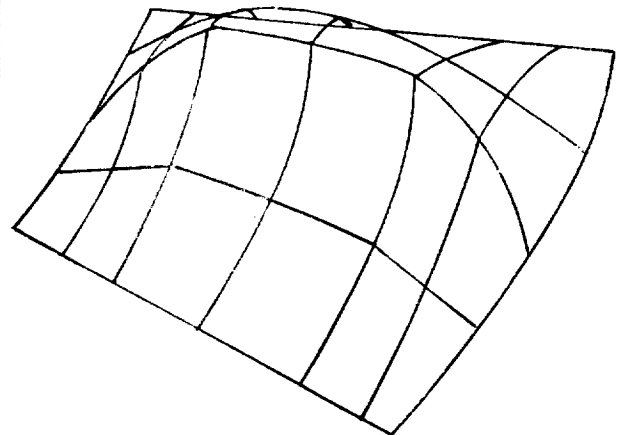
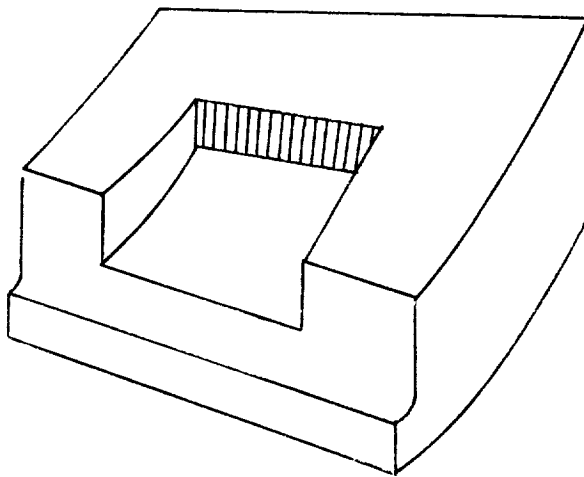


Fig. E-12 Pressure Rise in Bearing Gaps

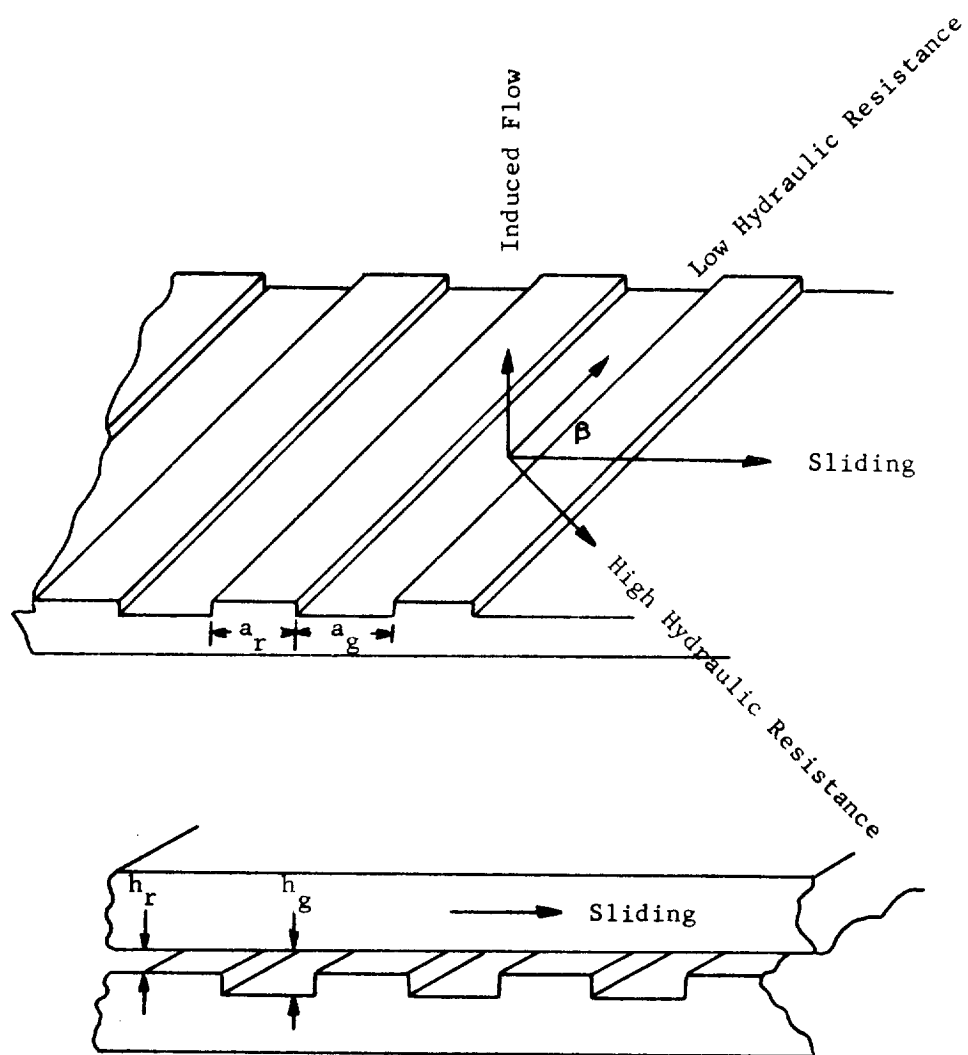


Figure E-13

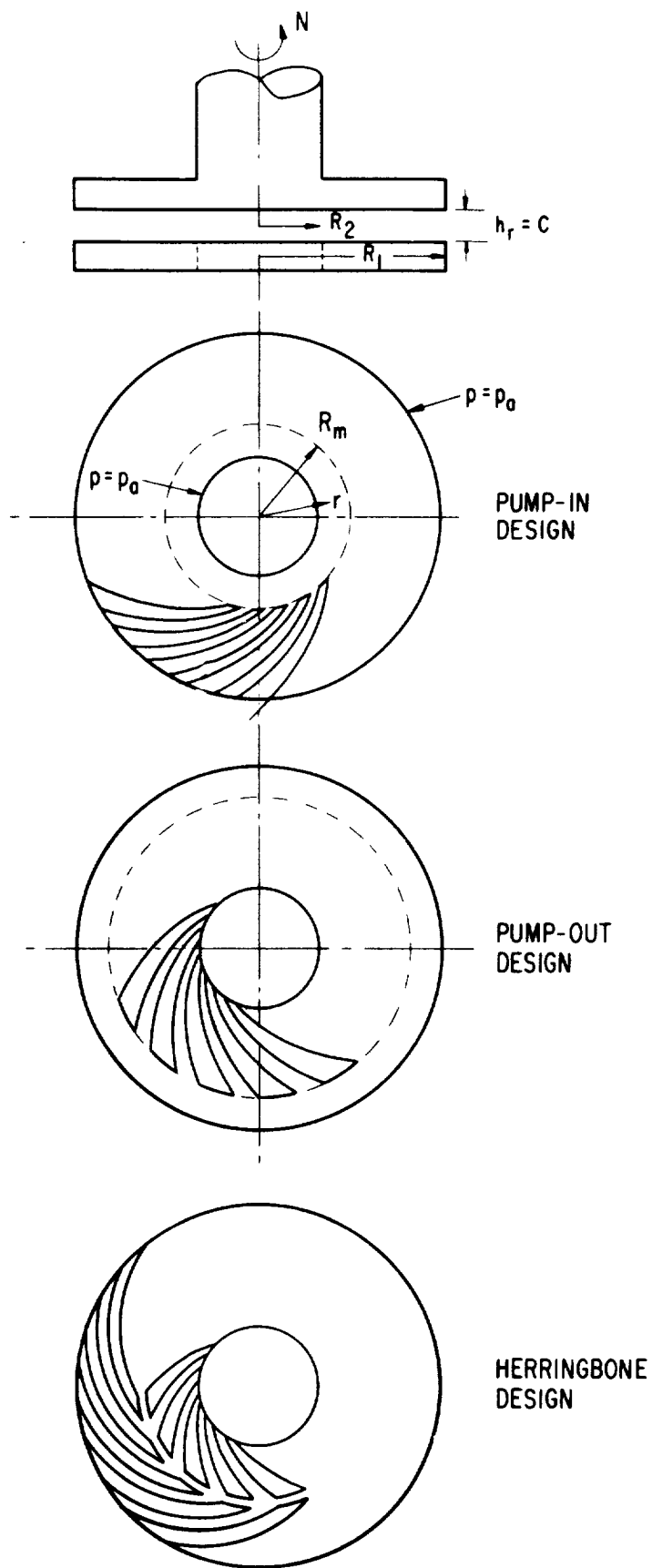


Fig. E-14 Three Common Variations of Spiral-Grooved Thrust Bearings

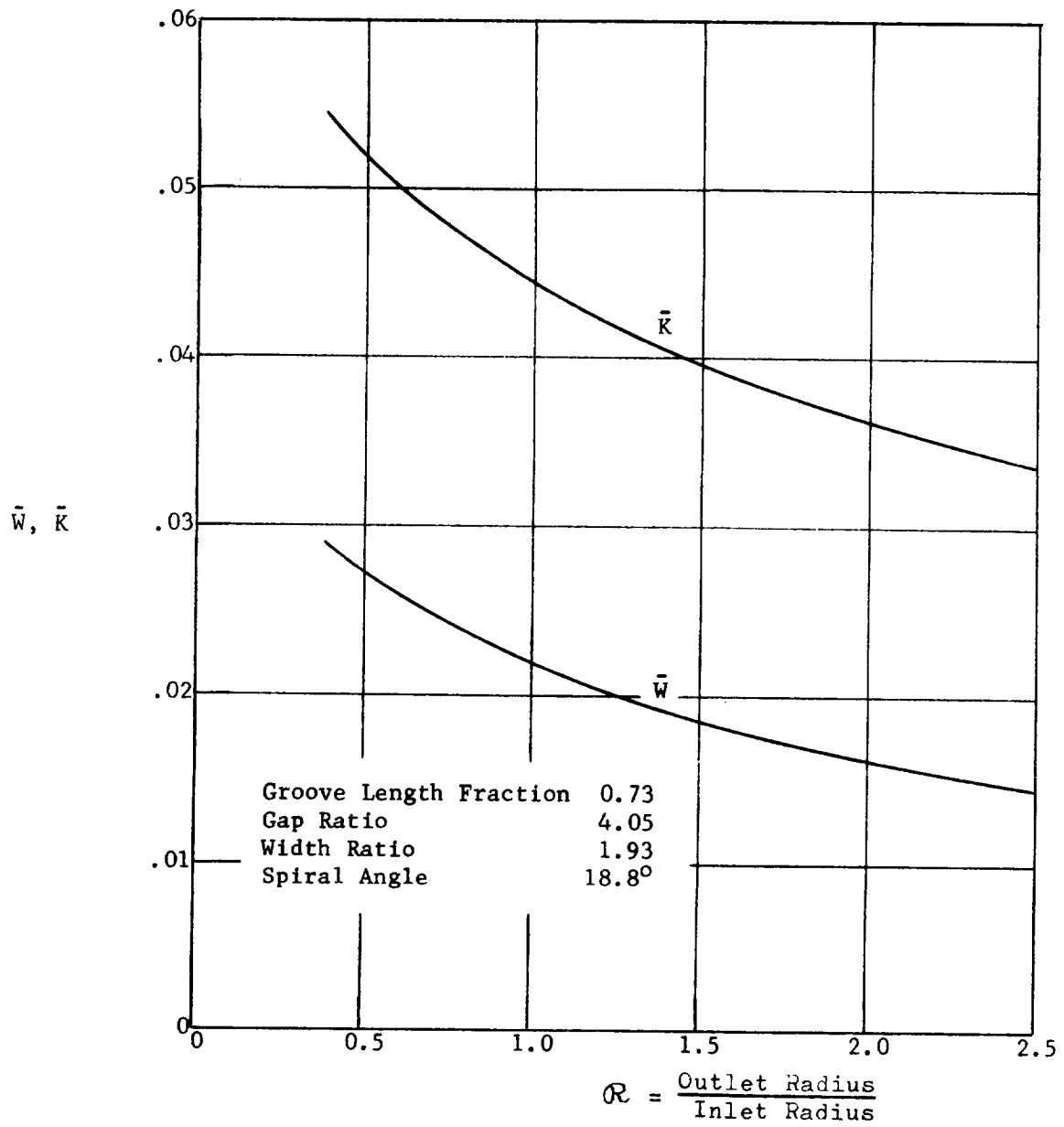


Fig. E-15 Curvature Effects on Load and Stiffness

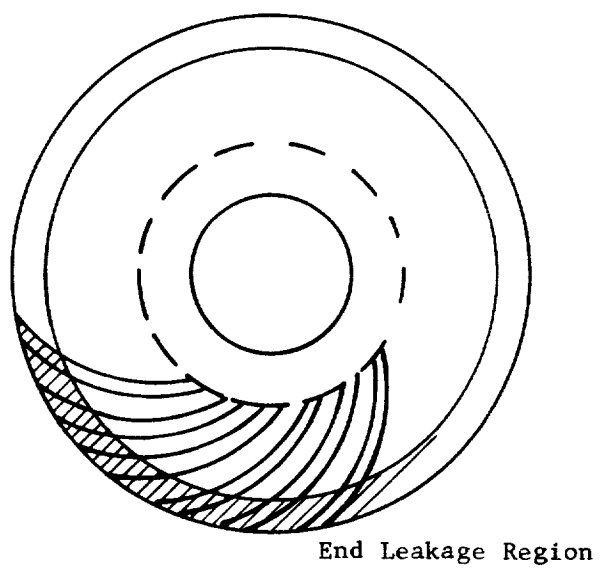


Fig. E-16 End Leakage in Spiral-Grooved Bearings

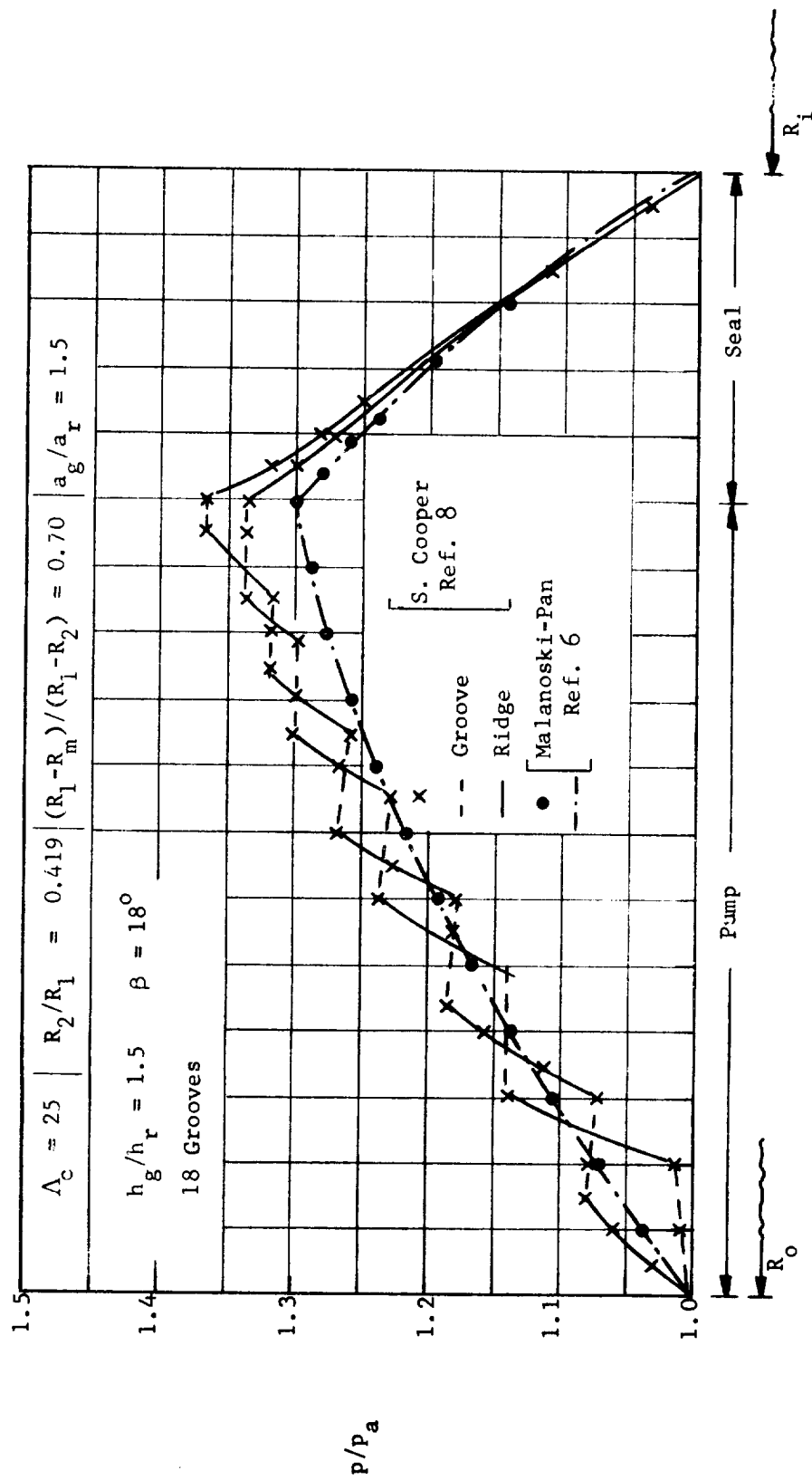
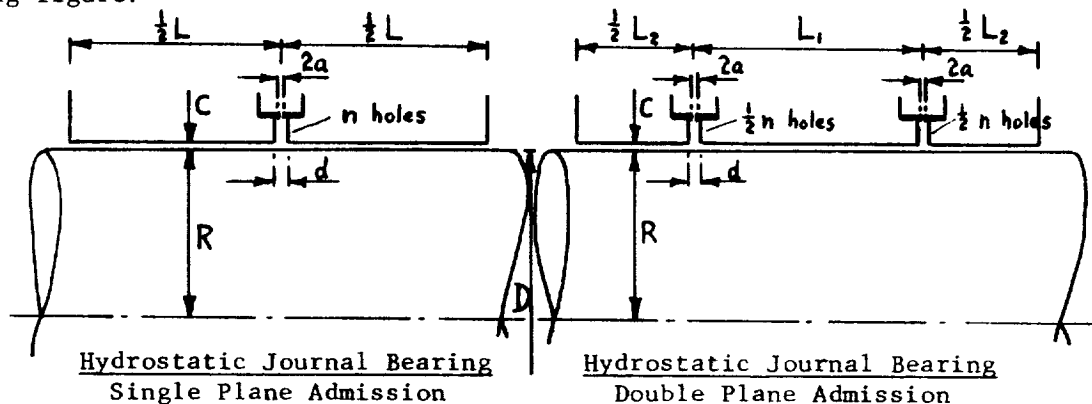


Fig. E-17 Effect of Finite Number of Grooves on Pressure Profiles

E. EXTERNALLY - PRESSURIZED JOURNAL BEARINGS

1. Introduction

In many applications where conditions make it desirable to use gas bearings, the rotor speed is too small, the required stiffness is too high, or the bearing load is too large to be carried by hydrodynamic action alone. In such cases pressurized gas may be supplied to the bearing making it the externally-pressurized (hydrostatic) gas bearing. The gas enters the bearing through feeding holes arranged in one or two planes (single plane admission, double plane admission). For the bearing to carry any load the feeding holes must restrict the flow. Schematically the bearing configuration can be shown by the following figure:



The flow restriction can either be provided by orifices (diameter = $2a$) or by the "curtain area" formed by the rim of the feeding hole and the surface of the journal (i.e., the area πdC). Accordingly, the bearing is called orifice restricted or inherently compensated. Frequently, both methods of restriction exist simultaneously. An alternate method is provided by a capillary restrictor (thin tubes, porous plugs, narrow circumferential slots) which may conveniently be classified as laminar restriction. Finally, the entire bearing wall may be made out of porous material such that the gas admission is distributed over the entire gas film and it is called the porous bearing. The present discussion is mainly devoted to the orifice restricted and inherently compensated bearing. The symbols used in this discussion are defined in the nomenclature list at the end of this section.

2. Selection of the Hydrostatic Bearing

The three major reasons for choosing the hydrostatic bearing instead of the self-acting bearing are:

1. Too large a bearing load
2. Too low a speed (e.g. low speed rotating machinery, gyro gimbal bearing)
3. The requirement of high stiffness (e.g. machine tool bearings, instrument bearings)

These considerations may be expressed approximately in terms of design parameters.

- a. Due to wear at starts and stops the properties of most bearing materials impose an upper limit on the load which can be carried by the self-acting bearing. Depending on the material used and the frequency of starts and stops the upper limit is approximately: *

$$\frac{W}{LD} \leq 4 \text{ to } 7 \text{ psi.}$$

For loads in excess of this value the hydrostatic bearing must be used, either as the actual bearing or, as an alternative, as an auxiliary bearing to be used at start-up and shut-down only.

- b. General experience indicates that in most applications the minimum gas film thickness should not be less than approximately 30 percent of the radial clearance. This means that the hydrostatic bearing should be used if:

$$\text{either: Sommerfeld No. } S = \frac{W}{\mu N D L} \left(\frac{R}{C}\right)^2 < \begin{cases} .2 & \text{for } \frac{L}{D} = .5 \\ .075 & \text{for } \frac{L}{D} = 1 \\ .05 & \text{for } \frac{L}{D} = 2 \end{cases}$$

$$\text{or: } \frac{W}{P_a LD} > 1 \text{ to } 1.5 .$$

*Note, that the numerical values depend strongly on the particular type of self-acting bearing. The above values are intended as a guide and they are in general not conservative.

- c. The obtainable stiffness with a self-acting bearing is in practice limited to:

$$\frac{CK}{P_a LD} < 1 \text{ to } 3$$

where the higher value requires a high load and very high speed. The hydrostatic bearing, on the other hand, can be designed to give a stiffness of:

$$\frac{CK}{P_a LD} = \left(\frac{P_s}{P_a} - 1 \right) 0.65$$

- d. Occasionally an additional consideration enters. When

$$\text{Rotor Speed, RPM} > \frac{650}{\sqrt{C}} \sqrt{\frac{W}{P_a LD}} \quad (C \text{ in inch, rotor horizontal})$$

or if the rotor mass is relatively large:

$$\frac{MP}{\mu L \left(\frac{R}{C} \right)^5} > 10 \text{ to } 20$$

it becomes difficult to ensure stability for a rotor supported by self-acting bearings of the fixed geometry type. If in addition other design requirements prevent the use of the self-acting, tilting pad bearing (too high a bearing load, susceptibility to pivot fretting) the hydrostatic bearing may be used. However, although superior to the plain geometry, self-acting bearing the hydrostatic bearing may also become unstable as discussed later.

3. Design for Steady-State, Operation, Non-Rotating Rotor

The governing design parameters for the hydrostatic gas journal bearing are:

- length-to-diameter ratio: $\frac{L}{D}$ (and $\frac{L_1}{D}$ for bearing with double plane admission)
- restrictor coefficient: $\Lambda_s = \frac{6\mu n a^2 \sqrt{RTg}}{P_s C^3 \sqrt{1+\delta^2}}$
- supply pressure ratio: P_s/P_a

The physical significance of the restrictor coefficient is that it gives the ratio between the flow resistance of the gas film and the resistance of the feeder hole restrictor. To illustrate, assume first that all the flow resistance takes place in the feeder hole restrictor (e.g. a very small orifice radius or a very big radial clearance) such that the entire available pressure drop is used up in the feeder hole. Hence, the pressure becomes ambient throughout the gas film and the bearing can carry no load. Conversely, assume that the gas film accounts for all flow resistance (e.g. a very small clearance or a big orifice radius). Then the pressure just downstream of all the feeder holes equals the supply pressure and there is no variation circumferentially in the gas film pressure. Again the bearing can carry no load. In summary, the load carrying capacity is zero for $\Lambda_s = 0$ and $\Lambda_s = \infty$ and it is seen that there must be an optimum value of Λ_s for which the load is a maximum. This value is determined to be:

$$\Lambda_s \frac{L}{D} = .5 \text{ to } .7 \quad \left(\text{for double plane admission use } \frac{L_1 + L_2}{D} \right)$$

The corresponding load, W , and stiffness, K , is given by (for $\frac{P_s}{P_a} > 2$):

$$\left[\frac{W}{(P_s - P_a)LD\epsilon} \right]_{\max} = \left[\frac{CK}{(P_s - P_a)LD} \right]_{\max} = \begin{cases} .65 & (\frac{L}{D} = .5, \text{ single plane admission}) \\ .51 & (\frac{L}{D} = 1, \text{ single plane admission}) \\ .29 & (\frac{L}{D} = 2, \text{ single plane admission}) \\ .66 & (\frac{L_1}{D} = .5, \frac{L_2}{D} = .5, \text{ dbl. plane admission}) \\ .42 & (\frac{L_1}{D} = 1, \frac{L_2}{D} = 1, \text{ dbl. plane admission}) \end{cases}$$

where: K = stiffness, lbs/inch

The given numerical values assume that the eccentricity ratio ϵ is small:

$$\epsilon < .4 - .5$$

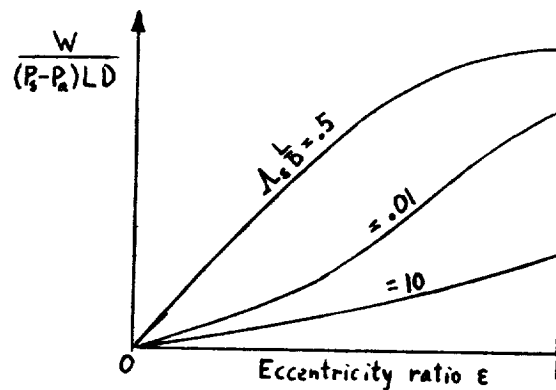
and that the load vs displacement relation is linear which is normally the case in the stated range of ϵ .

Under normal conditions the hydrostatic bearing should not be designed to operate at an eccentricity ratio in excess of .4. Hence, as a rule of thumb the maximum load carrying capacity available with a hydrostatic bearing is:

$$\left[\frac{W}{DL} \right]_{\max} = \begin{cases} .2 \cdot (P_s - P_a) & \text{(single plane admission)} \\ .25 \cdot (P_s - P_a) & \text{(double plane admission)} \end{cases}$$

which corresponds to 20 percent and 25 percent of the available pressure drop, respectively. Note that the above values apply for the orifice restricted bearing; for the inherently compensated bearing multiply by 2/3. More detailed information about the load carrying capacity is given through Figs. E-21 and E-22.

The reason for limiting the operating eccentricity ratio to $\epsilon < .4$ is a phenomenon called lock-up where the hydrostatic pressure forces the journal against the bearing wall and locks it in that position. Lock-up can be caused by an uneven flow distribution between the feeder holes due to manufacturing inaccuracies, but seems also to be connected somewhat with the inherent load characteristic of the hydrostatic bearing. Typical load curves are given below:



Since the operating value of the restrictor coefficient is approximately $\Lambda_s \cong .5$ to 1 it is found that the stiffness (i.e. the slope of the load curve) decreases rapidly for $\epsilon > .5$ thereby enhancing the susceptibility to lock-up. The best remedy against lock-up seems to be as large a number of feeder holes as practical.

The second consideration in designing a hydrostatic bearing is the flow requirements. The flow is most conveniently given in form of a dimensionless parameter:

$$\frac{6\mu Q T}{\pi P_s^2 C^3} \frac{L}{D} \cdot Q$$

where Q is the flow in lbs/sec. Typical curves are given in Figs. E-3 and E-4. From a design point of view it is important to note that, everything being equal, the flow increases with the cube of the clearance. Since stiffness is inversely proportional to the clearance, and since most applications call for a high stiffness with a minimum of flow, the most critical design consideration is to keep the clearance small.

With regard to Figs. E-23 and E-24 it may be remarked that the feeder hole restrictors are choked for small Λ_s -values, becoming unchoked at $\Lambda_s \cdot \frac{L}{D} = .2$ to $.25 \left(\frac{P_s}{P_a} > 3 \right)$. At a first glance Figs. E-23 and E-24 seem to show just the opposite.

The power required to pump the gas through the bearing is given by:

$$[\text{pumping power}]_{\text{gas through bearing}} = \frac{QQT}{6600} \cdot \log_e \left(\frac{P_s}{P_a} \right) \text{ HP}$$

Knowing the efficiency of the compressor allows computing the total pumping power.

If the rotor span is sufficiently long or if thermal expansion is present, an accurate rotor alignment becomes difficult to achieve. Therefore, the bearing is frequently mounted such that it is capable of self-alignment (e.g. flexible diaphragm supports). Then, in order to determine the support stiffness the bearing stiffness for an angular displacement must be considered. Although more accurate information is available, a rough estimate can be obtained by:

$$\text{Angular stiffness, } \frac{\text{lbs.in.}}{\text{radians}} = \frac{L^2}{16} \cdot K$$

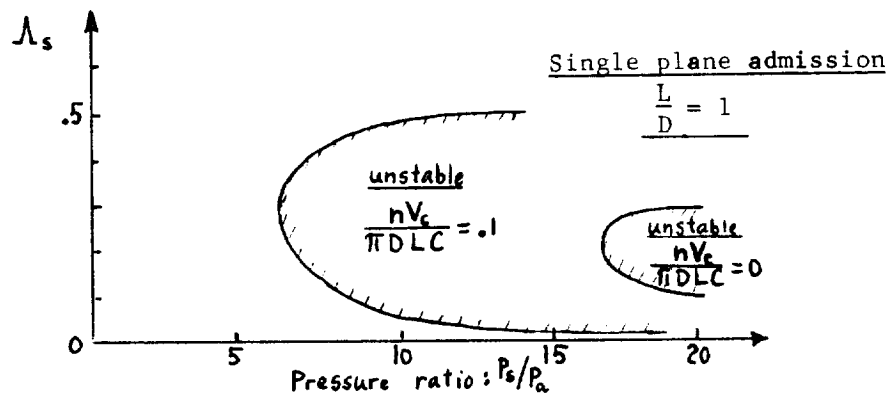
where $K, \frac{\text{lbs}}{\text{in.}}$ is the previously discussed bearing stiffness. This estimate is conservative.

The most serious problem encountered in designing a hydrostatic bearing is a self-excited pneumatic instability called pneumatic hammer. The instability

derives its energy from the pressurized gas and is controlled by the flow-vs-pressure time lag associated with the feeder hole restrictors and the gas film. In addition to the previously mentioned design parameters, the description of pneumatic hammer requires one more parameter:

$$\text{feeder hole volume parameter: } \frac{nV_c}{\pi DLC}$$

where V_c is the gas volume between the orifice and the entrance to the gas film. Thus the parameter gives the ratio between the total volume of all feeder holes and the total volume of the gas film. This ratio should be kept as small as possible, not exceeding .05 to .1, but even so pneumatic hammer may still be encountered. The region of instability may be illustrated by a graph:



Thus, for a single plane admission bearing with $\frac{L}{D} = 1$ and a feeder hole volume parameter of .1 pneumatic hammer sets in for pressure ratios exceeding 6 with a restrictor coefficient of less than .5. Increasing the $\frac{L}{D}$ -ratio or going to the double plane admission bearing greatly improves the stability. However, as a general rule pneumatic hammer occurs at high pressure ratios and for $\Lambda_s \frac{L}{D} \lesssim .5$ to .8 when using the orifice restricted bearing.

Because of the danger of encountering pneumatic hammer a hydrostatic bearing should never be provided with recesses, pockets or any excess volumes. As a further precaution experience indicates that the best method to avoid pneumatic hammer is to make the bearing completely inherently compensated, i.e., to have no orifices at all and instead dimension the feeder holes such that the flow restriction occurs at the entrance to the bearing film. This should always be done if the 33 percent loss in stiffness and load carrying capacity can be tolerated.

When the supply pressure ratio exceeds:

$$\frac{P_s}{P_a} > 6 \text{ to } 8$$

turbulent effects and shock in the gas film frequently become important and may affect the load carrying capacity adversely. Thus, if a high supply pressure is needed to meet a required load special precautions must be taken. The most important consideration is to keep the clearance small whereby the gas velocity is minimized. Thus, the following relationship should be satisfied if possible:

$$\frac{Q}{2\pi P_a DC} \sqrt{\frac{RT}{kg}} < .5 \text{ to } 1$$

where k is the ratio of specific heats (i.e., $k = 1.4$ for air). In addition, the edges of the feeding holes should be chamfered or rounded to smooth the air passage into the bearing.

4. Design for Dynamical Operation, Rotating Rotor

When the externally-pressurized bearing supports a rotating shaft the gas film is subjected to both hydrodynamic and hydrostatic action and the term the hybrid bearing is used to classify this type of bearing. The hydrodynamic action changes the performance of the hydrostatic bearing in several respects, of which the most significant are:

- a. The load carrying capacity and the stiffness increases for the same eccentricity ratio.
- b. The hybrid bearing is susceptible to fractional frequency whirl instability.

To describe the performance of the hybrid bearing one more design parameter is needed in addition to the previously listed hydrostatic bearing parameters. The new parameter is:

$$\text{compressibility no: } \Lambda = \frac{6\mu\omega}{P_a} \left(\frac{R}{C}\right)^2 .$$

In most applications, the increase in load carrying capacity due to hydrodynamic effects can be disregarded as being small. A typical example is given by Fig. E-25 where the dimensionless load is given as a function of Λ for a pressure ratio of 5,

an eccentricity ratio $\epsilon = .1$ and several values of the restrictor coefficient Λ_s . Since most hybrid bearings operate in the range $.2 < \Lambda_s \frac{L}{D} < 2$ it may be used as a rough estimate that the hydrodynamic effect can be neglected when $\Lambda < P_s/P_a$. Hence, as a general rule the load carrying capacity and the stiffness for a hybrid bearing is taken from the hydrostatic bearing data, which at least is conservative. The stiffness thus obtained can be used directly to calculate the critical speed of the rotor.

To calculate the amplitude response of the rotor to either unbalance forces or any external excitation it is necessary to know the damping of the bearing in addition to the already computed stiffness. It is very difficult to give even the order of magnitude of the damping without going into great detail since it depends strongly on the compressibility number, the frequency of the vibrations and actually becomes negative at the onset of pneumatic hammer. However, to give at least an indication of the numerical value of the damping assume the compressibility number to be small ($\Lambda \lesssim 2$) and assume that the bearing operates well outside the range of pneumatic hammer. Then, in very rough approximation:

$$\frac{B}{\mu L \left(\frac{R}{C}\right)^3} \sim \begin{cases} .8 & (\frac{L}{D} = .5) \\ 3 & (\frac{L}{D} = 1) \\ 10 & (\frac{L}{D} = 2) \end{cases}$$

where B, lbs.sec/in, is the damping coefficient. Note, that the damping becomes zero as Λ approaches infinity. On the other hand, in many applications the damping is sufficiently large to make the rotor-bearing system critically damped thereby effectively eliminating the critical speed.

The rotation of the shaft may induce instability (fractional frequency whirl) of the hybrid bearing. Within the conventional range of operation the instability sets in at twice the critical speed based on the purely hydrostatic bearing. With a few exceptions, this is a very realistic estimate.

The power loss of the hybrid bearing is closely given by:

$$\text{Power loss} = \frac{\pi^3 \mu L D^3 N^2}{6600 \cdot C \sqrt{1-\epsilon^2}} \quad \text{HP}.$$

NOMENCLATURE LIST FOR SECTION E: Externally-Pressurized Journal Bearings

a	- Orifice radius, inch
B	- Damping coefficient, lbs.sec/in
C	- Radial clearance, inch
D	- Bearing radius, inch
d	- Feeder hole diameter, inch
g	= 386.07 in/sec^2 , gravitational acceleration
K	- Stiffness, lbs/in
k	- Ratio of specific heats ($k = 1.4$ for air)
L	- Bearing length, inch
L_1	- Distance between gas admission planes, inch
L_2	= $L - L_1$, Combined bearing length outside admission planes, inch
L/D	- Length-to-diameter ratio (for double admission planes, use L_2/D)
M	- Rotor mass per bearing (\sim half total rotor mass), lbs.sec ² /in
N	- Rotor speed, rps
n	- Total number of feeding holes
P_a	- Ambient pressure, psia
P_s	- Supply pressure, psia
Q	- Gas flow, lbs/sec
R	= $\frac{1}{2} D$, Bearing radius, inch
$\mathcal{R} T$	- (Gas constant) \cdot (Total temperature, $^{\circ}\text{R}$), inch (for air at 70°F : $\mathcal{R} T = 342,500 \text{ in}^2/\text{lb}$)
S	= $\mu \text{NDL} (\frac{R}{C})^2 / W$, Sommerfeld number
W	- Load capacity, lbs.
δ	= a^2/dC , Inherent compensation factor
ϵ	- Eccentricity ratio

- Λ = $6\mu\omega (\frac{R}{C})^2 / P_a$, Compressibility number
 Λ_s = $6\mu na^2 \sqrt{RTg} / P_s C^3 \sqrt{1+\delta^2}$, Restrictor coefficient
 μ - Gas viscosity, lbs.sec/in²
 ω = $2\pi N$, Angular velocity, radians/sec.

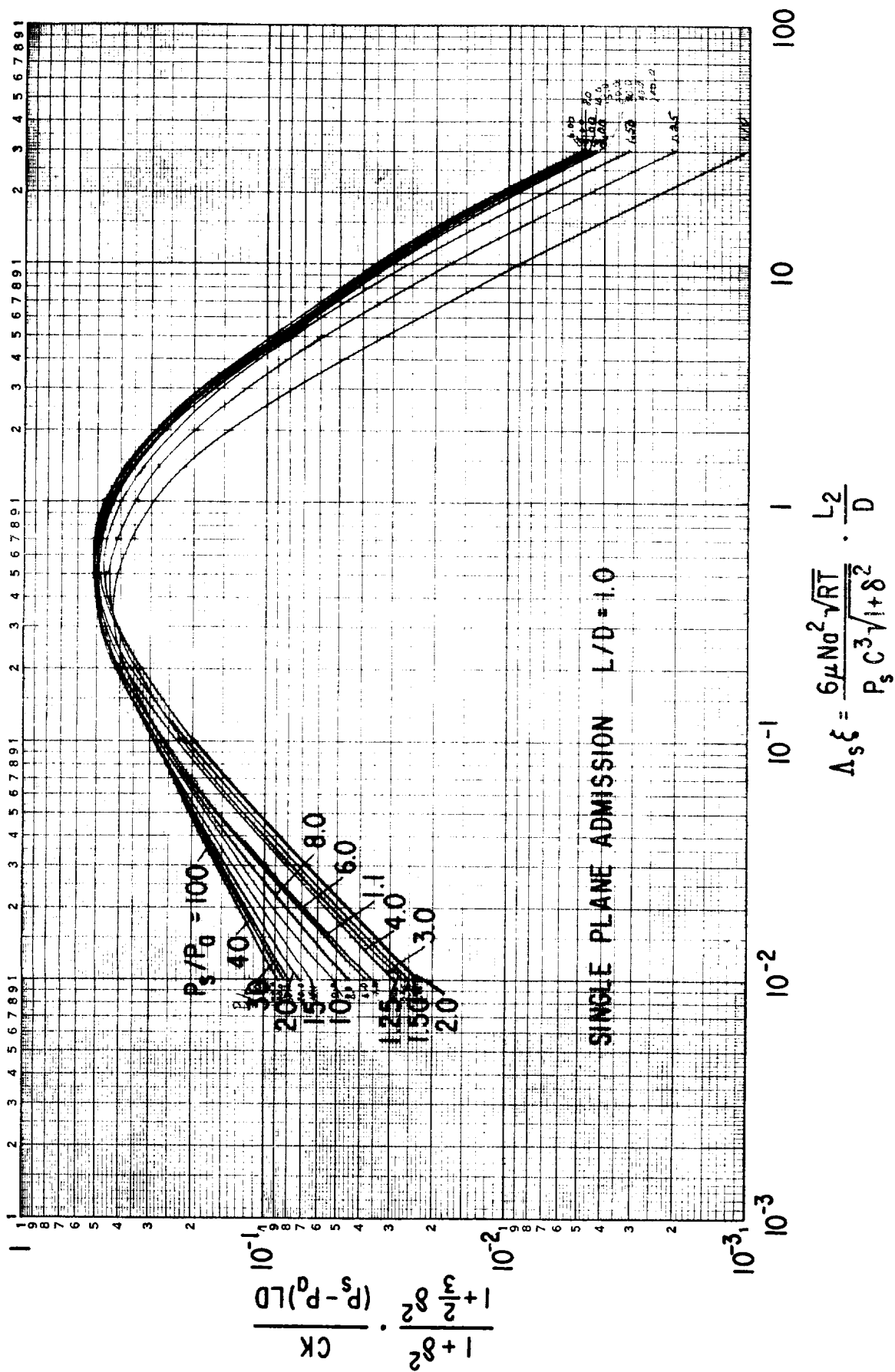


Fig. E-21 Hydrostatic Journal Bearing Stiffness vs Restrictor Coefficient

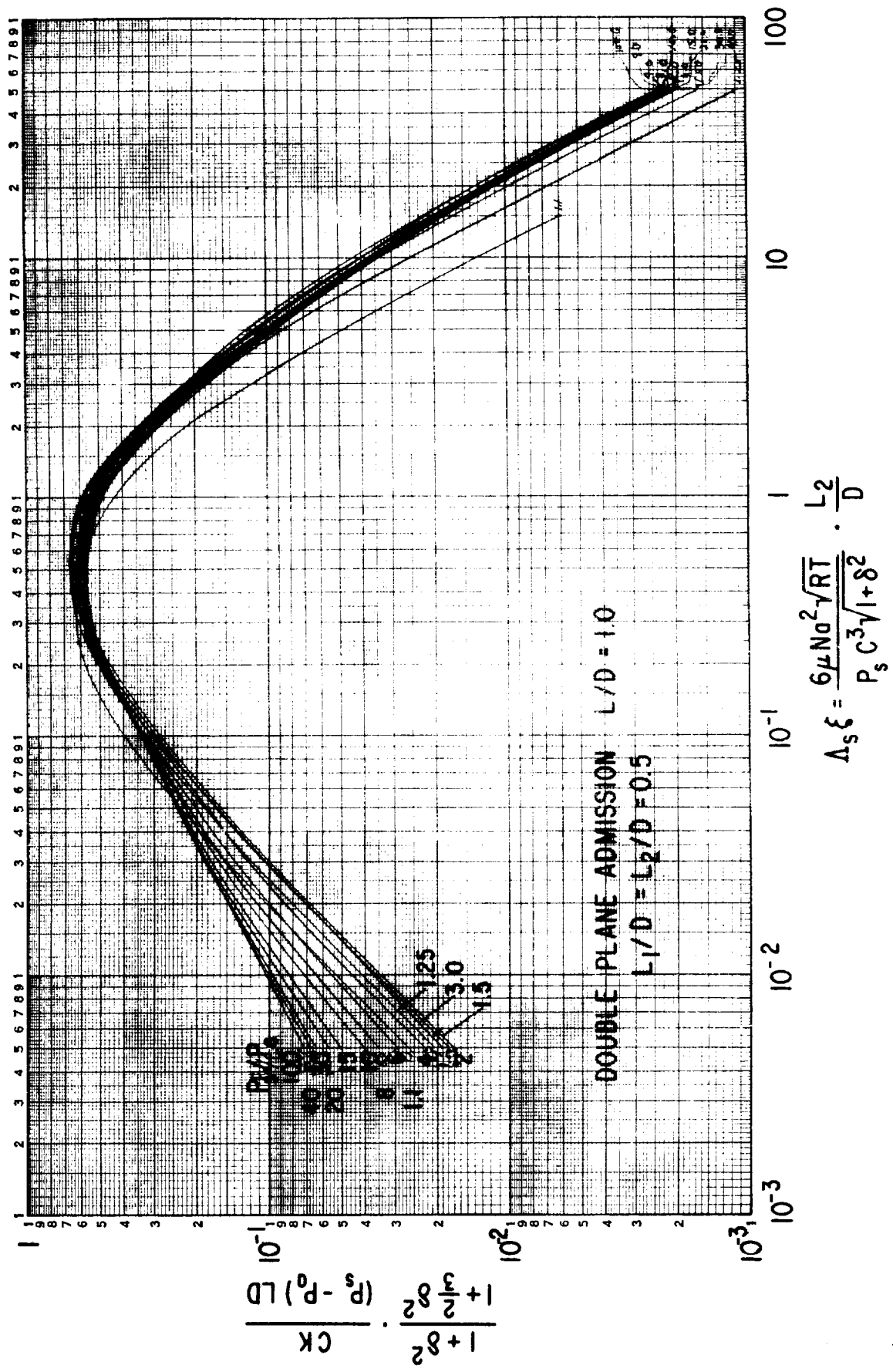


Fig. E-22 Hydrostatic Journal Bearing Stiffness vs Restrictor Coefficient

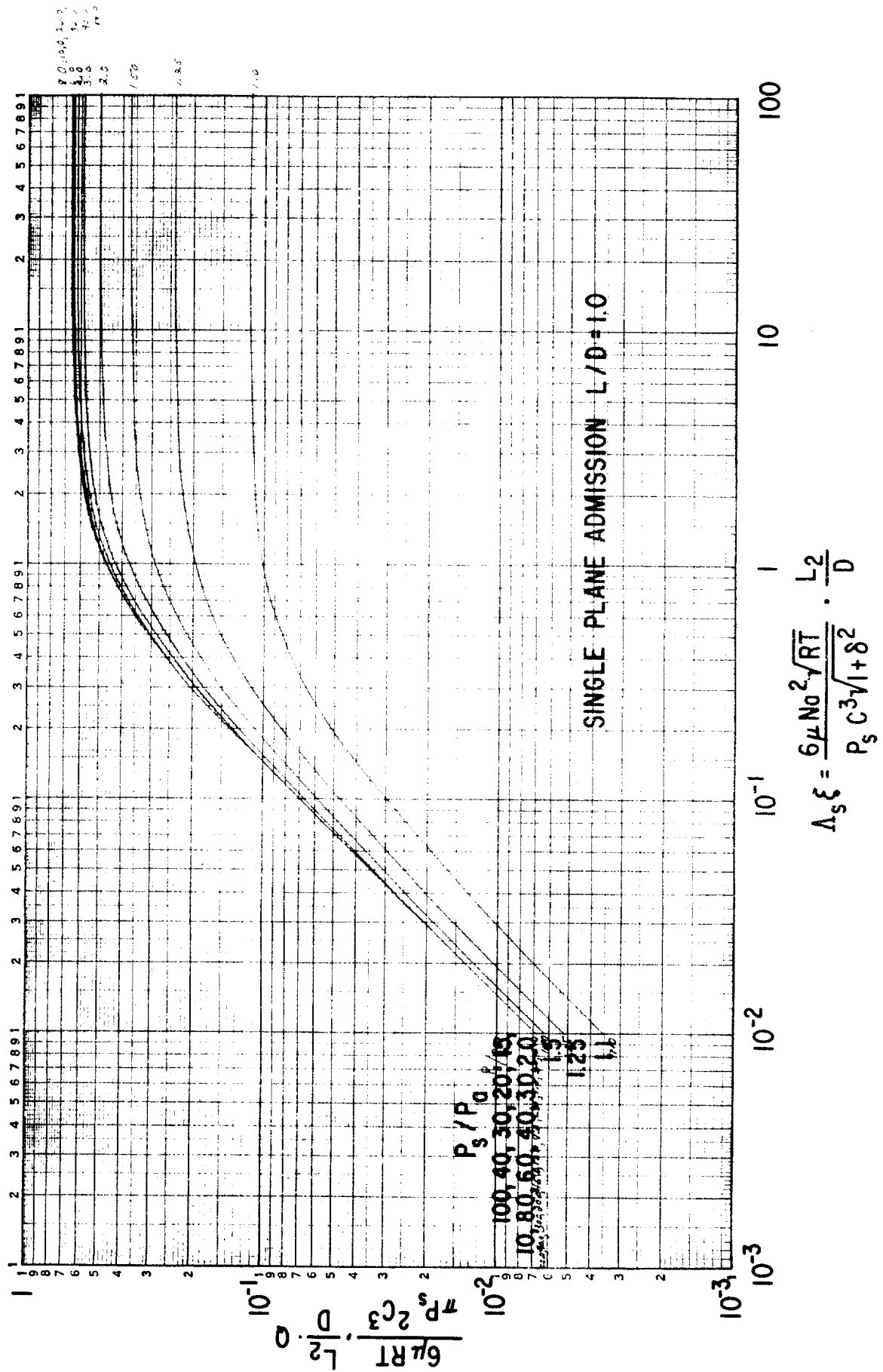


Fig. E-23 Hydrostatic Journal Bearing Flow vs Restrictor Coefficient

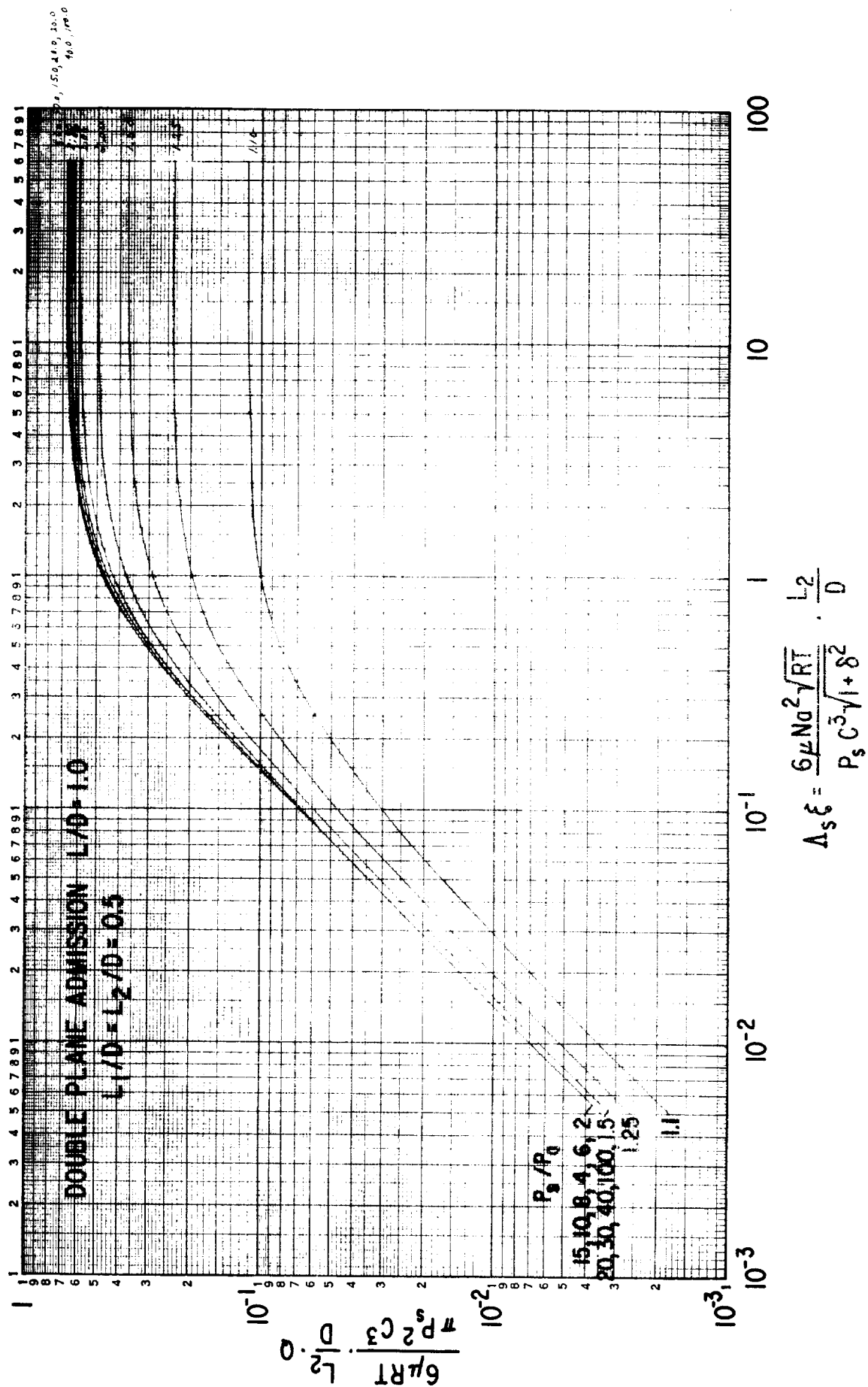


Fig. E-24 Hydrostatic Journal Bearing Film vs Restrictor Coefficient

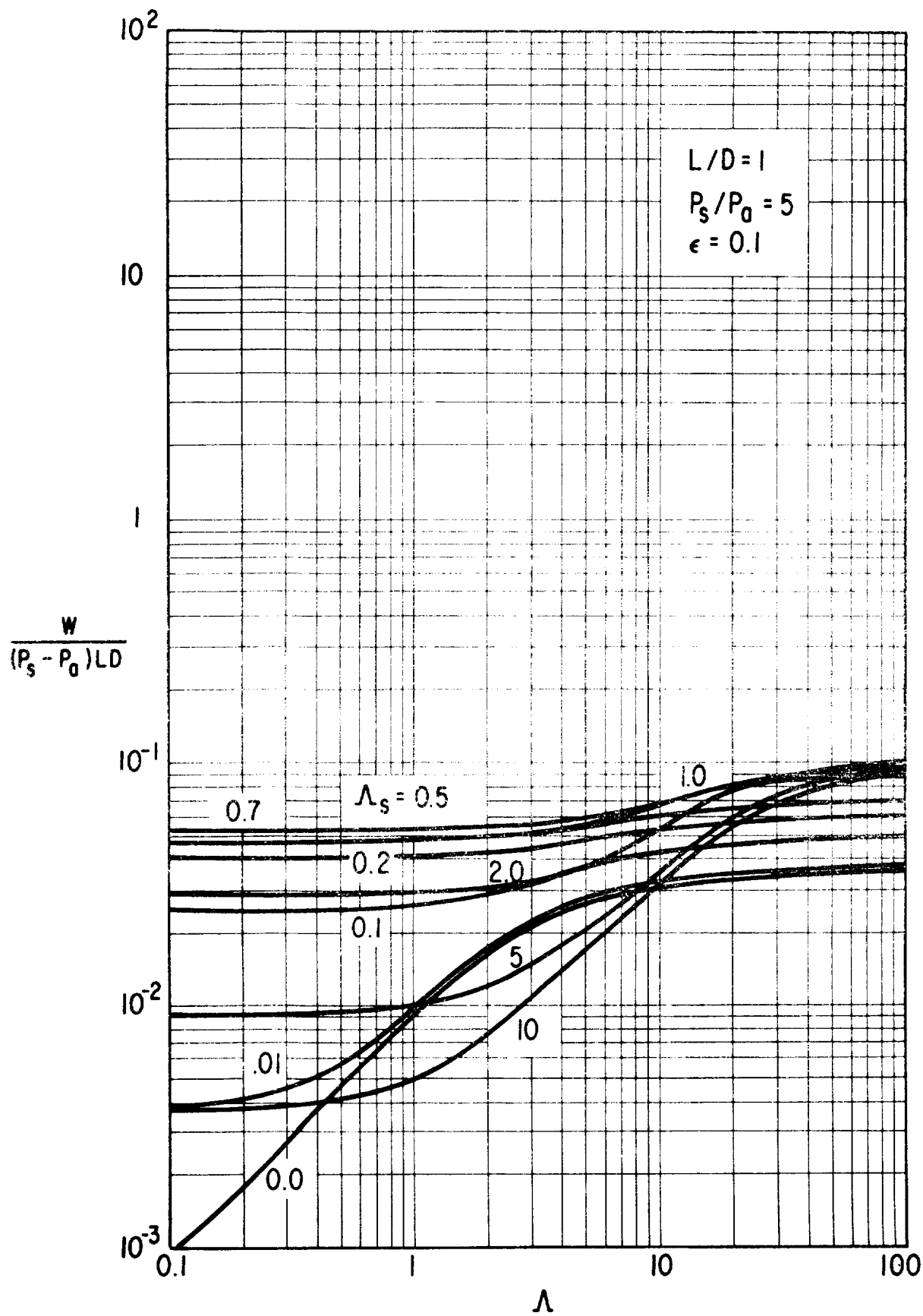


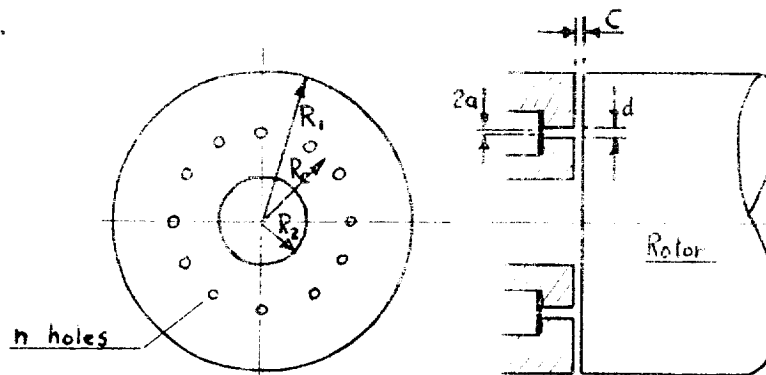
Fig. E-25 Hybrid Journal Bearing Load vs Compressibility Number

F. EXTERNALLY-PRESSURIZED THRUST BEARINGS

1. Introduction

The operating conditions for which an externally-pressurized thrust bearing is selected over a self-acting bearing (e.g. the spiral grooved bearing) are identical to the conditions discussed in connection with the externally-pressurized journal bearing (see Section E, Introduction). The determining factors are high load, high stiffness and low speed.

The externally-pressurized thrust bearing, also called the hydrostatic thrust bearing, is normally made as an annular, flat plate where the pressurized gas is supplied through a series of restricted feeding holes located on some mean diameter.



Hydrostatic Thrust Bearing

The various methods of flow restriction described previously for the hydrostatic journal bearing also apply to the thrust bearing (orifice restriction, inherent compensation, laminar restriction, porous walls). The emphasis in the present discussion is on the orifice restricted and inherently compensated bearing.

In many existing designs the thrust bearing is provided with an annular pocket into which the feeding holes enter, or the pocket may be a circular recess at the center of the bearing. This bearing type can conveniently be called the pocket bearing. The purpose of the pocket is to extend the high pressure region over a larger area of the bearing, thus increasing the load carrying capacity but at a penalty in flow. However, the same may be accomplished by arranging

the feeding holes in two "circles" instead of one as shown above, i.e., completely analogous to the single plane admission and the double plane admission for the hydrostatic journal bearing. The latter arrangement is preferable to a pocket since it reduces the susceptibility to pneumatic hammer.

The following discussion makes frequent use of dimensionless parameters as a convenient method to describe the characteristics of the bearing. The various symbols are explained in the nomenclature list at the end of the section (see also the figure above showing the bearing dimensions).

2. Selection of the Hydrostatic Bearing

When an application calls for a gas lubricated thrust bearing there is a choice between a self-acting bearing or a hydrostatic bearing. As with the journal bearing, the determining factors are load, speed and stiffness. The most widely used self-acting thrust bearing is the spiral-grooved thrust bearing. Its maximum load carrying capacity is approximately given by:

$$\frac{W}{\Delta P_a R_1^2} \approx .03$$

where

$$\text{bearing no. } \Lambda = \frac{6\mu\omega}{P_a} \left(\frac{R_1}{C}\right)^2$$

and the corresponding stiffness is approximately

$$\frac{CK}{\Delta P_a R_1^2} \approx .06$$

where K , lbs/in, is the stiffness

Thus, the maximum unit loading for the self-acting bearing can be given as:

$$\frac{W}{\pi(R_1^2 - R_2^2)P_a} \approx .015 \cdot \Lambda \quad (\approx .3 \text{ to } .5 \text{ in general}) .$$

For load requirements exceeding this value the hydrostatic bearing must be used. It can be designed to give a load of

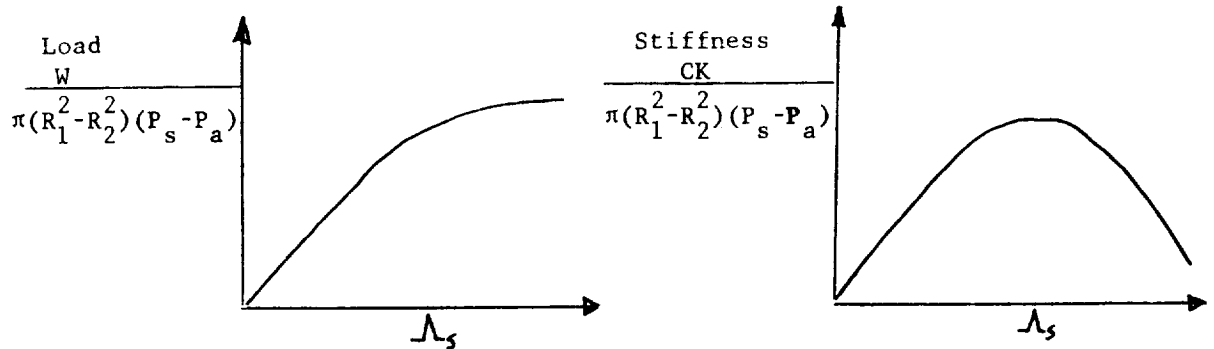
$$\frac{W}{\pi(R_1^2 - R_2^2)P_a} \approx \left(\frac{P_s}{P_a} - 1\right) \cdot \begin{cases} .4 & \text{(single row admission)} \\ .6 & \text{(double row admission)}. \end{cases}$$

Design for Steady-State and Dynamic Operating Conditions

The governing design parameters for the hydrostatic thrust bearing are:

- a) ratio of outer to inner radius: R_1/R_2
- b) restrictor coefficient: $\Lambda_s = \frac{6\mu n a^2 \sqrt{RTg}}{P_s C^3 \sqrt{1+\delta^2}}$
- c) supply pressure ratio: P_s/P_a .

The restrictor coefficient Λ_s gives the ratio between the flow resistance of the gas film and the resistance of the feeding hole restrictors. When $\Lambda_s = 0$ the gas film pressure is equal to ambient throughout the gas film and the bearing has neither load carrying capacity nor stiffness. As Λ_s approaches infinity the gas film resistance becomes very large such that the pressure downstream of the feeding holes equals the supply pressure. Hence, the load carrying capacity is the maximum possible whereas the stiffness is zero. This may be illustrated by the following figures.



Hydrostatic Thrust Bearing, Load and Stiffness vs.
Restrictor Coefficient

The maximum stiffness occurs at

$$\frac{1}{2} \Lambda_s \cdot \log_e \left(\frac{R_1}{R_2} \right) \approx .45$$

With respect to stiffness and flow, there is a close similarity between the hydrostatic journal bearing and the hydrostatic thrust bearing. The flow and stiffness data are almost the same under the condition

$$\frac{L}{D} = \frac{1}{2} \log_e \left(\frac{R_1}{R_2} \right) .$$

Hence, the required flow is determined as described previously for the journal bearing (section E). With respect to load carrying capacity the load characteristic of the thrust bearing differs markedly from that of the journal bearing (compare the first of the above figures with Fig. E-21, section E). The basic reason is that the thrust bearing load derives from a plane pressure distribution whereas in the journal bearing the pressure distribution is "wrapped around", i.e., the thrust bearing uses the pressure level directly whereas the journal bearing depends on a circumferential change in the pressure level. On the other hand, if the thrust load may reverse direction such that two thrust bearings are needed instead of one, the effective thrust load carrying capacity is the difference in load between the two bearings. This combined bearing is called the double-acting thrust bearing to distinguish it from the previously discussed unidirectional bearing which is called the single-acting thrust bearing. The load characteristic of the double-acting bearing is completely analogous to the characteristic of the journal bearing, i.e., it has a maximum value for the same value of the restrictor coefficient, as given above in connection with the optimum stiffness. As a matter of fact, for displacements not exceeding 40 percent of the film thickness C , the load carrying capacity of the double-acting thrust bearing is in close approximation equal to:

$$\text{Load, double-acting brg.} \approx 2 \cdot (\text{displacement}) \cdot (\text{stiffness of single-acting brg}).$$

The maximum load to be obtained with a single-acting bearing (single "row" of feeding holes) can roughly be given by

$$\left[\frac{W}{\pi(R_1^2 - R_2^2)} \right]_{\max} \approx (.4 \text{ to } .5) \cdot (P_s - P_a)$$

i.e., the thrust bearing can utilize 40 to 50 per cent of the available pressure drop. This value can be raised to 60 or 70 per cent by arranging the feeding holes in two "circles" instead of one. However, only in very special cases (e.g. lifting bearings), should a thrust bearing be designed for its maximum load carrying capacity since the corresponding stiffness is virtually zero. Instead, the bearing should be dimensioned to operate near its maximum stiffness. The maximum stiffness and the corresponding single-acting bearing load are approximately given by

$$\left[\frac{CK}{\pi(R_1^2 - R_2^2)(P_s - P_a)} \right]_{\max} \approx .4$$

and

$$\left[\frac{W}{\pi(R_1^2 - R_2^2)} \right]_{\max. \text{stiffness}} \approx (.25 \text{ to } .3) (P_s - P_a) \cdot$$

Thus, a single-acting bearing should not be designed for a unit loading exceeding 30 per cent of the available pressure difference (or 50 per cent with two "rows" of feeding holes) unless the stiffness is of no importance. Similarly, the double-acting bearing is also limited to 30 per cent as seen from the given value of the maximum stiffness in connection with the requirement that the maximum displacement should not exceed 40 per cent of the film thickness to avoid lock-up.

Frequently, the thrust bearing is mounted such that it is self-aligning (e.g. flexible supports). In order to estimate the alignment capacity of the bearing the angular stiffness of the gas film must be known. In approximation:

$$\text{Angular stiffness, lbs.in/radian} \approx \frac{R_1^2}{3} \cdot K$$

where K, lbs/in, is the previously calculated bearing stiffness.

The power required to pump the gas through the bearing is given by

$$[\text{pumping power}]_{\text{gas through bearing}} = \frac{QRT}{6600} \log_e \left(\frac{P_s}{P_a} \right), \text{ HP.}$$

Including the compressor efficiency allows for calculating the total required pumping power.

The power loss imparted to the rotor by the hydrostatic thrust bearing is given by

$$\text{Power Loss} = \frac{\pi^3 \mu N^2 (R_1^4 - R_2^4)}{3300 \cdot C}, \text{ HP}.$$

In studying axial vibrations of the rotor it is occasionally needed to know the damping of the thrust bearing in addition to the already obtained stiffness. As in the case of the journal bearing it is almost impossible to give even the order of magnitude of the damping since it strongly depends on the restrictor coefficient, the pressure ratio and the frequency of the rotor vibrations. Detailed data are available but it would be outside the scope of this discussion to furnish such data. Instead, an indication of the magnitude shall be given under the assumption that the bearing operates well outside the range of pneumatic hammer. Then, for low vibratory frequencies (squeeze number: $\sigma = 12\mu\nu(\frac{R_1}{C})^2/P_2 < 1$ to 2, where ν = vibration frequency, radians/sec) the damping is roughly given by:

$$\frac{B}{\mu R_1 (\frac{R_1}{C})^3} \sim \begin{cases} .003 \left(\left(\frac{R_1}{R_2} \right) = 1.25 \right) \\ .02 \left(\left(\frac{R_1}{R_2} \right) = 1.5 \right) \\ .1 \left(\left(\frac{R_1}{R_2} \right) = 2 \right) \\ .3 \left(\left(\frac{R_1}{R_2} \right) = 3 \right) \end{cases}$$

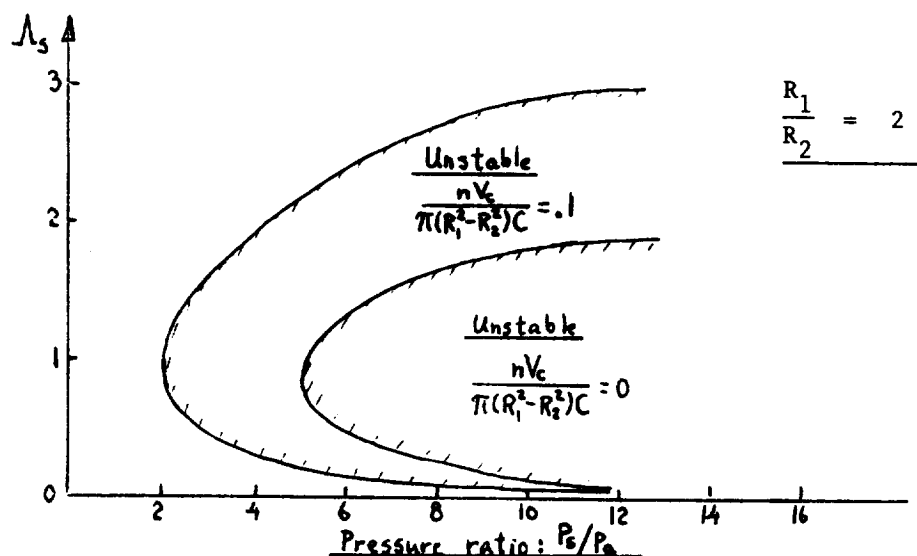
The most serious problem encountered in designing and operating a hydrostatic gas thrust bearing is pneumatic instability, called pneumatic hammer. The hydrostatic thrust bearing is much more sensitive to pneumatic hammer than the hydrostatic journal bearing, and the whole thrust bearing design frequently centers around methods to avoid unstable operation.

A critical factor is the air volume contained in pockets, grooves and the feeder holes themselves. It is of extreme importance to reduce this volume to a minimum, preferably eliminating it all together. Even so, pneumatic hammer may still set in. The effect of any air volume is defined by means of a feeder hole volume parameter:

$$\frac{nV_c}{\pi(R_1^2 - R_2^2) \cdot C}$$

(V_c = volume of feeder hole and pockets or grooves per feeder hole, in³).

This parameter gives the ratio between the total volume, given the feeder hole downstream pressure and the total volume of the gas film. The ratio should be as small as possible (10 per cent is high). The parametric range in which pneumatic hammer occurs is illustrated in the figure below.



"Boxing-in" the above shown regions of instability, the range of parameters for which pneumatic hammer is encountered can be given in approximation by:

Region of Pneumatic Hammer for the Orifice Restricted Thrust Bearing

$\frac{R_1}{R_2}$	$\frac{nV_c}{\pi(R_1^2 - R_2^2)C} = 0$		$\frac{nV_c}{\pi(R_1^2 - R_2^2)C} = .1$	
	$\Lambda_s <$	$\frac{P_s}{P_a} >$	$\Lambda_s <$	$\frac{P_s}{P_a} >$
1.25	5.5	5	12.5	1
1.5	3	5	6	2
2	1.8	5	3	2.5
3	1.1	5	1.6	3

This represents a severe limitation on the design conditions for a hydrostatic gas thrust bearing. Therefore, it is in general recommended that the bearing be designed as inherently compensated, thus eliminating all orifices and providing for the necessary flow restriction at the rim of the feeder holes. In

most cases the inherently compensated bearing does not experience pneumatic hammer as long as the bearing is free from pockets and grooves. It should be noted that the stiffness of the inherently compensated bearing is $2/3$ of the stiffness of the orifice restricted bearing.

NOMENCLATURE LIST FOR SECTION F: Externally-Pressurized Thrust Bearings

- a - Orifice radius, inch
- B - Damping coefficient, lbs.sec/in
- C - Film thickness, inch
- d - Feeder hole diameter, inch
- g = 386.07 in/sec^2 , gravitational acceleration
- K - Stiffness, lbs/in
- N - Rotor speed, rps
- n - Total number of feeding holes
- P_a - Ambient pressure, psia
- P_s - Supply pressure, psia
- Q - Gas flow, lbs/sec
- R_1 - Outer radius of bearing, inch
- R_2 - Inner radius of bearing, inch
- $Q T$ - (Gas Constant) · (Total temperature, °R), inch (for air at 70°F: $Q T = 342,500 \text{ in}$).
- W - Load capacity, lbs.
- δ = a^2/dC , Inherent compensation factor
- Λ = $6\mu\omega(\frac{R_1}{C})^2/P_a$, Compressibility number
- Λ_s = $6\mu n a^2 \sqrt{Q T g}/P_s C^3 \sqrt{1+\delta^2}$, Restrictor coefficient
- μ - Gas viscosity, lbs.sec/in²
- ν - Frequency, radians/sec
- σ = $12\mu\nu(\frac{R_1}{C})^2/P_a$, Squeeze number
- ω = $2\pi N$, Angular velocity, radians/sec

G. GAS BEARING MATERIALS

1. Summary

This section is concerned with the selection of materials for hydrodynamic, gas-lubricated bearings. Emphasis is placed on bearings which will operate in an inert environment at temperatures up to 1000 F.

To eliminate problems of matching thermal expansion characteristics, it is recommended that the same base materials be used for both the bearings and the shaft. Low-alloy steels appear to be suitable in this application. Surface coatings should be applied to achieve sliding compatibility.

The most promising bearing surface coatings for start-stop operation are:

1. Resin bonded MoS_2 film vs. hardened shaft.
2. Oxide or carbide coatings on shaft and bearings.

These coatings are suitable for use in an inert gas environment. The final choice of one specific combination will be governed, to some extent, by the operating temperature range.

The major unknowns in material selection are the ability of bearing materials to withstand a high speed contact and the optimum types of materials which should be used for the pivots of tilting-pad bearings.

2. Materials for Gas-Lubricated Bearing Applications

a. General

From the materials standpoint, reliable operation of any rotating machinery in which gas-lubricated bearings are used will require that the following two conditions be satisfied. First, it must be possible to fabricate the bearings and shaft with a high degree of accuracy. Second, these dimensions must remain constant during the operating life of the equipment. These conditions are particularly important where hydrodynamic bearings are being used.

Specifically, the material requirements which must be considered for any application include the following:

1. Dimensional stability of the bearing and shaft materials.
 - a) Intrinsic stability of the materials themselves to long-time stress relaxation, centrifugal forces at high speed, metallurgical changes or similar effects.
 - b) Resistance of the material to permanent deformation under load at the maximum temperature of usage.
2. Corrosion resistance of the bearing and shaft materials.
3. Matched coefficients of thermal expansion between the bearings and the shaft throughout the operating temperature range.
4. Sliding compatibility of the materials, both under start-stop conditions and during a high-speed rub.

The requirements listed above are not presented in any order of importance. Any one could be the difference between success and failure in a particular piece of machinery.

The actual selection of materials for gas-lubricated bearing systems is difficult, largely because so little factual data is available on the results of using particular materials in practical hardware. A review of the open literature has turned up just three articles (Refs. 1-3) which supplied any useful information on this subject. A study of materials for small, high-precision gyro bearing has recently been completed for the Navy (Ref. 4). These reports appear to sum up most of the published information on materials.

The purpose of the following discussion is to describe some of the practical experience which has been gained in selecting materials for gas-lubricated bearings and to point out some of the problem areas which must still be overcome. Major emphasis is being placed on bearing systems which will operate under the following conditions:

Environment: Inert gas (such as argon)
Speed range: 0-18,000 rpm or 0-60,000 rpm
Temperature range: Ambient to 1000 F
Shaft diameter: 1 to 2 inches
Bearings: Hydrodynamic thrust and journal

While the primary concern of this discussion is with the materials considerations, it is never possible to divorce materials completely from bearing design. For this reason, an attempt has been made to show where material selection and materials problems can be affected by the specific design.

In the following paragraphs, each of the material requirements is discussed briefly:

1. Dimensional Stability

This requirement is not considered to be a major problem as long as good engineering and metallurgical practices are followed. For high-speed operation, centrifugal growth of the shaft must be factored in, especially if high temperatures will be encountered. Every effort should be made to assure that the materials are stabilized above the maximum anticipated temperature and that no residual stresses remain in the surfaces as the result of machining operations.

2. Corrosion Resistance

Since the operating environment will be an inert gas, such as argon, corrosion should be a problem only during fabrication, assembly and check-out. Careful cleaning and handling procedures must be followed to prevent the initiation of corrosion centers. It is recommended that all ferrous surfaces be protected with a surface coating such as Turco Products' "Paintite" (or equivalent), which is a very light phosphating treatment. Storage and shipping should be made under dry conditions and all precision surfaces should be handled with lint-free gloves to prevent corrosion by chemicals from the skin.

3. Differential Thermal Expansion

For operation over a wide temperature range, differential thermal expansion may cause serious changes in the conformity and clearances between the bearings and the shaft. To minimize this problem, the approach has been taken that the bearings and shaft should be made of the same base material wherever possible. Coatings or surface modifications should then be used to provide adequate surface properties such as sliding compatibility. Experience has shown that this approach is generally satisfactory although it restricts the number of possible combinations to materials which can be applied as thin films.

In Table E-26 a list of alloys which could be used for the base materials of the shaft and bearings is given. Normally, low-alloy steels are preferable but, where weight is a factor, materials such as titanium, aluminum or even beryllium should be considered as long as the temperature and strength requirements are not exceeded.

4. Sliding Compatibility

Of all the material requirements imposed on gas-lubricated bearings, the selection of materials for adequate sliding compatibility is certainly the most difficult and least understood aspect of the problem. Because gases are very low viscosity fluids, extremely tight clearances must be maintained between the bearings and the shaft in order to keep the load capacity as high as possible. Any abrasive wear debris or surface damage could penetrate the gas film and cause failure by jamming or by a high-speed contact.

There are two conditions under which sliding contact could occur between the the bearing and the shaft. First, since these are self-acting bearings, low-speed sliding will take place under design stress levels during starts and stops. The lift-off and touchdown sliding velocities could vary over a wide range depending on a number of factors including: clearances, conformity, surface finish, bearing design, stress, etc. A well-designed bearing system will develop some hydrodynamic lift after the first few revolutions, although complete separation may not be achieved until a rotational speed of a few hundred rpm is reached.

The second sliding condition is the case of a high-speed rub during operation. This contact could result from shock or vibration being imposed on the system, or it could be caused by unstable operation of the shaft.

In stationary gas bearing machinery, the possibility of high-speed rubs should not be a problem once satisfactory balancing has been achieved. However, for space power systems, sudden shock loads or vibration must be considered a part of the operational specification. A high-speed rub on a one inch diameter shaft rotating at 50,000 rpm will result in a peripheral sliding velocity of about 220 ft./sec. under a momentary load of possibly several g's. Fortunately,

the time in contact should be extremely short. At the present time, some material combinations appear to be capable of surviving this condition. Very careful experimentation work is required to demonstrate the actual shock load and contact times which could be tolerated. A much more serious case of high-speed sliding contact could occur if the shaft went into whirl and rubbed against the bearing.

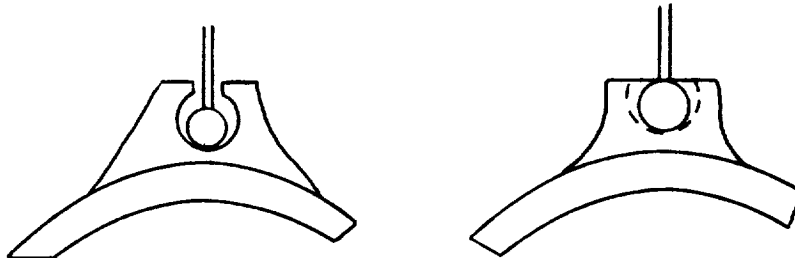
One of the major disadvantages of rigidly-mounted hydrodynamic bearings, such as plain sleeve bearings or fixed pads, is the low threshold value of instability. If the shaft goes into whirl and rubs the bearing, centrifugal forces would impose very high bearing stresses, particularly since the bearing would be edge loaded. Practical experience has shown that this condition will always result in catastrophic failure because of the surge of energy which must be dissipated in a very short period of time.

In the case of tilting-pad bearings, the same sliding contact problems exist. However, since the bearing can follow the shaft motions, the problem of shaft whirl is practically nil in well designed tilting-pad bearings. The tilting pad is also less susceptible to jamming or abrasion damage by loose wear debris because the pad can adapt itself somewhat to accommodate particles. The interrupted surfaces permit debris to escape while the plain sleeve bearing will trap any loose particles in the bearing clearances.

On the other hand, the use of tilting pads imposes a new materials problem insofar as the pivot points are concerned. Since the bearing must adjust to the shaft continuously, the pivot will be subjected to a very high frequency, low amplitude motion. This could result in serious pivot damage in a very short period of time if a significant amount of relative slip was taking place.

One alternative to the pivot designs which involve relative motion between surfaces is to use flexurally-supported bearings. This introduces other material problems and will also involve a sacrifice in radial stiffness. Experimental work on this configuration is now being done by MTI under an Air Force Contract (Ref. 5). At the present time, the ball-socket or

ball-sleeve pivot design shown below appears to be the simplest and most practical arrangement for pivoted pad bearings.



In summary, the most questionable area in the selection of materials is concerned with material compatibility. The following section on sliding contacts discusses the state-of-the-art of bearing material selection in greater detail.

b. The Selection of Compatible Sliding Combinations for the Shaft and Bearings

At this point, it should be emphasized that there is no material combination that can slide in contact without some degree of wear or surface damage taking place. The best that one can hope to attain is an insignificant amount of surface degradation in a finite period of time.

Because of the importance of this problem, considerable emphasis has been placed on the selection and evaluation of materials for adequate compatibility. In making a choice for a particular application, the following operating variables should be considered:

1. Operating Temperature Range

This will affect the choice of materials and will also determine the severity of the problem of matching thermal expansion.

2. Environment

In the normal atmosphere, materials are covered by thin, protective oxide or hydrated oxide films which generally minimize surface damage. In a

non-oxidizing, inert gas, these films will be worn away rapidly and no replenishment is possible. Therefore, materials must be selected which are inherently compatible — regardless of the presence or absence of these surface films.

3. Bearing Design

The choice of a particular bearing design, such as a tilting pad, may also rule out certain materials because of fabrication difficulties or the physical properties of the materials. For example, carbon-graphites are often used in gas-lubricated bearing applications because of their self-lubricating characteristics. To use these low expansion materials over a wide temperature range, it is necessary to shrink the bearing into a housing having the desired thermal expansion characteristics. Unfortunately, this concept is only applicable to a full journal bearing and could not be used with a tilting pad.

Along these same lines, most dissimilar material combinations will present problems of matching the thermal expansion of the bearing to the expansion of the shaft. To circumvent this difficulty, the same base material can be used for both the bearing and the shaft, and coatings or surface modifications can be applied to improve sliding compatibility.

In addition, there is a fabrication problem involved in selecting thrust bearing materials which can be grooved accurately to form patterns such as the Whipple type of spiral grooving. This is discussed later in the section on Fabrication Problems.

As far as the sliding characteristics of the material combinations are concerned, the criteria for selection falls generally into one or more of the following categories:

<u>Criteria</u>	<u>Typical Examples</u>
1. Hard, wear resistant material combinations	Ceramics*, carbides*, nitrided or mal-comized alloys, etc.
2. Self-lubricating materials (mated against hard, lapped shaft)	Carbon-graphite, DU**, Powder compresses containing solid lubricants
3. Soft phase materials (mated against hard, lapped shaft)	Leaded bronzes, Powder compresses containing infiltrated phase
4. Solid lubricant films (mated against hard, lapped shaft)	Resin or ceramic-bonded solid lubricant films

* Could be solid members or flame-sprayed coatings.

** Proprietary bearing material supplied by Glacier Metals. Made by sintering spherical bronze particles on thin steel backing and impregnating the surface with Teflon and lead.

For operation in an inert environment, the following are least affected by the absence of oxide films or moisture in the environment:

1. Hard material combinations
2. Self-lubricating materials which depend on Teflon for sliding properties
3. Solid lubricant films containing molybdenum disulfide.

For general background information, a partial list of materials which have been used in gas-lubricated bearings is given in Table E-27. Of the combinations described in this table, the following appear to be most promising for this application:

<u>Shaft Material</u>	<u>Bearing Material</u>	<u>Temperature Limitation</u>
Hard, lapped material such as tool steel, chrome plate or nitrided steel	Resin-bonded MoS ₂ film on steel	600 F
Flame-sprayed oxide on steel substrate	Flame-sprayed oxide or carbide on steel substrate	750 to 1000 F*

* Depends on coating

These coatings can be applied readily, have excellent slow-speed compatibility at stress levels up to at least three psi, and have been evaluated and used in a number of applications. Satisfactory performance can be obtained, both in air and in an inert environment. Based on tests which were made at MTI on a single, tilting-pad test bearing, operating hydrodynamically, it is reasonable to design for a minimum of 1000 starts and stops without significant deterioration in bearing performance.

For the case of high-speed rubs, it has been qualitatively shown that the oxide vs. oxide or carbide combinations will tolerate a rub of very short duration at 20,000 rpm on a two inch diameter shaft without destroying the bearing. However, the exact loads and contact times were not determined in these tests. Much more effort is required to evaluate the high-speed rub problem since a bearing failure under these conditions could destroy a complete power system.

c. The Selection of Pivot Materials for Tilting-Pad Bearings

The major problem in the pivot appears to be one of design although suitable materials must also be selected. The tracking capability of the bearing is affected by pivot radius and is also affected if moments due to pivot friction are not negligibly small compared to moments due to hydrodynamic pressures. The amplitudes of oscillation will also affect long-term pivot performance. These will be functions of the dynamic loading and the rotor geometry.

Assuming that the pivot must undergo some adjustment with each revolution of the shaft, it is apparent that the pivot will be subjected to high-frequency, small-amplitude motions which could result in surface damage. Improperly designed pivots, where the motions have a large component of sliding, will exhibit serious damage very rapidly. It is very important to design the pivots so that the motions are as close to pure rolling as possible. Since some degree of slip will always take place, the materials combination used in the pivots is also an important aspect.

The stress level in the pivots must be kept sufficiently low to prevent brinelling, fatigue or material fracture — particularly if a brittle material, such as tungsten carbide, is used. The stress level can be reduced, for example, by

using a ball vs. socket design instead of a ball vs. flat design. Care must be exercised, however, to assure that the percentage of sliding motion is not increased. Even with relatively low contact stress, sliding motion will cause considerably more surface damage than will rolling motion. The mathematical expressions for calculating pivot stresses, deflections and compliance are available, adapted from similar analyses for rolling element bearings.

To sum up, long-term satisfactory operation of the pivots will depend on:

1. Configuration and degree of sliding motion
2. Materials combination
3. Stress level
4. Amplitudes of oscillation

At temperatures below 350 F, 52100 steel hardened to 59-62 Rc has been used for both the ball and the sleeve material. Up to 600 F, M-1 or M-10 tool steel was selected for its dimensional stability and hot hardness. Above 600 F, cemented tungsten carbide is preferred. The carbide oxidizes rapidly in air above 900 F, but would be suitable for higher temperatures in argon. For better run-in and surface conditioning, a resin bonded MoS_2 film is generally applied to the surface of the sleeve.

Practical gas-bearing machines employing steel pivots of the type described above have been built by MTI and have accumulated more than 5000 hours of running time with no significant change in bearing performance.

In spite of these successes, there is still much to be learned about these tilting-pad bearing pivots. The design is empirical and the effects of variables such as stress, temperature, shaft speed and shaft balance are not clearly understood.

d. Fabrication Problems

The surface coatings described in the previous sections are supplied by a number of vendors and can be applied to a variety of metallic substrates. Hard, flame-sprayed materials, such as the oxides and carbides, are generally applied to a thickness of about .007 in. and then ground and lapped to a finish thickness of about .003 in. The surface finish should be on the order of one to two rms.

As a general rule, the surface finish on any hard surface, including steel, should never exceed four rms.

The softer coatings, such as the resin-bonded MoS_2 , can be applied with reasonable accuracy to a thickness of .0002 to .0005 in. These coatings should be lapped down to a smooth surface. This removes excess material which would be rapidly worn off in any case. A finished coating thickness of about .0001 to .0002 in. is desirable.

Since the thrust bearings will require some type of grooving for pumping, techniques must be available to make these patterns. At least one coating vendor uses a metal shim mask to blank off the areas where grooves are needed and sprays carbides or oxides to build up the lands. Then the thrust surface is ground and lapped back until the desired groove depth is obtained. Abrasive blasting is also used to cut grooving in the surface.

MTI has had very satisfactory results with photo-etching processes. The patterns obtained are extremely accurate. Most metals are readily etched. If a hard bearing surface is desired, it should be noted that photo-etching can only be done on electrical conductors. Straight oxides cannot be used but metal-bonded carbide are generally suitable.

The greatest problem in the fabrication area is the fact that techniques and skills are the determining factors in the construction of gas bearing machinery. There is no substitute for experience, nor is there any satisfactory way to describe these techniques on paper.

REFERENCES FOR SECTION G: Gas Bearing Materials

1. Macks, E. F., "Gas Lubrication of Radial and Thrust Bearings at High Temperature, High Speeds and Low Lubricant Flow Rates". WADD TR61-83. Feb. 1961.
2. Drescher, H., "Special Features of Self-Acting Air Bearings and Their Effect on Practical Application". First International Symposium Gas Lubricated Bearings, Edited by Dudley D. Fuller, October 26-28, 1959. ACR-49 ONR.
3. Adams, C. R., "Step Gas Bearings". SAE Journal, pp. 29-31. June 1960.
4. Murray, S. F. and M. B. Peterson, "The Selection and Evaluation of Materials and Lubricant Films for Gas-Lubricated Gyro Bearings". MTI 64TR1, June 6, 1964. Prepared for Director, SP-24 under Contract NOBS-88615(FBM).
5. Air Force Contract AF 33(657) 10694. "Research on Gas Lubrication at High Temperature and Low Flow Rates". Now in progress at Mechanical Technology Incorporated.

TABLE E-26 SOME ALLOY CLASSES USEFUL AS BASE MATERIALS FOR SHAFT AND/OR BEARINGS

Alloy Class	Typical Alloy	Nominal Coeff. of Thermal Expansion in./in./°F	Approx. Density	Estimated Useful Temp. Range (in-ert environment)	Problem Areas and Limitations (a)
Low Alloy Steel	4340 or M-1	7.7 (+68 to 752 F)	0.28	ambient to 1000 F	High temp. strength and stability
Martensitic stainless	416	6.4 (+68 to 752 F)	0.28	ambient to 1000 F	High temp. strength and stability
Nickel-base alloys	Inconel X	7.5 (80 to 600 F)	0.3	ambient to 1200 F	Metallurgical trans-formation at high temp. Fabrication. Cost.
Cobalt-base alloys	Haynes 25 (wrought)	7.8 (68 to 800 F)	0.31	ambient to 1200 F	Metallurgical trans-formation at high temp. Fabrication. Cost.
Titanium alloys	Ti-6Al-4V	5.2 (68 to 752 F)	0.16	ambient to 550 F	Dimensional stability after prolonged exposure at temp. Fabrication. Cost. High temp. strength
Aluminum alloys	2024 T-4	12.9 (68 to 212 F)	.09	ambient to 300 F	High temp. strength

(a) Compatibility is a problem common to all of these materials. A self-lubricating bearing material and/or surface coatings must be used for protection.

TABLE E-27 MATERIAL COMBINATIONS WHICH HAVE BEEN USED FOR LARGE BEARINGS

Shaft Material	Bearing Material	Application	Experience
1. Hardened Steel	Bronze (SAE 64)	Hydrostatic journal bearing	Seemed to be suitable for start-stop use. Severe transfer from high speed rub.
2. Hard, lapped Chrome plate	U.S. Graphite Graphitar 80	Hydrodynamic journal and thrust bearings. About 1 psi stress	Excellent compatibility. Survived several rubs at 13,000 to 18,000 rpm at light loads. Poor dimensional stability.
3. Same as 2	National Carbon CCA72	Same as 2. About 3 psi stress.	Excellent stop-start compatibility. Excellent dimensional stability. Would not survive a high speed rub, scored chrome plate badly.
4. Same as 2	Pure Carbon P-303C	Same as 2. About 3 psi stress.	Excellent compatibility and stability. No experience with high speed rubs.
5. Same as 2	Copper-filled carbon-graphite. Morganite MY3A	Hydrodynamic thrust bearing	Same as 4.
6. Same as 2	Pure Carbon P658RC	Hydrodynamic journal bearing	Excellent start-stop compatibility. No experience with high speed rubs.
7. Same as 2	Resin bonded MoS ₂ on phosphated 4130 steel (.0005" thick)	Tilting pad shoes, journal and thrust. About 1-2 psi.	In excellent condition after many start-stop tests.
8. Nitrided Nitralloy	Nitrided Nitralloy	Hydrodynamic journal bearing	200 starts and stops at 2.5 psi. Performance shaky at first, but improved. Test at 3.8 psi very marginal after 50 starts and stops.
9. Vapor blasted, hard, Electroless nickel with fused Teflon film	Same as shaft	Hydrodynamic tilting pad bearing, about 1 psi stress	Satisfactory after about 25 starts and stops. No high speed experience.

TABLE E-27 (continued)

Shaft Material	Bearing Material	Application	Experience
10. Hard, lapped Chrome plate	Epoxy coating with MoS ₂ and low expansion ceramic powder fillers	Hydrodynamic journal bearing	Excellent after about 200 starts and stops. No high speed experience.
11. Hard, lapped Chrome plate	Hardened tool steel	Hydrostatic journal	Used rubbed film of MoS ₂ which seemed to help. OK for starts and stops unless edge loaded. Would not tolerate high-speed rubs.
12. Hard, lapped Chrome plate	Silver impregnated carbon-graphite Pure carbon P5 Ag	Hydrostatic journal and thrust bearings	Normally, bearing only contacted shaft when power failure occurred (on coastdown). Light cleanup of shaft was sufficient for repair.
13. Arc-sprayed Molybdenum coating (Metco)	Aluminum Bronze	Hydrostatic journal bearing	Very little experience but looked promising.
14. Sprayed Stellite over steel	Hard, lapped Chrome plate	Hydrodynamic journal and thrust bearings	Excellent corrosion resistance. Seems good for starts and stops. Very little experience
15. Hard, lapped Chrome plate	S-Monel	Hydrodynamic journal bearing	Good for starts and stops. Quality of Monel was critical. No high speed data.
16. Hard, lapped Chrome plate	Meehanite	Hydrodynamic journal bearing	Good for starts and stops. Poor corrosion resistance.
17. Lapped nitrided Nitralloy	DU bonded to steel backing	Hydrodynamic tilting pad	Excellent compatibility at low and high speeds but limited load capacity. Difficult to fabricate bearing accurately.
18. Flame sprayed oxide	Flame sprayed oxide	Hydrodynamic tilting pad	Excellent start-stop behavior, no high speed data available.
19. Flame sprayed Al ₂ O ₃	Flame sprayed tungsten carbide	Hydrodynamic tilting pad	Excellent start-stop behavior, no high speed data available.

H. SPECIAL CONSIDERATIONS IN GAS BEARING DESIGN

Design procedures and materials considerations have been discussed above for various kinds of gas bearings. The designer, however, should be cautioned that there are several other factors which could cause failure if not properly considered in the design phase. These include:

1. Proper pivot design for tilting-pad bearings
2. Thermal growth and distortion of parts
3. Centrifugal growth of the rotor
4. Tolerance to shock loads .

Proper pivot design to assure that severe fretting or other damage will not occur remains at present an empirical art, based on prior successful experience. Several geometries which have been successfully used include:

- (a) ball on flat
- (b) ball in cylinder
- (c) ball in spherical socket .

Whichever design is used, it is essential to analyze the motion to assure that there is almost entirely a rolling motion. Extensive sliding motions at the pivot must be avoided to prevent fretting or other damage. Also, contact stresses should be kept low. Based on past experience, pivot stresses of about 100,000 psi are used with hardened pivot materials. The pivot materials should be compatible and surface coatings used, where practical.

Gas bearing clearances are generally quite small — of the order of 0.5 to 1×10^{-3} inches per inch. Thus, it is extremely important to make certain that there is adequate cooling to remove the heat generated in the bearings. Suitable heat dams and heat shunts should be used to maintain the bearing region as nearly isothermal as possible and to prevent large thermal gradients due, for example, to the proximity of parts of the rotor that are at very high or very low temperatures. It is strongly recommended that temperature maps of the rotor be included in the design phase, for both steady-state and transient operations, to calculate the resulting distortions. If these are an appreciable part of the clearance, their effect on bearing performance should be verified by cal-

ulation. Where significant temperature rises are expected, the coefficients of expansion of the shaft and bearing should be matched.

At high speeds, there is appreciable centrifugal growth of the rotor. This must be calculated during the design phase and allowance made for it in the ground clearance of the bearing. The change in bearing clearance with speed should also be factored into the calculations, over the full speed range.

Gas bearings have generally poor tolerance to rapidly applied shock loads because the fluid film damping is small and approaches zero for rapid applications of load. If shock loads are anticipated, the bearings should be designed to have very small eccentricity at the steady-state condition, to allow a large margin of load capacity for the shock loads. In any case, the maximum load capacity of the bearing should be checked to assure that it is not exceeded by shock loads.

In closing this discussion, it should be noted that the design procedures discussed in the earlier parts of this review were made assuming laminar condition in the fluid film. This assumption however, is valid over very wide operating ranges, since gases have generally very high kinematic viscosity. For example, developed turbulence will occur when the Reynolds' number is about 1000, i.e.,

$$Re_{crit} = \frac{Uh}{\nu} \approx 1000$$

A one inch diameter bearing with a clearance ratio of 0.001 inches/inch and operating in air at 100 F would achieve this value of Reynolds' number at speeds greater than 900,000 RPM. In general, therefore, gas bearings operate in laminar regime except in cases where the bearing size, clearance and speed are extremely large.

ROLLING CONTACT BEARINGS

For space applications, two general ball bearing applications are of interest. They are high-speed bearings with good lubricant, and low-speed bearings in the space vacuum environment. For the latter application, the bearing companies are coating the bearings with dry-film lubricants and even teflon in a number of ways. These bearings are still being developed so the bearing companies should be contacted for the vacuum environment applications.

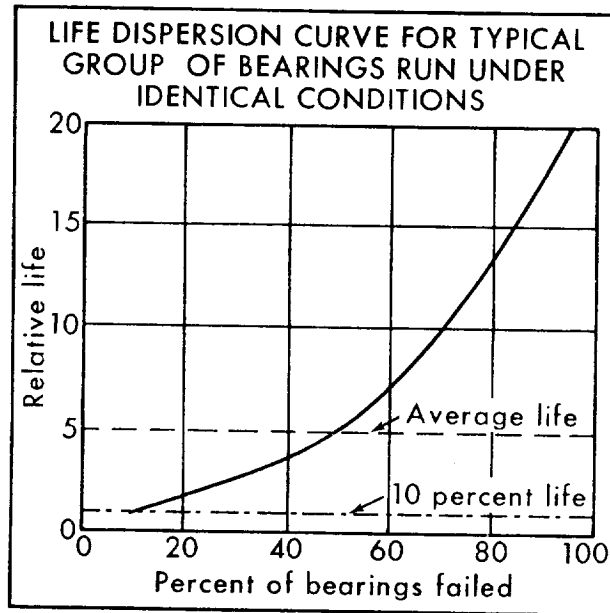
For those applications where a good lubricant can be used, the bearing application information has been well standardized and verified by many tests.

The life of a rolling-contact bearing is usually limited by fatigue. Heavy loads naturally cause greater distortion of the metal in the contact region and fatigue is more rapid with heavy loads than with light loads.

Load ratings of rolling-contact bearings are determined statistically from actual tests.

Two designations for bearing life are B-10 life which is the time at which 10% of the bearings in the test quantity have failed, and B-50 life which is the time at which 50% of the bearings in the test group will have failed. A typical distribution of fatigue failures for a test group of rolling-

contact-bearings will look like this:



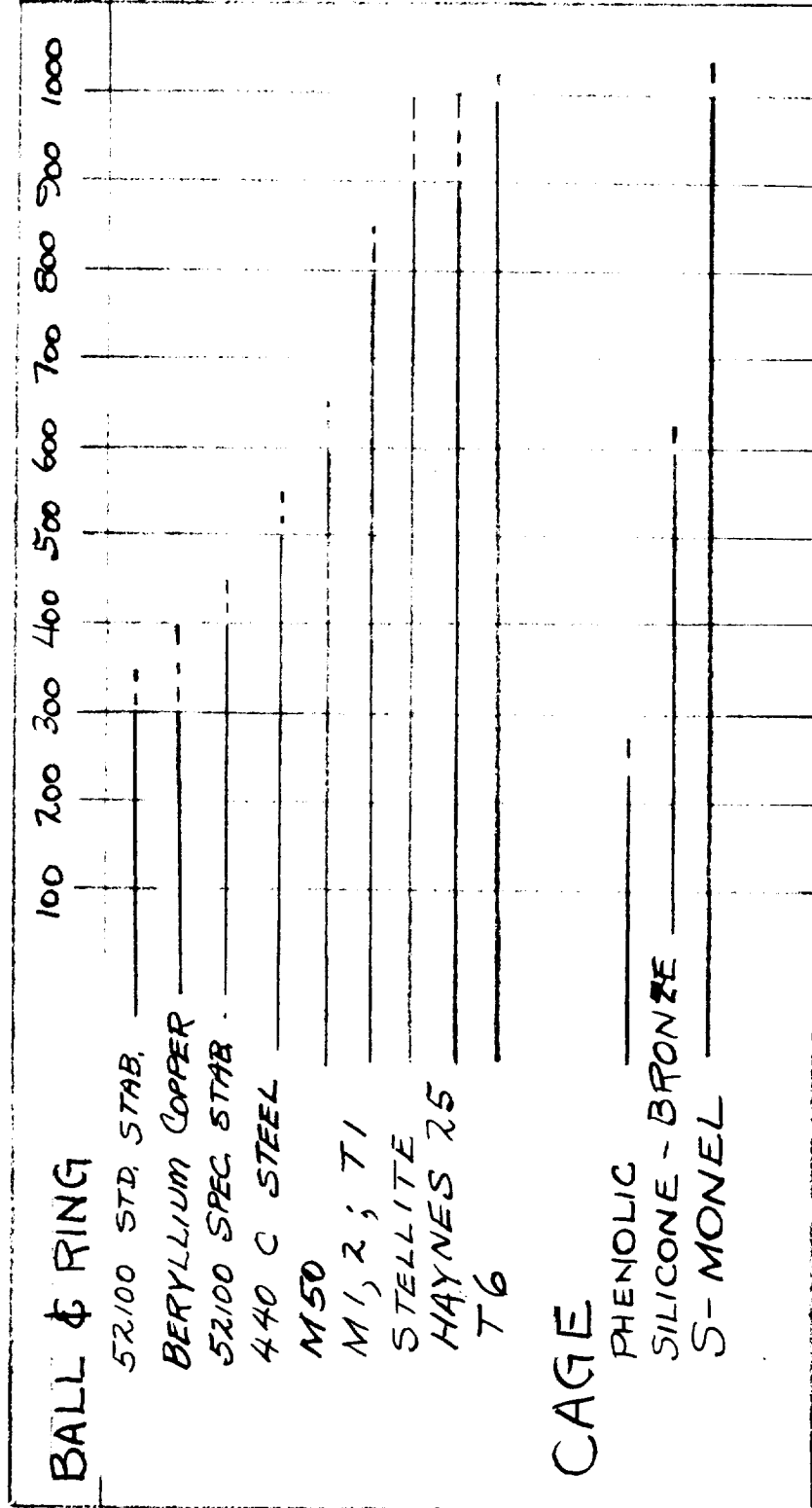
The early fatigue failures in a group of test bearings are believed, by some bearing manufacturers, to be due to inclusions, too small to be seen by a microscope, and by hydrogen in the steel. The hydrogen and inclusions are now removed by various

vacuum melting processes and the earlier fatigue failures in a test group of bearings are fewer. Revised life data based upon the use of vacuum melt steels is not presently available.

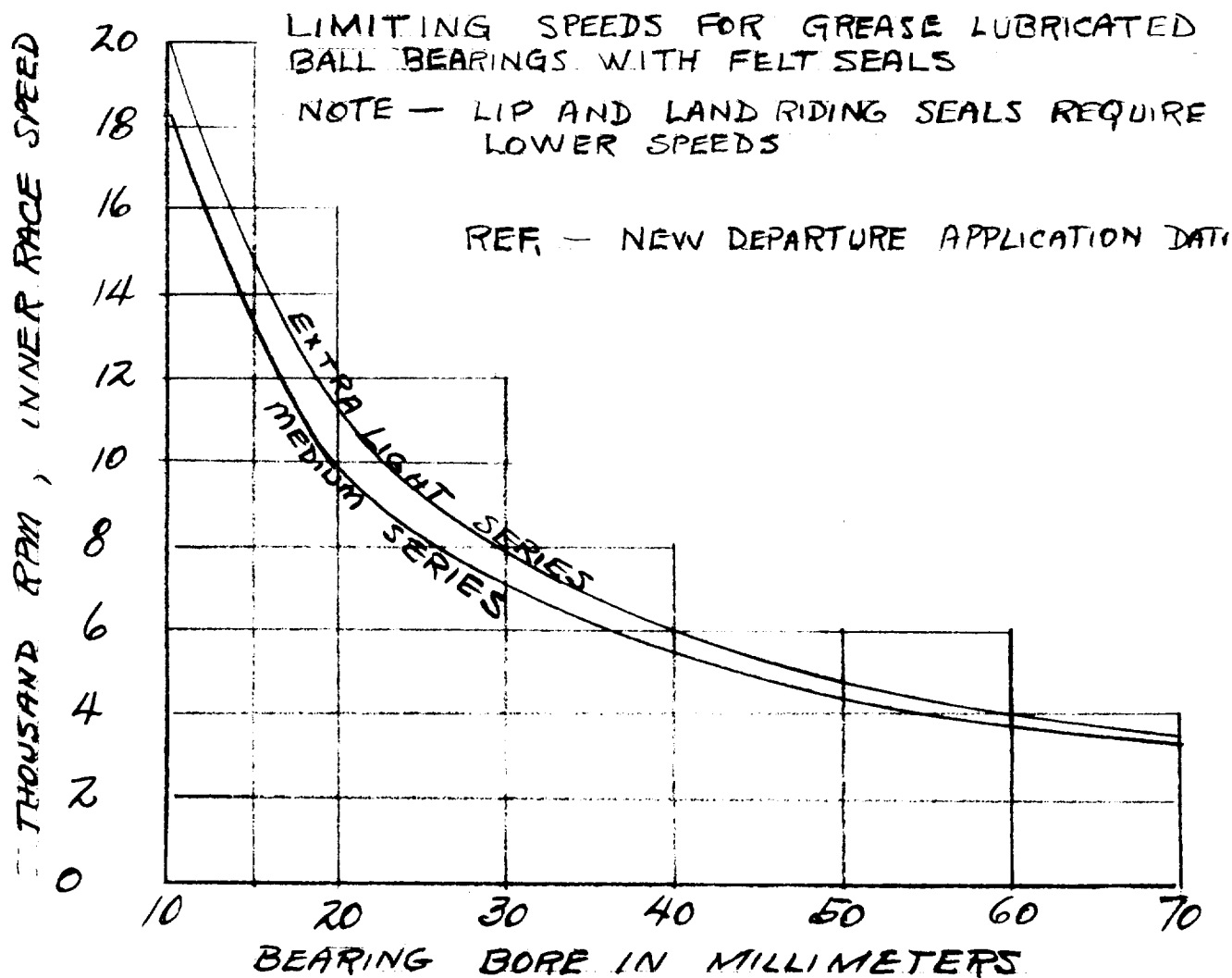
TEMPERATURE LIMITATIONS OF BALL, RING, AND CAGE MATERIALS IN BALL BEARINGS

REF: CHIRONIS, "TODAY'S BALL BEARINGS" PRODUCT ENGINEERING, DEC. 12, 1960
PP 63-78

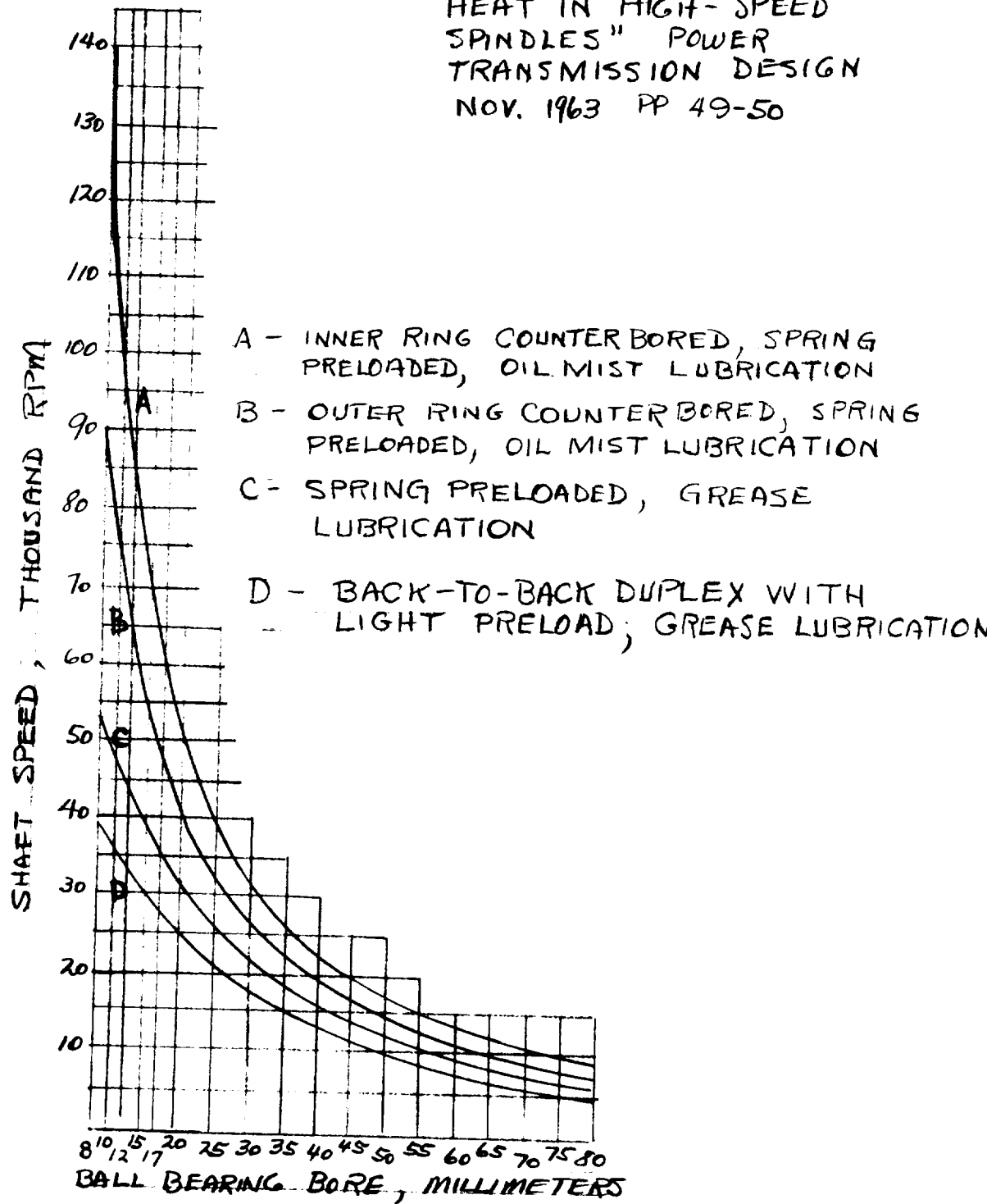
MATERIALS TEMPERATURE °F



NOTE - DASHED LINES MERELY SHOW THAT LIMITS ARE NOT SHARPLY DEFINED



SPEED AND SIZE OF LIGHT AND EXTRA-LIGHT
 SUPERPRECISION BALL BEARINGS FOR FOUR (4)
 KINDS OF APPLICATIONS — FROM-MORAN, "BEARING
 HEAT IN HIGH-SPEED
 SPINDLES" POWER
 TRANSMISSION DESIGN
 NOV. 1963 PP 49-50



INNER-RACE OR SHAFT RPM
FOR OIL JET OR OIL MIST
LUBRICATED, LIGHT SERIES,
RADIAL BALL BEARINGS

15000 FT./MIN. INNER RING RACEWAY SPEED

SERVICE LIFE = 3000 HRS.

BRGS. ARE UNSEALED AND
PROPERLY ALIGNED

REF. NEW DEPARTURE

